Regulation of sphingolipid long-chain bases during cell death reactions and abiotic stress in *Arabidopsis thaliana*

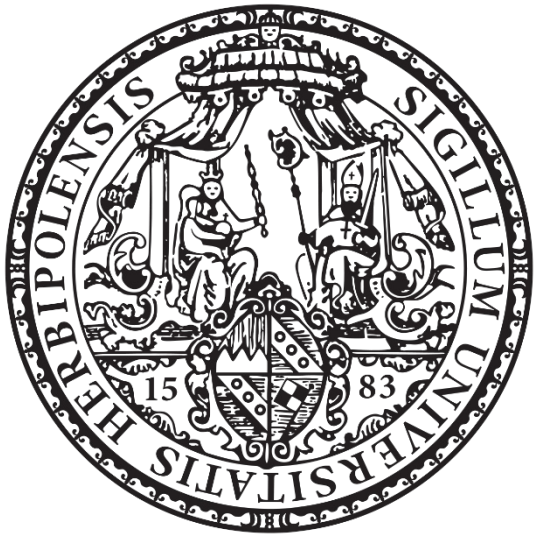

Dissertation zur Erlangung des
naturwissenschaftlichen Doktorgrades
der Julius-Maximilians-Universität Würzburg

vorgelegt von

Benjamin Lambour

Geboren in
Villeneuve-d'Ascq (France)

Würzburg, 2022

Eingereicht am : ……

Mitglieder der Promotionskommission:

Vorsitzender: ……..
Gutachter: PD Dr. Frank Waller
Gutachter: Prof. Dr. Dirk Becker

Date of Public Defense: ……
Date of Receipt of Certificates: ……

Affidavit

I hereby confirm that my thesis entitled "Regulation of sphingolipid long-chain bases during cell death reactions and abiotic stress in *Arabidopsis thaliana*" is the result of my own work. I did not receive any help or support from commercial consultants. All sources and / or materials applied are listed and specified in the thesis.

Furthermore, I confirm that this thesis has not been yet submitted as part of another examination process neither in identical nor in similar form.

Besides I declare that if I do not hold the copyright for figures and paragraphs, I obtained it from the rights holder and that paragraphs and figures have been marked according to law or for figures taken from the internet the hyperlink has been added accordingly.

Place, Date Signature

Eidesstattliche Erklärung

Hiermit erkläre ich an Eides statt, die Dissertation "Regulation von Sphingobasen während der Zelltodreaktion und abiotischem Stress in *Arabidopsis thaliana*" eigenständig, d.h. insbesondere selbständig und ohne Hilfe eines kommerziellen Promotionsberaters, angefertigt und keine anderen als die von mir angegebenen Quellen und Hilfsmittel verwendet zu haben.

Ich erkläre außerdem, dass die Dissertation weder in gleicher noch in ähnlicher Form bereits in einem anderen Prüfungsverfahren vorgelegen hat.

Weiterhin erkläre ich, dass bei allen Abbildungen und Texten bei denen die Verwer-tungsrechte (Copyright) nicht bei mir liegen, diese von den Rechtsinhabern eingeholt wurden und die Textstellen bzw. Abbildungen entsprechend den rechtlichen Vorgaben gekennzeichnet sind sowie bei Abbbildungen, die dem Internet entnommen wurden, der entsprechende Hypertextlink angegeben wurde.

Ort, Datum Unterschrift

Table of contents

Abbreviations

AAL: *Alternaria alternate f. sp. lycopersici*
ABA: Abscisic Acid
acd5: accelerated cell death 5
ACD11: Accelerated Cell Death 11
ACER: Alkaline Ceramidase
Al: Aluminum
BP: Base Pair
CDB: Czapek Dox Broth
CERK: Ceramide Kinase
Cer-P: Ceramide Phosphate
cfu: colony forming unity
CID: collision induced dissociation
CTAB: Hexadecyltrimethyl-Ammonium bromide
DAMP: Damage-Associated Molecular Patterns
DMSO: Dimethyl Sulfoxide
DNA: Deoxyribonucleic acid
DPL1: Dihydrosphingosine-1-Phosphate Lyase
ER: Endoplasmic Reticulum
ERH1: enhancing *RPW8*-mediated HR-like cell death
ESI: Electro Spray Ionisation
ETI: Effector-Triggered Immunity
ETS: Effector-Triggered Susceptibility
FA: Fatty Acid
FB_1: Fumonisin B_1
GC: gas chromatography
GCS: Glucosylceramide Synthase
GIPC: Glycosyl Inositol Phosphate Ceramide
GlcA: Glucuronic Acid
Glc-Cer: Glycosyl-Ceramide
HCl: Hydrogen chloride
hpi: hours post-inoculation
HR: Hypersensitive Response
IPC: Inositol Phosphorylceramide
IPCS: Inositol Phosphorylceramide Synthase
IPUT1: Inositol Phosphorylceramide-Glucuronosyl-Transferase
IS: Internal Standard
kb: kilo base
KB: King's B
KOH: Potassium hydroxide
LAG: Longevity Assurance Gene
LB: Left Border
LCB: Long-Chain Base
LCBK: Long-Chain Base Kinases

LCB-P: Long-Chain Base Phosphate
LOH: Longevity Assurance Gene Homolog
LP: Left Primer
LRR: Leucine-Rich Repeat
M: Molar
MAPK: Mitogen-Activated Protein Kinase
$MgCl_2$: Magnesium Chloride
MRM: Multiple Reactions Monitoring
MS: Murashige and Skoog
m/z: Mass to charge ratio
MS/MS: tandem Mass Spectrometry
NB: Nucleotide Binding
NCER: Neutral Ceramidase
ORM: Orosomucoid
PAMP: Pathogen-Associated Molecular Patterns
PCD: Programmed Cell Death
PCR: Polymerase Chain Reaction
PDB: Potato Dextrose Broth
PR: Pathogenesis-Related
PRR: Pattern Recognition Receptors
Pst: *Pseudomonas syringae pv. tomato*
PTI: Pattern-Triggered Immunity
qPCR: quantitative Polymerase Chain Reaction
RB: Right Border
RF: Reference Factor
RNA: Ribonucleic acid
RNAi: RNA interference
ROS: Reactive Oxygen Species
RPW8: Resistance to powdery mildew 8
Rt: Room temperature
RT: retention time
SPHK: Sphingosine Kinase
SPHK-KD: Sphingosine Kinase Knockdown
SPL: Sphingolipids
SPP: Sphingoid Phosphate Phosphatase
SPT: Serine Palmitoyltransferase
TAE: Tris-Acetate EDTA
TCA: Trichloroacetic Acid
TOF: time-of-flight
UPLC: Ultra Performance Liquid Chromatography
UPLC-MS/MS: Ultra Performance Liquid Chromatography - tandem Mass Spectrometry
UV: Ultraviolet
VLCFA: Very-Long-Chain Fatty Acid
VPE: Vacuolar Processing Enzyme
x G: x-folding acceleration

Summary

Sphingolipid long-chain bases (LCBs) are the building blocks of the biosynthesis of sphingolipids. They are defined as structural elements of the plant cell membrane and play an important role determining the fate of the cells. Complex ceramides represent a substantial fraction of total sphingolipids which form a major part of eukaryotic membranes. At the same time, LCBs are well known signaling molecules of cellular processes in eukaryotes and are involved in signal transduction pathways in plants. High levels of LCBS have been shown to be associated with the induction of programmed cell death as well as pathogen-derived toxin-induced cell death. Indeed, several studies confirmed the regulatory function of sphingobases in plant programmed cell death (PCD): (i) Spontaneous PCD and altered cell death reaction caused by mutated related genes of sphingobase metabolism. (ii) Cell death conditions increases levels of LCBs. (iii) PCD due to interfered sphingolipid metabolism provoked by toxins produced from necrotrophic pathogens, such as Fumonisin B_1 (FB_1). Therefore, to prevent cell death and control cell death reaction, the regulation of levels of free LCBs can be crucial.

In the present study, we first investigated the role of sphingobases and sphingolipids in PCD by using sphingolipid (SPL) biosynthesis mutant lines. The levels of LCBs and LCB-Ps were reported to be different within the distinct mutant lines. These mutants were subjected to biotic and abiotic stresses and the levels of sphingolipids were measured to determine how SPL species vary and if their levels correlate with or are required for survival or fitness under the established conditions. The investigation of the role of sphingobases and sphingolipids in PCD were conducted on several sphingolipid mutant lines after pathogen infection (*Pseudomonas syringae* and *Verticillium longisporum*) and after variations of temperature (heat shock, and heat and cold acclimation). The results showed significant accumulations of sphingobases such as d18:0 and t18:0, and of sphingolipids such as d18:0-16:0 and t18:0-16:0, in all the mutants tested post *P. syringae* infection. Regarding to *V. longisporum* infection, strong accumulations of phosphorylated sphingobases were exhibited from some of the sphingolipid biosynthesis mutant lines. That was correlating to lower susceptibility to *V. longisporum* for the mutant line *sphk1*-OE / *spp1.2*. Regarding abiotic stresses, increases of LCBs, LCB-Ps but also d18:0-16:0 and t18:0-16:0 were observed for *sphk1*-OE but no correlation in tolerance to high temperature was demonstrated.

Secondly, we studied the flux of sphingolipids in *Arabidopsis thaliana* ecotype Col-0 after providing deuterium labeled free LCBs (D_7-d18:0). This experiment could be the precursor on the discovery of new pathways of regulation of LCB levels to regulate PCD. The examination of the flux was conducted by both, targeted and untargeted analysis, to define a profile on the synthesis of *de novo* sphingolipids containing D_7-d18:0 and to establish how high amount of free LCBs (D_7-d18:0) could be reduced. We showed high turnover rates for d18:0-P, t18:0, and t18:0-P and that they contained high amounts of labeled D_7-d18:0. Turnover of ceramides was lower, with the highest steady state levels detected for d18:0-16:0, followed by d18:0-24:0, t18:0-16:0 and t18:0-22:0. LCB-P steady state levels, that showed more than 50-fold increase, pointed out the fact that the degradation of LCBs via LCB-Ps was important, and that LCB-P degradation could be a rate-limiting step to reduce high levels of LCBs. We also generated a list of non-characterized compounds that were induced by high LCB levels that could be further analyzed to reveal new pathways to regulate PCD.

The results of the present study challenged the comprehension of sphingobases and sphingolipid levels during PCD. We provided detailed analysis of sphingolipids levels that revealed correlations of certain sphingolipid species with cell death. Moreover, the investigation of sphingolipid biosynthesis allowed us to understand the flux after the accumulation of high LCB levels. However, further analysis of degradation products or sphingolipid mutant lines, would be required to fully understand how high levels of sphingobases are being treated by the plant.

Zusammenfassung

Sphingobasen (LCBs) sind die Bausteine der Biosynthese von Sphingolipiden. Sie werden als Strukturelemente der pflanzlichen Zellmembran definiert und spielen eine wichtige Rolle für das Schicksal der Zellen. Komplexe Ceramide machen einen wesentlichen Teil der gesamten Sphingolipide aus, die einen großen Teil der eukaryotischen Membranen bilden. Gleichzeitig sind LCBs bekannte Signalmoleküle für zelluläre Prozesse in Eukaryonten und sind an Signalübertragungswegen in Pflanzen beteiligt. Es hat sich gezeigt, dass hohe LCB-Konzentrationen mit der Induktion des programmierten Zelltods sowie mit dem durch Pathogene ausgelösten Zelltod in Verbindung stehen. Mehrere Studien haben die regulierende Funktion der Sphingobasen beim programmierten Zelltod (PCD) in Pflanzen bestätigt: (i) Spontaner PCD und veränderte Zelltodreaktionen, die durch mutierte verwandte Gene des Sphingobasen-Stoffwechsels verursacht werden. (ii) Zelltodbedingungen erhöhen den Gehalt an LCBs. (iii) PCD aufgrund eines gestörten Sphingolipid-Stoffwechsels, der durch von nekrotrophen Krankheitserregern produzierte Toxine wie Fumonisin B1 (FB1) hervorgerufen wird. Um den Zelltod zu verhindern und die Zelltodreaktion zu kontrollieren, kann daher die Regulierung des Gehalts an freien LCBs entscheidend sein.

In der vorliegenden Studie untersuchten wir zunächst die Rolle von Sphingobasen und Sphingolipiden bei PCD, indem wir Sphingolipid (SPL)-Biosynthesemutantenlinien verwendeten. Es wurde festgestellt, dass der Gehalt an LCBs und LCB-Ps innerhalb der verschiedenen Mutantenlinien unterschiedlich ist. Diese Mutanten wurden biotischen und abiotischen Stressfaktoren ausgesetzt, Ihr SPL-Gehalt wurde gemessen, um festzustellen, ob und wie die verschiedenen SPL-Spezies variieren und ob ihr Gehalt mit dem Überleben oder der Fitness unter den festgelegten Bedingungen korreliert oder dafür erforderlich ist. Die Rolle der Sphingobasen und Sphingolipiden bei PCD wurde an mehreren Sphingolipid-Mutantenlinien nach einer Pathogeninfektion (*Pseudomonas syringae* und *Verticillium longisporum*) und nach Temperaturschwankungen (Hitzeschock, sowie Hitze- und Kälteakklimatisierung) untersucht. Die Ergebnisse zeigten eine signifikante Akkumulation von Sphingobasen wie d18:0 und t18:0 sowie von Sphingolipiden wie d18:0-16:0 und t18:0-16:0 in allen getesteten Mutanten nach einer Infektion mit *Pseudomonas syringae*. Im Hinblick auf eine Infektion mit *Verticillium longisporum* wurde bei einigen der Sphingolipid-Biosynthese-Mutantenlinien eine starke Akkumulation phosphorylierter Sphingobasen festgestellt. Dies korrelierte mit einer geringeren Anfälligkeit für *V. longisporum* bei der Mutantenlinie *sphk1*-OE / *spp1.2*. In Bezug auf abiotische Stressfaktoren wurde für *sphk1*-OE ein Anstieg von LCBs, LCB-Ps, aber auch von d18:0-16:0 und t18:0-16:0 beobachtet, aber es wurde keine Korrelation mit der Toleranz gegenüber hohen Temperaturen nachgewiesen.

Zweitens untersuchten wir den Flux von Sphingolipiden in *Arabidopsis thaliana* Ökotyp Col-0, nachdem wir mit Deuterium markierte freie LCBs (D_7-d18:0) gefürttert hatten. Dieses Experiment könnte der Wegbereiter für die Entdeckung neuer Wege zur Regulierung des LCB-Spiegels sein, um PCD zu regulieren. Die Untersuchung des Fluxes der Deuterium markierten Sphingobase wurde sowohl durch gezielte als auch durch ungezielte Analyse durchgeführt, um ein Profil der Synthese von de novo gebildeten Sphingolipiden, die D_7-d18:0 enthalten, zu erstellen und um festzustellen, wie hohe Mengen an freien LCBs (D_7-d18:0) reduziert werden können. Wir konnten hohe Umsatzraten für d18:0-P, t18:0 und t18:0-P nachweisen und feststellen, dass sie große Mengen an markiertem D_7-d18:0 enthalten. Der Umsatz von Ceramiden war geringer, wobei die höchsten Steady-State-Werte für d18:0-16:0 festgestellt wurden, gefolgt von d18:0-24:0, t18:0-16:0 und t18:0-22:0. LCB-P-Steady-State-Werte, die um mehr als das 50-fache anstiegen, wiesen darauf hin, dass der

Abbau von LCBs über LCB-Ps wichtig war und dass der LCB-P-Abbau ein ratenbegrenzender Schritt zur Verringerung hoher LCB-Werte sein könnte. Wir erstellten auch eine Liste von nicht charakterisierten Verbindungen, die durch hohe LCB-Konzentrationen induziert wurden und die weiter analysiert werden könnten, um neue Wege zur Regulierung von PCD aufzuzeigen.

Die Ergebnisse der vorliegenden Studie stellten das Verständnis der Sphingobasen und Sphingolipidspiegel während der PCD in Frage. Wir lieferten eine detaillierte Analyse der Sphingolipidspiegel, die Zusammenhänge zwischen bestimmten Sphingolipidarten und dem Zelltod aufzeigte. Darüber hinaus ermöglichte uns die Untersuchung der Sphingolipid-Biosynthese ein Verständnis des Fluxes nach Akkumulation hoher LCB-Konzentrationen. Weitere Analysen von Abbauprodukten oder Sphingolipid-Mutantenlinien wären jedoch erforderlich, um vollständig zu verstehen, wie die Pflanze mit hohen Mengen an Sphingobasen umgeht.

1. INTRODUCTION.

Plants are sessile organisms that are affected by abiotic and biotic environmental changes around them, which can ultimately determine their fate. In response to stressful conditions, plants have developed varied and complex strategies through molecular, metabolic, and physiological adaptations. For a multicellular organism, it is particularly important to regulate during the cell life cycle if a cell is going to survive or die. An important mechanism that controls growth and development is programmed cell death (PCD), which is also a crucial component of defense mechanisms in response to a variety of biotic and abiotic stresses (Berkey *et al*. 2012). PCD is defined as a sequence of events that lead to the controlled and organized destruction of cells (Lockshin and Zakeri, 2004). It is an established process found in eukaryotes as a physiological aspect essential for their life as well as in prokaryotes as a benefit for the population (Allocati *et al*., 2015). It results in the possibility of certain cells essential for development (or bacteria, in the case of prokaryotes) sacrificing themselves to save the whole organism.

There are different forms of PCD that regulate cell death and most of them have been studied in detail. Nowadays, the molecular fundamentals of apoptosis, which is a non-inflammatory, silent process found in mammalian cells, is the best characterized and well-understood process from PCD. Processes such as apoptosis activation by effective proteins along its regulatory pathway, the release of cytochrome *c* from the mitochondria into the cytosol, activation of the caspase 3 cascade to mediate apoptosis and killing cells, or macrophages engulfing dead cells for further degradation have been described in detail in animals (Nagata, 2018) and are outside the scope of this thesis.

In animals, a classification of the different cell death modalities as well as a description of the pathways at morphological, biochemical, and functional levels have been well defined (Galluzzi *et al*., 2018). However, in plants, the molecular mechanisms and signaling pathways involved in PCD have been described to a lesser extent. Based on morphological criteria, two different classes of PCD can be distinguished in plants: vacuolar cell death (autolytic cell death) and necrosis cell death (non-autolytic cell death; van Doorn, 2011). Vacuolar cell death is characterized by the formation and increase in volume of lytic vacuoles with subsequent rupture of the tonoplast and release of hydrolases, leading to the degradation of the components of the cytoplasm. During this plant immune response, a cysteine proteinase localized in the vacuole known as vacuolar processing enzyme (VPE) is responsible for the vacuolar rupture and initiating the proteolytic cascade that leads to PCD (Hatsugai *et al*., 2015). The caspase-like VPE defines a clear process in plant cells in comparison to the apoptosis occurring in animal cells (Hara-Nishimura and Hatsugai, 2011). In necrosis cell death, the plasma membrane ruptures and provokes the shrinkage of the tonoplast while the remaining constituents of the cytoplasm remain mainly undamaged (van Doorn, 2011). Necrotic cell death occurs mainly under abiotic or biotic stress conditions whereas vacuolar cell death occurs during developmental processes such as tissue formation (aerenchyma formation, unisexual flower formation and leaf shape) or xylogenesis (Fukuda, 1996; Gunawardena, 2008).

Despite the previously mentioned PCD classification, some examples of plant PCD do not clearly fall under one of the two major categories described and are therefore considered as separate modalities, which can exhibit mixed features of both major cell death forms. This is the case of a unique PCD type known as the hypersensitive response (HR), which occurs upon interaction of plants with biotrophic pathogens. The HR is triggered by the detection of pathogens by the plant and displays most of the characteristics of necrotic cell death. Yet, at the same time, HR also displays features of vacuolar cell death, such as the increase in volume of lytic vacuoles and destruction of the

tonoplast (van Doorn, 2011). As a result, either the spread of the pathogen is decreased by the HR or the pathogen infests the plant (Coll *et al*., 2011). The HR is further described in a later section of this thesis (1.1.2. Hypersensitive Response).

1.1. Plant-pathogen interaction.

During evolution, and due to their sessile way of life, plants have developed a primary cell-autonomous immune system, which is the result of the lack of a circulatory system and cells being framed within a rigid cell wall (Coll *et al*., 2011). Plants represent a large reservoir of nutrients in the environment where they grow, and they are exposed to many microorganisms that can potentially utilize them as a source of nutrients. In nature, many microorganisms interact in symbiosis with the plants in different ways, including, for example, mutualistic, commensalism, or parasitic relationships. Based on the type of interaction of the microorganisms with the host plant, they can be classified into three different categories: biotrophic, hemibiotrophic, and necrotrophic. In simple terms, a biotrophic interaction between two different species occurs when the parasite obtains nutrients from the living cells of the host plant without causing significant harm. On the contrary, necrotrophic organisms are geared towards breaking down plant cell walls through the secretion of hydrolytic enzymes, killing host cells and feeding off the released nutrients. In the practice, there are many intermediate states between biotrophy and necrotrophy, which are referred to as hemibiotrophic relations (Vleeshouwers and Oliver, 2014). A hemibiotrophic interaction is a dual-life style in which there is an initial biotrophic lifestyle that causes minimum damage to the plant tissues and a later lifestyle change into a highly destructive necrotrophic phase (Oliver and Ipcho, 2004). This is the case of some phytopathogens, such as the bacterium *Pseudomonas syringae*, characterized by an initial biotrophic phase with a posterior change to necrotrophy.

The interaction between pathogens and plants is sophisticated and dynamic. During evolution, plants have developed a complex set of strategies to respond to the stresses generated by microbial pathogens. The first line of defense is a physical barrier that consists of a cell wall surrounding the plant cells. This wall is composed of cellulose, pectin, hemicellulose, proteins and, in some cases, lignin. Changes in lignin content and composition have been shown to provide protection against biotic stress (De Gara *et al*., 2003; Hamann, 2012). However, in the leaves, phytopathogenic fungi and bacteria are able to penetrate these structures through various openings such as wounds, stomata, and pores (Chisholm *et al.*, 2006). In addition to the physical barriers, plants continuously produce secondary metabolites with antimicrobial activity that are stocked in specific cell compartments and ready to be used in the defense against phytopathogen infection (De Gara *et al*., 2003). Even if these constitutive protective mechanisms are overcome by a pathogen and a plant gets infected, there are defense mechanisms to fight pathogens that are considered as the plant immune response and remain to be further characterized. Unlike animals, plants lack mobile immune cells and therefore must own an adaptive immune system in every single cell to respond to infections. The plant immune system is composed of several distinguishable phases, which result from the evolutionary pressure imposed on plants and pathogens and will determine the fate of the interaction between these organisms (Coll *et al*., 2011).

Phytopathogens use different methods to infect plants. As mentioned previously, bacteria can invade leaves through wounds or natural openings in the leaves, like gas pores (stomata) or water pores (hydathodes), and colonize the apoplastic space in the tissue. Pathogenic fungi (such as *Verticillium longisporum*, which is employed in this thesis), symbiotic fungi, and oomycetes penetrate the plant

into or between epidermal cells by means of hyphae (Jones and Dangl, 2006). Then, these pathogens develop specialized feeding structures called haustoria which penetrate the host cell wall to obtain the nutrients from the space between the cell wall and the plasma membrane. An intimate association between the host plasma membrane and the haustorial plasma membrane is established and determines the outcome of the plant-pathogen interaction. A different method to infect plants has been developed by nematodes and aphids, which feed by inserting a stylet directly through the cell wall and thereby obtain nutrients (Jones and Dangl, 2006).

1.1.1. Plant immune system.

Traditionally, the performance of the plant immune system upon an attack by a pathogen can be represented as a four-phased "zigzag" model (**Figure 1**). This simplified model was proposed by Jones and Dangl to describe the continuous steps that occur during plant-pathogen interaction (Jones and Dangl, 2006).

In phase 1, pathogenic microorganisms exude molecules into the environment known as pathogen-associated molecular patterns (PAMPs). These are perceived by the plant's transmembrane pattern recognition receptors (PRRs) leading to the activation of a basal immune response (Jones and Dangl, 2006). In the same way, microorganisms that are not necessarily pathogenic produce microbe-associated molecular patterns (MAMPs) and trigger the same immune response in the plant (Ausubel, 2005). PAMPs and MAMPs can be evolutionary conserved molecules within organisms such as bacterial proteins (e.g., flagellin), peptidoglycans, polysaccharides (e.g., chitin), or lipopolysaccharides (Bigeard *et al*., 2015). In addition, endogenous peptides in the plants as well as degradation products derived from pathogenic invasions, which are known as damage-associated molecular patterns (DAMPs), are also recognized by the PRRs, inducing a plant immune response (Boller and Felix, 2009; Bigeard *et al*., 2015). The plant transmembrane PRRs are composed of an extracellular domain for ligand binding and an intracellular kinase domain. Ligand binding results in the opening of ion channels with rapid influx of extracellular calcium ions, formation of reactive oxygen species (ROS), activation of mitogen-activated protein kinase (MAPK) cascades, transcription of specific defense genes, cell wall thickening, and formation of antimicrobial metabolites called phytoalexins (Boller and Felix, 2009; Bigeard *et al*., 2015). In every case, the binding of PAMPs/MAMPs/DAMPS to PRRs triggers the induction of the primary, broad-range defense response of the plant, referred to as PAMP-triggered immunity or pattern-triggered immunity (PTI), which limits pathogen growth and halts colonization (Jones and Dangl, 2006; Bigeard *et al*., 2015).

Pathogens have developed counter strategies to overcome PTI, circumventing or suppressing this form of plant resistance. In phase 2, they deploy effector molecules into the host cells or the extracellular matrix that contribute to pathogen virulence and counteract the induction of PTI (Jones and Dangl, 2006). To perform this, bacteria transmit the effectors via the type III secretion system. Type III effectors promote bacterial multiplication by suppressing plant innate immunity and by interfering with cellular processes such as proteasome-dependent protein degradation, phytohormone signal conduction, inhibition of MAPK cascades, formation of cytoskeleton, vesicle transport, or gene expression (Büttner, 2016). The virulence of the pathogen depends on the recognition of these effectors by the plant. Successful recognition can lead to prevention of the pathogen spread. Conversely, if the plant is not able to recognize those effectors, effector-triggered susceptibility (ETS) develops (Chisholm *et al*., 2006).

Subsequently, in phase 3, plants have evolved to recognize the specific secreted pathogen effectors and to mount a robust and amplified defense response. This secondary defense line is referred to as effector-triggered immunity (ETI) and is mediated by resistance proteins. These resistance proteins either act directly on the pathogen effectors by recognizing and binding to them or indirectly by modifying the host target proteins upon recognition of specific pathogen effectors (Jones and Dangl, 2006; van der Hoom and Kamoun, 2008). In most cases, these proteins are localized intracellularly and consist of a nucleotide binding (NB) domain and leucine-rich repeat (LRR) motifs (Lukasik and Takken, 2009). ETI leads to an accelerated and intensified PTI that results in HR, a form of PCD, at the site of infection (Jones and Dangl, 2006). Colonization by plant-specific biotrophic and hemibiotrophic pathogens, which require living host cells to survive and complete their life cycle, is stopped by ETI. However, ETI as mechanism of resistance, is not capable of impeding plant colonization by necrotrophic pathogens, which kill host tissues as they colonize and thrive on the contents of dead or dying cells (Glazebrook, 2005).

Last, evolution has showed that ETI can be counteracted and suppressed by pathogens. In phase 4, pathogens are able to avoid ETI by employing a new variety of effectors by expression of novel genes. In turn, novel NB-LRR resistance proteins can be generated in the plant to recognize the newly acquired effectors, triggering once again the activation of the ETI. The zigzag model described here represents in a simple way the co-evolution of pathogens and plants and the repertoire of effectors and resistance proteins that will ultimately define an outcome (Jones and Dangl, 2006; Bigeard *et al*., 2015).

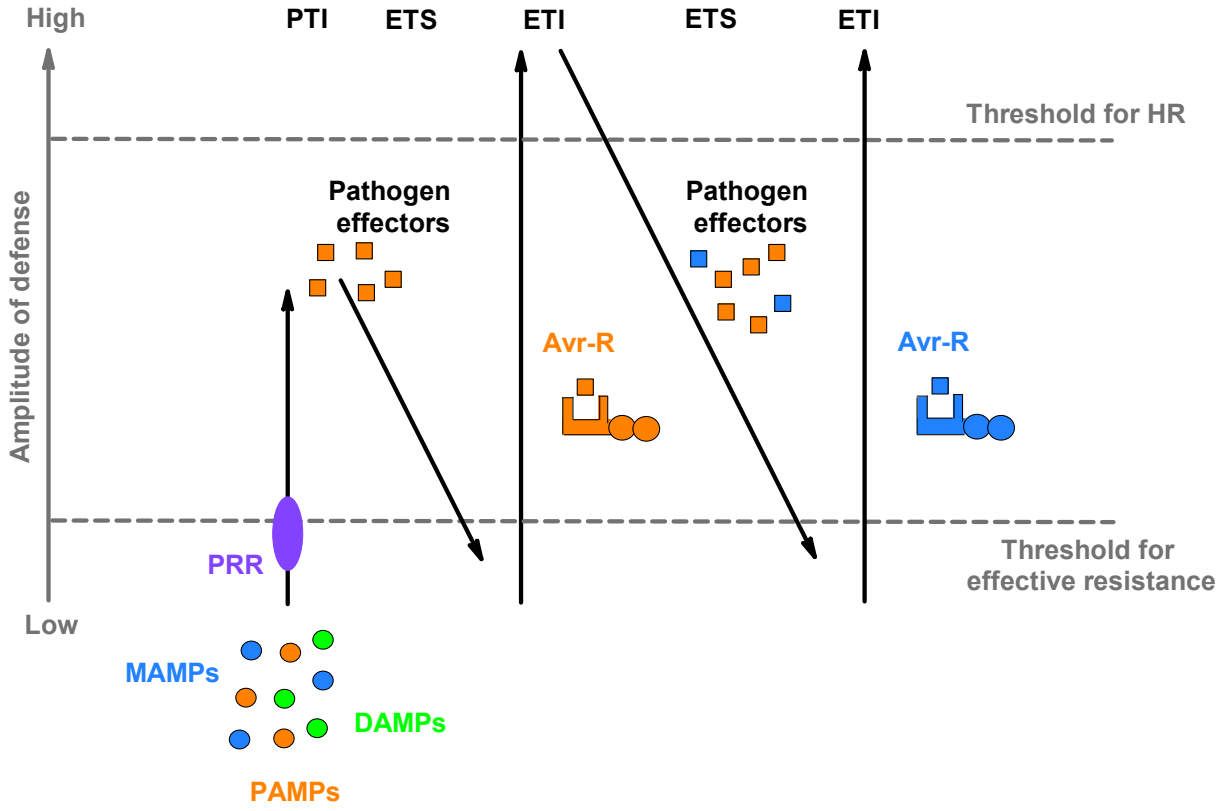

Figure 1. Zigzag model of plant immune system. In phase 1, microbe/pathogen/damaged-associated molecular patterns (MAMPs/PAMPs/DAMPs shown in blue, orange, and green dots, respectively) are detected by the plant via PRR and induce PTI. In phase 2, pathogens display effectors (shown as orange squares) that interfere with PTI, resulting in ETS and allowing them to feed from plant nutrients. In phase 3, specific effectors (shown as orange squares) are recognized by NB-LRR proteins, enhancing ETI and intensifying PTI, which results in HR. In phase 4, ETI can be counteracted or suppressed by new effectors (shown as blue squares) through expression of novel genes. New plant NB-LRR can be then generated to recognize the newly acquired effectors, triggering once again the activation of ETI. Figure adapted from Chisholm *et al*., (2006); Jones and Dangl (2006).

1.1.2. Hypersensitive Response.

The morphological characteristics of the HR as a special modality of PCD have been previously described. However, the features observed with effector-dependent immunity associated with PTI overlap with those that can be observed with the molecular mechanisms of the HR, acting in many ways as an accelerated and intensified immunity (Jones and Dangl, 2006; Coll *et al*., 2011). The transcription of resistance genes and the activation of MAPK cascades initiated by the HR lead to an increase in calcium ions in the cytoplasm that affect the production of ROS, nitric oxide, salicylic acid, and sphingolipids (SPLs; Mur *et al*., 2008; Ogasawara *et al*., 2008; Thuleau *et al*., 2013). Biological processes such as growth, development, and responses to biotic and abiotic stresses are regulated by ROS, which play an integral role as signaling molecules.

As signaling function and in regulatory mechanisms, the sudden increase in ROS, also called oxidative burst, is the best way to detect HR experimentally (e.g., hydrogen peroxide, hydroxyl radical, hyperoxide anion, singlet oxygen). The production of a ROS oxidative burst by peroxidases and NADPH oxidases in the plasma membrane, in the chloroplasts and/or mitochondria occurs in numerous cell pathways, including photosynthesis and respiration via the electron transport chain (Baxter *et al.*, 2014). Moreover, some other oxidases, such as glycolate oxidase and amine oxidase, as well as other mechanisms, such as FA oxidation, have been shown to be involved (Mittler, 2002). As a result, lipid peroxidation could trigger cell death within the plant (Mur *et al*., 2008).

Despite many studies on the regulation of HR and PCD, the accurate mechanism and molecules involved in triggering cell death remains to be further established in plants. Nevertheless, sphingolipids have been suggested to play an important role in the regulation of PCD by acting as second messengers in signal transduction in plant cells (Shi *et al*., 2007; Peer *et al*., 2011). These molecules, which are described and discussed in detail in the sections below, are the focus of this thesis.

1.2. Sphingolipids in plants.

Sphingolipids are a class of complex lipids derived from the different sphingobases existing. They constitute essential components of the plasma membrane of the cells and play a role in signaling. SPLs are produced ubiquitously in eukaryotes as well as in a few prokaryotes. In the latter, their production is restricted to a small subset of bacterial phyla, mainly bacteria belonging to the Bacteroidetes phylum (Heaver *et al*., 2018). There are about 500 different species of SPLs described in animals and 168 different species described in the model plant *Arabidopsis* (Futerman and Hannun, 2004; Markham and Jaworski, 2007) but, in general, their metabolism is broadly conserved in animals, yeast, and plants.

1.2.1. Structure and nomenclature.

Despite their high level of complexity and structural diversity, all SPLs are composed of two moieties: a *N*-acylated fatty acid (FA) condensed with a sphingosine backbone called long-chain base (LCB). These two elements together are known as ceramide, which composes the basic unit of SPLs. In addition to this basic structure, polar head groups of different nature can be linked to the ceramide resulting in more complex SPLs (Gault *et al*., 2010; Pata *et al*., 2010). The extremely high structural diversity of SPLs depends on several parameters: the type of headgroup, the length, the saturation, and the hydroxylation of the FA, as well as the length and configurational isomerism of the sphingoid LCB. In plants, LCBs are typically composed of 18 carbon atoms and can contain double bonds at the Δ4 or Δ8 positions. The Δ4 double bond is found only in the *trans* configuration, while the Δ8 double bond can be found in either the *trans* or *cis* configurations (**Figure 2**). Altogether, these variations generate a great array of sphingolipid isoforms, known as sphingolipidome (Spassieva and Hille, 2003; Merrill *et al*., 2009).

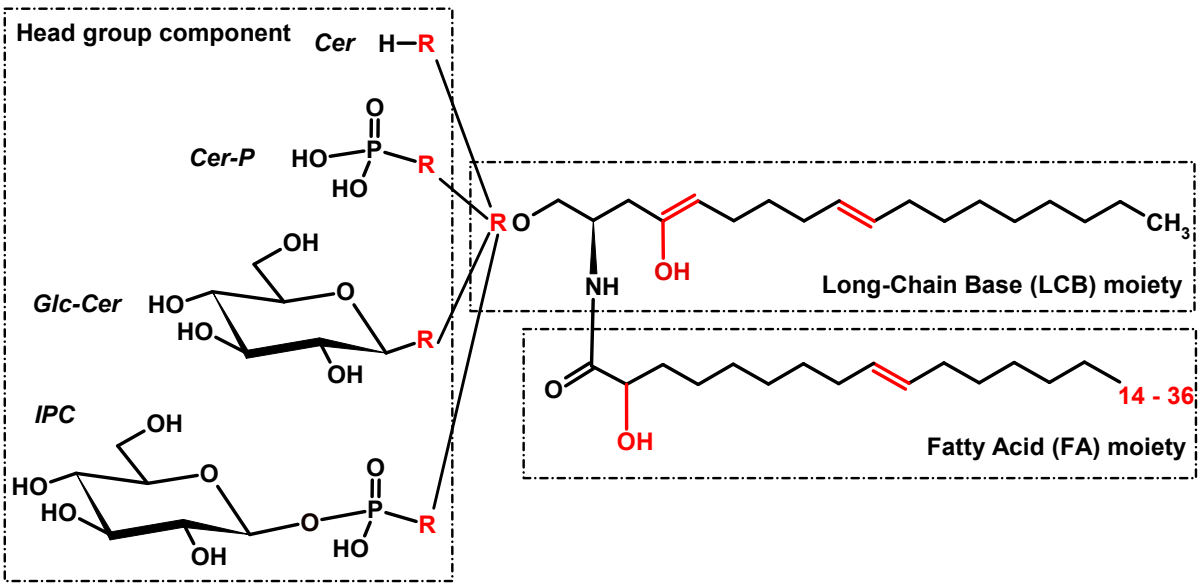

Figure 2. Basic structure and structural diversity of sphingolipids. Complex sphingolipids are composed of a sphingobase (LCB), a fatty acid (FA), and a head group. The four main classes of sphingolipids in plants are shown: free sphingobases (LCB/LCB-P), ceramides (Cer/Cer-P), glycosyl-ceramides (Glc-Cer), and glycosyl inositol phosphate ceramides (GIPC). The structural diversity that results from modification of the LCB or FA moieties or from a different glycosylation of the head group are highlighted in red. The fatty acid structure is variable in length (between 14 to 36 carbons), degree of saturation, and hydroxylation. LCBs with 18 carbon atoms can be hydroxylated or unsaturated and have a double bond at the C4 or C8 positions with configurational (*E*) or (*Z*) isomerism; here, (*E*) arrangement is shown. Figure adapted from Pata *et al*., (2010); Berkey *et al*., (2012).

In animals, the most common LCB is 4-sphingenine, known as sphingosine, which has a double bond at the C4 position. This LCB was the first to be isolated (Spiegel and Milstien, 2003). In plants and fungi, the free sphingobase phytosphinganine (4-hydroxysphinganine), which presents a hydroxy

group at the C4 position, is predominant (Markham and Jaworski, 2007; Shi *et al*., 2007). The name of sphingobases can be described with a short-hand nomenclature to facilitate their differentiation and simplify their names (Chen *et al*., 2010; Merrill, 2011). For example, the dihydrosphingosine (or sphinganine) with 18 carbons and 1 double bond is referred to as d18:1. The trihydroxisphingosine (or phytosphingosine) with 18 carbons and 0 double bond is referred to as t18:0. In addition, modifications at different positions can also be precisely indicated. For example, modifications at the C4 or C8 positions of the sphingosine d18:1 can be indicated as d18:1$^{\Delta 4E}$ or d18:1$^{\Delta 8E}$, respectively.
Ceramides can also be described using a short-hand nomenclature by specifying the LCB-FA with the chain length and the number of double bonds for each. As an example, the N-palmitoyl-D-*erythro*-sphinganine is written as d18:0-16:0, which specifies that the molecule contains a saturated 18-carbon sphingoid base with an attached saturated hexadecanoyl fatty acid side chain. The diversity of SPLs increases with the variety of head groups that can be linked to the C1-hydroxy group. For instance, both free sphingobases and ceramides can be phosphorylated at this position to obtain a long-chain base phosphate (LCB-P) or a ceramide phosphate (Cer-P). Other modifications of the head group at the C1 position in ceramides are possible, including glycosylation with mostly glucose or mannose (glycosyl-ceramide, Glc-Cer) or the addition of glycosyl inositol phosphate (glycosyl inositol phosphate ceramide, GIPC; Lynch and Dunn, 2004; Pata *et al*., 2010; Michaelson *et al*., 2016). GIPCs are exclusively produced in plants and fungi whereas other complex sphingolipids have been observed in animals, such as sphingomyelin (Pata *et al*., 2010; Merrill, 2011).
Combinations of different LCBs, FAs / very-long-chain fatty acids (VLCFAs), and attachment of different head groups create a great variety of SPLs within the organisms. The sphingolipid species can also vary widely between the individual plant phylogenetic groups, especially regarding the sphingobase component (Pata *et al*., 2010; Islam *et al*., 2012). In plant cells, GIPCs and Glc-Cers are present at much higher concentrations (at least ten times) compared to free LCBs and ceramides (Markham *et al*., 2006; Markham and Jaworski, 2007) and represent most of the different sphingolipid species.

1.2.2. Sphingolipid biosynthesis and metabolism.

Despite the diversity in structure and function of sphingolipids, their production and degradation are governed by common synthetic and catabolic pathways. The main steps in the biosynthesis and metabolism of sphingobases are largely preserved in animals, yeast, and plants (Merrill, 2011; Hannun and Obeid, 2018). Therefore, many insights from the basic research on SPL metabolism from animals and yeast can be transferred to plants (Dickson, 1998; Dunn *et al*., 2004; Michaelson *et al*., 2016). The creation of the various sphingolipid classes and their further alterations depend on a great number of different enzymes. In the case of *Arabidopsis thaliana,* many of these enzymes have already been characterized (Berkey *et al*., 2012; Michaelson *et al*., 2016; **Figure 3**). SPLs can be formed via two major pathways: the salvage pathway, in which ceramides and LCBs as products of SPL catabolism are reused within the synthetic pathway, and the *de novo* biosynthesis pathway (Kitatani *et al*., 2008; Pata *et al*., 2010; Merrill, 2011). The first steps of the *de novo* biosynthesis of SPLs, from the creation of the first LCB to the creation of the basic ceramide, occur in the endoplasmic reticulum (ER). Subsequently, ceramides are transported to the Golgi apparatus and undergo further modifications to become more complex ceramides. In the following subsections, the individual steps of SPL biosynthesis and metabolism will be described (**Figure 3**).

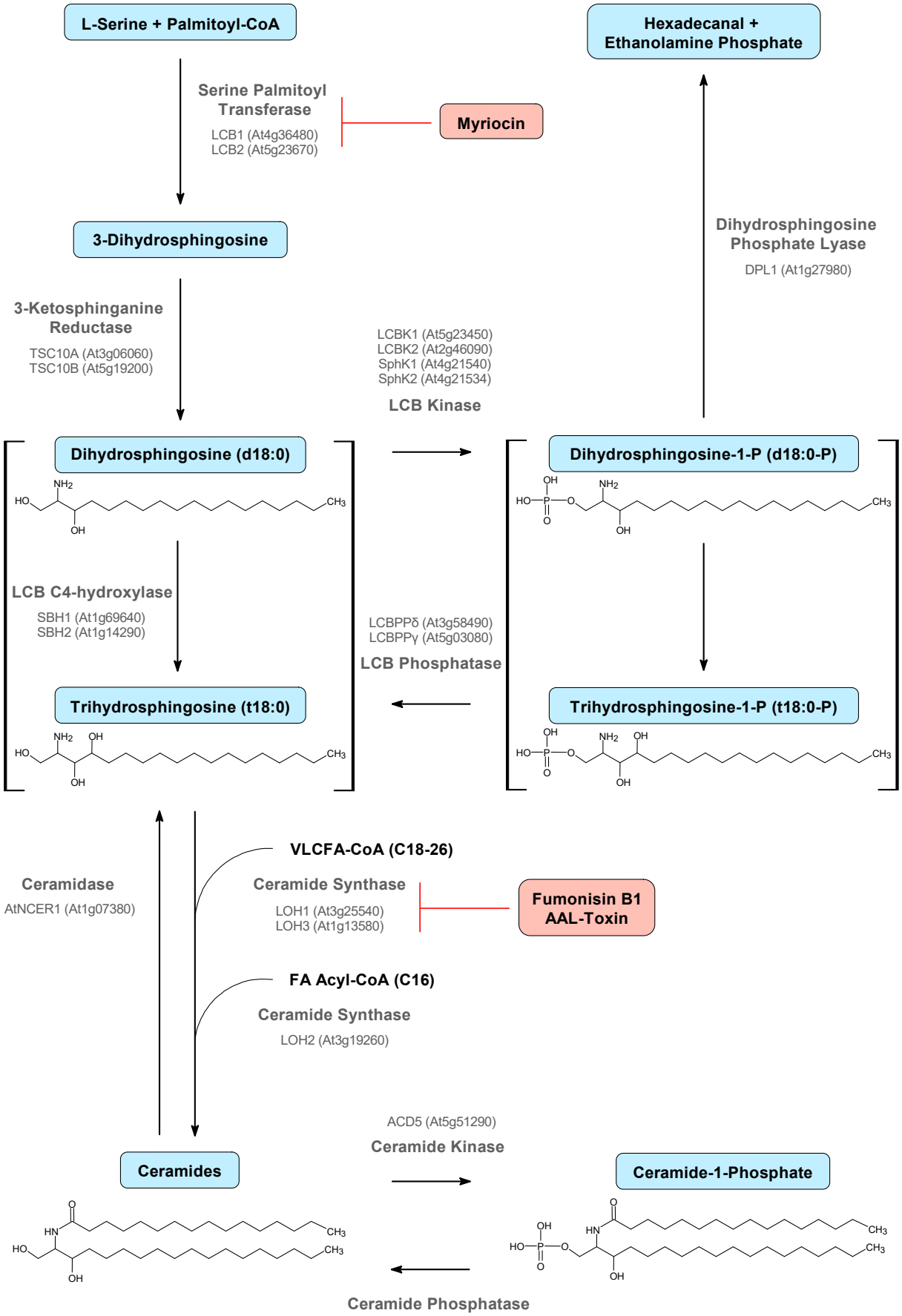
L-Serine + Palmitoyl-CoA
Serine Palmitoyl Transferase
LCB1 (At4g36480)
LCB2 (At5g23670)
Myriocin
3-Dihydrosphingosine
3-Ketosphinganine Reductase
TSC10A (At3g06060)
TSC10B (At5g19200)
Dihydrosphingosine (d18:0)
LCB C4-hydroxylase
SBH1 (At1g69640)
SBH2 (At1g14290)
Trihydrosphingosine (t18:0)
LCBK1 (At5g23450)
LCBK2 (At2g46090)
SphK1 (At4g21540)
SphK2 (At4g21534)
LCB Kinase
Dihydrosphingosine-1-P (d18:0-P)
LCBPPδ (At3g58490)
LCBPPγ (At5g03080)
LCB Phosphatase
Trihydrosphingosine-1-P (t18:0-P)
Hexadecanal + Ethanolamine Phosphate
Dihydrosphingosine Phosphate Lyase
DPL1 (At1g27980)
Ceramidase
AtNCER1 (At1g07380)
VLCFA-CoA (C18-26)
Ceramide Synthase
LOH1 (At3g25540)
LOH3 (At1g13580)
Fumonisin B1
AAL-Toxin
FA Acyl-CoA (C16)
Ceramide Synthase
LOH2 (At3g19260)
Ceramides
ACD5 (At5g51290)
Ceramide Kinase
Ceramide-1-Phosphate
Ceramide Phosphatase

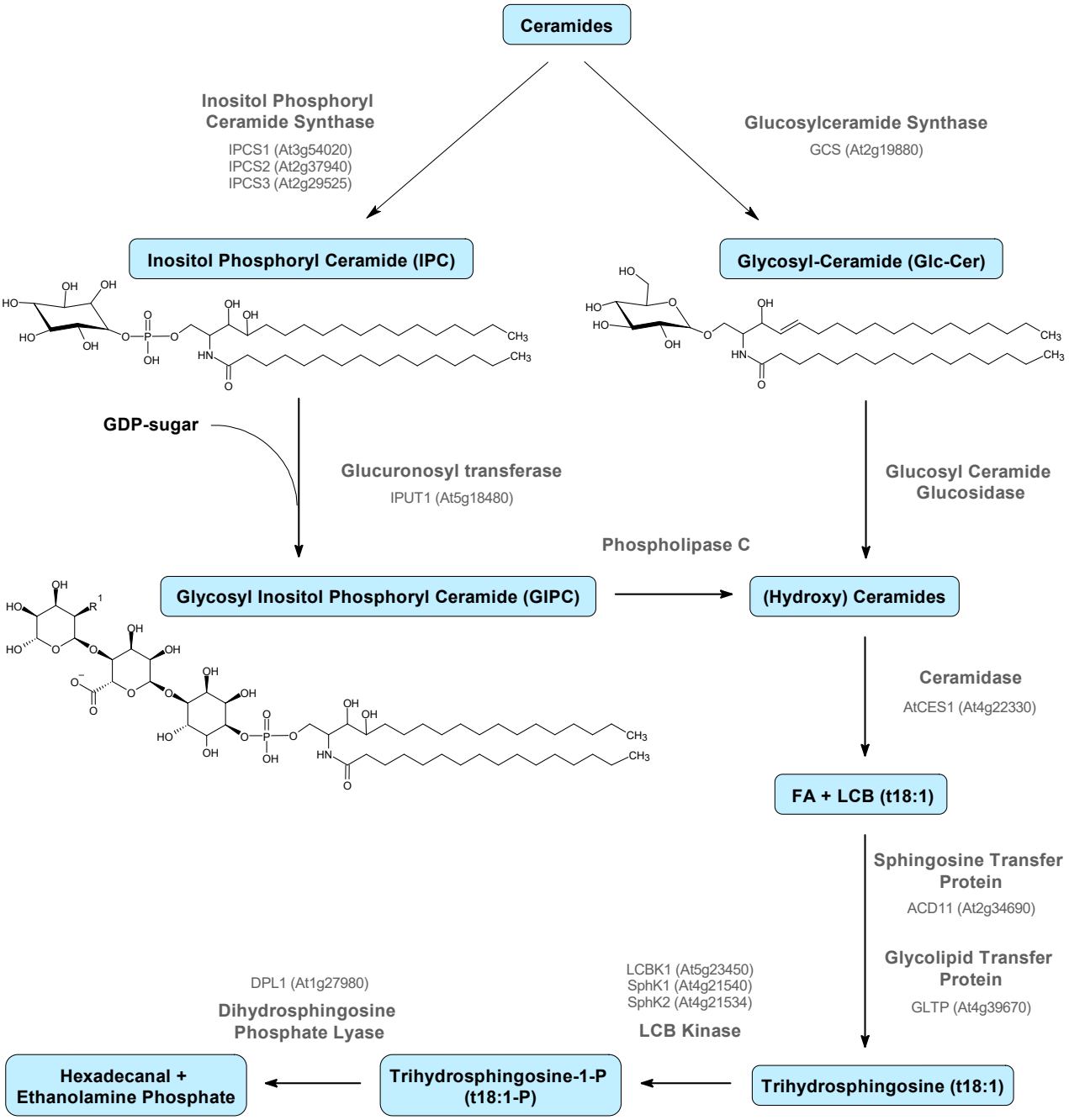

Figure 3: Main steps of sphingolipid metabolism in plants. *De novo* biosynthesis of free sphingobases (LCBs) occurs in the ER and starts with the condensation of serine and palmitoyl-CoA to create 3-dihydrosphinganine and, after reduction, dihydrosphingosine (d18:0). LCBs can be either reversibly phosphorylated at the C1 position (LCB-Ps) and be cleaved into hexadecanal and ethanolamine phosphate in the degradation pathway or be converted into ceramides by N-acylation with a fatty acid (FA/VLCFA). Modification of ceramides takes place in the Golgi apparatus and occurs at the C1 head group to be metabolized into Glc-Cers, IPCs, or GIPCs. (Hydroxy)ceramides can be hydrolyzed into FA and LCB by ceramidases. LCBs are transferred back to the ER and can either enter the degradation process or be reused. The main molecules of the pathway are shown in light blue boxes. The names of the enzymes that catalyze the different reactions are written in bold grey. Genes genetically characterized from *A. thaliana* coding these enzymes are written in grey. Mycotoxins affecting the sphingolipid metabolism pathway are indicated in red boxes. Figure adapted from Pata *et al*., (2010); Berkey *et al*., (2012); Michaelson *et al*., (2016).

1.2.2.1. LCB synthesis and metabolism.

The first step in the biosynthesis of SPLs is the generation of the basic LCB sphingobase 3-dihydrosphingosine (3-ketosphinganine) by condensation of L-serine and palmitoyl-CoA. The 3-ketosphinganine is defined as the first LCB in the SPL metabolism pathway (Tafesse and Holthuis, 2010; Merrill, 2011). This first reaction is catalyzed by the enzyme serine palmitoyltransferase (SPT) and is the rate-limiting step and control point in SPL biosynthesis and homeostasis (Hanada, 2003). SPT is a heterodimer composed of LCB1 and LCB2 subunits, which together form the active site of this enzyme. The importance of SPT as an essential enzyme and, therefore, also the importance of SPLs for cell viability, was demonstrated by employing knockout and knockdown mutants of the genes encoding the subunits LCB1 and LCB2, which resulted in lethality in both animals and plants. In the case of *Arabidopsis*, these SPT mutants resulted in the death of the embryo and male gametophyte (Chen *et al*., 2006; Dietrich *et al*., 2008; Teng *et al*., 2008; Kimberlin *et al*., 2013). The orosomucoid (ORM) proteins, which are conserved in animals, yeast, and plants, regulate sphingolipids levels by binding to the SPT subunits and acting as negative regulators of their activity (Kimberlin *et al*., 2016).

In the second step of LCB synthesis, the enzyme 3-ketosphinganine reductase catalyzes the conversion of 3-ketosphinganine to dihydrosphingosine, the simplest LCB found in plants. Further modifications of LCBs occur on dihydrosphingosine via hydroxylation or desaturation. On one hand, total extracts of LCBs from *Arabidopsis* revealed that the majority of LCBs were di- and tri-hydroxylated (d18 and t18, respectively). Dihydroxy LCBs have two hydroxy groups at the C1 and C3 carbons (dihydrosphingosine). Trihydroxy LCBs, which are more predominant in plants, have an additional third hydroxy group at the C4 carbon, leading to trihydrosphingosine (phytosphingosine). This third additional hydroxy group is introduced by a LCB C4 hydroxylase. The two genes that encode this enzyme in *Arabidopsis* are designated *Sphingoid Base Hydroxylase 1* and *2* (*SBH1* and *SBH2,* respectively). Double *sbh1*/*sbh2* mutants displayed a lack in trihydroxy LCBs and resulted in significant defects in plant growth, demonstrating the importance of the C4-hydroxylase and the third hydroxyl group. Also, dwarfed plants were unable to progress from vegetative to reproduction growth and the expression of cell death-associated genes was enhanced (Chen *et al*., 2008). Interestingly, it has been observed that dihydroxy LCBs are preferentially incorporated into shorter fatty acyl chain SPLs (mostly generating LCFA-SPLs), while trihydroxy LCBs are preferentially incorporated into larger fatty acyl chain SPLs (mostly generating VLCFA-SPLs). As example, trihydroxy LCB null showed a differential ceramide composition in plants, exhibiting a higher content of short chain fatty acid C_{16}-SPL in comparison to wild-type plants, which accumulated more VLCFA-SPL (Chen *et al*., 2008). Therefore, the hydroxylation level of LCBs is crucial in SPL biosynthesis. On the other hand, LCBs may also be unsaturated by the action of desaturases. The LCB Δ8 desaturase can introduce a *cis* or *trans* double bond between the C8 and C9 carbons (Δ8 position) of dihydroxy or trihydroxy LCBs (Sperling *et al*., 2001; Michaelson *et al*., 2009, Pata *et al*., 2010; Peer *et al*., 2010; Michaelson *et al*., 2016). Two homologs, SLD1 (*At3g61580*) and SLD2 (*At2g46210*), were identified in *Arabidopsis* and confirmed to be Δ8 desaturases through yeast and *in planta* studies (Sperling *et al*. 1998; Chen *et al*. 2012). The LCB Δ4 desaturase can introduce a *trans* double bond between the C4 and C5 carbons (Δ4 position) of dihydroxy LCBs, leading to sphingosine. LCB Δ4 unsaturation occurs almost entirely in combination with LCB Δ8 unsaturation in dihydroxy LCBs. The resulting LCBs (d18:2) are mostly found in Glc-Cer and absent from GIPCs (Sperling *et al*. 2005; Markham *et al*. 2006; Markham and Jaworski 2007). *Arabidopsis* contains one Δ4 desaturase gene (*At4g04930*) that encodes a LCB Δ4 desaturase. In contrast to the LCB Δ8 desaturase, it introduces double bonds

exclusively in the *trans* configuration. Given that both LCB C4 hydroxylases and LCB Δ4 desaturase can use d18:0 as substrates, C4 hydroxylation precludes Δ4 desaturation, and conversely, Δ4 desaturation prevents C4 hydroxylation.

Additionally, the LCB moiety can be phosphorylated by LCB kinases (LCBKs) at the C1 hydroxy group to form LCB-Phosphates (LCB-P). Four LCB kinases have been identified in *A. thaliana* and are named after their homologs in animals: LCBK1, LCBK2 (LCB kinase 1 and 2, respectively), SPHK1, and SPHK2 (sphingosine kinase 1 and 2, respectively). Putative *Arabidopsis* SPHK and AtLCBK1 show partial amino acid sequences alignment within the five characteristic conserved domains of sphingosine kinases (Worrall *et al*., 2008). *SPHK2* is also a directly adjacent gene of *SPHK1* with a high sequence similarity. Phosphorylation of the sphingobases d18:0 and t18:0 occurs *in vitro* by the enzymes LCBK1, SPHK1, and SPHK2 (Coursol *et al*., 2003, 2005; Imai and Nishiura, 2005; Guo *et al*., 2011; Dutilleul *et al*., 2012). These enzymes are expressed differentially in the different tissues of plants (Worrall *et al*., 2008; Guo *et al*., 2011; Qin *et al*., 2017). It has been shown that the phosphorylated molecules sphingosine-1-P and phytosphingosine-1-P are lipid messenger molecules involved in abscisic acid (ABA) regulation of guard cell turgor (Ng *et al*. 2001, Coursol *et al*. 2003, 2005). The enzyme SPHK is activated by ABA in *A. thaliana* and is involved in both ABA inhibition of stomatal opening and promotion of stomatal closure. The stomata of a knockdown mutant of SPHK1 (SPHK1-KD) were less sensitive to ABA than the wild-type plants, while mutants overexpressing SPHK1 exhibited increased sensitivity and promoted light-induced stomatal opening (Coursol *et al*., 2003, 2005; Worrall *et al*., 2008). Similar findings have been reported regarding the other kinase AtLCBK2. Cold temperature exposure triggered a rapid and transient production of phytosphingosine-1-P, which required the presence of the putative LCBK2 but not the two other LCB kinase isoforms, SPHK1 and LCBK1. This transient cold-induced phytosphingosine-phosphate synthesis was reduced by addition of LCB kinase inhibitors and completely abolished in a knockout mutant of *LCBK2* (*lcbk2*). Moreover, the *lcbk2* knockout mutant exhibited an abnormal regulation of the cold-responsive mitogen-activated protein kinase 6 (AtMPK6) which allowed the plants to grow at 22°C or 4°C with no phenotypical distinction (Dutilleul *et al*., 2012).

The LCB-Ps synthesized by LCBKs can either be dephosphorylated by an LCB-P phosphatase to LCBs or be degraded by LCB-P lyase to C16 fatty aldehydes and ethanolamine phosphate. On the basis of sequence homology with a LCB-P phosphatase from yeast, the gene coding for a LCB-P phosphatase in *A. thaliana*, designated as sphingoid phosphate phosphatase 1 (AtSPP1), was identified and characterized by Nakagawa and colleagues. Loss-of-function mutants of SPP1 presented increased levels of dihydrosphingosine-1-phosphate in comparison to wild-type plants, suggesting a role of SPP1 in the regulation of LCB-P levels. In addition, stomata of these mutants also showed higher sensitivity to ABA, suggesting a role of SPP1 in stomatal responses through LCB-P-mediated ABA signaling (Nakagawa *et al*., 2012). There has been a sole LCB-P lyase, known as dihydrosphingosine-1-phosphate lyase (AtDPL1), identified and characterized in *A. thaliana* (Tsegaye *et al*. 2007; Nishikawa *et al*. 2008). Two independent mutants, *dpl1.1* and *dpl1.2*, which present T-DNA insertions in the At*DPL1* gene, have been characterized, presenting indistinguishable phenotypes from that of wild-type plants under normal growth conditions. However, the rates of decrease of the fresh weight of these mutant plants were significantly slower than those of the wild-type plants, suggesting that At*DPL1* expression influences transpiration rates in stomata and a role in dehydration stress (Tsegaye *et al*., 2007; Nishikawa *et al*., 2008; Nakagawa *et al*., 2012; Magnin-Robert *et al*., 2015). The knockout mutant of *DPL1* has also been shown to be more resistant to the necrotrophic fungus *Botrytis cinerea* but more sensitive to the hemibiotrophic bacterium *P. syringae* (Magnin-Robert *et al*., 2015).

Accordingly, a mutant with a combined knockdown of *SPP1* / *DPL1* also exhibited compromised stomatal responses to ABA (Worrall *et al*., 2008).

1.2.2.2. Ceramide synthesis and metabolism.

Ceramides can be formed via two different pathways: FA-CoA-dependent and free FA-dependent pathways. In plants, the FA-CoA-dependent pathway is the major route through which ceramides are synthesized. The formation of the ceramide core, which comprises the LCB and the FA moieties, occurs via the condensation of a FA with the amino group of the LCB dihydrosphingosine (**Figure 3**). This reaction is catalyzed by ceramide synthases (Sperling and Heinz, 2003; Lynch and Dunn, 2004; Pata *et al*., 2010) and is FA-CoA-dependent. Ceramides can be modified on the sphingobase moiety in the same way as it has been previously described for free LCBs. In addition, modifications on the FA moiety have also been observed, such as α-hydroxylation resulting in the creation of hydroxy-ceramide (**Figure 3**). The members of the gene family *LAG1* (Longevity Assurance Gene 1) encode ceramide synthases and are present in all eukaryotes studied, from fungi to plants and animals (Winter and Ponting, 2002). In *Arabidopsis*, the incorporation of FAs into SPLs is catalyzed by three ceramide synthases known as LOH1, LOH2, and LOH3 (LAG Homolog 1, 2, and 3), which are homologs to the ceramide synthase LAG1 (Markham *et al*., 2011). These enzymes present distinct substrate specificities: LOH1 and LOH3 use VLCFA (C_{20}-C_{26}) and trihydroxy LCB substrates for the formation of ceramides, whereas LOH2 uses C_{16}-FAs and dihydroxy LCB (Luttgeharm *et al*., 2015). Accordingly, the knockout double mutant *loh1 / loh3* is lethal due to a severe lack of VLCFA-derived ceramides and the accumulation of free LCBs (d18:0 and t18:0) (Markham *et al*., 2011). Single knockout mutant *loh1* plants were phenotypically small with spontaneous cell death and enhanced expression of the pathogenesis-related gene *PR-1* under short-day conditions (Ternes *et al*., 2011). Such spontaneous cell death may be triggered either by the accumulation of free trihydroxy sphingoid bases or ceramide species with C_{16}-FA (Ternes *et al*., 2011). Overexpression of *LOH1* and *LOH3* showed biomass increase in comparison to wild-type plants, which exhibited higher cell division rate promoted by a greater synthesis of VLCFAs and t18:0 LCB ceramides. LOH2 overexpression resulted in phenotypically dwarf plants that accumulated SPLs with C_{16}-FAs and dihydroxy LCB ceramides, promoters of the induction of PCD (Luttgeharm *et al*., 2015).

Inhibitors of SPL metabolism known as mycotoxins have attracted worldwide attention because they are important contaminants with numerous effects on human and animal health that cause significant agroeconomic problems. Mycotoxins such as the AAL toxins produced by *Alternaria alternate f. sp. lycopersici* and the Fumonisin B_1 (FB_1) toxin produced by *Fusarium moniliforme* are structurally related and are known to inhibit the activity of ceramide synthases (Mirocha *et al*., 1992; Pruett *et al*., 2008; Peer *et al*., 2010). In fact, the effects observed in ceramide synthases knockout mutants on ceramide and sphingobase contents can be mimicked by treatment with the fungal toxin FB_1, which inhibits the activity of ceramide synthases by disrupting ethylene signaling, perturbing SPL homeostasis and thus inducing cell death (Luttgeharm *et al*., 2015; Wu *et al*., 2015). FB_1 is the most abundant mycotoxin and is classified as a human carcinogen due to its neurotoxic, hepatotoxic, and nephrotoxic effects that cause oxidative stress, apoptosis and cytotoxicity at the cellular level (Stockmann-Juvala *et al*., 2008). FB_1 presents a similar basic structure to sphingobases, but the presence of an additional hydroxy group and tricarballylic acid allows it to interact with the binding sites of FA-CoA for sphinganine. This leads to the inhibition of ceramide synthase activity and, thus, to a strong accumulation of free LCBs and their metabolites (Merrill *et al*., 2001). In plants, FB_1 triggers apoptosis-like PCD with similarities to the hypersensitive response. This response is

associated with the modified expression of pathogen-associated defense genes and requires jasmonate-, ethylene- and salicylate-dependent signaling pathways (Asai *et al*., 2000). Treatment with FB_1 leads to an increase in free LCBs and ceramides with short chain fatty acids (C_{16}), while the levels of ceramides with VLCFAs (C_{24}-C_{26}) are completely devoid (Abbas *et al*., 1994; Shi *et al*., 2007; Markham *et al*., 2011). In *Arabidopsis*, double knockout mutant *loh1 / loh3* leads to an almost complete absence of VLCFA sphingolipids, demonstrating the specificity of LOH1 and LOH3 for VLCFA, while LOH2 is specific for C_{16}-FA (Markham *et al*., 2011). Due to distinct substrate specificities and affinities to FB_1 and their preference for unsaturated LCB substrates, LOH2 and LOH3 overexpression led to an increased resistance to FB_1. In contrast, overexpression of LOH1 showed no difference in comparison to wild-type plants, indicating that FB_1 is a stronger inhibitor of this ceramide synthase (Luttgeharm *et al*., 2015). There have been other toxins described, such as myriocin, which acts as an inhibitor of serine palmitoyltransferase at the very first step of the SPL synthesis pathway (Wadsworth *et al*., 2013).

As it occurs for LCBs, ceramides can also be phosphorylated at the C1 position (**Figure 3**). In *Arabidopsis*, a mutant of the proposed ceramide kinase (CERK; *At5g51290*), encoded by accelerated cell death 5 (acd5), accumulates more ceramides and ceramide substrates and displays spontaneous PCD in late developmental stages. Moreover, in comparison to wild-type plants, *acd5* knockout mutant plants show more susceptibility to *P. syringae* and *B. cinerea* but more resistance to powdery mildew (*Golovinomyces cichoracearum*) (Greenberg *et al*., 2000; Liang *et al*., 2003; Wang *et al*., 2008; Bi *et al*., 2014). In addition, this *acd5* mutant line, which has a reduced rate of seed germination, is hypersensitive to cold temperature and ABA. After germination at low temperature, ABA-dependent gene expression was modified in *acd5* mutant seeds (Dutilleul *et al*., 2015). Currently, the reverse reaction corresponding to the dephosphorylation of the ceramide-1-phospate remains largely uncharacterized and no ceramide phosphatases have been described in plants so far. Nevertheless, it has been shown that ceramides and protein phosphatases 1 and 2A require a very particular structure to be able to interact between each other. This feature demonstrates a specific regulation between ceramides and ceramide-activated protein phosphatases (Chalfant *et al*., 2004).

Ceramidases are enzymes that break down ceramides by hydrolyzing their N-acyl linkage, resulting into sphingosine and fatty acids. Several ceramidases have been identified, which show differences in their subcellular localization, substrate specificities, and their optimal pH preferences. Based on the latter, ceramidases can be divided into three classes: acid, neutral, and alkaline ceramidases (Mao and Obeid, 2008; Michaelson *et al*., 2016). In contrast to the situation in animals and yeast, much less is known about ceramidases in plants, for which so far only homologs of neutral and alkaline ceramidases have been identified, but not for acid ceramidases. The genome of *Arabidopsis* encodes three neutral ceramidases (NCER1, 2 and 3) and two alkaline ceramidases (ACER and *Arabidopsis* turgor regulation defect 1). However, their roles remain to be further characterized (Chen *et al*., 2015; Li *et al.*, 2015; Wu *et al*., 2015; Zheng *et al*., 2018). On one hand, a knockout and a knockdown mutant of *AtACER1* accumulate ceramides with a slight reduction of free LCBs, while *NCER1* mutants show only a significant accumulation of hydroxyceramides and a slight accumulation of free LCBs. These findings suggest that these enzymes exhibit different substrate specificities. Such knockout / knockdown mutants of *AtACER1* showed increased sensitivity to salt stress, FB_1 and *P. syringae*. In the case of *AtNCER1* mutants, an increased sensitivity to oxidative stress induced by methyl viologen treatment was observed. On the other hand, overexpression of *AtACER1* exhibited more resistance to salt, FB_1 and *P. syringae*, while overexpression of *AtNCER1* displayed more resistance to oxidative stress (Wu *et al.*, 2015; Li *et al*., 2015).

1.2.2.3. Synthesis of complex ceramides.

Ceramides can undergo further modifications and become more complex sphingolipids by linkage of a variety of sugar residues as head groups to their C1 position. These complex ceramides are known as glycosphingolipids. In contrast to the synthesis of ceramides, this process does not take place exclusively in the ER but also requires the transport of ceramides to the Golgi apparatus via the plant secretory pathway (Melser *et al*., 2010). There are two classes of glycosphingolipids in plants: Glc-Cers and GIPCs. GIPCs are primarily found in plants and fungi, while Glc-Cers are found in more eukaryotic organisms, including mammals, insects, plants, and fungi.

In Glc-Cers, the headgroup is a single hexose, either β-glucose or β-mannose. In addition to this head group, the FA moiety of plant Glc-Cers is usually α-hydroxylated (Lynch *et al*., 1992; Norberg *et al*., 1996; Sullards *et al*., 2000; Bohn *et al*., 2001). In many species, α-OH C16 is the predominant FA. The enzyme responsible for catalyzing the transfer of the hexose from guanosine diphosphate-hexose to the ceramide is known as glucosylceramide synthase (GCS). In *Arabidopsis*, GCS mutant lines lacking or deficient in Glc-Cers exhibited a dwarfed phenotype and were only viable in the early seedling stage, illustrating the importance of this type of sphingolipids in plant organ development and cell differentiation (Msanne *et al*., 2015).

In GIPCs, the headgroup is composed of phosphoinositol with up to seven hexoses or pentoses in *Arabidopsis* (Cacas *et al*. 2013). The initial step of GIPC synthesis is the formation of inositol phosphorylceramide (IPC), which requires the transfer of the phosphoinositol group from phosphatidylinositol to the ceramide. This reaction results in the release of diacylglycerol byproducts and is catalyzed by an IPC synthase (IPCS). So far, three inositol phosphorylceramide synthases (IPCS1/2/3) have been described in *Arabidopsis* (Mina *et al*., 2010) and they are able to employ both non-hydroxy and hydroxyceramides as substrates for IPC synthesis. In *Arabidopsis*, the loss of function of IPCS2 encoded by the gene *ERH1* (enhancing *resistance to powdery mildew 8* (*RPW8)*-mediated HR-like cell death) results in salicylic acid accumulation. This accumulation enhances the transcription of the resistance gene *RPW8*, which triggers the HR to restrict the spread of powdery mildew during plant infection (Wang *et al*., 2008). Accordingly, the knockout mutant *erh1* presents enhanced transcription of *RPW8*, *RPW8*-dependent spontaneous HR-like cell death in leaf tissues and accumulation of ceramides (Wang *et al*., 2008). Then, the following step of GIPC synthesis involves further glycosylation of the head group of IPC, which varies among plant species and tissues. In monocots, GIPCs containing three saccharides attached to the head group were mostly found, whereas in eudicots, GIPCs containing two saccharides were more predominant (Cacas *et al*., 2013). The conserved glucuronic acid (GlcA) is one of the glycan decorations that can be found among plant GIPCs. The inositol phosphorylceramide-glucuronosyl-transferase (IPUT1) has been described to be the enzyme that transfers GlcA to IPCs to obtain GIPCs. Overexpression of *IPUT1* results in accumulation of GIPCs in the plant, whereas homozygous knockout mutants do not transmit GIPCs through pollen despite normal pollen development. The knockdown of *IPUT1* also leads to an accumulation of IPCs, ceramides, and Glc-Cers (Rennie *et al*., 2014). This highlights the importance of this type of sphingolipids in plants. In fact, it has been shown that even the lack of a single GIPC type (as example here: glucuronosyl-IPC) already has a significant impact on the development of plants.

In addition to the enzymes described and listed here for the sphingolipid metabolism pathway in *A. thaliana* (**Figure 3**), enzymes characterized in other plants with homologous functionality exist (Berkey *et al*., 2012; Michaelson *et al*., 2016). As previously mentioned, ceramide and complex ceramide structures vary greatly due to the large component possibilities of the LCB and FA moieties,

the addition of head groups, and the presence of different sets of enzymes within individual species. The biosynthesis described in this thesis offers an overview of sphingolipid metabolism in *A. thaliana*.

1.2.3. Sphingolipids functions.

The role of sphingolipids in plants has been overlooked for a long time. However, they are now recognized as abundant and essential components of the plasma membrane and other endomembranes of plant cells, including ER, Golgi, or the tonoplast (Mongrand *et al*. 2004; Sperling *et al*. 2005; Bayer *et al*. 2014). From the great structural diversity of the individual sphingolipid classes emerge plenty of different functions within plants. Some of these functions can be inferred from the phenotype of mutants described in the previous section (Section 1.2.2.2. Ceramide synthesis and metabolism), from studies using heterologous expression of recombinant proteins (for example, in yeast), or from *in vitro* experiments employing sphingolipids. Regarding the total content of sphingolipid classes in plants, there is a large difference of ratio between complex ceramides (Glc-Cers and GIPCs) and simple ceramides/LCBs. Complex SPLs are abundant and represent a substantial fraction of total sphingolipids, being around ten times more abundant than ceramides and LCBs. They are considered to act as building blocks and signaling molecules. Simple ceramides or LCBs are rather intermediate and are generally defined as structural elements of the plant cell membrane. They play an important role determining the fate of cells (Markham *et al*., 2006; Markham and Jaworski, 2007).

1.2.3.1. Glycosyl-Ceramides (Glc-Cers).

Glc-Cers are important membrane lipids in eukaryotes. In plants, this lipid class is found in the plasma membrane, in the tonoplasts as well as in the vesicles and represents between 6 to 27 % of the total lipid content (Warnecke and Heinz, 2003). In these organisms, the hexoses attached to the head group at C1 of Glc-Cers are either β-glucose or β-mannose and the FA moiety is usually α-hydroxylated (Pata *et al*., 2010). Several functions for Glc-Cers have been described in plants such as membrane stability, membrane permeability, and pathogenesis (Spassieva and Hille, 2003; Warnecke and Heinz, 2003; Lynch and Dunn, 2004).
Numerous studies have shown that variations in Glc-Cers composition have an impact on membrane stability, thus on cold adaptation or frost tolerance. Glc-Cers containing α-OH monounsaturated VLCFAs have been shown to be increased during chilling/freezing tolerance experiments in chilling-resistant plants (Cahoon and Lynch, 1991). By contrast, Glc-Cers containing saturated α-OH FAs have been shown to be increased in chilling-sensitive plants (Imai *et al*., 1995). Other studies show that Glc-Cers are also involved in drought tolerance by increasing their concentration in drought-adapted crassulacean acid metabolism plants (Warnecke and Heinz, 2003) or by increasing their content at the plasma membrane of the resurrection plant *Ramonda serbica* under desiccated conditions in comparison to normal growth conditions (Quartacci *et al*., 2001). Finally, Glc-Cers have been shown to be involved in plasma membrane stability to reduce ion permeability, such as to aluminum (Al), which is highly phytotoxic for plant growth. In this case, a slight increase in Glc-Cers was observed in Al-resistant cultivar of wheat, whereas Glc-Cers content was reduced in Al-sensitive cultivar of wheat (Zhang *et al*., 2006). These comparative studies on membrane composition establish a relationship between the abundance of lipid species and the adaptation of plants to abiotic stress but do not show direct evidence of the function of Glc-Cers. In this respect, experiments that employed *Arabidopsis* lines deficient in Glc-Cers, either by knockout or by RNA interference (RNAi) of the GCS gene, indicated that this type of complex sphingolipids are essential for cell-type differentiation and

organogenesis but not for cell viability (Msanne *et al*., 2015). These mutants were viable and fertile with protein trafficking defects. Also in tobacco leaves, it has been observed that a decrease in Glc-Cers has an impact on the transport of soluble and membrane secretory proteins to the cell surface, which remain retained at the beginning of the plant secretory pathway, between the ER and the Golgi apparatus (Melser *et al*., 2010).

1.2.3.2. Glycosyl-Inositol-Phospho-Ceramides (GIPCs).

The sphingolipid class of GIPCs is exclusively synthesized in plants and fungi but not in animals. GIPCs are mainly built from t18:0 or t18:1 as an LCB linked to a VLCFA with up to 26 carbon atoms. In addition, various types of glycosylation can lead to differences within plant species. The number of saccharides linked to the IPCs can be large, with up to 19 in tobacco leaves and up to 20 in *Candida albicans* leaves (Trinel *et al*., 2002). In *A. thaliana*, the majority of GIPCs are composed of a hexose bound to the IPC via a hexuronic acid and up to 7 saccharides (Buré *et al*., 2011; Cacas *et al*., 2013). GIPCs are found to be particularly enriched in the plasma membrane of cells with the polar head group localized in the outer layer. They have been shown to offer resistance to detergents and to act as anchors of proteins into the lipid rafts (Borner *et al*., 2005; Pata *et al*., 2010). Moreover, in lipid rafts of two plasma membrane monolayers, VLCFAs which compose GIPCs might also contribute to the interaction with other lipids, such as sterols (Cacas *et al*., 2016). Moreover, in detergent-insoluble membrane “Bright Yellow 2” cell suspension of tobacco (*Nicotiana tabacum*), GIPCs have been found to be up to 40 % of the total lipids of the plasma membrane (Cacas *et al*., 2016). *Arabidopsis* mutants of GONST1 (Golgi-Localized Nucleotide Sugar Transporter 1), which are unable to provide sugar to the Golgi lumen for GIPCs synthesis, exhibit a dwarfed phenotype and a constitutive hypersensitive response associated with increased levels of salicylic acid (Mortimer *et al*., 2013). Together, observations derived from mutants of IPCS2 (reference to the previously described mutant named ERH1) and IPUT1 (Wang *et al*., 2008; Rennie *et al*., 2014) not only show a role of GIPCs as essential structural elements in development but also a potential role in plant PCD associated with defense or in plant pathogen defense (Michaelson *et al*., 2016).

1.2.3.3. Ceramides (Cers/Cers-P).

Ceramides with an unmodified head group constitute the basic framework on which more complex ceramides are built. This type of sphingolipids is found in lower concentrations in comparison to GIPCs. In *A. thaliana*, the most common LCB components found in ceramides are t18:0 and t18:1, while the fatty acid component is very variable (Markham *et al*., 2006; Markham and Jaworski, 2007). Assessing the function of ceramides is complex since their alteration commonly has an impact on the whole sphingolipid homeostasis. Changes in the levels of ceramides directly interfere with the function of other sphingolipid classes, such as free LCBs. This can be particularly observed in the phenotypes of mutants of the ceramide synthases LOH1/2/3 and ceramidases ACER and NCER1 (Section 1.2.2.2. Ceramide synthesis and metabolism). Several studies have shown that ceramides may play a role in the response to salt and oxidative stress. In fact, the level of ceramides and hydroxyceramides as well as the level of free sphingobases, although to a lesser extent, are altered in response to those stresses (Li *et al*., 2015; Wu *et al*., 2015). Also, others have reported that ceramides with unsaturated VLCFAs may play a role in hypoxia tolerance in *Arabidopsis*. In this case, the contents of ceramides and hydroxyceramides significantly increased in plants that were submerged in water and kept in the dark. In this study, when employing knockout mutants of the

ceramide synthases LOH1/2/3, a decrease of ceramides with unsaturated VLCFAs was observed, which resulted in increased sensitivity to these treatments (Xie *et al*., 2015). Another relevant function of ceramides is the modulation of PCD. Indications of such a function come primarily from the animal kingdom, in which a connection between the production of these lipid species and the onset of the PCD has been established (Hannun and Obeid, 2018). Plants are known to have exogenous uptake of ceramides with short FA constituents (C2) which induce cell death in *Arabidopsis* cell cultures and protoplasts. This is preceded by a transient increase in calcium and the formation of ROS. By inhibiting such calcium increase, cell death could be prevented, while inhibition of ROS generation had no effect on survival. These findings suggest a role for calcium signaling, but not ROS generation, in ceramides-induced PCD. In addition, partial reduction of PCD could be achieved by addition of phosphorylated ceramides (Cer-Ps), indicating a role of this form of ceramide modification in modulating PCD (Liang *et al*., 2003; Townley *et al*., 2005). Further evidence for a participation of Cers and Cer-Ps in PCD regulation in plants lays on the characterization of the CERK mutant *acd5* and the sphingolipid transfer protein ACD11 (Accelerated Cell Death 11). Both *Arabidopsis* mutants were identified in studies with spontaneous PCD (Brodersen *el al*., 2002; Liang *et al*., 2003). The loss of function of ACD5 ceramide kinase leads to the accumulation of ceramides, formation of ROS, cell death, and impaired defense against pathogens (Bi *et al*., 2014). Regarding the ACD11 loss-of-function mutant, *in vitro* experiments demonstrated a transport activity across membranes of ceramide-1-phosphate, while other sphingolipid classes (LCBs, Glc-Cers and GIPCs) were not transported or only to a small extent. In addition, there was a high accumulation of ceramides that correlated with spontaneous cell death which in turn is dependent on salicylic acid (Simanshu *et al*., 2014). Finally, a mutant of inositol phosphorylceramide synthase (*ipcs2*) also provides additional evidence for the function of ceramides in PCD by strongly enhancing the transcription of *RPW8* and *RPW8*-dependent spontaneous HR-like cell death (Wang *et al*., 2008).

1.2.3.4. Sphingobases (LCBs/LCB-Ps).

It is known that sphingobases act as relevant regulators in animal cellular processes, but their function as signaling molecules in plants have been characterized to a lesser extent. So far, the signaling pathways involving sphingosine and its derivates, such as sphingosine-1-phosphate, have been studied (Hannun and Obeid, 2018). Several functions have been described for sphingosine, including apoptosis, arrest of the cell cycle and cell differentiation, while functions such as cell stability, inflammation, cell migration and cell invasion have been described for sphingosine-1-phosphate. Five G protein-coupled receptors of sphingosine-1-phosphate have been identified to be responsible for these functions downstream in the pathway (Siehler and Manning, 2002). The importance of the knowledge on sphingobases in animals is reflected by their application in the development of therapeutics. For example, the active ingredient of the medication Fingolimod is a sphingosine analog that is employed as an immunomodulatory drug for the treatment of multiple sclerosis (Brinkmann *et al*., 2010).

Several roles of sphingobases as signaling molecules have also been identified in plants despite limited knowledge regarding the receptors involved and the signal transmission route. Like in animals, in plants, non-phosphorylated (LCB) and phosphorylated sphingobases (LCB-P) mostly exhibit antagonistic functions, as inferred from the phenotypes of mutant enzymes of the sphingobase metabolism, such as SPHK1 and LCBK2, mentioned in Section 1.2.2.1. LCB synthesis and metabolism. First, LCB-Ps have been shown to play a role in ABA-dependent stomatal closure. Knockout and overexpression lines of *SPHK1* show a reduction and an increase, respectively, in the

sensitivity of their stomata in comparison to wild-type plants (Worrall *et al*., 2008). In the knockout mutants, which present dehydration due to the excessive stomata opening, a direct treatment with LCB-Ps led to stomatal closure (Ng *et al*., 2001; Coursol *et al*., 2005). In *Arabidopsis*, such closure induced by LCB-Ps appears to require the prototypical G protein α-subunit GPA1. In guard cells, LCB-Ps signals are transduced through GPA1, which in turn regulates ion channels and stomatal closure. In contrast, *gpa1* knockout mutants present insensitive stomata: LCB-Ps do not inhibit stomatal opening nor promote stomatal closure (Coursol *et al*., 2003, 2005). Second, LCB-Ps may also play a role in the response of plants to cold. In mutant lines deficient of LCBK2, a transient and amplified formation of t18:0-P was detected in response to cold stress as well as an increase in root growth at moderately low temperatures (Dutilleul *et al*., 2012). Third, there are many studies on the function of sphingobases in plants, which often involve exogenous addition of sphingobases, that have established a relationship with the regulation of PCD. It has been shown that direct treatment with LCBs led to PCD in leaves and cell cultures in *A. thaliana* and *N. tabacum* (Shi *et al*., 2007; Lachaud *et al*., 2010; Peer *et al*., 2011), while treatment with LCB-Ps appeared to lead to inhibition or reduction of PCD (Shi *et al*., 2007). However, there is conflicting evidence regarding the role of LCB-Ps in PCD. On one hand, an inhibiting effect on PCD by LCB-Ps was observed in *A. thaliana* cell cultures in response to a range of stresses (heat- and C2 ceramide-induced stresses; Alden *et al*., 2011) as well as in pathogen-infected plants (by *P. syringae* or *B. cinereal*; Magnin-Robert *et al*., 2015). On the other hand, a promoting effect by LCB-Ps on cryptogein-induced PCD was observed in tobacco and *Arabidopsis* cells. In contrast, an antagonistic effect (inhibition of cell death) was observed by LCB treatment (Coursol *et al*., 2015). A strong inhibitory effect of LCBs (d18:0) in cell death induced by *P. syringae* was also demonstrated (Magnin-Robert *et al*., 2015). The theory of an antagonizing effect of LCB-Ps on PCD was disapproved in a recent study: indeed, external application and *in vivo* levels of LCB-Ps did not reduce FB_1-induced cell death whereas a positive correlation between levels of non-phosphorylated LCBs and cell death was observed (Glenz *et al*., 2019).

Sphingobases have also been shown to regulate the hypersensitive response, a localized cell death reaction. For instance, in *Arabidopsis*, upon inoculation with an avirulent strain of *P. syringae* carrying the avirulence factor *AvrRPM1*, the levels of phytosphingosine t18:0 increased and remained high for a longer period when compared to inoculation with a virulent strain of this pathogen. The increase of t18:0 likely results from *de novo* synthesis from dihydrosphingosine (d18:0), the second most abundant LCB in plants after t18:0. In the sphingobase hydroxylase SBH1 knockout mutant, an increase in the levels of d18:0 in response to *Pseudomonas* infection was observed whereas the levels of d18:0 did not increase in wild-type plants. This lack of increase may indicate that t18:0 represents the most relevant LCB in the regulation of the hypersensitive response (Peer *et al*., 2010).

Other important findings regarding the involvement of sphingobases in regulating PCD in plants are provided by studies using inhibitors of ceramide synthesis, such as FB_1 and AAL toxin. These toxins, which inhibit various *Arabidopsis* ceramide synthases, can induce the activation of the hypersensitive response, eventually leading to cell death. Cell death induced by FB_1 or AAL was correlated with a higher content of sphingobases that increased through *de novo* biosynthesis (Asai *et al*., 2000; Shi *et al*., 2007). Several mutants of the sphingobase metabolism, such as mutants of the serine palmitoyltransferase or LCB-P lyase DPL1, show higher sensitivity to FB_1 (Spassieva *et al*., 2002; Tsegaye *et al*., 2007). The regulatory role of sphingobases in PCD is the consequence of changes in their metabolism. By using FB_1 in the experiments, several components of the signal transmission route could be associated with cell death triggered by sphingobases. FB_1-induced PCD is not only dependent on jasmonate, salicylic acid, and ethylene signaling pathways, but also requires the activation of MAPK cascades (Asai *et al*., 2000; Igarashi *et al*., 2013). In *Arabidopsis*, the

orosomucoid-like proteins ORM1 and ORM2 suppress the activity of the serine palmitoyltransferase subunits and play an important role in the regulation of sphingolipid homeostasis and PCD (Kimberlin *et al*., 2016). Mutants of these proteins show altered FB_1 sensitivity. In addition, the use of FB_1 has also shed some light on some of the consequences of the increase in LCB levels. An external application of LCBs triggers a rapid increase in the concentration of calcium ions in the cytosol and, later, in the nucleus. Also, it has been shown in tobacco cell cultures that cell death triggered by addition of the LCB d18:0 acts as a selective inhibitor of the calcium influx. Altogether, it seems that the calcium increase in the nucleus is required for triggering PCD (Lachaud *et al*., 2010). In addition to the influx of calcium, LCB-mediated cell death also induces an increase in ROS and nitrogen monoxide. In contrast to the calcium influx, these increases take place later and are not required for cell death (Shi *et al*., 2007; Lachaud *et al*., 2010; Da Silva *et al.*, 2011; Peer *et al*., 2011; Saucedo-García *et al*., 2011).

The findings summarized in this section together with the mutant phenotypes of enzymes involved in sphingobase metabolism mentioned previously (Section 1.2.2. Sphingolipid biosynthesis and metabolism) highlight the importance of the regulatory function of LCBs/LCB-Ps in PCD and hypersensitive response upon pathogen infection.

1.2.4. Metabolome analysis.

Metabolomics is the characterization of the metabolome, which refers to small molecules, commonly known as metabolites, within cells, biofluids, tissues, or organisms (Oliver *et la*., 1998). The goal of metabolomics is to understand the distribution of metabolites in time and space present in a biological system by using qualitative and quantitative analyses (Kueger *et al*., 2012). Over the last two decades, plant metabolomics has benefited from pre-existing methodological approaches and analytical strategies for the high throughput analysis and characterization of the many chemically diverse classes of metabolites (Hegeman, 2010). Yet, significant challenges in these analytical approaches, such as compound identification and quantification, still exist. On one hand, mass spectrometry-based analysis of metabolites has advanced considerably in recent years (Allwood and Goodcare, 2010). This is mostly due to the enhancement of mass spectrometers, with improved mass range and resolution capabilities, coupled with progresses in various chromatographic separation techniques and software developments. The latter facilitate data extraction and processing (Benton *et al*., 2010; Pluskal *et al*., 2010) and increase the quality and accessibility to public databases (Tohge and Fernie, 2009; Wang *et al*., 2009). On the other hand, recent progresses in the application of stable isotope dilution and compound annotation, such as stable isotopic metabolic labeling, are very useful to elucidate the metabolite's structures, allowing their partial determination (Kueger *et al*., 2012).

Stable isotope dilution analysis is a process that uses the mass difference between two compounds due to the substitution of one or more atoms by stable isotopes, allowing the co-purification and then, the determination of the isotopic enrichment after isolation. This method provides a good internal control where labeled compounds are fed in the earliest stages of the organism. Moreover, stable isotope labeled compounds are also used as internal standards (IS), which enables the absolute quantification of metabolites (Hegeman, 2010). The availability of labeled compounds remains one of the most common limitations in the analysis of metabolomics. One of the solutions, called "metabolic labeling", is to use the incorporation of labeled nutrients, such as $^{13}CO_2$ or ^{15}N-nitrate, into organisms and analyze every labeled molecule (Beynon and Pratt, 2005). This approach was first used in quantitative analysis in proteomics (Kikuchi and Hirayama, 2007) and its

application has been extended to metabolomics in plant suspension cells (Engelsberger *et al*., 2006; Harada *et al*., 2006) as well as in whole plants (Hegeman *et al*., 2007; Giavalisco *et al*., 2009). The analysis of all metabolites found in a biological system in mass spectrometry-based metabolomics depends on the biological question and on the nature of the compounds to be measured (Kueger *et al*., 2012). Two different methods exist for the analysis of metabolites distributions. The first approach, commonly called targeted metabolomics, measures and profiles known metabolites with known chemical structures (Albinsky *et al*., 2010; Dudley *et al*., 2010). Both, ultra-performance liquid chromatography (UPLC) and gas chromatography (GC) are techniques used for targeted analysis. In contrast to UPLC, GC is limited to volatile compounds or needs further chemical derivatization prior to the analysis. GC coupled either with time-of-flight (TOF) or quadrupole mass spectrometers has proven to be the best-established system (Lisec *et al*., 2006). However, targeted metabolomic profiling techniques require reference compounds for the identification and quantification in order to establish a profile. Internal standards remain the major limitation for the profiling due to their commercial unavailability (Nakabayashi *et al*., 2009) or inexistent identification (Kim *et al*., 2011). The second approach, commonly called non-targeted analysis, studies compounds beyond the known targets including signals of unknown identity (Hanhineva *et al*., 2008; Tianniam *et al*., 2009). Metabolites are obtained in positive- and negative-ionization mode of the polar fraction, and elemental composition annotation of these peaks is determined with databases according to their structures (Giavalisco *et al*., 2011). To perform non-targeted analysis, there are two different procedures established. The first procedure, known as metabolomic fingerprinting, is often combined with a chromatographic separation of the samples upstream of the mass spectrometry-based measurement and is to identify differences between two metabolomes (Last *et al*., 2007). The second procedure, known as metabolite profiling, is performed by including a chromatographic separation step upstream of the mass spectrometry measurement and is generally employed to describe a larger set of compounds within a single class of compounds (Last *et al*., 2007; Allwood and Goodacre, 2010). Metabolomic signatures obtained by non-targeted analysis can be analyzed by multivariate statistical methods and provide significantly different metabolic features between the analyzed samples (Bylesjö *et al*., 2007; Sumner *et al*., 2007b). More sophisticated analytical technologies, such as the use of higher-dimension NMR methods with extensive purification and compounds enrichment (Kim *et al*., 2011), can be applied to unravel exact chemical structures upon identification of important markers (Kueger *et al*., 2012). As in the targeted approach, the unavailability of authentic reference materials, important for peak annotation and distinction between biological and non-biological compounds, is one of the main limitations of this technique (Saito and Matsuda, 2010).

In this thesis, the sphingolipid profiles of different genotypes of the model plant *A. thaliana* were investigated in response to several stresses using different metabolomics approaches. Sphingolipids were measured after application of deuterium-labeled d18:0 in order to identify the major metabolites present by targeted and non-targeted analyses. Both targeted and untargeted analyses of labeled-isotope sphingobase d18:0 were performed to identify the major metabolites being newly synthesized as well as determine their rate of synthesis. In these feeding assays, this sphingobase was considered as the first precursor in the sphingolipid pathway.

1.3. Motivation and objectives of this work.

In plants, the function of sphingobases acting as signaling molecules has been less characterized than in animal cellular processes. However, sphingolipids have been suggested to play an important role in the regulation of PCD by acting in signal transduction in plant cells (Shi *et al*., 2007; Peer *et al*., 2011). In plants, FB_1, a toxin produced by *Fusarium moniliforme*, triggers apoptosis-like PCD by inhibition of ceramide synthase activity, leading to a strong accumulation of free LCBs and their metabolites (Merrill *et al*., 2001; Peer *et al*., 2010). The hypersensitive response, a form of PCD, induced by avirulence factors from *P. syringae*, has also been demonstrated to correlate with the increase of LCBs levels (t18:0; Peer *et al*., 2010). A previous work suggests an antagonism in cell death between LCBs and LCB-Ps; LCBs promoting cell death and LCB-Ps obstructing cell death (Magnin-Robert *et al*., 2015). However, this hypothesis was disproved by Glenz *et al*. (2019) who showed that cell death was depending predominantly on LCB levels.
Sphingobases are building blocks of membrane-localized sphingolipids. Remodeling of the membrane lipid composition occurs during temperature changes (Dutilleul *et al*., 2012; Mittler *et al*., 2012; Huang *et al*., 2017; Mueller *et al*., 2017). Membranes adapt their lipid composition in response to environmental changes to maintain optimal properties (Huby *et al*., 2019). However, it is not well known which SPL species are regulated when temperatures change and if these changes are required for survival or fitness under these conditions. When submitted to a stress, the composition of lipids, and therefore sphingolipids, might evolve to allow the plant to adapt. The understanding of the sphingolipid pathway in *A. thaliana* under such conditions remains poorly described. Studying the flux of sphingolipids under specific conditions could grant the discovery of new pathways of regulation of LCB levels and thereby PCD regulation.

Therefore, the main aims of this thesis work were:

(i) Investigate *Arabidopsis* sphingolipid biosynthesis mutant lines during biotic and abiotic stresses. These mutant lines were known to have different LCB and LCB-P levels and, therefore, enable to test the influence of distinct LCB levels on several biological processes. For that purpose, survival rates, plant-pathogen infection responses, and sphingolipid levels were analyzed.

Cell death quantification and sphingolipid analysis will be conducted on several sphingolipid mutant lines after *P. syringae* infection.

Cell death symptoms, spread of the pathogen and sphingolipid contents will be analyzed on several sphingolipid mutant lines after *V. longisporum* infection.

Survival rates and sphingolipid analysis will be performed on several sphingolipid mutant lines after heat stress.

Plant growth and sphingolipid analysis will be performed on several sphingolipid mutant lines after heat and cold acclimations.

(ii) Investigate the flux of sphingolipids in *A. thaliana* ecotype Col-0 leaves after providing high levels of deuterium-labeled LCBs (D_7-d18:0). In order to better understand how high levels of LCBs are regulated in the plant, the contribution of different enzymatic pathways which metabolize free LCBs will be assessed.

A targeted analysis will be performed to quantify the major labeled SPLs and thereby identify the contribution of the synthesis of sphingolipids containing D_7-d18:0.
An untargeted analysis will be performed which will enable the identification of yet unknown compounds and, possibly, pathways which are involved in the downregulation of elevated LCB levels. Also, the regulation of sphingolipid compounds synthesized *de novo* to reduce high amount of free LCBs will be studied.

2. Materials and Methods.

2.1. Materials.

2.1.1. Chemicals, materials and water.

Commercially available chemicals and material products used in this study are mentioned in the following table (**Table 1**). Manufacturers related: AppliChem (Darmstadt, Germany); Becton, Dickinson and Company (Le Pont de Claix, France); Biosolve Chimie SARL (Valkenwaard, Netherlands); Duchefa Biochemie (Haarlem, Netherlands); A. Hartenstein (Würzburg, Germany); Merck (Darmstadt, Germany); Carl ROTH (Karlsruhe, Germany); Sigma-Aldrich (Deisenhofen, Germany); VWR chemicals (Darmstadt, Germany). Solutions were used with ultrapure water from an ultrapure water system, consisting of a RiOs™ Essential 5 and a Milli-Q® gradient water purification system (Merck, Darmstadt, Germany). For molecular biological methods, water used was provided from AppliChem (Darmstadt, Germany).

Table 1: Special chemicals and materials

Chemical Products	Company supplier
Agar Kobe I	AppliChem
Ammonium Formate	Biosolve Chimie SARL
Bacto™ Proteose peptone No. 3	Becton, Dickinson and Company
Butan-1-ol	VWR chemicals
ß-Mercaptoethanol	Carl ROTH
Chloral Hydrate	VWR chemicals
Chloroform	AppliChem
Citric Acid	AppliChem
Czapek Dox Broth	Duchefa Biochemie
di-Potassium Hydrogen Phosphate	AppliChem
di-Sodium Hydrogen Phosphate di-hydrate	AppliChem
Dimethyl Sulfoxide	Merck
Ethanol 99.8%	Carl ROTH
Ethylene di-amine tetra-acetic Acid	AppliChem
Formic Acid	Merck
Glycerin anhydrous BioChemica	AppliChem
Glycerol anhydrous BioChemica	AppliChem
Hexa-decyl-trimethyl -Ammonium bromide	Merck
Hydrochloric Acid	AppliChem
Lactic Acid	AppliChem
Magnesium Sulfate hepta-hydrate	Merck
Mannitol	Merck

Methanol	Merck
Murashige and Skoog	Duchefa Biochemie
N-Lauroylsarcosine	AppliChem
Paper filter (d = 125 mm)	A. Hartenstein
Phyto agar	Duchefa Biochemie
Potassium Hydroxide	AppliChem
Potato Dextrose Broth	Sigma-Aldrich
Sodium Chloride	AppliChem
Tri-Chloro Acetic Acid	AppliChem
Tris Buffer	AppliChem
Trypan Blue	Sigma-Aldrich

2.1.2. Media.

All media were prepared with ultrapure water and then sterilized for 20 min at 121 °C in a Tuttnauer 5075 ELV autoclave (Tuttnauer Europe B.V., Breda, Netherlands). For solid media, a defined agar concentration was added to the corresponding medium before autoclaving it (**Table 2**). For selection, media were cooled down to about 50 °C and selection antibiotics were added at defined concentrations (**Table 3**).

Table 2: Summary of media

Seedling growth medium: Murashige and Skoog (MS) medium	
MS 1B micro and ½ macro elements including vitamins	2.286 g/L
Phyto agar	12 g/L
pH adjusted	5.7

P. syringae pv. tomato strain *AvrRPM1* growth medium: King's B (KB) medium	
Bacto™ Proteose peptone No. 3	20 g/L
Glycerin anhydrous BioChemica	10 mL/L
di-Potassium Hydrogen Phosphate	1.5 g/L
Agar Kobe I	15 g/L
Magnesium Sulfate heptahydrate	1.5 g/L
pH adjusted	7.2

V. longisporum sporulation medium:
Czapek Dox Broth is used at 33.4 g/L and contains

Sodium Iron EDTA	0.013 g/L
Magnesium glycerophosphate	0.5 g/L
Potassium Chloride	0.5 g/L
Potassium Sulfate	0.35 g/L
Sodium Nitrate	2.0 g/L
Sucrose	30 g/L

2.1.3. Antibiotics.

All antibiotic stock solutions (ordered from Duchefa Biochemie, Haarlem, Netherlands) were prepared at a thousand times concentration, dissolved in ultrapure water (Dimethyl Sulfoxide (DMSO) for rifampicin) and sterilized. Antibiotics were added at the indicated concentration to the media for selection of the appropriate bacterial or fungal strains (**Table 3**).

Table 3: Summary of antibiotics

Antibiotics	**Final concentration for selection of:**	
	P. syringae	***V. longisporum***
Cefatoxim	-	500 µg/mL
Rifampicin	50 µg/mL	-
Tetracycline	5 µg/mL	-

2.1.4. Organisms.

2.1.4.1. Plant material.

A. thaliana ecotype Columbia (Col-0) was used in this study. All mutants of *A. thaliana* were in the Col-0 background (**Table 4**). The T-DNA insertion mutants lines were created by SALK (Alonso *et al.*, 2003), SAIL (McElver *et al.*, 2001) and GABI-Kat (Kleinboelting *et al.*, 2012), respectively, and obtained from the Nottingham *Arabidopsis* Stock Centre (NASC, University of Nottingham, Loughborough, UK (Scholl *et al.*, 2000)). Double mutants *dpl1.1* / *spp1.2* and sphk1-OE / *spp1.2* were kindly provided by R. Glenz (obtained by crossing homozygote parental lines; Julius Von-Sachs-Institute, Würzburg University, Germany). The double mutant *cyp79 b2*/*b3* was kindly provided by C. Fröschel (Julius Von-Sachs-Institute, Würzburg University, Germany).

Table 4: T-DNA insertion mutant lines

Name	Gene locus	T-DNA Insertion	Reference
dpl1.1	At1g27980	SALK_020151	Tsegaye *et al.*, 2007
dpl1.2	At1g27980	SALK_093662	Tsegaye *et al.*, 2007
sphk1-KD	At4g21540	SAIL_794_B01	Worrall *et al.*, 2008
sphk1-OE	At4g21540	GK-288D07	Worrall *et al.*, 2008
spp1.1	At3g58490	SALK_035202	Nakagawa *et al.*, 2012
spp1.2	At3g58490	SALK_027084	Nakagawa *et al.*, 2012
lcbk1	At5g23450	SALK_152371	Dutilleul *et al*., 2012
lcbk2.1	At2g46090	SALK_129175	Dutilleul *et al*., 2012
lcbk2.2	At2g46090	SALK_141351	Dutilleul *et al*., 2013
spp1-OE	At3g58490	GK-126D07	Glenz *et al*., 2019
dpl1.1 / *spp1.2*	At1g27980 At33g58490	Crossed T-DNA insertion	In this study
sphk1-OE / *spp1.2*	At4g21540 At33g58490	Crossed T-DNA insertion	In this study
cyp79 b2/*b3*	At4g39950 At2g22330	Crossed T-DNA insertion (SALK)	Zhao *et al*., 2002

2.1.4.2. Bacteria.

The bacterial leaf pathogen *P. syringae pv. tomato* strain *AvrRPM1* (Mishina and Zeier, 2007) was used in this study. Source: F. Waller (Julius Von-Sachs-Institute, Würzburg University, Germany). Resistance to antibiotics from this bacterial strain is mentioned in **Table 3**.

2.1.4.3. Fungi.

The vascular fungal pathogen strain *V. longisporum* isolate Vl43 (Zeise and von Tiedemann, 2002) was used in this study. Source: C. Fröschel (Julius Von-Sachs-Institute, Würzburg University, Germany). Resistance to antibiotics from this bacterial strain is mentioned in **Table 3**.

2.1.5. Primers.

2.1.5.1. PCR primers.

Primers used in standard PCRs were synthesized by Thermo Fisher (Thermo Fisher Scientific Inc., Waltham, MA, USA) at the defined temperature with desalinated purity. Primers were received lyophilized and dissolved in HPLC Grade H_2O. For the verification of T-DNA insertion, primer sequences were used with the online software SIGnAL T-DNA Express (Salk Institute Genomic Analysis Laboratory, La Jolla, CA, USA; http://signal.salk.edu/tdnaprimers.2.html). A list of primers employed in this thesis is shown in **Table 5.** LP and RP stand for left (forward) and right (reverse) primers, respectively.

Table 5: Primers for the verification of T-DNA insertion

Name	T-DNA Insertion	Primer sequences (5' → 3')
dpl1.1	SALK_020151	LP: CATGCCATCACACATAGCAAC RP: AGAAAGGCCTCAAAGCTTGTC
dpl1.2	SALK_093662	LP: CATGCCATCACACATAGCAAC RP: ATCCATGTTGATTCAAGCTCG
sphk1-KD	SAIL_794_B01	LP: TCCCAAAAGCAATTCCTCTTAC RP: CGTCATAGCTAAGAGGAGGGG
sphk1-OE	GK-288D07	LP: AACGGATTCACAAACACAAGC RP: ATTCCCTTGTGGTTGTGTGTG
spp1.1	SALK_035202	LP: ATTGGCAGCAATCACAAAATC RP: GGCAGTAATCCTTCTAACCGG
spp1.2	SALK_027084	LP: ACCACTGACGATATCGACGAC RP: ATCAATGGAAGGTTCAGGGAC
lcbk1	SALK_152371	LP: ACACGAGACAGCGTCCAATAG RP: TTTCGCCCTATTTTGGTTAGG
lcbk2.1	SALK_129175	LP: AAAGGCAGGATTTTACGCTTC RP: GCAACTCACTCCAGTTGCTTC
lcbk2.2	SALK_141351	LP: GAAGCAGTGGAGCGCATTGC RP: TGGCACCGGGTAACACCTGA
spp1-OE	GK-126D07	LP: CCATGTCATGAAGTAATCGGC RP: ACAATACCAACGAGCACCAAG
SALK-line	LBb1.3	ATTTTGCCGATTTCGGAAC
SAIL-line	LB3_SAIL	TAGCATCTGAATTTCATAACCAATCTCGATACAC
GK-line	LB_GK (o8474)	ATAATAACGCTGCGGACATCTACATTTT

2.1.5.2. qPCR primers.

Actin and *V. longisporum* primers for quantitative PCR (qPCR) used in this study were provided by C. Fröschel (**Table 6**; Julius Von-Sachs-Institute, Würzburg University, Germany).

Table 6: qPCR primers

Name	Primer sequences (5' → 3')	Reference
Act8gen fwd	GGTTTTCCCCAGTGTTGTTG	Fröschel *et al*., 2019
Act8gen rev	CTCCATGTCATCCCAGTTGC	
OLG70 fwd	CAGCGAAACGCGATATGTAG	Eynck *et al*., 2007
OLG71 rev	GGCTTGTAGGGGGTTTAGA	

2.1.6. Sphingolipids.

Sphingolipid references and a stable isotope sphinganine labeled (D_7-d18:0) were purchased from Avanti Polar Lipids (Avanti Polar Lipids Inc., Alabaster, AL, USA). Stock solutions of LCBs and ceramides were dissolved in Chloroform:Methanol (50:50; v:v) at a concentration of 1 mg/ml. Working solutions were prepared by evaporating at 60 °C for 30 min the appropriate amount of stock solution, dissolving it in methanol by ultrasonication for 15 min and diluting it for the required concentration in H_2O (2 % methanol final concentration). Working solutions were stored at -20 °C. Sphingolipids purchased are listed in **Table 7**, with the abbreviation name (label), the molecular weight (MW) and the respective CAS number (Chemical Abstracts Service, Columbus, OH, USA).

Table 7: Sphingolipids internal standards

Substances	Label	MW	CAS Number
[C17]-D-*erythro*-Sphingosine	d17:1$^{\Delta4}$	285.3	6918-48-5
D-*erythro*-Sphingosine	d18:1 $^{\Delta4}$ (Sphingosine)	299.3	123-78-4
D-*erythro*-Sphinganine	d18:0 (Sphinganine)	301.3	764-22-7
D-*erythro*-Sphinganine-d7	D_7-d18:0	308.3	1246304-35-7
D-ribo-4-hydroxysphinganine	t18:0 (Phytosphingosine)	317.2	388566-94-7
[C20]-D-*erythro*-Sphingosine	d20:1 $^{\Delta4}$	327.3	6918-49-6
[C17]-D-*erythro*-Sphingosine-1-Phosphate	d17:1$^{\Delta4}$-P	365.2	474923-27-8
D-*erythro*-Sphingosine-1-Phosphate	d18:1 $^{\Delta4}$-P	379.3	26993-30-6
D-*erythro*-Sphinganine-1-Phosphate	d18:0-P	381.3	19794-97-9
D-ribo-4-hydroxysphinganine-1-Phosphate	t18:0-P	397.3	383908-62-1
N-decanoyl-D-*erythro*-sphingosine	d18:1 $^{\Delta4}$-c10:0	453.4	111122-57-7

N-palmitoyl-D-*erythro*-Sphinganine	d18:0-c16:0	539.5	5966-29-0
N-palmitoyl-Phytophingosine	t18:0-c16:0	555.5	111149-09-8
N-oleoyl-D-*erythro*-Sphinganine	d18:0-c18:1(9Z)	565.5	34227-83-3
N-stearoyl-D-*erythro*-Sphinganine	d18:0-c18:0	567.6	2304-80-5
N-lignoceroyl-D-*erythro*-Sphingosine	d18:1 $^{\Delta 4}$-c24:0	649.6	102917-80-6
N-nervonoyl- D-*erythro*-Sphinganine	d18:0-c24:1(15Z)	649.6	352518-80-0
N-lignoceroyl-Phytosphingosine	t18:0-c24:0	667.6	34437-74-6

2.2. Methods.

2.2.1. Methods for *A. thaliana* plants.

2.2.1.1. Plant growth conditions.

All seeds were gas sterilized in a desiccator with 100 mL of Danklorix (commercial hygiene cleaner with active chlorine) and 10 mL 37 % HCl for 2 h before use. After transfer to growth soil/medium, the seeds were incubated at 4 °C in the dark for 2 days for stratification.
For feeding experiments, wild-type *A. thaliana* ecotype Col-0 plants were transferred to a growth chamber under a 9 h light/15 h dark cycle condition at 22/20 °C (70 % humidity) for 6 weeks before use.
For heat shock, short-term heat adaptation, long-term heat adaptation or long-term cold acclimation experiments, seedlings were sown on Murashige and Skoog (MS) agar medium in petri dishes and incubated in climate chamber under photoperiod of 16 h light/8 h dark at 22/20 °C (70 % humidity) for 2 weeks before use.
For *P. syringae* infection experiments, plants were grown in soil in a growth chamber under a 9 h light/15 h dark short-day cycle at 22/20 °C (70 % humidity) for 6 weeks before use.
For *V. longisporum* infection experiments, plants were grown in mix of sand/soil (20 %/80 %) in climate chamber under photoperiod of 16 h light/8 h dark at 22/20 °C (70 % humidity) for 3 weeks before infection. After infection with the fungus, the plants were transferred to soil for 3 more weeks of growth in climate binder with 12 h light/12 h dark at 22/20 °C (70 % humidity).

2.2.1.2. Trypan blue staining for *A. thaliana* leaves.

In order to observe the spread of the pathogen inside *A. thaliana* leaves after infection, biological materials were fixed for 1 day with Ethanol/Chloroform/TCA solution (Fixing solution, **Table 8**; Hückelhoven and Kogel, 1998).
Leaves were washed 3 times with 10 mL H_2O and incubated with 5 mL of 10 % KOH at 80 °C for 5 min. KOH solution was exchanged by 5 % HCl and let for 3 min at Rt. HCl solution was removed and trypan blue was added at 0.1 % in H_2O to stain the leaves at 80 °C for 5 min. Dye solution was replaced by ethanol 99.8 % for 2 min at 80 °C and then changed to lacto-solution (**Table 8**) for 10 min at Rt. Samples were washed 3 times with 10 mL H_2O and distained with a high concentrated chloral hydrate solution (1.2 kg /L H_2O). The leaves were finally stored in H_2O before analysis by microscopy using a binocular.

Table 8: Fixing solution and Lacto-solution

Ethanol/Chloroform/TCA:	0.15 % TCA (w/v), chloroform (4:1; v/v) in ethanol
Lacto-solution:	Lactic acid, 87 % glycerol anhydrous, in H_2O (1:2:1; v:v:v)

2.2.1.3. Feeding experiment of *A. thaliana* leaf discs.

Twenty leaf discs per replicate were excised from 6-week-old *A. thaliana* Col-0 plants using a biopsy puncher (5.0 mm diameter; Servoprax GmbH, Wesel, Germany) and equilibrated in Milli-Q® water overnight. Leaf discs were then transferred to a control solution (H_2O + 2 % DMSO) or to a treatment solution (100 µM D_7-d18:0 + 2 % DMSO; **Table 7**). Leaf discs were incubated in a growth chamber under a 9 h light/15 h dark cycle condition at 22/20 °C (70 % humidity). Leaf discs were collected at 0, 1, 3, 6, 24 and 48 hpi, immediately frozen in liquid nitrogen and stored at -80°C for subsequent sphingolipid extraction.

2.2.1.4. Temperature-related experiments.

Two-week-old seedlings grown on MS agar plates were used for heat shock assays at 45 °C for 90 min. Half of the seedlings were then collected for sphingolipids analysis. The other half was transferred back to the climate chamber for two weeks recovery period before calculating survival rate.
Short-term heat adaptation was performed incubating *A. thaliana* ecotype Col-0 plates for 1, 2, 4, 8 and 24 h at 37 °C after the two weeks growth. For long-term heat and cold acclimations, the plates were incubated for 1, 3, 5 and 7 days at 37 °C or 10 °C, respectively, with photoperiod 16 h light/8 h dark (70 % humidity) after the two weeks growth. For all assays, control plates remained at growth conditions of 16 h light/8 h dark at 22/20 °C (70 % humidity).

2.2.2. Microbiology methods.

2.2.2.1. Pathogen growth and inoculation.

P. syringae
The bacterial leaf pathogen *P. syringae pv*. *tomato* strain *AvrRPM1* was cultured overnight at 28 °C on solid King´s B medium, supplemented with rifampicin (50 µg/mL) and tetracycline (5 µg/mL). Bacterial cells were then washed twice by centrifugation and resuspended in 10 mM $MgCl_2$. Bacterial concentration was determined with Fuchs-Rosenthal cell-counting chamber (Superior Marienfeld, Lauda-Königshofen, Germany) and prepared to a final density of 10^7 cfu/mL (optical density = 0.01). The bacterial solutions were infiltrated from the abaxial side into the leaves using a 1 mL syringe without needle (Dispomed, Gelnhausen, Germany). Control inoculations were performed with 1 mM $MgCl_2$. Leaves were collected from 0 to 48 hpi, frozen in liquid nitrogen, and stored at -80 °C until use.

V. longisporum

V. longisporum isolate Vl43 (Zeise and von Tiedemann, 2002, kindly provided by C. Fröschel, Julius Von-Sachs-Institute, Würzburg University, Germany) was stored at -20 °C in 25 % glycerin/75 % Czapek Dox Broth (CDB) medium until use. Two baffled Erlenmeyer flasks containing 150 mL Potato Dextrose Broth (PDB) medium at 22 g/L and 0.5 g/L Cefotaxim antibiotic were used to grow the fungus at 5 million spores/mL, final concentration. The flasks were incubated in the dark at Rt on a shaker plate for 10 days to get *V. longisporum* actively growing. After this period, the medium was replaced by 100 mL of CDB medium as sporulation medium containing Cefotaxim at 0.5 g/L for an additional 4 days on a shaker plate in the dark at Rt. The spore solution was filtered from the mycelium using filter paper (d = 125 mm). Spore concentration was determined with Thoma cell-counting chamber (Superior Marienfeld, Lauda-Königshofen, Germany) and was adjusted to $2*10^6$ spores/mL in ¼ liquid MS medium including vitamins (1.25 g/L) before the experiment.

2.2.2.2. Pathogen assays *in planta*.

Cell death determination

Bacterial infections were performed as described previously (Magnin-Robert *et al*., 2015). In short, five foliar leave discs per replicate were excised using a biopsy puncher (5.0 mm diameter; Servoprax GmbH, Wesel, Germany) and washed with Milli-Q® water for 1 h. The different replicates were placed into a 24 wells plate containing Milli-Q®water. The water was changed to start the experiment and the conductivity was measured in µS cm^{-1} using a LAQUATwin EC-11 conductivity meter (Horiba, Kyoto, Japan) from 0 to 24 h. The total conductivity representing 100 % of cell death was measured after boiling the leaves for 1 h at 100 °C and cooling the samples to Rt. Due to some variations within the results, this experiment was performed 10 times in quadruplicate. Data are reported as mean of percentage cell death.

V. longisporum infection

V. longisporum was prepared as mentioned before at $2*10^6$ spores/mL in ¼ liquid MS medium including vitamins and 40 mL were poured into a petri dish. The roots of three-week-old plants grown in mix of sand/soil were rinsed with water. The roots were incubated with the infection solution in the petri dish for 1 h at Rt. Control plants were incubated in water for 1 h. All plants were transferred to pots with fresh soil to grow and incubated in climate chamber with a photoperiod of 12 h light/12 h dark at 22/20 °C. The rosettes were collected 3 weeks post-infection and frozen in liquid nitrogen before being stored at -80 °C until further extraction.

2.2.3. Molecular biology methods.

2.2.3.1. DNA extraction.

The concentration of nucleic acids in aqueous solution can be measured by photometric absorption at 260 nm. Absorption of 1 at 260 nm corresponds to a concentration of 50 µg/mL double strand DNA. Genomic DNA concentration was determined with a spectrophotometer (NanoDrop 1000; Thermo Fisher Scientific Inc., Waltham, MA, USA).

For the isolation of genomic DNA from *A. thaliana* leaf material, a Hexa-decyl-trimethyl-Ammonium Bromide (CTAB) method was used.

About 50 to 100 mg of frozen plant material were grinded with mortar and pestle or with zirconia beads 3 times at 24 frequencies/sec with mixer mill. Crushed samples were incubated with 400 µL DNA extraction buffer (**Table 9**) and 400 µL chloroform for 60 min at 65 °C in a water bath. Two phases were separated by centrifugation at 7500 x G for 10 min at Rt. The aqueous phase was transferred to a new tube and mixed with an equal volume of isopropanol. After mixing the solution, genomic DNA was pelleted by centrifugation (10 min, 12000 x G, 4 °C). After two washing steps with ethanol 75 %, the DNA was dried at Rt and dissolved in 50 µL of water. The samples were stored at -20 °C before use.

Table 9: DNA extraction solution

DNA extraction buffer:	0.22 M Tris-HCl pH 7.8; 0.022 M EDTA; 0.8 M NaCl; 0.14 M Mannitol; 1 % N-Lauroylsarcosine; 0.8 % CTAB; H_2O Add fresh 14 µl/10 ml ß-Mercaptoethanol

2.2.3.2. Polymerase Chain Reaction (PCR).

To amplify specific DNA fragments, the PCR method was applied using DreamTaq™ polymerase purchased at Thermo Fisher Scientific Inc., Waltham, MA, USA (**Table 10** and **11**; Saiki *et al*., 1988). In the present work, the PCR technique was used to amplify genomic DNA from *A. thaliana* to check for the presence of certain T-DNA sequences (Alonso *et al*., 2003) using defined primers from **Table 5**. LP/LB stands for left primer/border and RB stands for right border.

Table 10: PCR reaction solution (25 µL) for genotyping

Template DNA	1 µg
DreamTaq™ buffer	1 X
dNTPs	2.5 mM
LP/LB Primer	10 µM
RB Primer	10 µM
DreamTaq™ polymerase	1-2 U
Sterile H_2O	To 25 µL

A Mastercycler® ep Gradient S (Eppendorf AG, Hamburg, Germany) was used to perform the PCRs. The different settings of the PCR (temperatures and times) from each different step (denaturation, annealing and elongation) were based on the information provided by the manufacturer of polymerases. The annealing temperature was calculated based on the melting temperature (Tm) of the primers (**Table 5**) according to the formula Tm = 4*(number G + number C) + 2*(number A + number T), where the letters represent the bases. Optimal annealing temperature for each primer pair was tested by temperature gradient.

Table 11: PCR program for genotyping

Step	Temperature	Time	Cycles number
Initial denaturation	94 °C	5 min	1
Denaturation	94 °C	45 s	40
Annealing	55 °C	45 s	
Elongation	72 °C	1.5 min	
Final elongation	72 °C	5 min	1

Using LB, LP and RB primers (**Table 5**) in wild-type DNA samples showed a PCR product (length 900 to 1200 BP) corresponding to the wild-type gene (no T-DNA insertion). PCRs carried out with homozygous mutant lines (T-DNA insertion in both chromosomes) showed a PCR product of length 410 BP + N (difference of the actual insertion side and the position of the flanking sequence; 0 - 300 BP). In heterozygous insertion lines (only one allele of a chromosome contains the T-DNA insertion) both PCR products were present.

2.2.3.3. Agarose electrophoresis gel.

After PCR of the samples, DNA fragments were separated using 1 % agarose gel electrophoresis prepared in Tris-Acetate EDTA (TAE) buffer (**Table 12**). In order to detect the DNA in the gel under UV light (364 nm), 5 µL DNA staining was added before pouring the gel. To increase the density of the DNA samples for migration, 1 µL loading dye (6X) was mixed with 5 µL PCR product sample. 5 µL 1 kb of DNA GeneRuler (Thermo Fisher Scientific Inc., Waltham, MA, USA) was used as size marker. Generally, electrophoresis gels were run at a voltage of 100 V in 1X TAE buffer for 45 min. After that, the bands could be detected in a gel documentation chamber with UV light produced by a transilluminator (Intas Science Imaging Instruments GmbH, Göttingen, Germany).

Table 12: TAE buffer for agarose electrophoresis gel

TAE buffer:	40 mM Tris-Acetate; 1 mM EDTA; in H_2O

2.2.3.4. Quantitative Polymerase Chain Reaction (qPCR).

For the quantification of gene expression from the growth of *V. longisporum*, qPCRs were performed in a CFX Connect Real-Time PCR Detection System (Bio-Rad Laboratories Inc., Hercules, CA, USA). The qPCRs were performed following the reaction protocol with ABsolute qPCR SYBR® Green Capillary Mix (**Table 13**; Thermo Fisher Scientic Inc.) and adding Actin or *V. longisporum* primers mentioned in **Table 6**. Quality of PCR products was checked by performing a melting curve from 60 °C to 95 °C during the initial denaturation step of the qPCR program (**Table 14**).

Table13: qPCR reaction protocol

Template DNA (70 ng/µL)	2 µL
Primer Mix (2 µM)	8 µL
ABsolute qPCR Sybr® Green capillary Mix (2X)	10 µL

Table 14: qPCR program for quantifying *V. longisporum*

Step	Temperature	Time	Cycles number
Initial denaturation	95 °C	15 min	1
Denaturation	95 °C	15 s	40
Annealing	55 °C	20 s	
Elongation	72 °C	20 s	
Final elongation	95 °C	10 min	1

2.2.4. Analytic methods.

The determination of the levels of different sphingolipids was carried out by high-performance liquid chromatography coupled with tandem mass spectrometry (HPLC-MS/MS). This method has been used in several previous works for the detection of sphingolipids (Sullards, 2000; Sullards and Merrill, 2001; Markham *et al*., 2006; Markham and Jaworski, 2007; Haynes *et al*., 2009; Scherer *et al*., 2010; Glenz PhD thesis, 2019).
The settings for the measurement of sphingobases and ceramides by HPLC-MS/MS and the quantification based on internal standards has been carry out as in M. Peer (2010).

2.2.4.1. Sphingolipid extraction.

In the present work, all sphingolipids were isolated using a single-phase extraction from leaf material or whole seedlings due to the amphiphilic nature of SPLs in a classical lipid extraction, which can be very variable, as described by (Shaner *et al*., 2009).
For feeding and *P. syringae* infection experiments, 20 leaf discs were used per sample for SPL extraction. Regarding to *V. longisporum* infection, whole rosettes were used for SPL extraction. For all heat-related experiments, about 40 to 60 mg of whole seedlings (approximately 100 seedlings) were used to perform SPL extraction.
Plant materials were placed into 2 mL screw-cap tubes and grinded with zirconia beads 3 times at 21 Hz for 45 sec with mixer mill (with intermediate cooling in liquid nitrogen) and extracted with the first SPL solution (**Table 15**; 18000 x G, 15 min; Upper phase). The residual solution was extracted with the second SPL solution (**Table 15**; 18000 x G, 15 min; Upper phase). The combined upper phases were dried in a vacuum concentrator (60 °C, 2 h; RVC 2-25 CDplus, Christ®, Osterode am Harz, Germany). The residual powder obtained was resuspended in 70 µL Methanol:Formic acid (99:1; v:v)

for 30 min, centrifuged at 18000 x G, 10 min and transferred to a 300 µL screw-fixed insert vial (Thermo Fisher Scientific Inc., Waltham, MA, USA). The tubes were stored at -20 °C until their analysis by HPLC-MS/MS or UPLC-ESI-MS/MS.

Table 15: Buffer and SPL extraction solutions

SPL extraction solutions:	
First SPL extraction solution:	500 µL Butan-1-ol, 170 µL H2O, 30 µL citrate-phosphate-buffer pH 4.0 and 0.9 µL of four internal standards (d17:1, d20:1, d17:1-P, d18:1-10:0) at 0.1 µg/µL
Second SPL extraction solution:	165 µL Butan-1-ol, 85 µL H2O
Citrate-phosphate buffer:	
Solution 1:	19.21 g Citric acid water-free/L H2O
Solution 2:	35.60 g di-Sodium Hydrogen Phosphate di-hydrate (Na2HPO4 . 2H2O)/L H2O

Autoclave bottles and mix Solution1:Solution2 (61.4:38.6; v:v) to get Citrate-phosphate buffer solution at pH 4.0.

For the measurement and quantification of sphingobases and ceramides obtained from the experiments in this thesis, four internal standards (IS; d17:1, d20:1, d17:1-P, d18:1-10:0) were added to each sample during SPL extraction. In addition, IS at 300 ng/ 70 µL (**Table 7**) were directly transferred into glass vials as reference materials. Immediately before the measurement, all samples were transferred to an ultrasonic bath for 5 min. All samples and IS were measured by HPLC-MS/MS for quantification.

2.2.4.2. Targeted analysis.

UPLC-MS/MS

Chromatographic separation of the analytes was carried out by ultra-performance liquid chromatography System (UPLC®, Waters Corporation, Milford, MA, USA). Analytes were then ionized by electrospray ionization (positive ESI mode) and detected by tandem mass spectrometry using a Quattro Premier Triple Quadrupole instrument (Waters Corporation, Milford, MA, USA).

Chromatographic separation

Reversed phase chromatography was performed with an ACQUITY UPLC® BEH C18 column (2.1 x 50 mm; particle size 1.7 µm) with a VanGuard pre-column (BEH C18; 2.1 x 5 mm; particle size 1.7 µm; In-Line particle filter 0.2 µm; flow rate: 350 µL/min; Water Corporation). Eluent A and Eluent B are mentioned in **Table 16** and the solvent compositions for gradient elution of SPLs are displayed in **Table 17**. Autosampler UPLC® system temperature was 20 °C, the column temperature was 30 °C, and the volume of samples injected was 8 µL.

Table 16: UPLC-ESI-MS/MS Eluents

UPLC-ESI-MS/MS Eluent A:	58 % Methanol v/v; 41 % H2O v/v; 1 % Formic acid v/v; 5 mM Ammonium formate
UPLC-ESI-MS/MS Eluent B:	99 % Methanol v/v; 1 % Formic acid v/v; 5 mM Ammonium formate

Table 17: HPLC gradients for separation of sphingolipids

Time (min)	Eluent A (%)	Eluent B (%)
0.0	60	40
2.0	60	40
4.0	20	80
5.5	15	85
8.0	5	95
14.0	0	100
20.0	0	100
20.1	60	40
24.0	60	40

MS/MS conditions

After chromatographic separation, the compounds were analyzed in positive ESI mode and detected by multiple reactions monitoring (MRM). The conditions for ionization and fragmentation of sphingolipids were taken from M. Peer (2010). The general device settings are listed in **Table 18**.

Table 18: General parameters for electrospray ionization (ESI)

Ionization mode	+ES
Capillary voltage (kV)	3
Source temperature (°C)	120
Desolvation temperature (°C)	450
Cone gas flow - N_2 (L/h)	50
Desolvation gas flow - N_2 (L/h)	800

Mass to charge ratios (m/z) in MRM mode of the individual sphingolipids with a dwell time of 25 ms for each transition and the specific cone voltage and collision energy are shown in **Table 19**. Argon was used as collision gas for the collision induced dissociation (CID) with a flow rate of 0.3 mL/min. Mass to charge ratios of the precursors (precursor ions) and products (product ions) of the analyzed

sphingolipids are specified in MRM transition. MS/MS parameters of Deuterium 7 (D_7) labeled sphingolipids measured are listed in **Table 20**.

Table 19: MS/MS parameters of sphingolipids

Sphingolipids	MRM transition (m/z)	Cone voltage (V)	Collision energy (eV)
d17:1 (IS)	286.2 → 268.1	20	11
d18:1	298.2 → 282.2	22	17
d18:0	302.2 → 284.2	28	18
t18:1	316.1 → 298.2	22	20
t18:0	318.1 → 282.2	22	20
d20:1 (IS)	328.1 → 310.2	18	22
d17:1-P (IS)	366.1 → 250.1	22	15
d18:1-P	380.0 → 264.2	20	17
d18:0-P	382.1 → 284.1	30	15
t18:1-P	396.2 → 298.2	24	20
t18:0-P	398.1 → 300.0	40	15
d18:1-10:0 (IS)	454.4 → 264.2	11	22
d18:0-16:1	538.7 → 266.3	45	35
d18:0-16:0	540.5 → 266.3	36	37
t18:1-16:0	554.5 → 262.3	30	30
t18:0-16:0	556.5 → 264.3	30	30
d18:1-18:1	564.7 → 264.3	35	35
d18:0-18:1	566.7 → 266.3	36	37
d18:0-18:0	568.5 → 266.3	36	37
d18:1-20:0	594.6 → 264.2	30	30
t18:1-22:0	638.6 → 262.3	35	40
t18:0-22:0	640.6 → 264.3	35	40
d18:1-24:0	650.6 → 264.2	28	32
d18:0-24:1	650.7 → 266.3	45	35
d18:0-24:0	652.7 → 266.3	45	35
t18:1-24:1	664.6 → 262.3	35	40
t18:1-24:0	666.6 → 262.3	35	40
t18:0-24:1	666.6 → 264.3	35	40
t18:0-24:0	668.6 → 264.3	35	40
d18:1-26:0	678.7 → 264.2	30	32
d18:0-26:0	680.7 → 266.3	43	35
t18:1-26:1	692.7 → 262.3	35	40
t18:1-26:0	694.7 → 262.3	35	40
t18:0-26:0	696.7 → 264.3	35	40

Table 20: MS/MS parameters of labeled D_7 sphingolipids

Sphingolipids	MRM transition (m/z)	Cone voltage (V)	Collision energy (eV)
d17:1 (IS)	286.2 → 268.1	20	11
D_7-d18:1	307.2 → 282.2	22	17
D_7-d18:0	309.2 → 291.2	28	18
D_7-t18:1	323.1 → 305.2	22	20
D_7-t18:0	325.1 → 289.2	22	20
d20:1 (IS)	328.1 → 310.2	18	22
d17:1-P (IS)	366.1 → 250.1	22	15
D_7-d18:0-P	389.1 → 291.1	30	15
D_7-t18:0-P	405.1 → 307.0	40	15
d18:1-10:0 (IS)	454.4 → 264.2	11	22
D_7-d18:0-16:1	545.6 → 273.3	45	35
D_7-d18:0-16:0	547.5 → 273.3	36	37
D_7-t18:1-16:0	561.5 → 269.3	30	30
D_7-t18:0-16:0	563.5 → 271.3	30	30
D_7-d18:1-18:1	571.5 → 269.2	30	30
D_7-d18:0-18:0	575.5 → 273.3	36	37
D_7-t18:1-22:0	645.6 → 269.3	35	40
D_7-t18:0-22:0	647.6 → 271.3	35	40
D_7-d18:0-24:0	659.7 → 273.3	45	36
D_7-t18:1-24:1	671.6 → 269.3	35	40
D_7-t18:1-24:0	673.6 → 269.3	35	40
D_7-d18:0-h24:1	673.6 → 273.3	30	30
D_7-t18:0-24:0	675.6 → 271.3	35	40
D_7-d18:0-26:0	687.7 → 273.3	43	35
D_7-t18:1-26:0	701.7 → 269.3	35	40
D_7-t18:0-26:0	703.7 → 271.3	35	40
D_7-d18:0-h26:0	703.7 → 273.3	30	30

Data processing was carried out with MassLynx V4.1 (Waters Corporation). The concentration of the analytes was based on the amount of material used and IS using reference factors (RFs) based on authentic reference materials available. RF stands for the correction factor of the respective analyte, C for the amount of material of the analytes or IS and A for the integrated area (area) of the signal analyte or internal standard:

$$RF_{\text{Analyte}} = \frac{C_{\text{Analyte}} * A_{\text{IS}}}{C_{\text{IS}} * A_{\text{Analyte}}}$$

The correction factor was calculated during the measurement of each experiment by a standard mix of sphingobases and ceramides (each of them concentrated at 300 ng/µL) and used for the evaluation of the respective experiment (**Table 25**). Since most of the ceramides measured in this work were not commercially available in contrast to sphingobases measured (**Table 7**), a RF adapted

from the structurally closest sphingolipid available for the quantification was used. Only an approximate quantification was possible regarding those sphingolipids. The unknown concentration of the analytes in the samples was determined taking into account the RF and the following formula:

$$C_{\text{Analyte (sample)}} = \frac{RF_{\text{Analyte}} * C_{\text{IS (sample)}} * A_{\text{Analyte (sample)}}}{A_{\text{IS (sample)}}} \; X \; \frac{1}{FW_{\text{(sample)}}}$$

The concentration of the analyte (C Analyte (sample)) was determined using the respective integrated area under the curve of the signal of the analyte (A Analyte (sample)) and internal standards (A IS (sample)) of the sample and the known concentration of the internal standard (C IS (sample)). The quantity of plant material was also used (fresh weight, FW (sample)) to determine the final concentration of the specific analyte. The volume of the sample solutions was used instead of the fresh weight for the measurement of treatment solutions.

2.2.4.3. Untargeted analysis.

UPLC-Quadrupole-Time-of-flight-MS

A chromatographic separation method of the analytes was performed first by ultra-performance liquid chromatography System (UPLC®, Waters Corporation, Milford, MA, USA) coupled to a SYNAPT G2 High-Definition Mass Spectrometry™ Quadrupole Time of flight-MS (HDMS™; TOF™; Waters Corporation, Eschborn, Germany).

Chromatographic separation

Reversed phase chromatography was performed at 60 °C with an ACQUITY UPLC® BEH C18 column (2.1 x 100 mm; particle size 1.7 µm; Waters Corporation) and with a VanGuard pre-column (BEH C18; 2.1 x 5 mm; particle size 1.7 µm; flow rate: 300 µL/min; Waters Corporation).
Eluent A and Eluent B are mentioned in **Table 21** and the solvent compositions for gradient elution of SPLs are displayed in **Table 22**. Autosampler UPLC® system temperature was 20 °C, the column temperature was 60 °C and the volume of samples injected was 8 µL.

Table 21: UPLC-ESI-TOF-MS Eluents

Eluent A:	40 % Acetonitrile v/v; 60 % H2O v/v; 10 mM Ammonium acetate
Eluent B:	10 % Acetonitrile v/v; 90 % Isopropanol v/v; 10 mM Ammonium acetate

Table 22: HPLC gradient for separation of sphingolipids

Time (min)	Flow (mL/min)	Eluent A (%)	Eluent B (%)
0.0	0.3	70	30
10.0	0.3	1	99
12.0	0.3	1	99
12.1	0.3	70	30
15.0	0.3	70	30

Quadrupole-Tof-MS conditions

After the chromatographic separation, lipophilic metabolites were ionized in positive and negative ESI mode and detected with a Time-of-flight Mass spectrometer. The conditions for ionization and fragmentation of sphingolipids were taken from Mueller *et al*. (2017). The general device settings are listed in **Table 23**.

Table 23: General parameters for electrospray ionization (ESI)

Ionization mode	+/-ES
Capillary voltage (kV)	1.8
Source temperature (°C)	120
Desolvation temperature (°C)	350
Cone gas flow - N_2 (L/h)	30
Desolvation gas flow - N_2 (L/h)	800

The quadrupole was operated in a wide-band RF mode, and data was acquired over the mass range of 50-1200 Da in the centroid data mode for 0.3 seconds. Leucine-enkephaline ($[M+H]^+$: m/z 556.2771 and $[M-H]^-$: m/z 554.2615) was used as a reference compound in the lock spray. The lock spray had a scan time of 0.3 seconds which allowed for continuous mass correction and the data format was maintained as centroid with mass error of below 5 ppm. Data was acquired in low energy function. Data processing was carried out with the help of the software MassLynx V4.1 and Progenesis® QI (Waters Corporation).

Progenesis® QI analysis

Progenesis QI is a small molecule discovery analysis software for high resolution mass spectrometer data to obtain reliable and definitive IDs for compounds. Data format was created as centroid data with a resolution of 13000. Ionization polarities checked were in positive and negative ESI mode with possible adducts obtained (**Table 24**). Data from the experiment was aligned according to their m/s and retention time (RT) and a list of compounds was obtained.

Table 24: Adducts checked during analysis

Positive ESI mode	Negative ESI mode
$[M+H+]^+$	$[M-H^+]^-$
$[M-H_2O+H+]^+$	$[M-H_2O-H^+]^-$
$[M+NH_4^+]^+$	$[M+Acetate^-]^-$
$[M+Na^+]^+$	

In order to reduce the list of identified compounds (peaks) found, filters were applied (P value < 0.05; Max fold changes > 1000; Present in all replicates and not present in control) and a restricted list of marker peaks was acquired.

Marker peak identification

The list of marker peaks obtained after the feeding with D_7-d18:0 experiment was compared against lipid databases of LCBs, LCBs-P, Ceramides, Ceramides-P, Hydroxy-Ceramides, Hydroxy-Ceramides-P, Glycosyl-Ceramides-FA, Glycosyl-Ceramides-Hydroxy-FA, GIPC-FA and GIPC-Hydroxy-FA (LCBs stands for Long-chain Bases, P for phosphate, FA for Fatty Acid and GIPC for Glycosyl Inositol PhosphoCeramide). Parameter of the blast was a difference of Molecular Mass ≤ 3 mDa.

To compare identified marker peaks obtained after the feeding with D_7-d18:0 experiment to other experiments performed in our lab, parameters were a difference of Molecular Mass ≤ 3 mDa and RT ≤ 0.2 min.

Table 25: Standard mix composition of IS

d17:1	d18:1-10:0
d17:1-P	d18:0-16:0
d18:1	t18:0-16:0
d18:1-P	d18:0-18:1
d18:0	d18:0-18:0
d18:0-P	d18:0-24:1
t18:0	d18:1-24:0
t18:0-P	d18:0-24:0
d20:1	t18:0-24:0

2.2.4.4. Statistical analysis.

Tukey-Kramer Post hoc Test

A one-way ANOVA is used to determine whether there is a statistically significant difference between the means of three or more independent groups. Tukey-Kramer test compares the mean between each pairwise combination of groups (Tukey, 1949). The test is performed in three steps:

- Find the absolute mean difference between each group
- Find the Q critical value
- Determine which group means are different

Values less than 0.05 were considered statistically significant.

3. Results.

3.1. Study of sphingolipids metabolism after infection by pathogens.

Sphingolipids have been shown to be bioactive metabolites involved in PCD during plant defense against pathogen infection (Dunn *et al*., 2004; Peer *et al*., 2010; Berkey *et al*., 2012; Markham *et al*., 2013; Magnin-Robert *et al*., 2015). Therefore, in this study, a number of sphingolipid biosynthesis mutant lines of *A. thaliana* were employed to investigate this aspect. In particular, various responses of the plant and the levels of sphingolipids were analyzed in response to pathogen infection in order to better understand the role that sphingolipids have in plant resistance, which still remains largely unknown.

3.1.1. Basal levels of sphingolipid contents in sphingolipid metabolism mutant lines.

As an initial step, sphingolipid basal levels in leaves of the different plant genotypes, including wild-type and mutant lines, were analyzed by UPLC-MS/MS. The chromatographic separation of the analytes, the detection and the quantification of the sphingolipids have been described in section 2. 2. 4. 2. Targeted analysis. The most abundant sphingobases and phosphorylated sphingobases detected by the instrument are presented in **Figure 4**. *A. thaliana* Col-0 sphingolipid levels that were detected in the experiments within this thesis were between 3 (t18:0, **Figure 4**, **C**) to 10 (d18:0, **Figure 4**, **A**) times inferior in comparison to the quantities that have been described in the literature (Markham and Jaworski, 2007; Shi *et al*., 2007). Likewise, lower levels of sphingobases and phosphorylated sphingobases contents were also detected in the sphingolipid biosynthesis mutant lines *spp1.1*, *spp1.2*, *lcbk1*, *lcbk2.1*, *lcbk2.2* and *sphk1*-KD (Dutilleul *et al*., 2012; Nakagawa *et al*., 2012). Similar results to the ones described in the literature were obtained with the mutant line *dpl1.1* (Magnin-Robert *et al*., 2015). Two double mutants never described before in the literature were used in this study: *dpl1.1* / *spp1.2* and *sphk1*-OE / *spp1.2*. Significantly higher levels of d18:0, d18:0-P, t18:0 and t18:0-P were observed in *dpl1.1* / *spp1.2* mutant line compared to Col-0 (**Figure 4**). Similar results were obtained with the *sphk1*-OE / *spp1.2* mutant line, with the exception of d18:0, which content remained in comparable levels to those of Col-0 (**Figure 4**, **A**). The less abundant sphingobases and phosphorylated sphingobases measured in the different *Arabidopsis* sphingolipid metabolism mutant lines are shown in **Annex 1**.

Sphingolipid basal levels were also measured by the same procedure. The most abundant long-chain fatty acid and very-long-chain fatty acid ceramides are displayed in **Figure 5**. Sphingolipid quantities in *A. thaliana* Col-0 ecotype were either in the same range as mentioned in the literature (**Figure 5**, **A** and **B**; Markham and Jaworski, 2007) or slightly higher (**Figure 5**, **C** and **D**). LCB-phosphatase mutant lines *spp1.1* and *spp1.2* contained two to five times higher sphingolipid levels than Col-0 (**Figure 5**). Similar observations were made among the LCB-kinase mutants *lcbk1* and *lcbk2.2*, as for example in the levels of t18:0-16:0 and t18:0-24:0 (**Figure 5**, **B** and **D, r**espectively). The single mutant *dpl1.2*, but not *dpl1.1* or the double mutant *dpl1.1* / *spp1*.2, also showed a higher accumulation of sphingolipids compared to Col-0. Furthermore, the double mutant *sphk1*-OE / *spp1.2* contained significantly higher levels of trihydroxy-LCBs ceramides in comparison with the wild-type Col-0 (**Figure 5**, **B** and **D**). The rest of sphingolipid basal levels measured are displayed in **Annexes 2** and **3**.

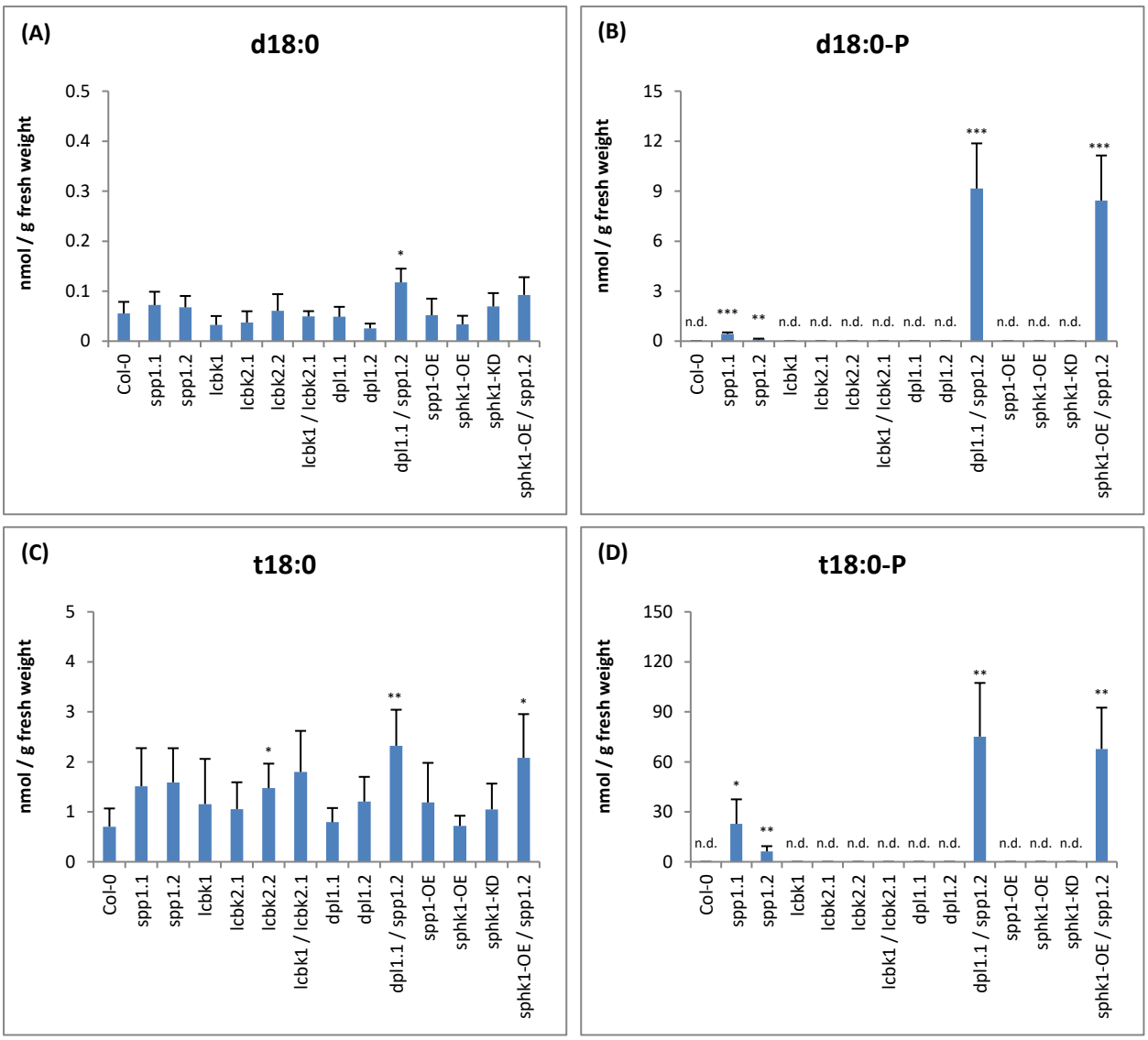

Figure 4: Sphingobase basal levels in *A. thaliana* ecotype Col-0 and *Arabidopsis* sphingolipid metabolism mutant lines. Sphingobases and phosphorylated sphingobases detected in six-week-old leaves of *A. thaliana* wild-type (Col-0) and *Arabidopsis* sphingolipid metabolism mutant lines. Levels were calculated by comparison to internal standards using correction factors (Section 2. 2. 4. 2. Targeted analysis) and presented as nano-mole per gram of fresh weight (nmol / g fresh weight). Asterisks indicate significant differences between Col-0 and the corresponding mutant line according to Student's *t*-Test: *, P < 0.05; **, P < 0.01; and ***, P < 0.001 (n.d. stands for non-detected). Results show means ± SD of four different technical replicates. The experiment has been repeated three times with similar results.

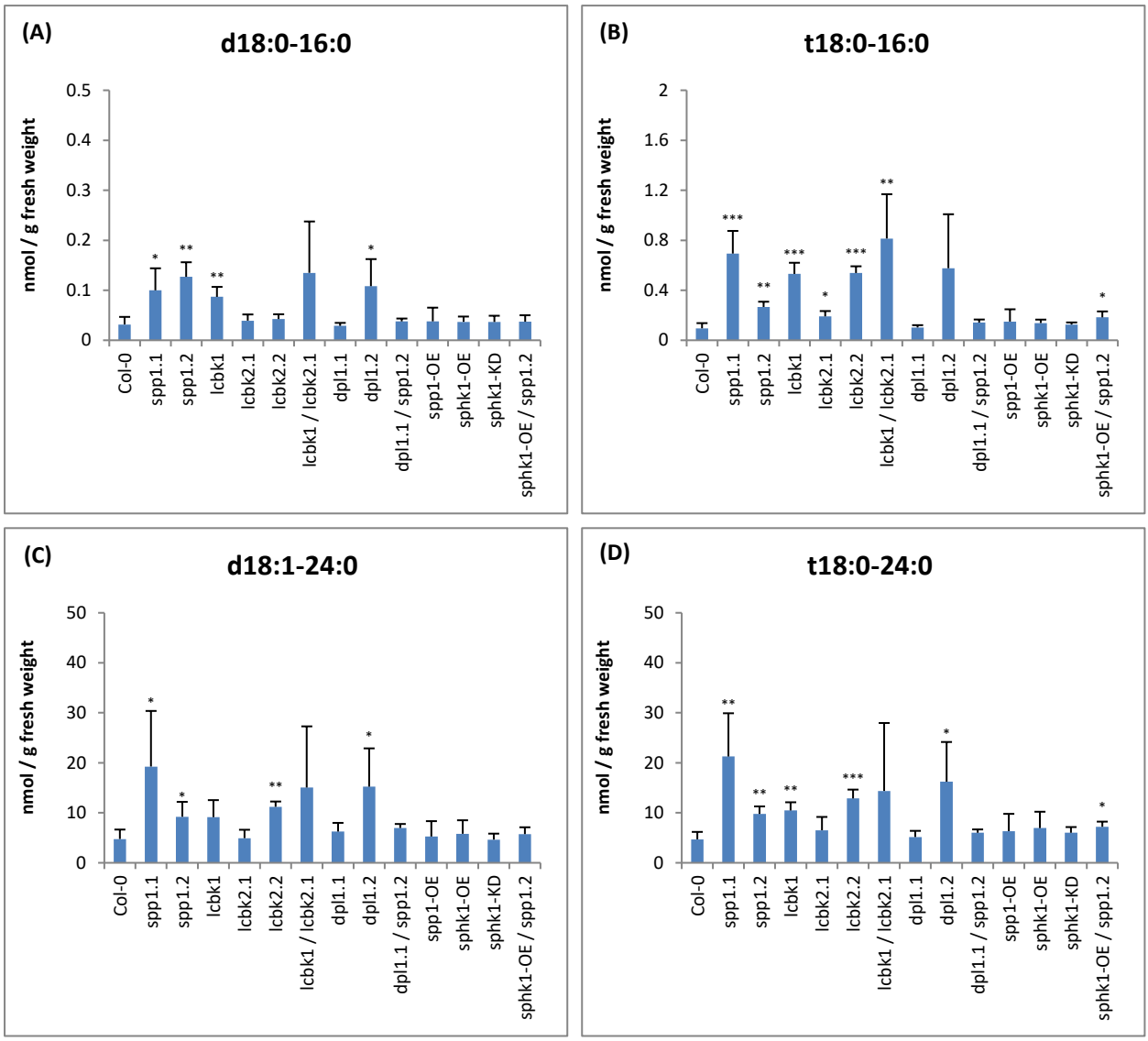

Figure 5: Long-chain fatty acid and very-long-chain fatty acid ceramide basal levels in *A. thaliana* ecotype Col-0 and *Arabidopsis* sphingolipid metabolism mutant lines. Long-chain fatty acid and very-long-chain fatty acid ceramides detected in six-week-old leaves of *A. thaliana* wild-type (Col-0) and *Arabidopsis* sphingolipid metabolism mutant lines. Levels were calculated by comparison to internal standards using correction factors (Section 2. 2. 4. 2. Targeted analysis) and presented as nano-mole per gram of fresh weight (nmol / g fresh weight). Asterisks indicate significant differences between Col-0 and the corresponding mutant line according to Student's *t*-Test: *, $P < 0.05$; **, $P < 0.01$; and ***, $P < 0.001$ (n.d. stands for non-detected). Results show means ± SD of four different technical replicates. The experiment has been repeated three times with similar results.

3.1.2. Study of *Arabidopsis* sphingolipid metabolism mutant lines after *P. syringae* infection.

Fluctuations in LCBs and LCBs-P contents have been shown to affect *Arabidopsis* tolerance and susceptibility to hemibiotrophic pathogens, such as the bacterium *P. syringae* (Magnin-Robert *et al*., 2015). The hypothesis of antagonism of PCD by LCB-Ps proposed in Magnin-Robert *et al.* (2015) has been refuted by Glenz *et al*. (2019). In this study, the authors showed that cell death depended predominantly on LCB levels. To further investigate this hypothesis, *A. thaliana* sphingolipid metabolism mutant lines, which accumulate either more LCBs or more LCB-Ps, were infected with *P. syringae.* Then, cell death was quantified by conductivity measurements and displayed with trypan blue staining. In addition, sphingolipids contents were quantified post-infection.

3.1.2.1. Cell death quantification after *P. syringae* infection.

In order to investigate the role of sphingolipids in the plant immune responses, cell death was quantified by measuring the electrolyte leakage (conductivity) of leaf discs from leaves infiltrated with $MgCl_2$ (control) or the pathogen *P. syringae pv. tomato* (*Pst*) *AvrRPM1* (**Figure 6**). The experimental procedure is described in section 2. 2. 2. 2. Pathogen assays *in planta*.
Previous results in this thesis have indicated that the mutant lines *dpl1.1* / *spp1.2* and *sphk1*-OE / *spp1.2* showed significantly higher accumulation of LCB and LCB-P under basal conditions (**Figure 4**) and, thus, they represented the most interesting cell lines to be investigated in this assay. In addition, the single mutant lines *dpl1.1*, *sphk1*-OE and *sphk1*-KD as well as Col-0 were tested in parallel.
In the control experiment (**Figure 6**, **A**), the percentages of relative cell death in the three mutant lines were not significantly different to Col-0 (referred as baseline). The observed variation of 0 to 5 % in the percentage of cell death is due to variations in the biological material from one experiment to another. Although not statistically significant (in comparison to wild-type), cell death quantified after *P. syringae* infection showed specific tendencies in the different genotypes **(Figure 6**, **B**). The mutant lines *dpl1.1*, *sphk1*-OE and the two double mutant lines *dpl1.1* / *spp1.2* and *sphk1*-OE / *spp1.2* exhibited between 12 to 18 % less cell death in comparison to Col-0. By contrast, the *sphk1*-KD mutant line exhibited the opposite tendency, with a higher cell death percentage than Col-0.
Cell death was then visually analyzed by staining leaves from Col-0, *dpl1.1*, *sphk1*-OE and *sphk1*-KD with trypan blue (**Annex 4**). In comparison to the control ($MgCl_2$-treated), cell death was higher in plants infected with *Pst AvrRPM1*. Nevertheless, in comparison to the previous conductivity experiments, this method did not allow to make distinctions between the different genotypes tested. Of note, the experiment was not performed with the two double sphingolipid metabolism mutant lines *dpl1.1* / *spp1.2* and *sphk1*-OE / *spp1.2*.

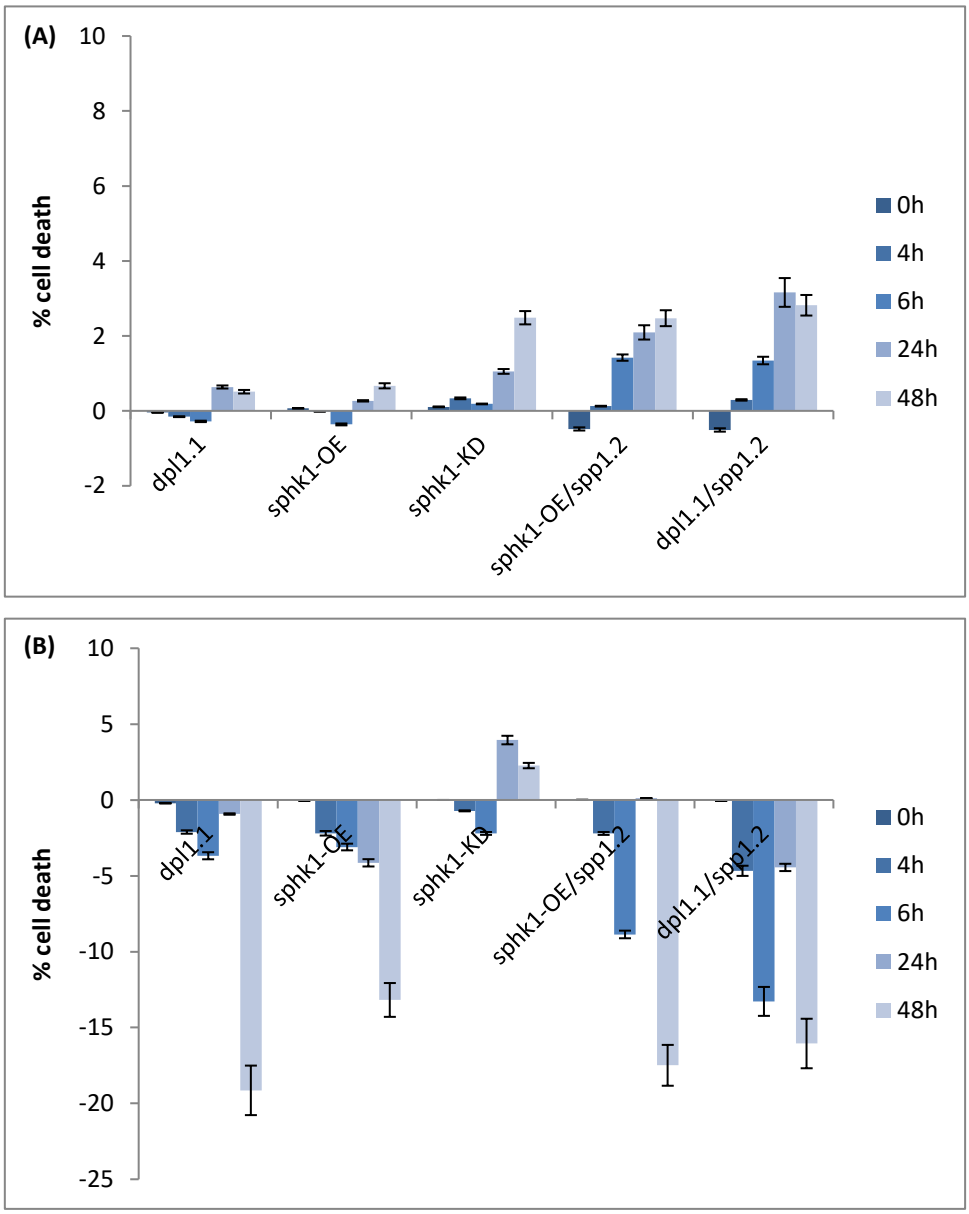

Figure 6: Relative cell death in *Arabidopsis* sphingolipid metabolism mutant lines after *P. syringae* infection. Cell death was quantified by electrolyte leakage measurements of leaf discs from leaves infiltrated with 10 mM $MgCl_2$ as control (A) or *Pst AvrRPM1* (B). Relative cell death (normalized to Col-0 data) using conductivity ($\mu S.cm^{-1}$) is shown for the solution containing leaf discs after infiltration. Results show means ± SE of four different technical replicates. The experiment was repeated four to ten times. No significant differences between Col-0 and the different sphingolipids metabolism mutant lines were found using the Student's *t*-Test: *, $P < 0.05$; **, $P < 0.01$; and ***, $P < 0.001$.

3.1.2.2. Sphingolipid analyses after *P. syringae* infection.

In order to establish a relationship between sphingolipid profile and cell death tendency and to investigate the hypothesis that cell death depends predominantly on the levels of LCBs, sphingolipid extraction and quantification were performed on the wild-type and the sphingolipid mutant lines during infection with *Pst AvrRPM1* (as explained in section 2. 2. 4.).

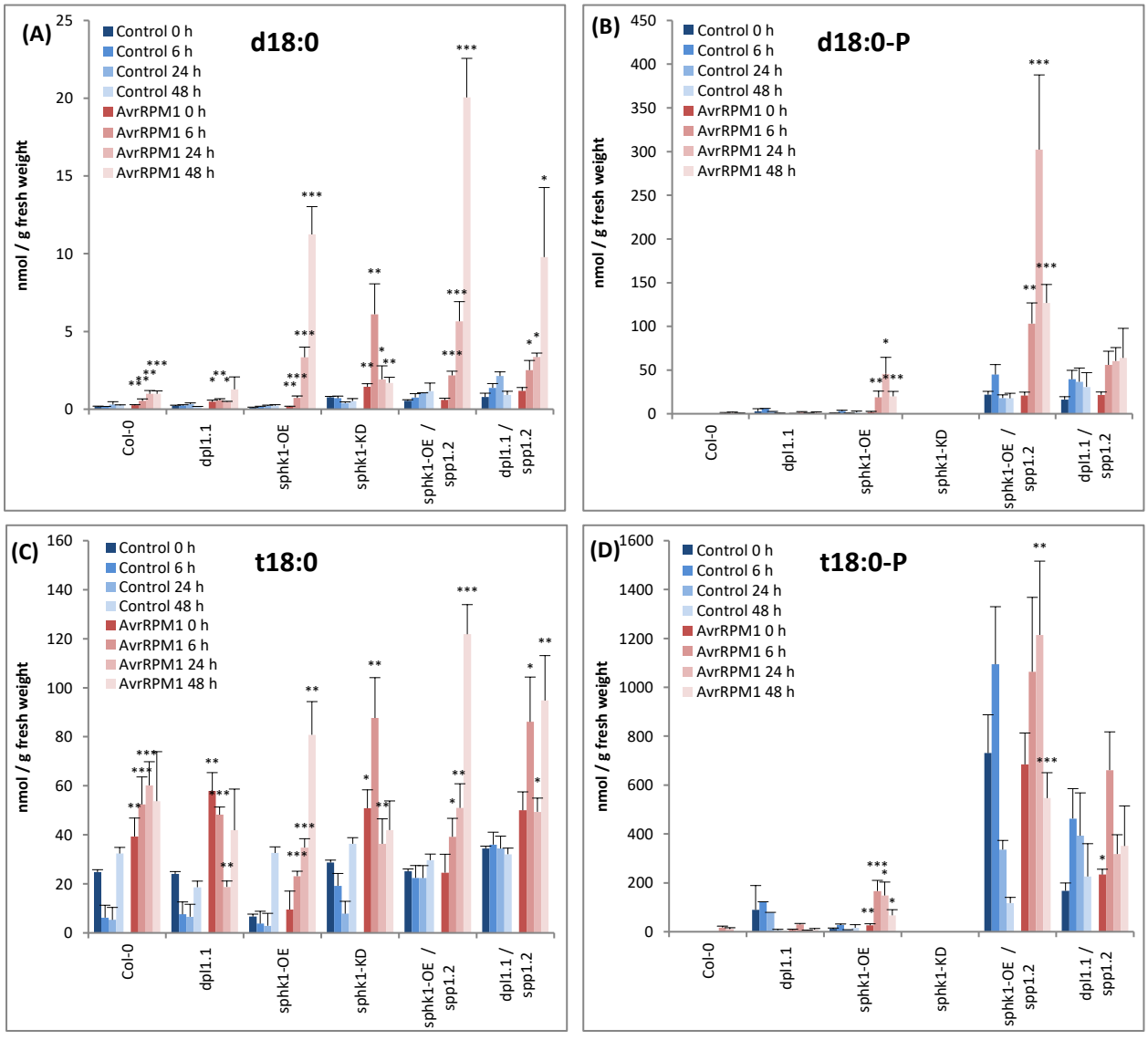

Figure 7: Free LCB and LCB-P accumulations after infection with *Pst AvrRPM1* in *Arabidopsis* sphingolipid metabolism mutant lines. Leaves of wild-type (Col-0) and sphingolipid metabolism mutant lines were infiltrated with 10 mM $MgCl_2$ (control) or *Pst AvrRPM1* bacteria solution. Quantification of LCBs (A and C) and LCB-Ps (B and D) was performed over time until 48 hpi. Asterisks indicate significant differences between control-treated samples and pathogen-treated samples according to Student's *t*-Test: *, $P < 0.05$; **, $P < 0.01$; and ***, $P < 0.001$. Results show means ± SD of four different technical replicates. The experiment was repeated three times with similar results.

Generally, *P. syringae* infection triggered a significant increase in the content of d18:0 and t18:0 between 0 h and 6 h post-inoculation in all the genotypes tested (**Figure 7**, respectively **A** and **C**). Phosphorylated sphingobases were particularly accumulated in *sphk1*-OE, *dpl1.1* / *spp1.2* and *sphk1*-OE / *spp1.2* mutant lines after *P. syringae* infection (**Figure 7**, **B** and **D**). Detection of phosphorylated sphingobases, especially t18:0-P, was possible in Col-0 only at later time points after infection (**Figure 7**, **D**).

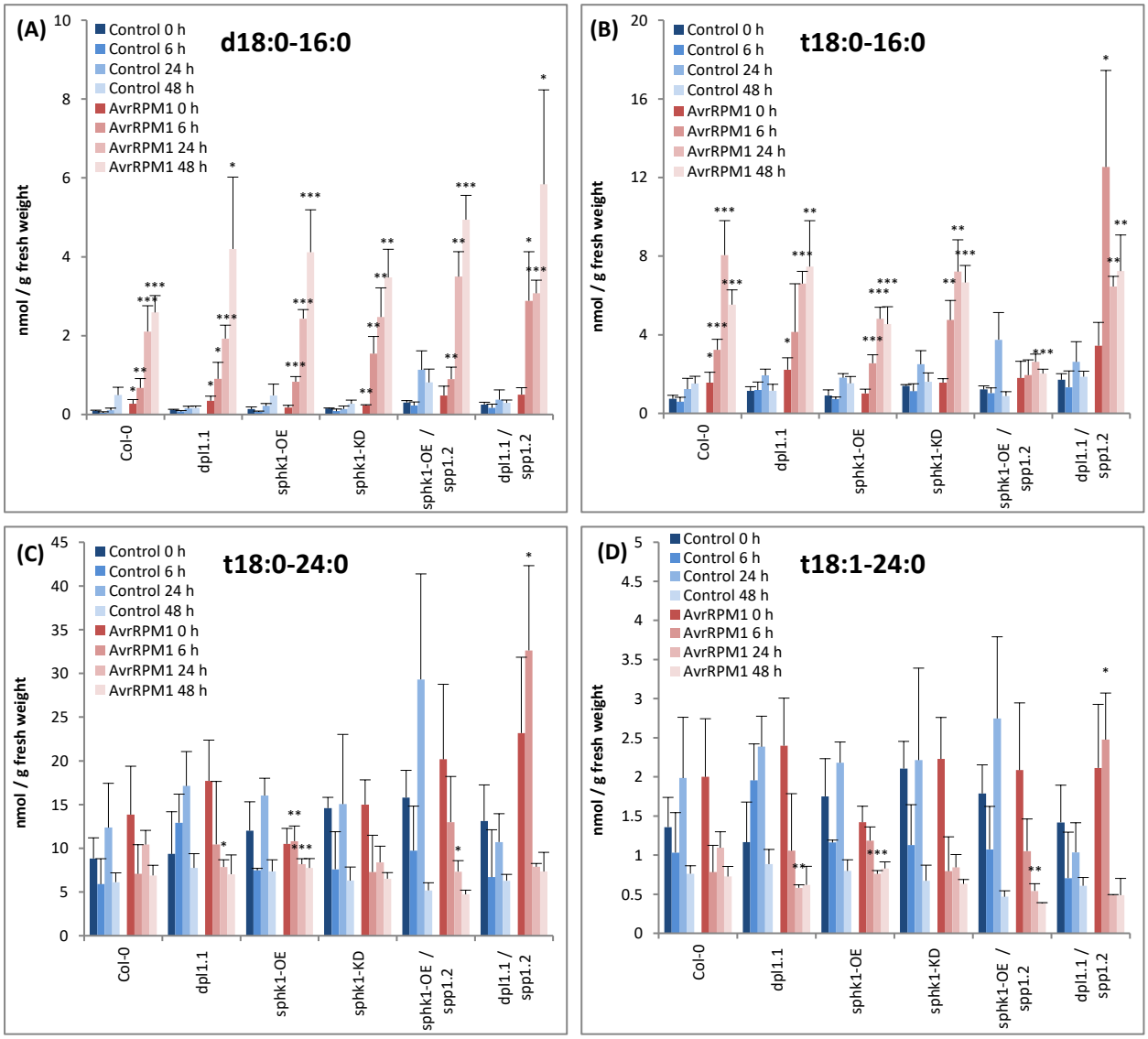

Figure 8: Long-chain fatty acid and very-long-chain fatty acid ceramide accumulations after infection with *Pst AvrRPM1* in *Arabidopsis* sphingolipid metabolism mutant lines. Leaves of wild-type (Col-0) and sphingolipid metabolism mutant lines were infiltrated with 10 mM $MgCl_2$ (control) or *Pst AvrRPM1* bacteria solution. Ceramide quantifications were performed over time until 48 hpi. Asterisks indicate significant differences between control-treated sample and pathogen-treated samples inside the same genotype according to Student's *t*-Test: *, $P < 0.05$; **, $P < 0.01$; and ***, $P < 0.001$. Results show means ± SD of four different technical replicates. The experiment was repeated three times with similar results.

Levels of the most abundant long-chain fatty acid and very-long-chain fatty acid ceramides are shown in **Figure 8**. It can be observed that infection by *Pst AvrRPM1* bacteria induced a significant increase in long-chain fatty acid ceramides, such as d18:0-16:0 and t18:0-16:0, in all the genotypes tested (**Figure 8**, **A** and **B**). No significant variations in the levels of very-long-chain fatty acid ceramides were found in Col-0 and *sphk1*-KD. A strong accumulation of trihydroxy sphingobase with very-long-chain fatty acid ceramides was detected in *dpl1.1* / *spp1.2* double mutant 6 h post-inoculation (**Figure 8**, **C** and **D**). Significant decreases in t18:0-24:0 and t18:1-24:0 were found in the mutant lines *dpl1.1*, *sphk1*-OE and *sphk1*-OE / *spp1.2* at 24 h post-inoculation (**Figure 8**, **C** and **D**).

In comparison to the levels of trihydroxy sphingobase with VLCFA ceramides, ten times less accumulation of dihydroxy sphingobase with VLCFA ceramides was detected in all the mutants tested (**Figure 9**). Also in this case, no variations were detected in the wild-type Col-0 and *sphk1*-KD over time. A strong accumulation of d18:0-24:0 and d18:1-24:0 was detected in *dpl1.1* / *spp1.2* double mutant 6 h post-inoculation while a significant decrease was observed in *dpl1.1* single mutant 24 h post-infection (**Figure 9**). An increase in d18:0-24:0 content and a decrease in d18:1-24:0 content were observed in *sphk1*-OE and *sphk1*-OE / *spp1.2*, respectively (**Figure 9**, respectively **A** and **B**). The rest of sphingolipids measured after *Pst AvrRPM1* infection are displayed in the **Annex 5**.

To conclude, at the late stage of the experiment (48 h), less cell death was observed in the mutant lines *dpl1.1*, *sphk1*-OE, *sphk1*-OE / *spp1.2* and *dpl1.1* / *spp1.2* in comparison to Col-0 after *Pst AvrRPM1* infection (**Figure 6**). In these lines, higher quantities not only of LCBs but also LCB-Ps and sphingolipids were detected upon infection (**Figure 7** and **8**). Therefore, this suggests that the cell death observed might not be dependent only on the levels of LCBs.

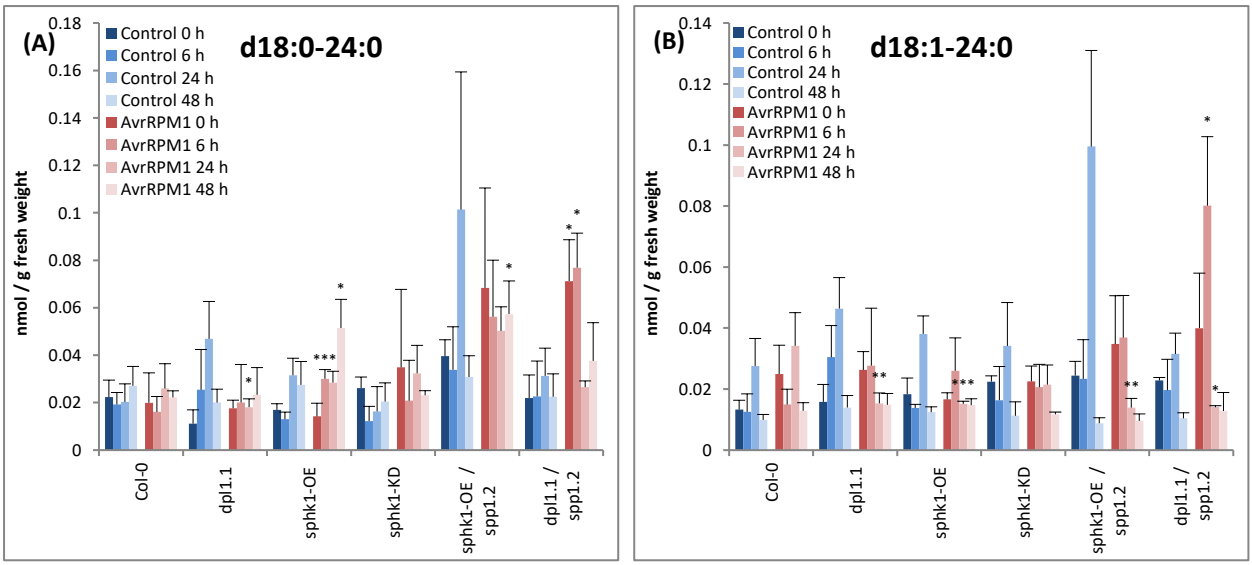

Figure 9: Very-long-chain fatty acid ceramide accumulations after infection with *Pst AvrRPM1* in *Arabidopsis* sphingolipid metabolism mutant lines. Leaves of wild-type (Col-0) and sphingolipid metabolism mutant lines were infiltrated with 10 mM $MgCl_2$ (control) or *Pst AvrRPM1* bacteria solution. Ceramide quantification was performed over time until 48 hpi. Asterisks indicate significant differences between control-treated sample and pathogen-treated samples inside the same genotype according to Student's *t*-Test: *, $P < 0.05$; **, $P < 0.01$; and ***, $P < 0.001$. Results show means ± SD of four different technical replicates. The experiment was repeated three times with similar results.

3.1.3. Study of *Arabidopsis* sphingolipid metabolism mutant lines in response to *V. longisporum* infection.

The hypothesis on this part of the thesis was in the same line as the one previously evoked regarding the infection by *P. syringae* and the fact that PCD is mainly dependent on the levels of LCBs. The vascular fungal pathogen *V. longisporum* was used in this study to investigate the impact of sphingolipid metabolism on its spread in the model plant *A. thaliana*. On one hand, phenotypical assays were first performed to examine the spread of the pathogen, which was then quantified by determining green leaf areas and leaves weight. On the other hand, sphingolipids quantities were analyzed post-infection.

3.1.3.1. Cell death after *V. longisporum* infection.

In order to investigate the role of sphingolipids in plant immune responses, root infection by *V. longisporum* was performed and cell death spread was analyzed. The experimental procedure is described in detail in section 2. 2. 2. 2. Pathogen assays *in planta*. The mutant line *cyp79 b2/b3*, an *Arabidopsis* glucosinolate mutant, was tested in parallel as control, since it has been already shown that this mutant is highly susceptible to infection by this pathogen (Iven *et al*., 2012). After visual examination of the plants, cell death symptoms were observed in several leaves as yellowish areas three weeks post-inoculation with *V. longisporum* in all the genotypes analyzed (**Figure 10**). However, no morphological distinctions between Col-0 and the different sphingolipid metabolism mutant lines tested could be observed. A significant decrease in green rosette areas was observed after inoculation with the pathogen in all the lines in comparison to the control plants (non-infected), with the exception of the mutant line *sphk1*-OE / *spp1.2*, which remained unchanged (**Figure 11**, **A**). Similar results were obtained when weighting the rosettes three weeks after infection (**Figure 11**, **B**). In both assays, *cyp79 b2/b3* showed the strongest pathogen-induced decrease in green rosette areas and rosette fresh weight compared to the control plants.

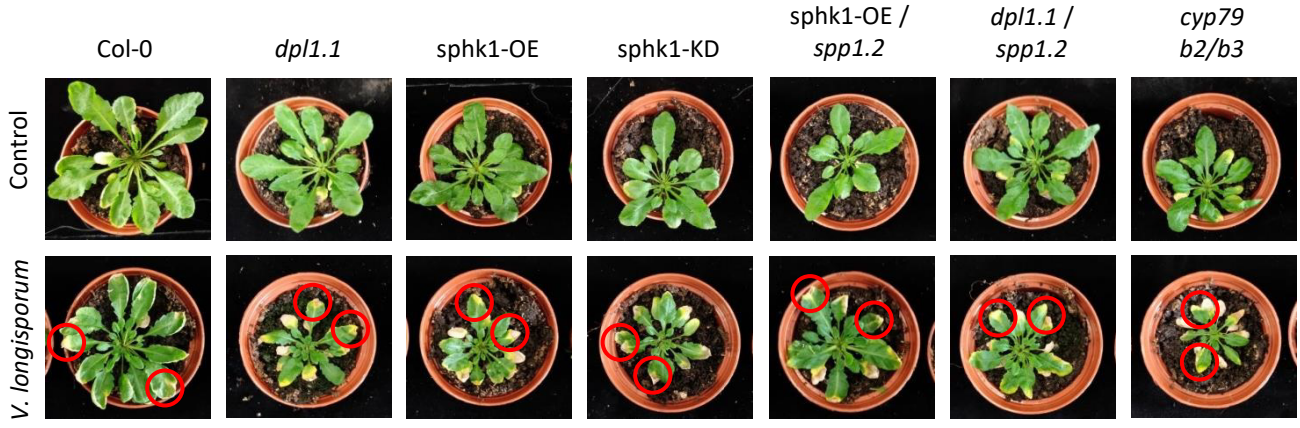

Figure 10: Cell death symptoms in *Arabidopsis* sphingolipid metabolism mutant lines after *V. longisporum* infection. Three-week-old plant roots of wild-type (Col-0), *Arabidopsis* sphingolipid metabolism mutant lines and a susceptible mutant line to *V. longisporum* (*cyp79 b2/b3*) were incubated with H_2O (control) or *V. longisporum* (pathogen-treatment solution) for 1 h. Plants were potted into soil and analyzed three weeks post-infection. Representative plants are shown. Cell death symptoms are circled in red. No macroscopic differences were observed between Col-0 and the other mutant lines.

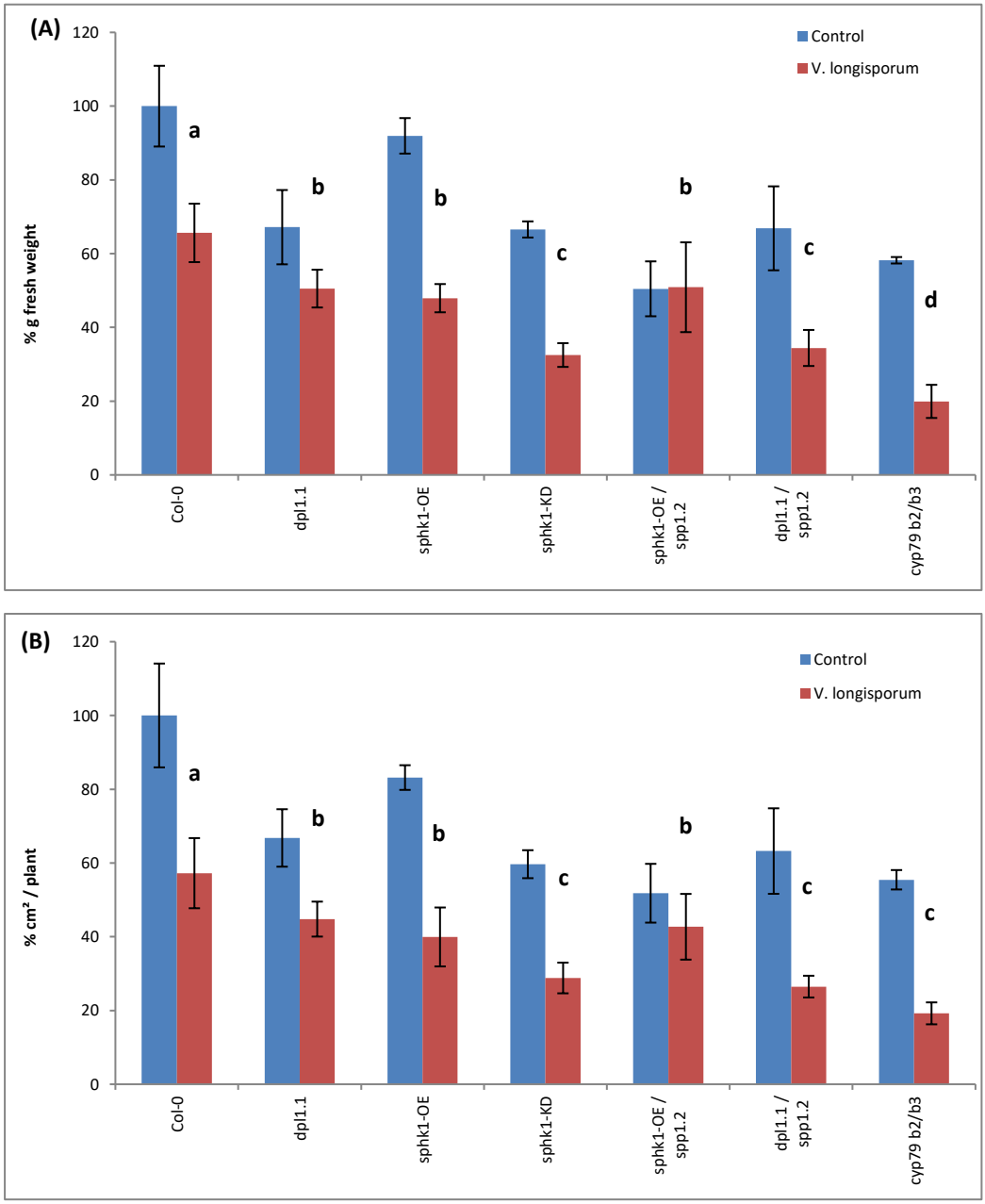

Figure 11: Green rosette areas and rosette fresh weight in *Arabidopsis* sphingolipid metabolism mutant lines after *V. longisporum* infection. Six-week-old rosettes were weighted three weeks after infection by *V. longisporum* (A). Green areas of six-week-old rosettes of wild-type (Col-0), *Arabidopsis* sphingolipid metabolism mutant lines and a susceptible mutant line to *V. longisporum* (*cyp79 b2/b3*) were determined three weeks after infection by *V. longisporum* (B). Different letters indicate statistical differences according to Tukey-Kramer-test value 4.54 (A) and 5.54 (B). Studentized range critical value 0.05, 9.76 (A) and 0.26 (B). Results show means ± SD of five technical replicates. The experiment was repeated two times with similar results.

3.1.3.2. Quantification of *V. longisporum* infection.

The spread of *V. longisporum* within the plants was analyzed by quantifying the expression of *OLG70* and *OLG71* genes by qPCR (Eynck *et al*., 2007). The procedure followed is described in section 2. 2. 3. 4. Quantitative Polymerase Chain Reaction, and results are presented in **Figure 12**. The relative gene expression of *V. longisporum* was set to 1 for Col-0. The mutant line *cyp79 b2/b3* had significantly higher levels of fungal DNA in the rosette in comparison to Col-0. Similar results were obtained for *sphk1*-OE, *sphk1*-KD, *sphk1*-OE / *spp1.2* and *dpl1.1* / *spp1.2 Arabidopsis* sphingolipid metabolism mutant lines. No significant changes of fungal DNA content in *dpl1.1* were observed.

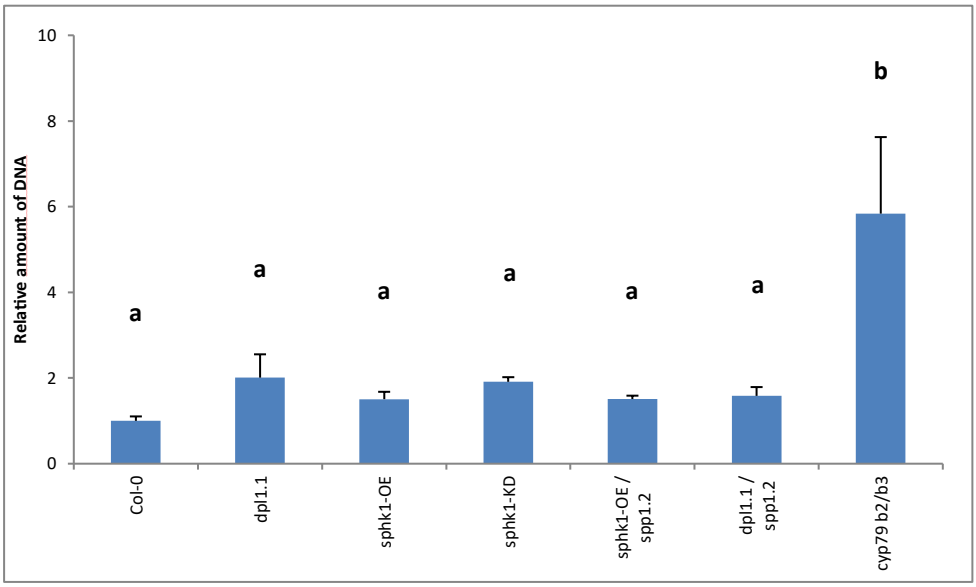

Figure 12: Relative amount of *V. longisporum* DNA in *Arabidopsis* sphingolipid metabolism mutant lines. *V. longisporum* was quantified by qPCR 21 days after pathogen infection in leaves of wild-type (Col-0), *Arabidopsis* sphingolipid metabolism mutant lines and a susceptible mutant line to *V. longisporum* (*cyp79 b2/b3*). Different letters indicate statistical differences according to Tukey-Kramer-test value 4.74. Studentized range critical value 0.05, 1.53. Results show means ± SD of four technical replicates and are representative of two independent experiments.

3.1.3.3. Sphingolipid analysis after *V. longisporum* infection.

In order to correlate a sphingolipids profile to the cell death observations previously made, sphingolipids extraction and quantification were performed (as described in section 2. 2. 4. Analytic Methods) three weeks after infection by *V. longisporum*. Results are presented in **Figure 13** and **Figure 14**.

Free LCB levels of d18:0 and t18:0 were significantly higher in *sphk1*-KD, *sphk1*-OE / *spp1.2*, *dpl1.1* / *spp1.2* and *cyp79 b2/b3* (**Figure 13**, respectively **A** and **C**). The quantity of t18:0, but not d18:0, was also higher in *dpl1.1* as compared to wild-type Col-0 (**Figure 13**, **C**). Importantly, a strong accumulation of phosphorylated sphingobases, d18:0-P and t18:0-P, was detected in the two double mutant lines *sphk1*-OE / *spp1.2* and *dpl1.1* / *spp1.2* (**Figure 13**, **B** and **D**).

The most abundant ceramides detected are shown in **Figure 14**. Significant increases in t18:0-16:0 in *sphk1*-OE / *spp1.2* (**Figure 14**, **A**), t18:1-26:0 in *cyp79 b2/b3* (**Figure 14**, **B**), t18:0-24:0 in *dpl1.1* (**Figure 14**, **C**) and t18:1-24:0 in *dpl1.1* and *dpl1.1* / *spp1.2* (**Figure 14**, **D**) were detected. No other significant differences were found among the other genotypes after infection. The rest of sphingolipids detected after *V. longisporum* infection are displayed in **Annex 6**.

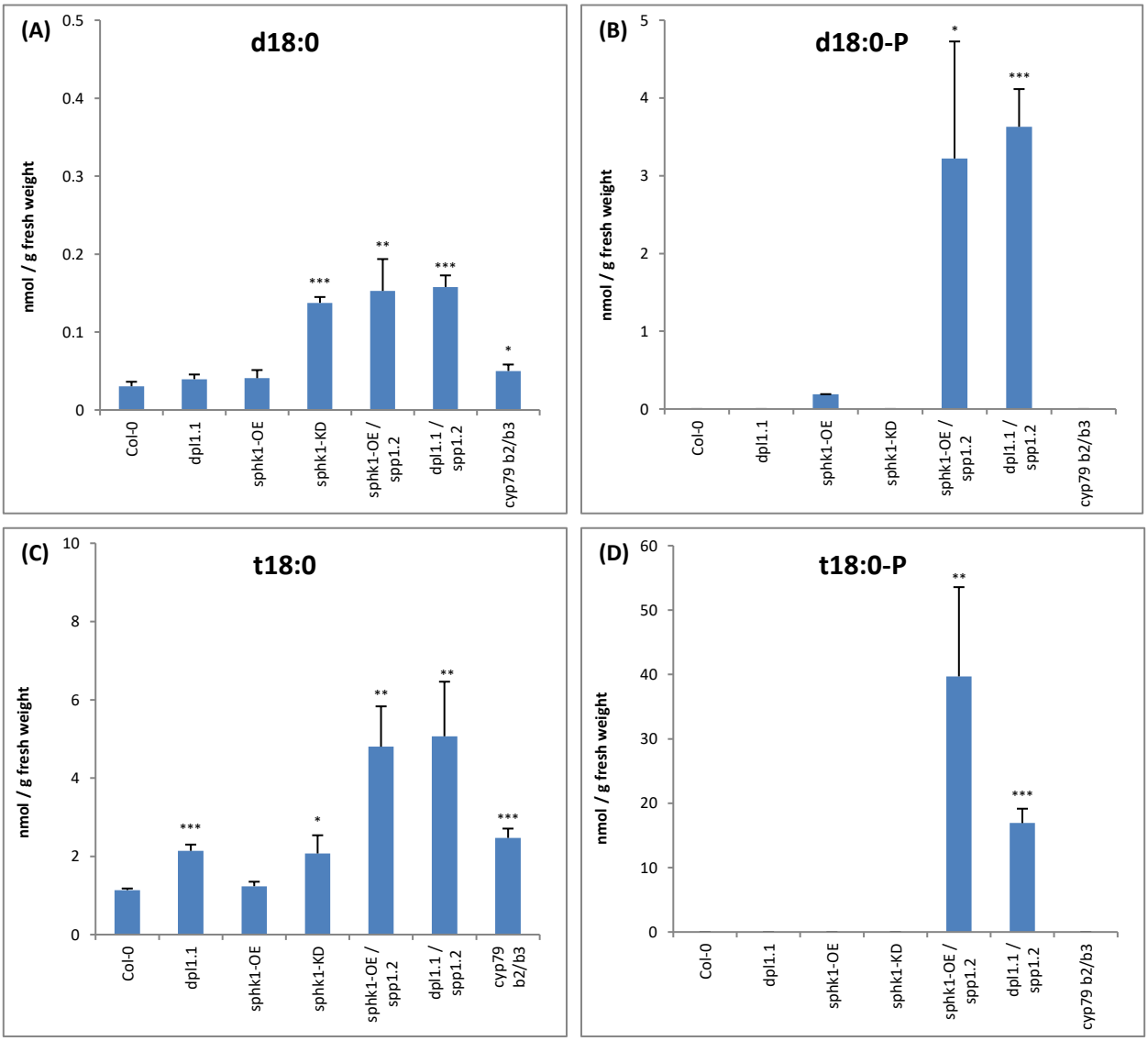

Figure 13: Free LCB and LCB-P accumulation after infection with *V. longisporum* in *Arabidopsis* sphingolipid metabolism mutant lines. Roots of wild-type (Col-0), sphingolipid metabolism mutant lines and the susceptible line *cyp79 b2*/*b3* were infected with $2*10^6$ spores/mL of fungi solution. LCB and LCB-P quantifications were performed three weeks post-infection in rosettes. Asterisks indicate significant differences between pathogen-treated Col-0 sample and the other pathogen-treated mutant lines samples according to Student's *t*-Test: *, $P < 0.05$; **, $P < 0.01$; and ***, $P < 0.001$. Results show means ± SD of three different technical replicates.

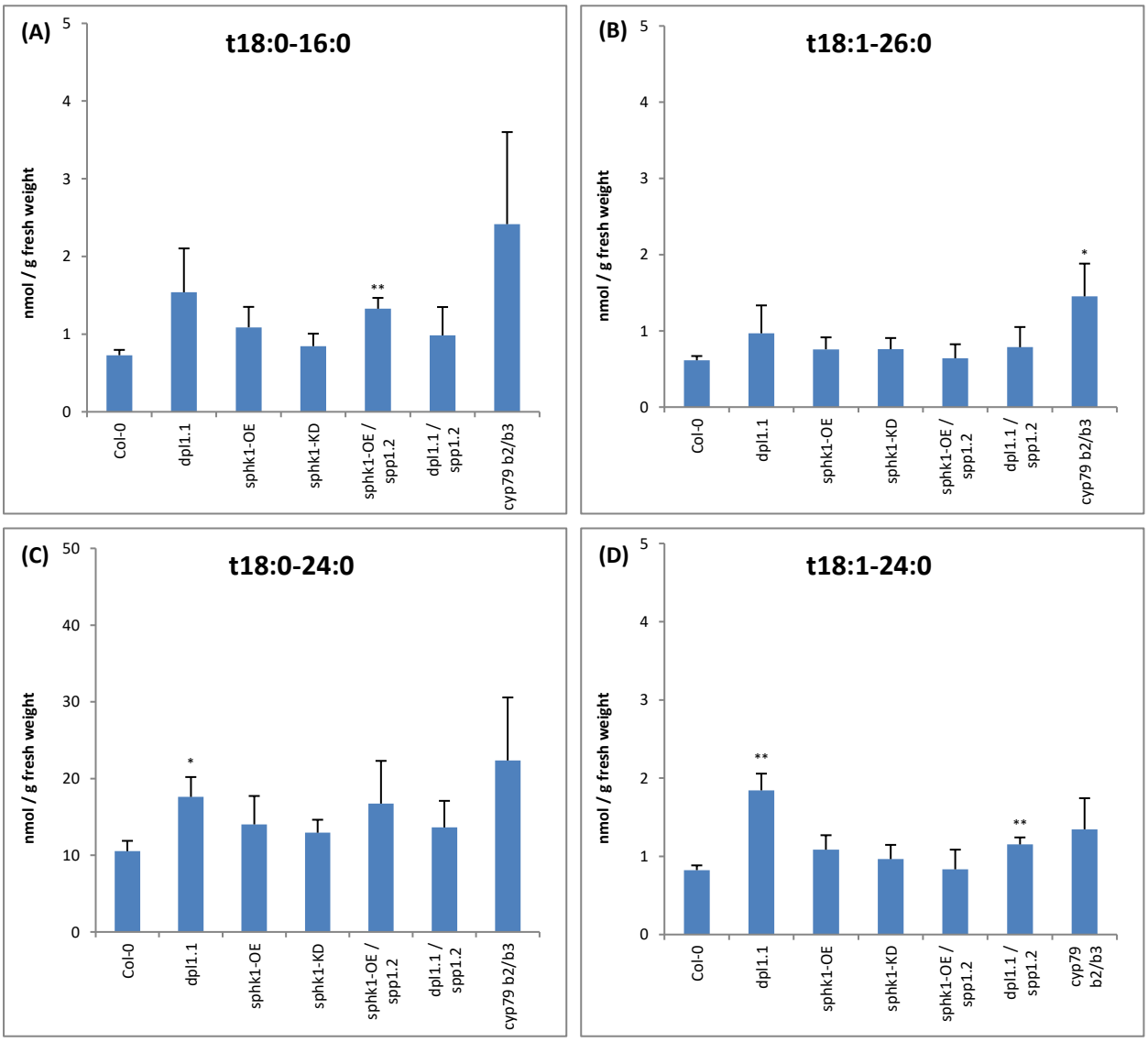

Figure 14: Long-chain fatty acid and very-long-chain fatty acid ceramides accumulation after infection with *V. longisporum* in *Arabidopsis* sphingolipid metabolism mutant lines. Roots of wild-type (Col-0), sphingolipid metabolism mutant lines and the susceptible line *cyp79 b2/b3* were infected with $2*10^6$ spores/mL of fungi solution. Ceramide quantification was performed three weeks post-infection in rosettes. Asterisks indicate significant differences between pathogen-treated Col-0 sample and the other pathogen-treated mutant lines samples according to Student's *t*-Test: *, $P < 0.05$; **, $P < 0.01$; and ***, $P < 0.001$. Results show means ± SD of three different technical replicates.

To conclude, all the mutant lines tested have been affected macroscopically by the infection of *V. longisporum*, except for the double mutant line *sphk1*-OE / *spp1.2* (**Figure 10** and **11**). Significant higher levels of both LCBs and LCB-Ps were detected in several mutant lines tested in comparison to Col-0 (**Figure 13**). Therefore, these data suggests that the cell death observed might not only be dependent on the level of LCBs.

3.2. Study of the effect of temperature on sphingolipid metabolism.

Plants are sessile organisms that need to evolve and adapt to changes affecting their surrounding environment, such as fluctuation of temperature. It has been shown that in order to survive to variations in temperature, plants modify their metabolism and perform structural remodeling and adaptation of membrane lipids (Dutilleul *et al*., 2012; Mittler *et al*., 2012; Huang *et al*., 2017). These modifications restrain plant growth and development rate but can potentially ensure survival. However, it is not well known which SPLs species are regulated upon temperatures change and whether these changes are required for plant survival or fitness under such conditions. Previous results with *A. thaliana* wild-type plants suggested that the content of some SPL species changes during temperature fluctuations. Therefore, in this study, the profile of sphingolipid metabolism mutant lines, defective in LCBs / SPLs regulation, was investigated in response to heat shock, cold and heat acclimation. These lines have been tested to find out if their genotype could lead to different SPL level changes upon temperature changes and / or are functionally required for the adaptation to different temperatures. The procedures followed are explained in section 2. 2. 1. 4. Temperature-related experiments. Sphingolipids were measured following the treatments, as mentioned in section 2. 2. 4. Analytic methods.

3.2.1. Study of sphingolipids metabolism mutant lines after heat shock.

3.2.1.1. Survival rate.

First, survival rate studies were performed employing Col-0 and the different sphingolipid metabolism mutant lines after heat shock at 45 °C for 90 min. As control, the survival rate of the lines was tested in parallel at 22 °C. Col-0 survival rate, which was approximately 70 %, indicated a significant decrease in the number of green seedlings after heat shock and was in agreement with unpublished data previously obtained in the laboratory (**Figure 15**). In addition, heat shock also affected the survival rate of the seedlings from the different sphingolipid metabolism mutant lines tested. Significant decreases, ranging from 41 % for the *dpl1.1* / *spp1.2* line to 78 % for the *dpl1.1* line, were observed. A survival rate of 64 % was observed for the mutant line *sphk1*-KD, although no statistical difference could be defined for this result.

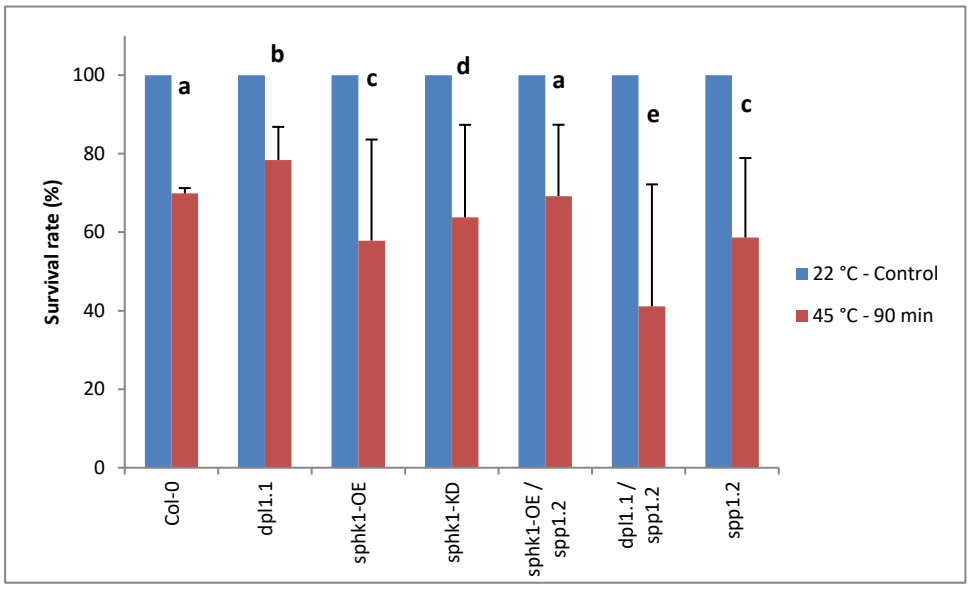

Figure 15: Survival rate of non-acclimated *A. thaliana* wild-type (Col-0) and *Arabidopsis* sphingolipid metabolism mutant lines after heat shock at 45 °C. Two-week-old seedlings of wild-type (Col-0) and sphingolipid metabolism mutant lines were incubated either at 22 °C for control or at 45 °C for heat shock for 90 min. After this period, seedlings were again incubated at 22 °C for two additional weeks. Survival rate was determined by counting green seedlings out of a total of 300. Different letters indicate statistical differences according to Tukey-Kramer-test value 4.83. Studentized range critical value 0.05, 1.56. Results show means ± SD of three different technical replicates. The experiment was repeated two times with similar results.

3.2.1.2. Study of sphingolipids levels after heat shock.

Heat shock is perceived by the plants as a stress, which could trigger structural rearrangements, such as the production or use of sphingolipids. The results in this thesis showed that, among the genotypes tested, only *sphk1*-OE showed a significant increase in d18:0 content after heat shock. On the contrary, a decrease in d18:0 content by as much as half was measured in *sphk1*-KD (**Figure 16**, **A**). Significant increases in the production of d18:0-P and t18:0 in both Col-0 and *sphk1*-OE seedlings, as well as t18:0-P in *sphk1*-OE seedlings, were detected after heat shock (**Figure 16**, **B**, **C** and **D,** respectively). Decreases in d18:0-P and t18:0 contents in the double mutant lines *sphk1*-OE / *spp1.2* and *dpl1.1* / *spp1.2* were observed (**Figure 16**, **B** and **C**, respectively). No drastic variations in long-chain base and phosphorylated long-chain bases were detected in the other sphingolipid metabolism mutant lines.

Ceramide analysis showed an increase in the content of the long-chain fatty acid sphingolipid d18:0-16:0 for Col-0, *dpl1.1*, *sphk1*-OE, *sphk1*-KD and *spp1.2* (**Figure 17**, **A**), and in the content of t18:0-16:0 for Col-0, *dpl1.1*, *sphk1*-OE and *sphk1*-KD (**Figure 17**, **B**). A slight decrease in t18:0-16:0 was observed for *sphk1*-OE / *spp1.2*, *dpl1.1* / *spp1.2* and *spp1.2*. Decreases in the contents of the very-long-chain fatty acid ceramides t18:0-24:0 and t18:0-26:0 were detected in the genotypes Col-0, *sphk1*-KD, *sphk1*-OE / *spp1.2*, *dpl1.1* / *spp1.2* and *spp1.2* after heat shock (**Figure 17**, **C** and **D**, respectively). Comparable decreases were obtained upon analysis of the following sphingolipids: t18:1-16:0, t18:1-22:0, t18:1-24:0, t18:0-24:1, t18:1-24:1, t18:1-26:0, d18:1-24:0 and d18:0-24:0 (**Annex 7**). No significant variations in the levels of those SPLs were detected in *dpl1.1* and *sphk1*-OE mutant lines. The rest of the sphingolipids measured are displayed in **Annex 7**.

To conclude, the heat shock treatment affected the SPL levels of all the genotypes tested (**Figure 15**). Exposure to a temperature of 45 °C did not affect LCBs and LCB-Ps levels, except for the mutant line

sphk1-OE for which the levels of LCBs, LCB-Ps but also d18:0-16:0 and t18:0-16:0 were increased (**Figure 16** and **17**). Some of the mutant lines exhibited decreases in SPLs after treatment (**Figure 17**). Other metabolites than the ones measured, such as triacylglycerols (as described in Mueller *et al.*, 2017) might be playing a more relevant role in the resistance or response of plants to high temperature.

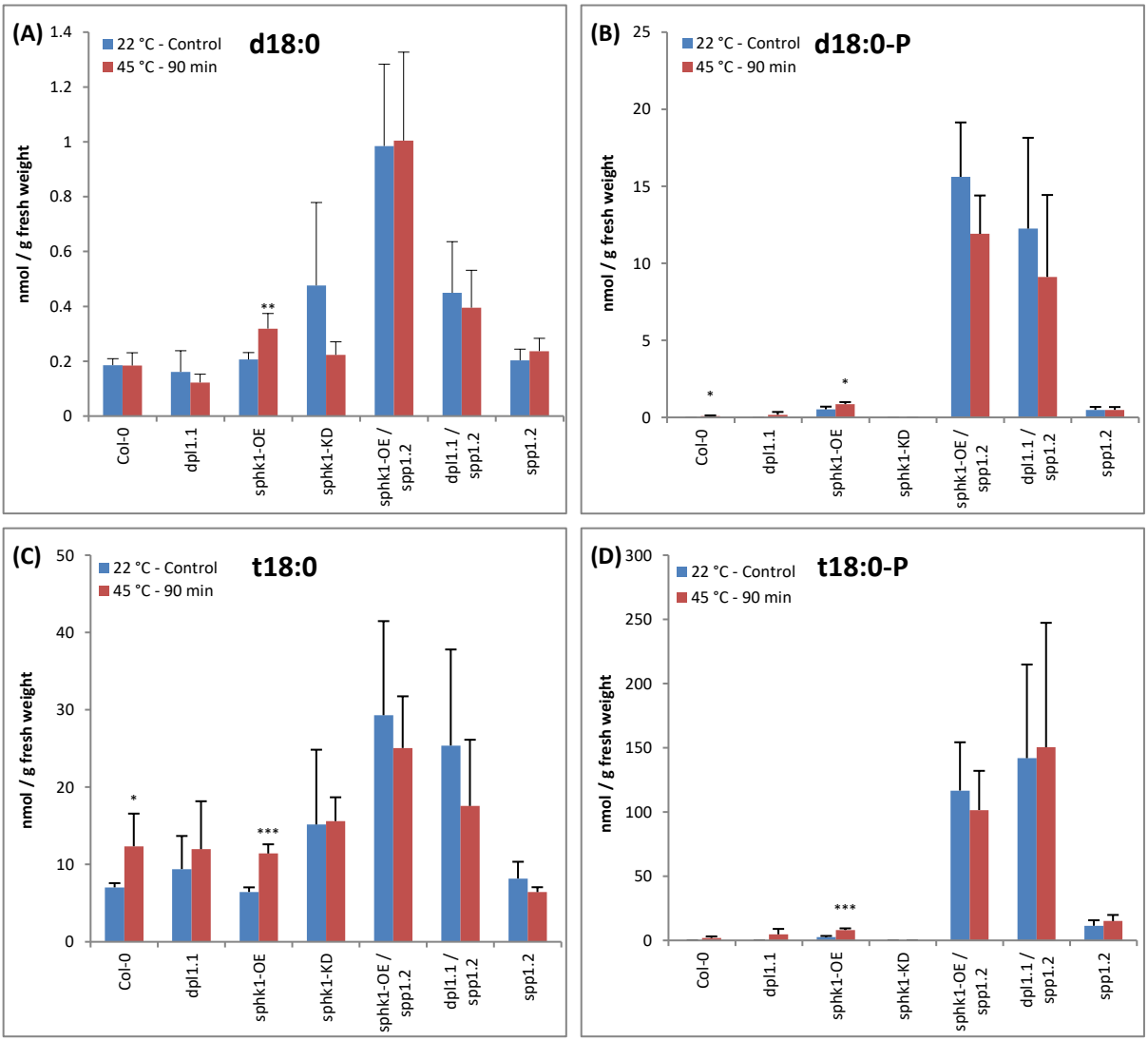

Figure 16: Free LCB and LCB-P accumulation after heat shock at 45 °C of *A. thaliana* wild-type (Col-0) and *Arabidopsis* sphingolipid metabolism mutant lines. Two-week-old seedlings of wild-type (Col-0) and sphingolipid metabolism mutant lines were incubated either at 22 °C for control or at 45 °C for heat shock. Free LCB and LCB-P quantification were measured after 90 min. Asterisks indicate significant differences between control-incubated samples and heat shock-incubated samples according to Student's *t*-Test: *, $P < 0.05$; **, $P < 0.01$; and ***, $P < 0.001$. Results show means ± SD of four different technical replicates. The experiment was repeated two times with similar results.

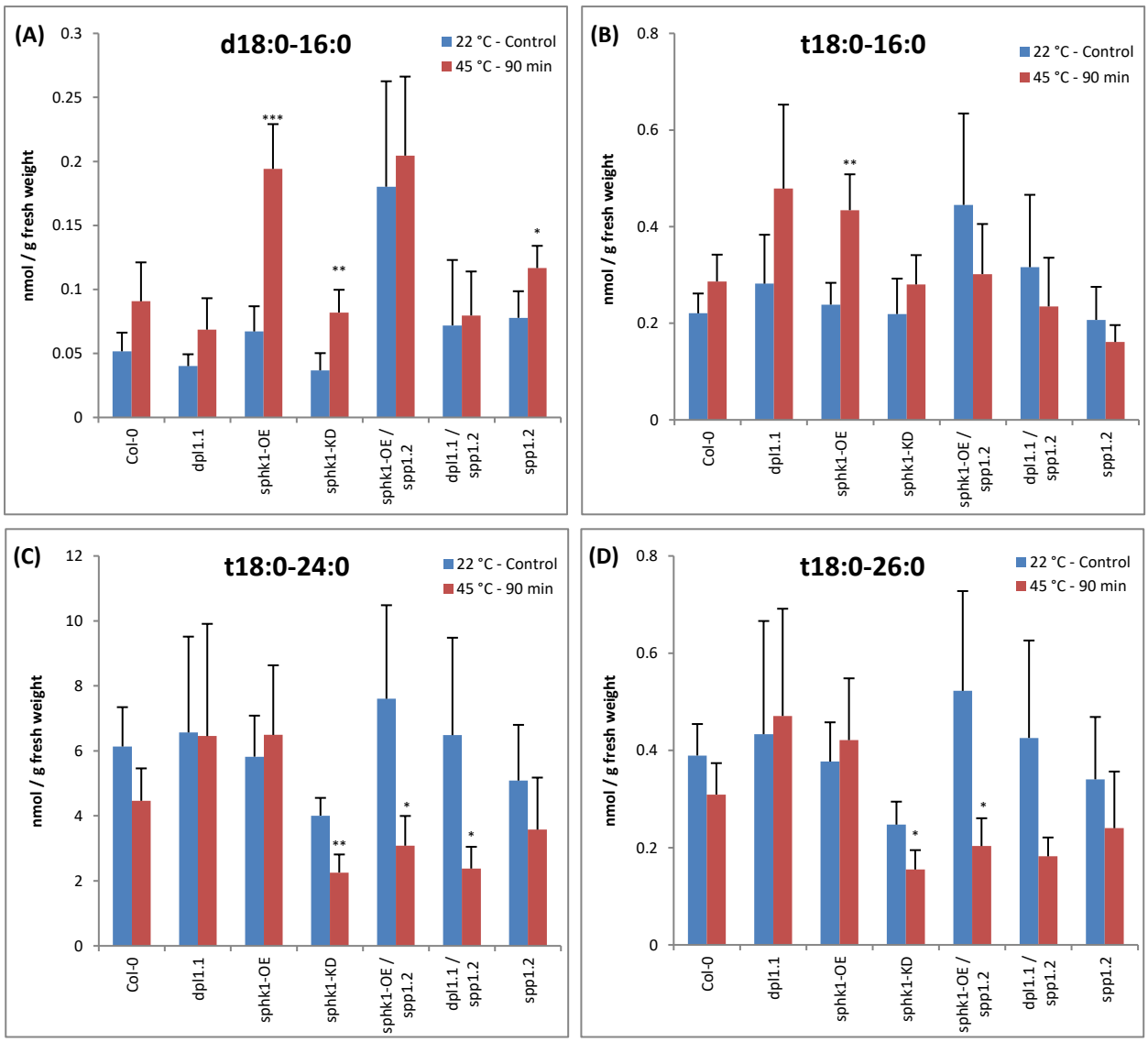

Figure 17: Long-chain and very-long-chain fatty acid ceramides accumulation after heat shock at 45 °C of *A. thaliana* wild-type (Col-0) and *Arabidopsis* sphingolipid metabolism mutant lines. Two-week-old seedlings of wild-type (Col-0) and sphingolipid metabolism mutant lines were incubated either at 22 °C for control or at 45 °C for heat shock. Long-chain and very-long-chain fatty acid ceramides quantification were measured after 90 min. Asterisks indicate significant differences between control-incubated samples and heat shock-incubated samples according to Student's *t*-Test: *, $P < 0.05$; **, $P < 0.01$; and ***, $P < 0.001$. Results show means ± SD of four different technical replicates. The experiment was repeated two times with similar results.

3.2.2. Study of sphingolipid metabolism mutant lines after cold and heat acclimation.

In order to define a sphingolipids profile during abiotic stresses, Col-0 and some sphingolipid metabolism mutant lines with deficiency in LCBs and LCB-Ps regulation were analyzed during cold and heat acclimation. The idea was to measure sphingolipid levels among those genotypes while avoiding lethal treatment conditions. Cold acclimation was represented by incubation at 10 °C, whereas heat acclimation was represented by incubation at 37 °C. Both treatments were performed

over the course of one week after two weeks of growth at 22 °C. Then, phenotypes were examined, and sphingolipid levels analyzed.

3.2.2.1. Phenotypical results.

Average seedling development after seven days of incubation at the different temperatures indicated are presented in **Figure 18**. In basal conditions (control, 22 °C), a notable difference could be observed regarding the germination rate: *sphk1*-KD presented a germination rate of 40 to 50 %, whereas the other genotypes tested (col-0, *sphk1*-OE and *sphk1*-OE / *spp1.2*) exhibited germination rates close to 100 %. Survival rate in the different incubation conditions remained unchanged over time among all the genotypes.
Regarding heat acclimation, some differences in the seedlings growth of plates incubated at 37 °C could be observed for the genotypes *sphk1*-OE, *sphk1*-KD and *sphk1*-OE / *spp1.2* in comparison to the control plates incubated at 22 °C. Seedlings were more bent with bigger cotyledons and longer first leaves than those from control plates were present. Regarding cold acclimation, seedlings from plates incubated at 10 °C were phenotypically unchanged in comparison to the seedlings in control plates incubated at 22 °C.

3.2.2.2. Study of sphingolipid levels during heat and cold acclimation.

In order to examine how the quantity of sphingolipids varies in response to early temperature changes exposure, a first experiment of short-term adaption (0 to 24 h incubation) was performed at 37 °C with wild-type ecotype Col-0. Significant accumulations of d18:0, t18:0, d18:0-P, t18:0-P, d18:0-16:0 and t18:0-16:0 were observed in Col-0 plants. Results are showed in **Annex 8**.
During long-term temperature acclimation, sphingobase and phosphorylated sphingobase contents were modified in the different mutant lines tested (**Figure 19**). No drastic variations neither in d18:0 nor t18:0 contents were observed at 22 °C during the incubation time (**Figure 19**, **A**; **Annex 9**). In contrast, at 37 °C, significantly higher levels of d18:0 were detected in several lines after 24 h. In addition, the transition peak detected after 24 h returned to basal level at day 3 or day 7. Acclimation to 10 °C did not markedly affect the concentration of d18:0 detected, with the exception of the double mutant *sphk1*-OE / *spp1.2*, which exhibited significantly high levels of this sphingobase even after 7 days of incubation.
Significant, although transient, increases in d18:0-P levels were observed in Col-0 after 24 h incubation for the two different temperature acclimations (**Figure 19**, **B**). Regarding the double mutant line *sphk1*-OE / *spp1.2*, notable decreases in d18:0-P (**Figure 19**, **B**), t18:0-P and t18:1-P levels (**Annex 9**) were observed over time at 22 °C and 37 °C. In contrast, at 10 °C, phosphorylated sphingobases remained unaltered over time.
Variations in the amount of long-chain fatty acid and very-long-chain fatty acid ceramides were also examined during this experiment. Significant increases were detected in the molecules d18:0-16:0, t18:0-16:0, t18:1-16:0 d18:0-18:0, t18:0-22:0, d18:0-24:0, d18:0-26:0 and t18:0-26:0 in the different mutant lines over time at 37 °C (examples for d18:0-16:0 and d18:0-26:0 are shown in **Figure 20**; examples for other molecules are shown in **Annex 10**). The other sphingolipids measured remained unaltered over time at 37 °C (**Annex 10**).
As a general observation, regarding the seedlings incubated at 10 °C, only minor or no variations were observed for all genotypes tested over time in comparison to control incubation (**Figure 20**). The rest of sphingolipids measured are shown in **Annex 9**.

To conclude, despite the fact that the genotypes *sphk1*-OE, *sphk1*-KD and *sphk1*-OE / *spp1.2* presented bigger seedlings in the plates incubated at 37 °C in comparison to control, no clear link to a sphingolipids profile could be established. Indeed, Col-0 presented the same range of increases in the LCBs, LCB-Ps and SPLs than the three other mutant lines but no phenotypical difference compared to control. At 10 °C, the seedlings remained phenotypically unchanged in comparison to control. This last observation is in line to unchanged sphingolipid levels measured for all the genotypes.

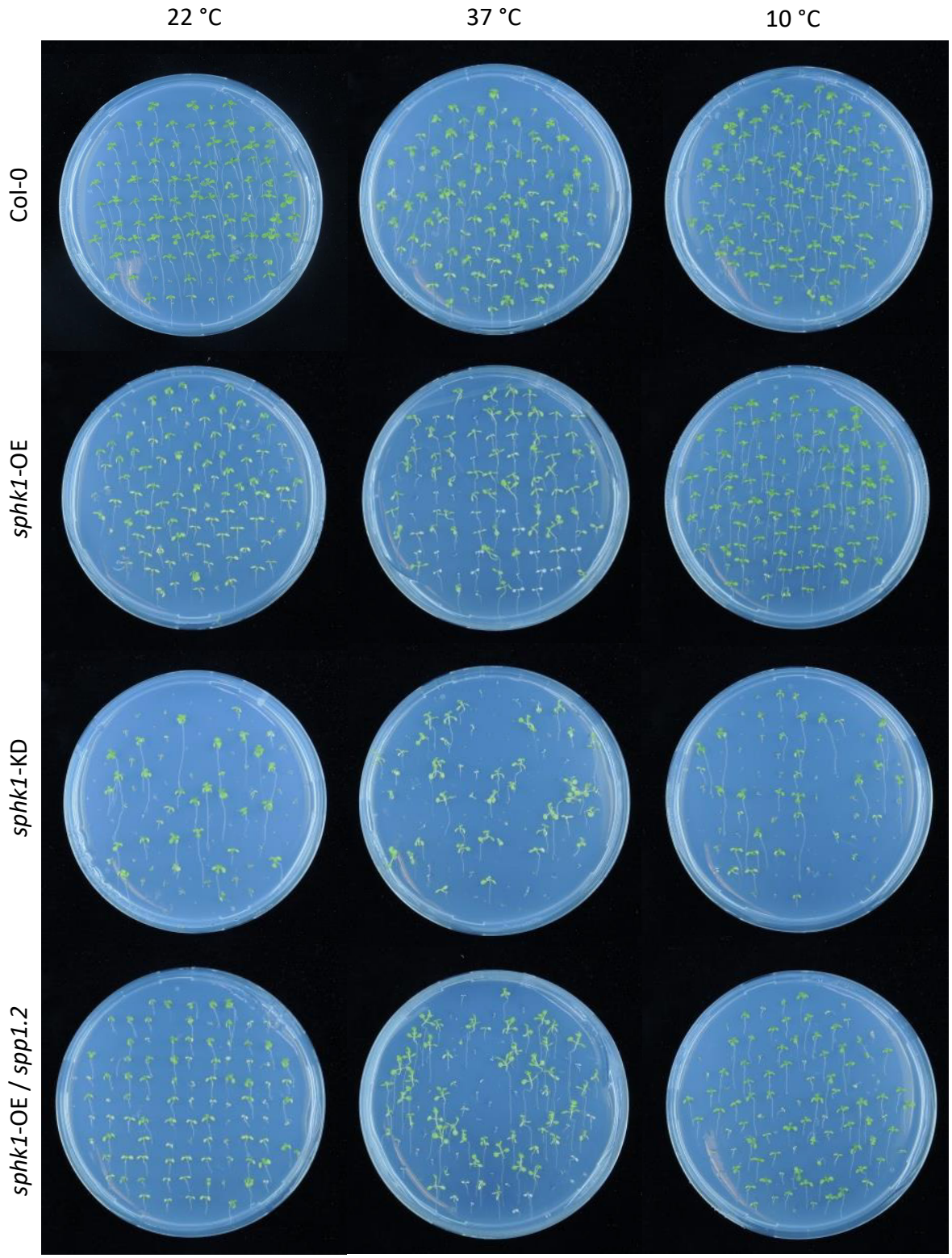

Figure 18: Growth differences in *A. thaliana* ecotype Col-0 and *Arabidopsis* sphingolipid metabolism mutant lines in response to temperature changes. Two-week-old wild-type (col-0), *sphk1*-OE, *sphk1*-KD and *sphk1*-OE / *spp1.2* seeds were grown on MS plates at 22 °C. Then, plates were transferred to 22 °C, 37 °C or 10 °C to grow for an additional week. Four plates per treatment and genotype were tested. One representative plate per genotype is shown.

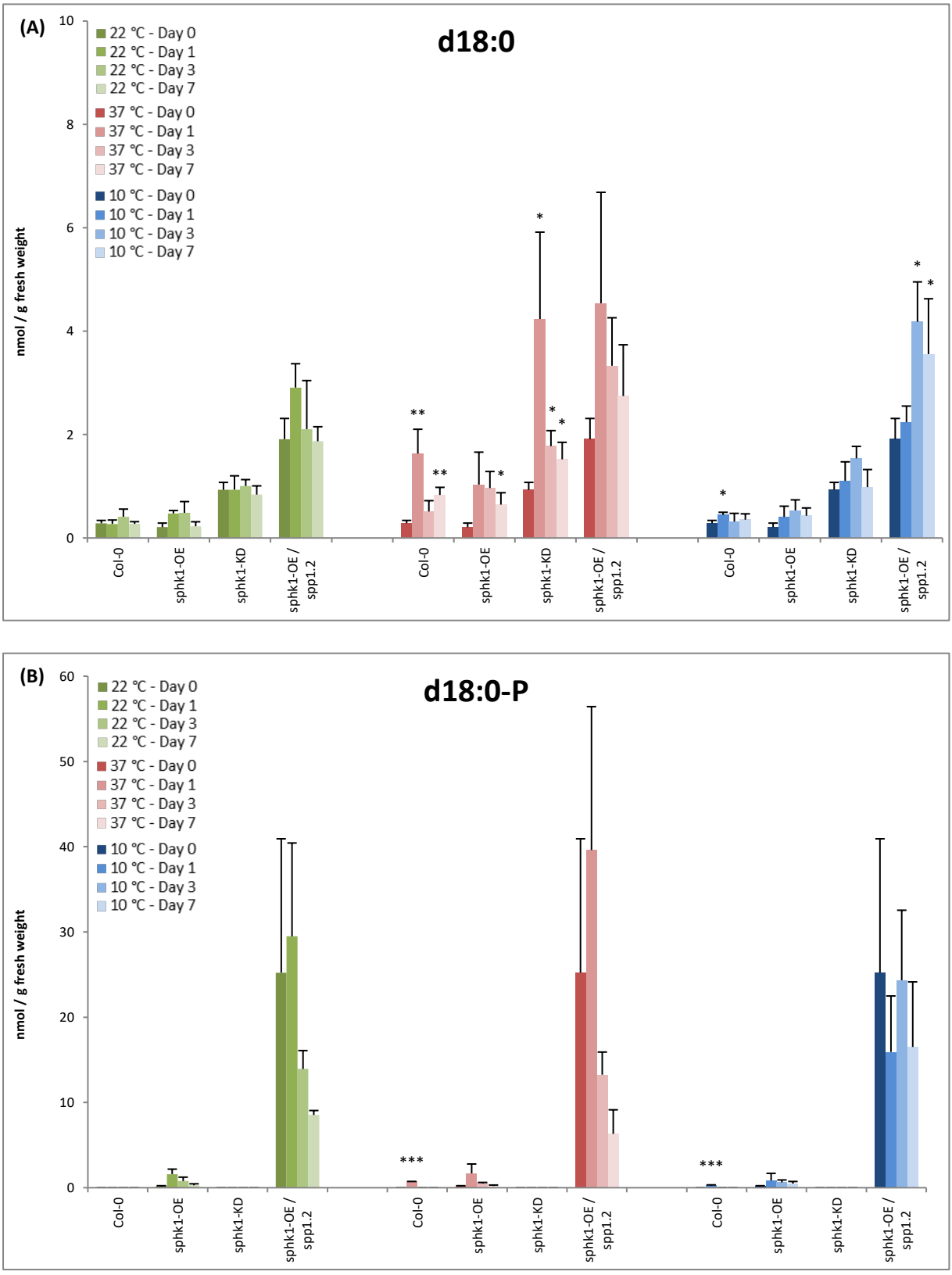

Figure 19: Free LCB and LCB-P accumulation in *A. thaliana* wild-type (Col-0) and *Arabidopsis* sphingolipid metabolism mutant lines in response to incubation at different temperatures. Two-week-old seedlings of wild-type (Col-0) and *Arabidopsis* sphingolipid metabolism mutant lines were incubated either at 22 °C for control, 37 °C for heat adaptation or 10 °C for cold adaptation. LCBs (A) and LCB-Ps (B) were measured at day 0, 1, 3 and 7. Asterisks indicate significant differences between control-incubated and heat-incubated samples or between control-incubated and cold-incubated samples for each genotype according to Student's *t*-Test: *, $P < 0.05$; **, $P < 0.01$; and ***, $P < 0.001$. Results show means ± SD of four different technical replicates.

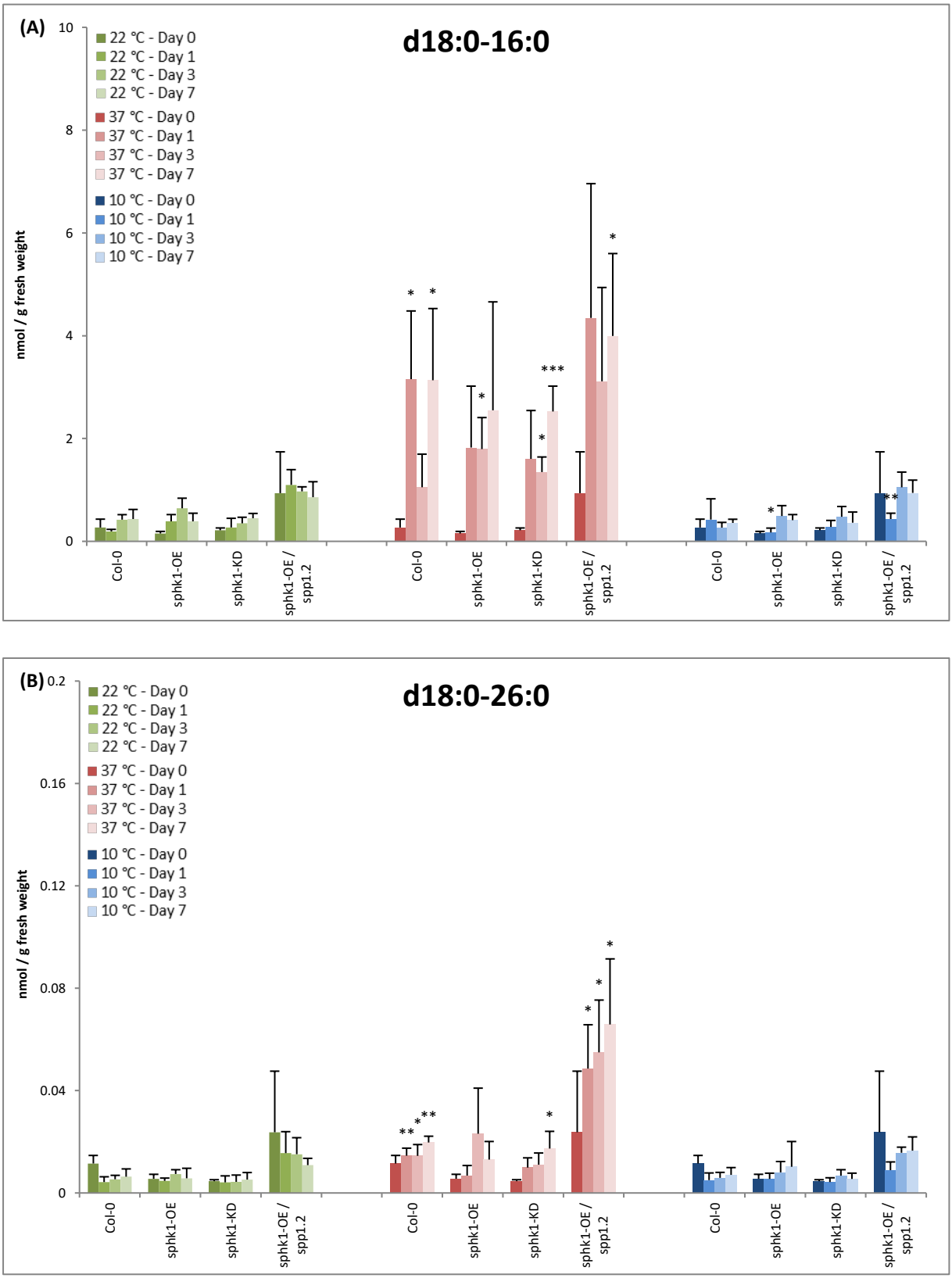

Figure 20: Ceramide accumulation in *A. thaliana* wild-type (Col-0) and *Arabidopsis* sphingolipid metabolism mutant lines in response to incubation at different temperatures. Two-week-old seedlings of wild-type (Col-0) and *Arabidopsis* sphingolipid metabolism mutant lines were incubated either at 22 °C for control, 37 °C for heat adaptation or 10 °C for cold adaptation. The quantities of d18:0-16:0 (A) and d18:0-26:0 (B) were measured at day 0, 1, 3 and 7. Asterisks indicate significant differences between control-incubated and heat-incubated samples or between control-incubated and cold-incubated samples according to Student's *t*-Test: *, $P < 0.05$; **, $P < 0.01$; and ***, $P < 0.001$. Results show means ± SD of four different technical replicates.

3.3. Feeding experiment with d18:0.

This section is focused on the study of sphingolipids metabolism in *A. thaliana* ecotype Col-0 and how this organism can reduce high levels of free LCBs. The flux of sphingolipids in *A. thaliana* is poorly known and only few studies have focused on sphingolipids metabolism. For example, in Shi *et al*. (2015), ^{15}N-labeled metabolic turnover analysis was used to measure sphingolipid contents and to predict significant changes in fluxes. In this thesis, in order to define the synthesis paths that the plant preferably uses and the speed of sphingolipids metabolism, feeding experiments were performed with the first sphingobase in the pathway, d18:0 (Protocol described in section 2. 2. 1. 3. Feeding experiment of *A. thaliana* leaf discs). A labeled version of this sphingobase, D_7-d18:0, was employed to be able to follow sphingolipids *de novo* synthesis over time. Experiments were performed by incubating leaf discs from *A. thaliana* ecotype Col-0 with a solution containing labeled- or unlabeled-d18:0 sphingobase (100 µM) and analyzing the changes in sphingolipid levels in leaf or solution over a time period of 48 hours. Analysis was done via UPLC-MS/MS.

3.3.1. Targeted quantification of labeled sphingolipids.

Initially, feeding experiments were performed using unlabeled d18:0. The sphingolipid profile results obtained are presented in **Annex 11**. In this case, it was not possible to differentiate between sphingolipids synthesized *de novo* using the fed sphingobase d18:0 and sphingolipids obtained by degradation. Therefore, the synthesis of new sphingolipids was next analyzed by using labeled D_7-d18:0 for feeding. The results are presented in **Figures 21** and **22**. On one hand, an increase in the concentration of D_7-d18:0 in leaves was observed within the first hour of incubation, whereas a decrease in the concentration of D_7-d18:0 in the incubation solution of the leaf discs was detected (**Figure 21**, **A** and **B**, respectively). On the other hand, the two closest newly synthesized molecules in the sphingolipid pathway using D_7-d18:0, which are D_7-t18:0 and D_7-d18:0-P, were detected after only 1 h of incubation and with at a concentration 10 times higher than the other sphingolipids measured (**Figure 21**, **C**). A transient increase peaking at 6 h post-incubation was observed for D_7-t18:0, while continuous increases during the timeframe of the experiment (48 h) were observed for D_7-d18:0-P, D_7-t18:0-P and D_7-d18:0-16:0 (**Figure 21**, **C** and **D**).

Labeled sphingolipids after feeding with D_7-d18:0 were detected in minor quantities in comparison to labeled sphingobases (around 0.05 nmol / g fresh weight) and, for most of them, after about 1 h of feeding (**Figure 22**). The most complex sphingolipids containing double bonds in the long-chain bases and/or in the long-chain fatty acid (e.g. D_7-t18:1-22:0, D_7-t18:1-24:1, **Figure 22**) appeared after 3 to 6 h of incubation with the labeled sphingobase. In these cases, the *de novo* synthesis of sphingolipids was transient, peaking at about 6 to 24 h post-feeding and markedly decreasing after 48 h.

To conclude, the targeted analysis showed rapid uptakes of D_7-d18:0 within the leaves. This sphingobase was quickly processed into other direct sphingobases and sphingolipids in the pathway, such as D_7-t18:0, D_7-d18:0-P and D_7-d18:0-16:0, which are among the most abundant ones measured. The following step was to expand the number of sphingolipid species analyzed in order to further understand the flux of sphingolipids synthesis when high amount of LCBs are present.

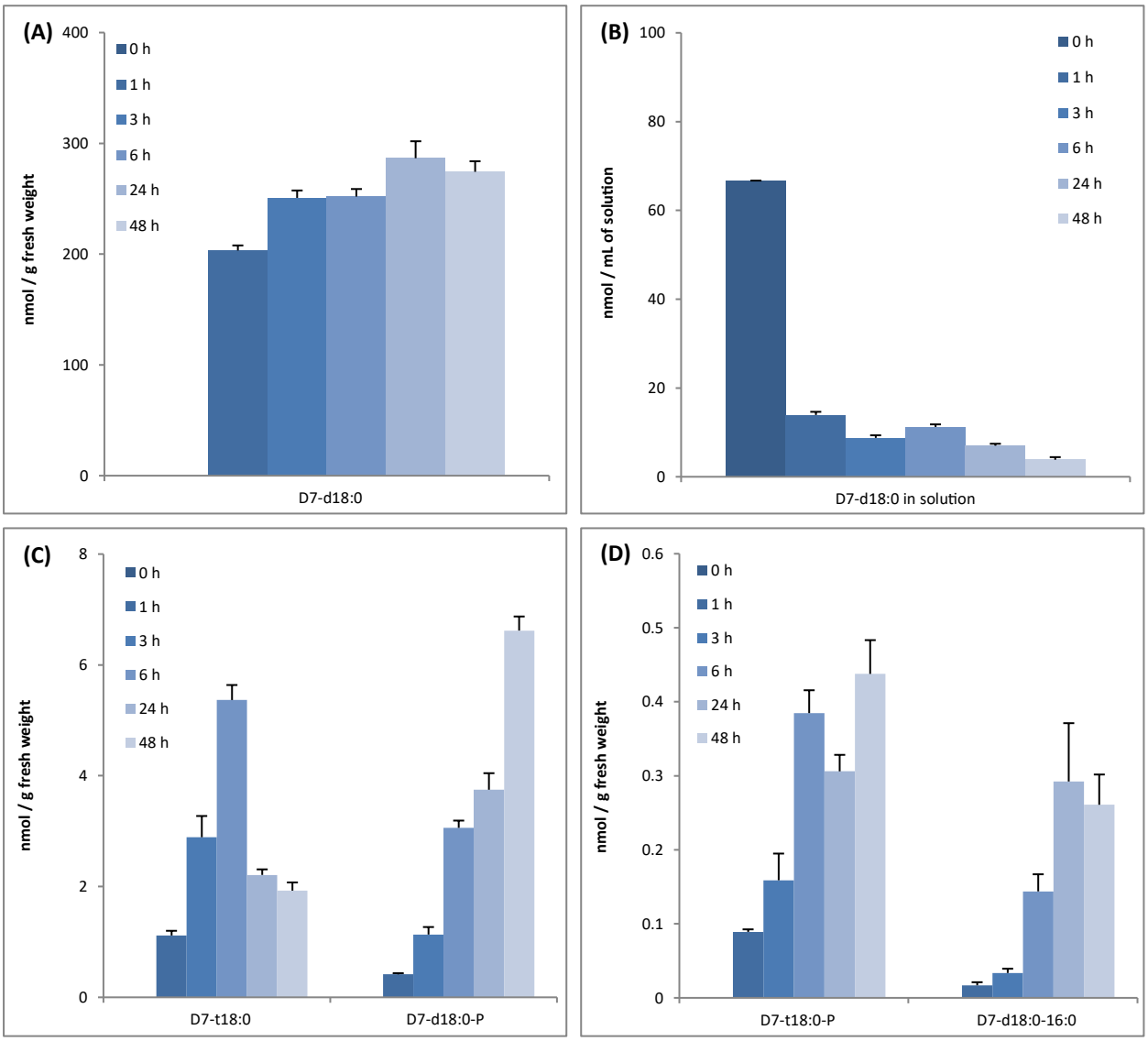

Figure 21: Deuterium-labeled sphingolipids detected during leaf discs feeding in *A. thaliana* wild-type (Col-0). Six-week-old leaf discs from *A. thaliana* ecotype Col-0 were incubated in a 100 µM D_7-d18:0 solution. Leaf discs and incubation solution were collected over time and labeled sphingobases and sphingolipids were quantified (D_7-d18:0 in leaf (A), D_7-d18:0 in solution (B), D_7-t18:0 and D_7-d18:0-P in leaf (C), and D_7-t18:0-P and D_7-d18:0-16:0 in leaf (D)). Results show means ± SD of four different technical replicates (pool of 20 leaf discs picked randomly). Similar results were obtained in two different biological replicates.

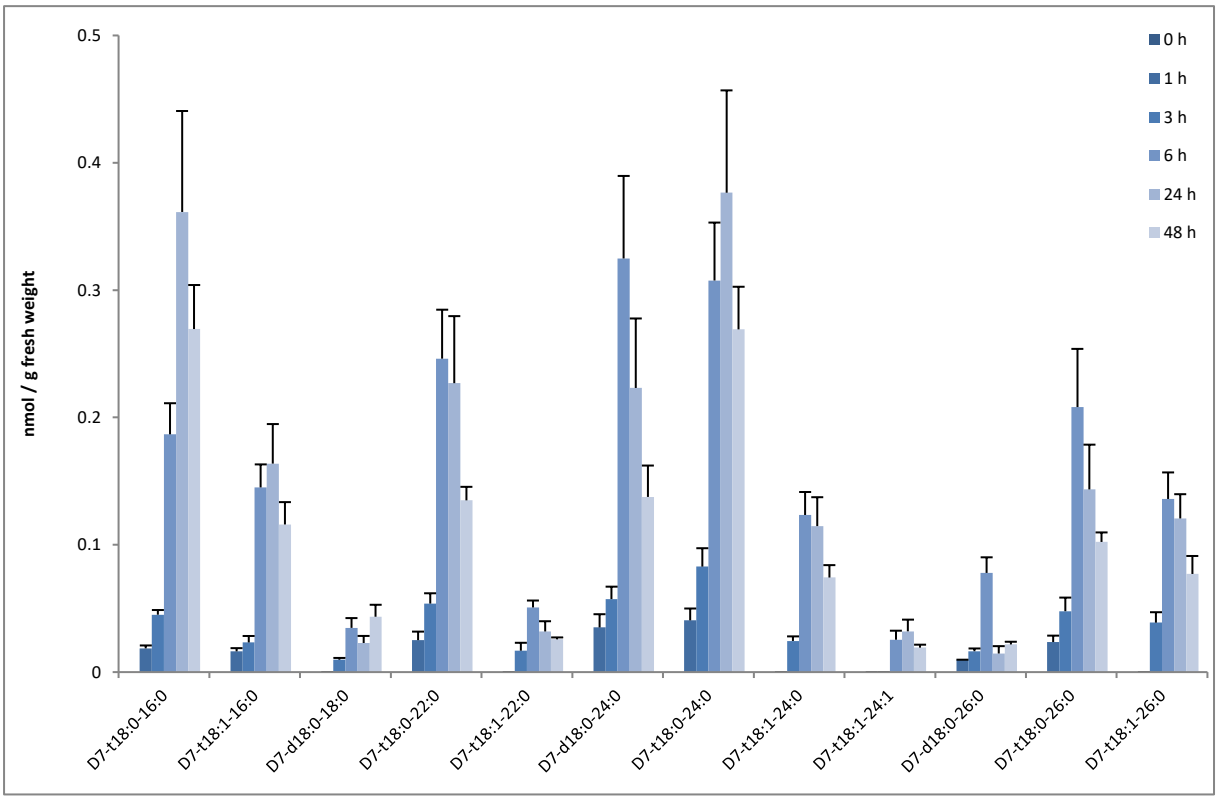

Figure 22: Deuterium-labeled sphingolipids detected during leaf discs feeding in *A. thaliana* wild-type (Col-0). Six-week-old leaf discs from *A. thaliana* ecotype Col-0 were incubated in a 100 µM D_7-d18:0 solution. Leaf discs were collected over time and labeled long-chain and very-long-chain fatty acids sphingolipids were quantified. Results show means ± SD of four different technical replicates (pool of 20 leaf discs picked randomly). Similar results were obtained in two different biological replicates.

3.3.2. Untargeted quantification of labeled sphingolipids.

3.3.2.1. Detection of marker peaks.

The analysis of metabolite profiles involved in the flux of sphingolipids was performed by untargeted analysis. This method is generally employed to describe a larger set of compounds within a single class of compounds (Last *et al*., 2007; Allwood and Goodacre, 2010). Performing this untargeted analysis allows the detection of many sphingolipid species involved in the flux when high quantities of LCBs are detected. Experiments were performed by incubating leaf discs from *A. thaliana* ecotype Col-0 with a solution containing D_7-d18:0 (100 µM) over the time period of 48 h. Then, leaf samples were analyzed by UPLC-qTOF-MS in positive and negative ESI modes (described in section 2. 2. 4. 3. Untargeted analysis). A list of 4548 peaks in positive ESI mode and a list of 3303 peaks in negative ESI mode were obtained (**Figure 23**, **A**). In order to target the most promising and abundant peaks, several filters were applied, which resulted in final lists of 287 positive marker peaks and 296 negative marker peaks defined by their molecular mass and their retention time (**Figure 23**, **A**). Evolution of unique positive marker peaks and unique negative marker peaks numbers over time are showed in **Figure 23 B** and **C,** respectively. Double hits of each marker peaks with both RT ≤ 0.02 min and m/z ≤ 0.003 Da from the positive and negative marker lists were sorted out. The final list of 203

marker peaks detected in positive ESI and 236 marker peaks detected in negative ESI are shown in **Annex 12**. All marker peaks were compared to marker peaks detected in previous experiments performed in the laboratory (see letters indicated in column "Found in experiment" of **Annex 12**; These letters correspond to **Annex 13**). Conditions of the previous experiments performed and used for comparison are presented in **Annex 13**.

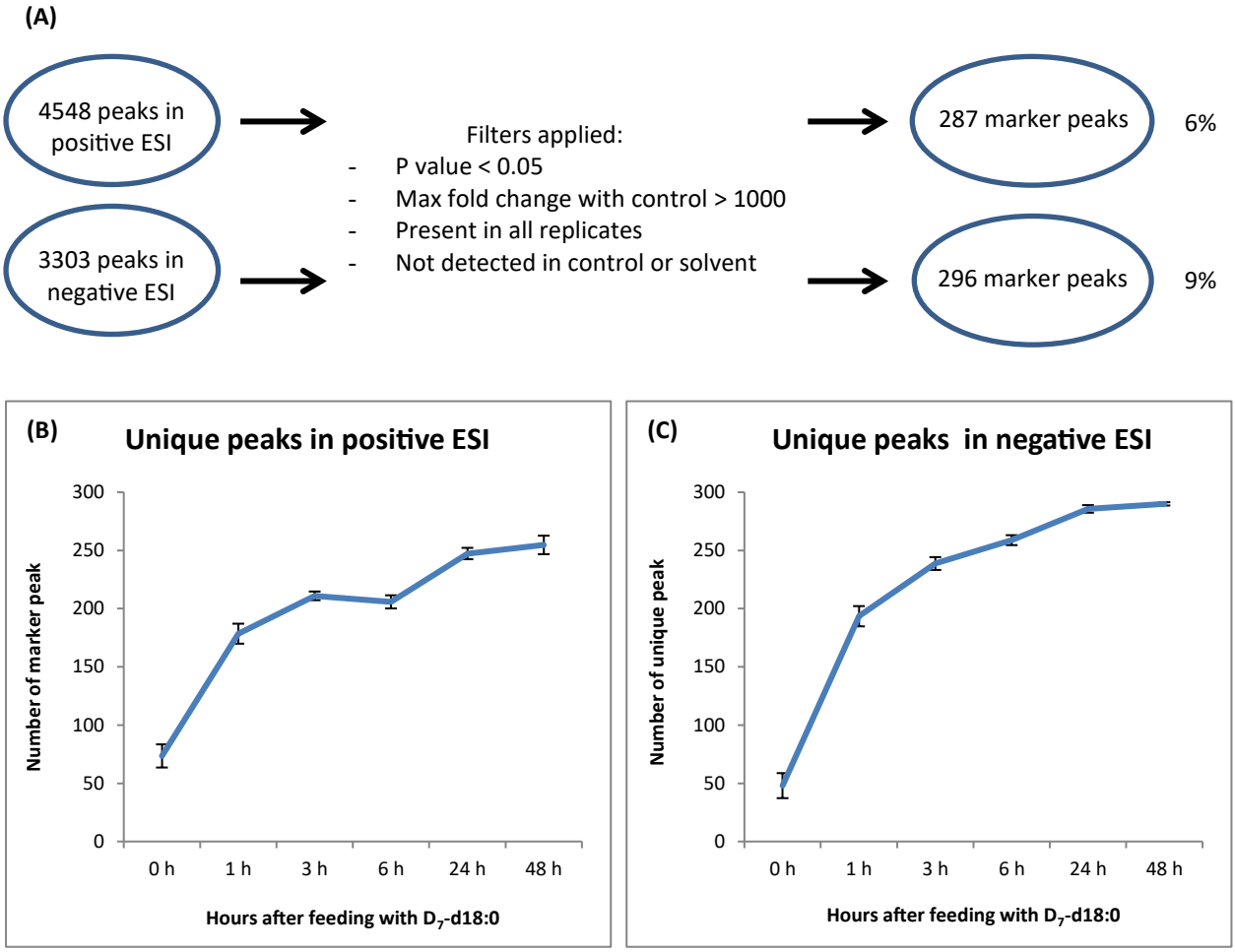

Figure 23: Untargeted analysis procedure performed with Progenesis® QI. Peaks obtained by UPLC-qTOF-MS after feeding leaf discs with D_7-d18:0. Analysis in positive and negative ESI were processed with Progenesis® QI and filtered: P value < 0.05; Max fold change with the control > 1000 ; presence in all 4 replicates and not detected in control or solvent (A). Average of positive ESI (B) and negative ESI (C) unique peaks. Results show means ± SD of four different technical replicates.

3.3.2.2. Identification of ceramides.

A database for the molecular mass of deuterium-labeled ceramides was created and is shown in **Annex 14**. The final list obtained with a total of 439 marker peaks was compared to this deuterium-labeled ceramide database, which generated 71 hits. A matching list composed of these 71 ceramides is displayed in **Figure 24** and are identified as level 2 on the identification scale from modified metabolomics standards initiative (Sumner *et al.*, 2007a). The 71 ceramides identified using

the database have been ordered from the highest average area at 24 h post-feeding to the lowest average area. The highest area measured was for the sphingobase d18:0 with which the experiment was performed, which presented an average area bigger by more than 100 times than the second ceramide identified (**Figure 24**, Area = 116472207). Long-chain fatty acid ceramide t18:0-16:0 and very-long-chain fatty acid ceramide t18:0-24:0 were detected with 2.5 and 3 times (**Figure 24**, Areas = 1529874 and 1892920 respectively) higher areas than the following ceramides identified. Smaller areas for the sphingobases d18:0-P and t18:0, coming from the direct synthesis pathway, were detected 24 h after the feeding (**Figure 24**, Areas = 267915 and 2719 respectively). Several ceramides identified presented the same retention time and mass to charge ratio (for example, d18:0-15:0 and ht18:0-h17:0).

Production over time of each of the 71 ceramides identified is displayed in **Figure 25** from the highest average area (top left) to the lowest average area (bottom right). Among these data, three graph types were observed: a continuous increase in the ceramide synthesis over time like t18:0-24:0 (first raw, 2nd graph, **Figure 25**), a transition in ceramides synthesis over time like Glc-d18:0-28:1 (seventh raw, 1st graph, **Figure 25**) and, finally, a decrease in ceramides synthesis over time like ht18:0-h28:2 (sixteenth raw, 4th graph, **Figure 25**).

Compound	RT	D_7-m/z	m/z	Adducts	Area at 24h
d18:0	3.62	308.3434	301.2993	Monoisotopic	116472207.19
t18:0-24:0	8.8	674.6938	667.6497	Monoisotopic	1892920.85
t18:0-16:0	7.36	562.5662	555.5221	Monoisotopic	1529874.58
d18:0-22:0	8.78	630.6668	623.6227	Monoisotopic	647201.95
d18:0-24:0	9.05	658.6963	651.6522	Monoisotopic	576777.01
d18:0-16:1	7.53	544.5558	537.5117	Monoisotopic	492725.36
t18:0-26:0	9.05	702.725	695.6809	Monoisotopic	471140.38
ht18:0-h18:0	3.88	605.5852	598.5411	$[M-H^+]^-$	456930.10
t18:0-24:1	8.65	672.6771	665.633	Monoisotopic	416179.82
d18:0-16:0	7.77	545.5651	538.521	$[M-H^+]^-$	293469.14
d18:0-P	2.54	389.3164	382.2723	$[M+H]^+$	267915.51
ht18:0-h25:1	3.94	703.6926	696.6485	$[M+H]^+$	263211.57
t18:0-16:1	7.14	561.558	554.5139	$[M+H]^+$	228356.00
d18:0-15:0	7.75	591.5703	584.5262	$[M+Acetate^-]^-$	220046.74
ht18:0-h17:0	7.75	591.5703	584.5262	$[M-H^+]^-$	220046.74
d18:1-P-26:2	2.48	379.3186	372.2745	$[M-2H^+]^-$	196035.66
Glc-d18:0-20:2	2.48	379.3186	372.2745	$[M-2H^+]^-$	196035.66
t18:2	2.48	379.3186	372.2745	$[M+Acetate^-]^-$	196035.66
Glc-t18:1-h28:2	4.3	450.3711	443.327	$[M-2H^+]^-$	188800.51
t18:0-26:1	8.93	701.7149	694.6708	$[M+H]^+$	180743.61
ht18:0-h24:2	8.18	686.6554	679.6113	Monoisotopic	167632.37
d18:0-P	2.55	387.3029	380.2588	$[M-H^+]^-$	134959.20
d18:0-26:0	9.28	745.7417	738.6976	$[M+Acetate^-]^-$	125528.62
ht18:0-h28:0	9.28	745.7417	738.6976	$[M-H^+]^-$	125528.62
Glc-d18:0-28:1	4.36	436.3914	429.3473	$[M-2H^+]^-$	100700.63
t18:0-24:2	5.75	693.6516	686.6075	$[M+Na^+]^+$	90842.25
Glc-d18:0-26:0	4.19	423.381	416.3369	$[M-2H^+]^-$	83702.73
d18:0-18:2	7.5	629.5874	622.5433	$[M+Acetate^-]^-$	79705.12
ht18:0-h20:2	7.5	629.5874	622.5433	$[M-H^+]^-$	79705.12
ht18:0-h22:1	8.2	660.6386	653.5945	Monoisotopic	77389.84
Compound	RT	D_7-m/z	m/z	Adducts	Area at 24h
d18:0-18:0	8.16	575.61	568.5659	$[M+H]^+$	62459.09
d18:0-22:1	8.38	687.6646	680.6205	$[M+Acetate^-]^-$	61577.57
ht18:0-h24:1	8.38	687.6646	680.6205	$[M-H^+]^-$	61577.57
d18:0-P-28:1	3.6	395.3503	388.3062	$[M-2H^+]^-$	59307.38
Glc-d18:0-22:0	3.6	395.3503	388.3062	$[M-2H^+]^-$	59307.38
Glc-d18:0-17:2	3.26	358.2961	351.252	$[M-2H^+]^-$	55700.22
Glc-t18:0-h24:0	3.43	425.3606	418.3165	$[M-2H^+]^-$	55700.22
t18:1	3.35	321.3133	314.2692	$[M-H^+]^-$	51832.34
ht18:0-h24:0	8.69	691.6958	684.6517	$[M+H]^+$	50067.07
Glc-d18:0-16:1	7.17	765.6226	758.5785	$[M+Acetate^-]^-$	38870.69
Glc-t18:0-h18:1	7.17	765.6226	758.5785	$[M-H^+]^-$	38870.69
t18:0-28:1	9.17	787.7532	780.7091	$[M+Acetate^-]^-$	38768.14
d18:0-14:1	6.97	575.5374	568.4933	$[M+Acetate^-]^-$	38567.94
ht18:0-h16:1	6.97	575.5374	568.4933	$[M-H^+]^-$	38567.94

Compound	RT	D_7-m/z	m/z	Adducts	Area at 24h
GIPC-d18:1-20:2	3.55	1176.6938	1169.6497	Monoisotopic	32223.35
t18:0-22:1	8.36	645.6524	638.6083	$[M+H]^+$	26675.84
d18:0-14:0	7.55	577.5559	570.5118	$[M+Acetate^-]^-$	20596.35
ht18:0-h16:0	7.55	577.5559	570.5118	$[M-H^+]^-$	20596.35
ht18:0-h20:0	3.56	657.6162	650.5721	$[M+Na^+]^+$	17785.91
ht18:1-h22:2	3.56	657.6162	650.5721	$[M+H]^+$	17785.91
Glc-t18:1-27:2	3.42	435.3665	428.3224	$[M-2H^+]^-$	15613.67
d18:0-18:1	7.35	631.5982	624.5541	$[M+Acetate^-]^-$	13240.66
ht18:0-h20:1	7.35	631.5982	624.5541	$[M-H^+]^-$	13240.66
ht18:0-P-h22:0	6.91	765.6129	758.5688	$[M+Na^+]^+$	12796.19
ht18:1-P-h24:2	6.91	765.6129	758.5688	$[M+H]^+$	12796.19
d18:0-23:0	8.92	703.6956	696.6515	$[M+Acetate^-]^-$	10312.86
ht18:0-h25:0	8.92	703.6956	696.6515	$[M-H^+]^-$	10312.86
ht18:0-h26:1	8.82	775.7177	768.6736	$[M+Acetate^-]^-$	9969.52
Glc-t18:0-h24:2	2.55	423.345	416.3009	$[M-2H^+]^-$	8622.40
d18:0-24:1	7.46	657.6864	650.6423	$[M+H]^+$	8067.37
ht18:1-P-h23:2	6.76	751.6005	744.5564	$[M+H]^+$	7714.60
t18:0-22:0	8.69	645.652	638.6079	$[M-H^+]^-$	6496.55
d18:0-28:0	9.49	773.7739	766.7298	$[M+Acetate^-]^-$	5158.66
ht18:0-h28:2	7.61	760.7505	753.7064	$[M+NH_4^+]^+$	4848.13
t18:0-20:1	8.01	675.628	668.5839	$[M+Acetate^-]^-$	4549.03
d18:0-19:0	7.89	589.6247	582.5806	$[M+H]^+$	4429.20
d18:0-25:0	9.17	731.7269	724.6828	$[M+Acetate^-]^-$	3021.42
ht18:0-h27:0	9.17	731.7269	724.6828	$[M-H^+]^-$	3021.42
t18:0	3.17	324.3363	317.2922	Monoisotopic	2719.05
Glc-t18:0-h24:1	8.31	851.7339	844.6898	$[M+H]^+$	2212.22
Glc-t18:0-16:1	7.07	723.6136	716.5695	$[M+H]^+$	1224.30

Figure 24: Detected labeled ceramides in *A. thaliana* leaves after feeding with D_7-d18:0. Six-week-old leaf discs from *A. thaliana* ecotype Col-0 were incubated in 100 µM D_7-d18:0. Compounds were detected by UPLC-qTOF-MS and compared to molecular weights contained in D_7-ceramides databases. The table includes: retention time: RT ; Deuterium labeled mass to charge ratio: D_7-m/z ; mass to charge ratio: m/z ; the detected adducts: Adducts ; and the average area at 24 h post-feeding: Area at 24h. Results are means of four different technical replicates.

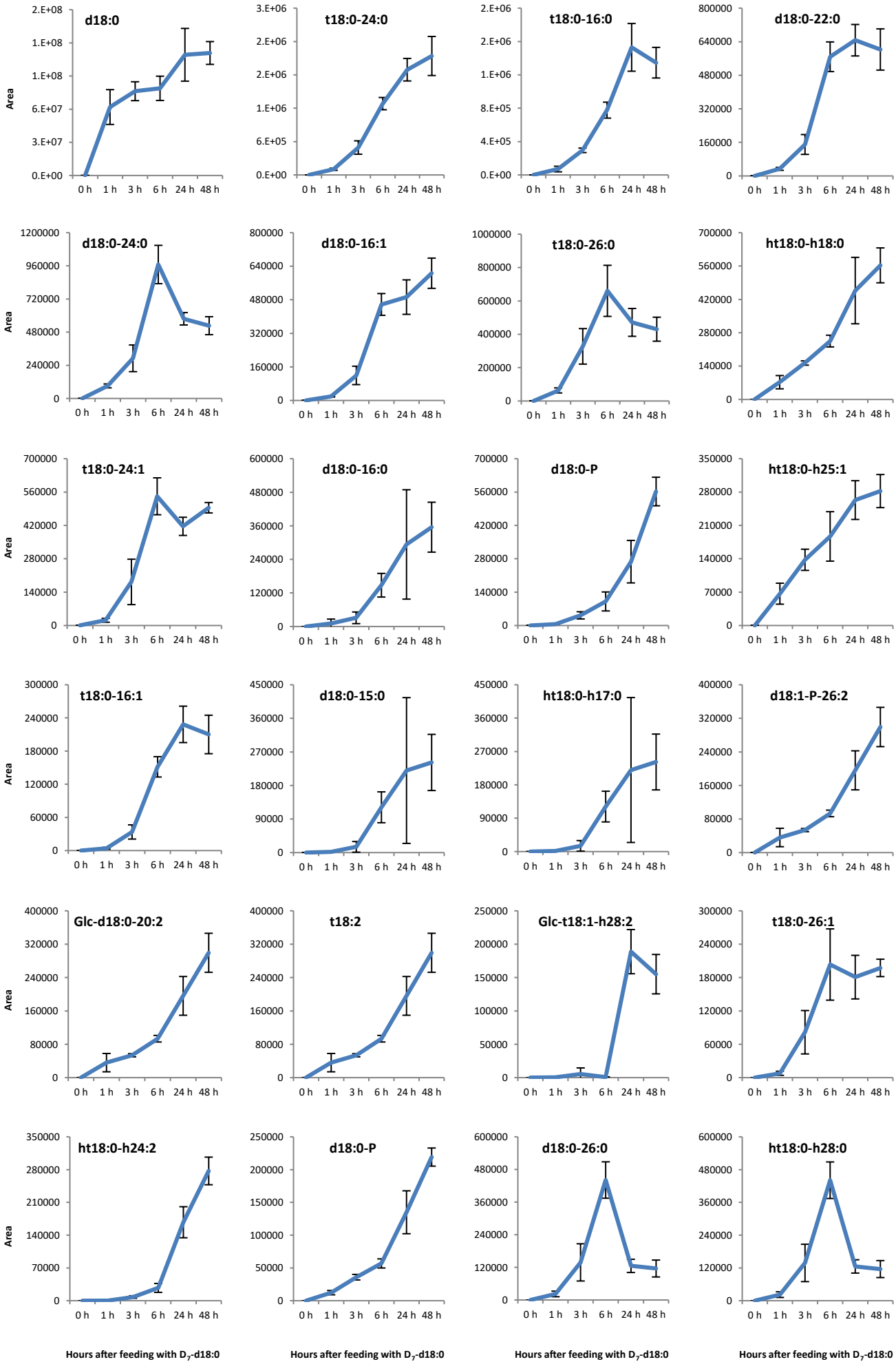
d18:0
t18:0-24:0
t18:0-16:0
d18:0-22:0
d18:0-24:0
d18:0-16:1
t18:0-26:0
ht18:0-h18:0
t18:0-24:1
d18:0-16:0
d18:0-P
ht18:0-h25:1
t18:0-16:1
d18:0-15:0
ht18:0-h17:0
d18:1-P-26:2
Glc-d18:0-20:2
t18:2
Glc-t18:1-h28:2
t18:0-26:1
ht18:0-h24:2
d18:0-P
d18:0-26:0
ht18:0-h28:0
Area
0 h 1 h 3 h 6 h 24 h 48 h
Hours after feeding with D7-d18:0

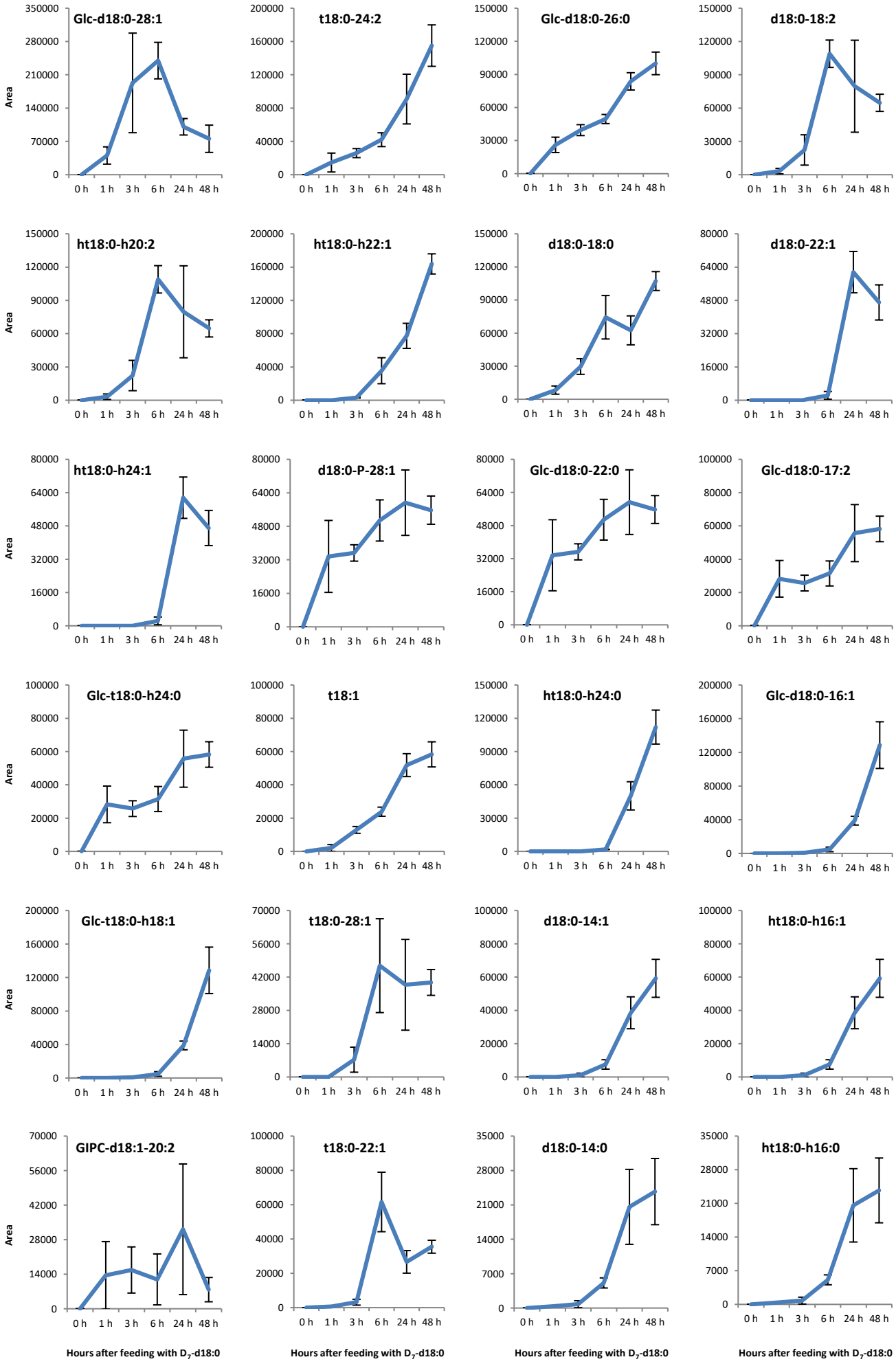
Glc-d18:0-28:1
t18:0-24:2
Glc-d18:0-26:0
d18:0-18:2
ht18:0-h20:2
ht18:0-h22:1
d18:0-18:0
d18:0-22:1
ht18:0-h24:1
d18:0-P-28:1
Glc-d18:0-22:0
Glc-d18:0-17:2
Glc-t18:0-h24:0
t18:1
ht18:0-h24:0
Glc-d18:0-16:1
Glc-t18:0-h18:1
t18:0-28:1
d18:0-14:1
ht18:0-h16:1
GIPC-d18:1-20:2
t18:0-22:1
d18:0-14:0
ht18:0-h16:0
Area
0 h 1 h 3 h 6 h 24 h 48 h
Hours after feeding with D7-d18:0

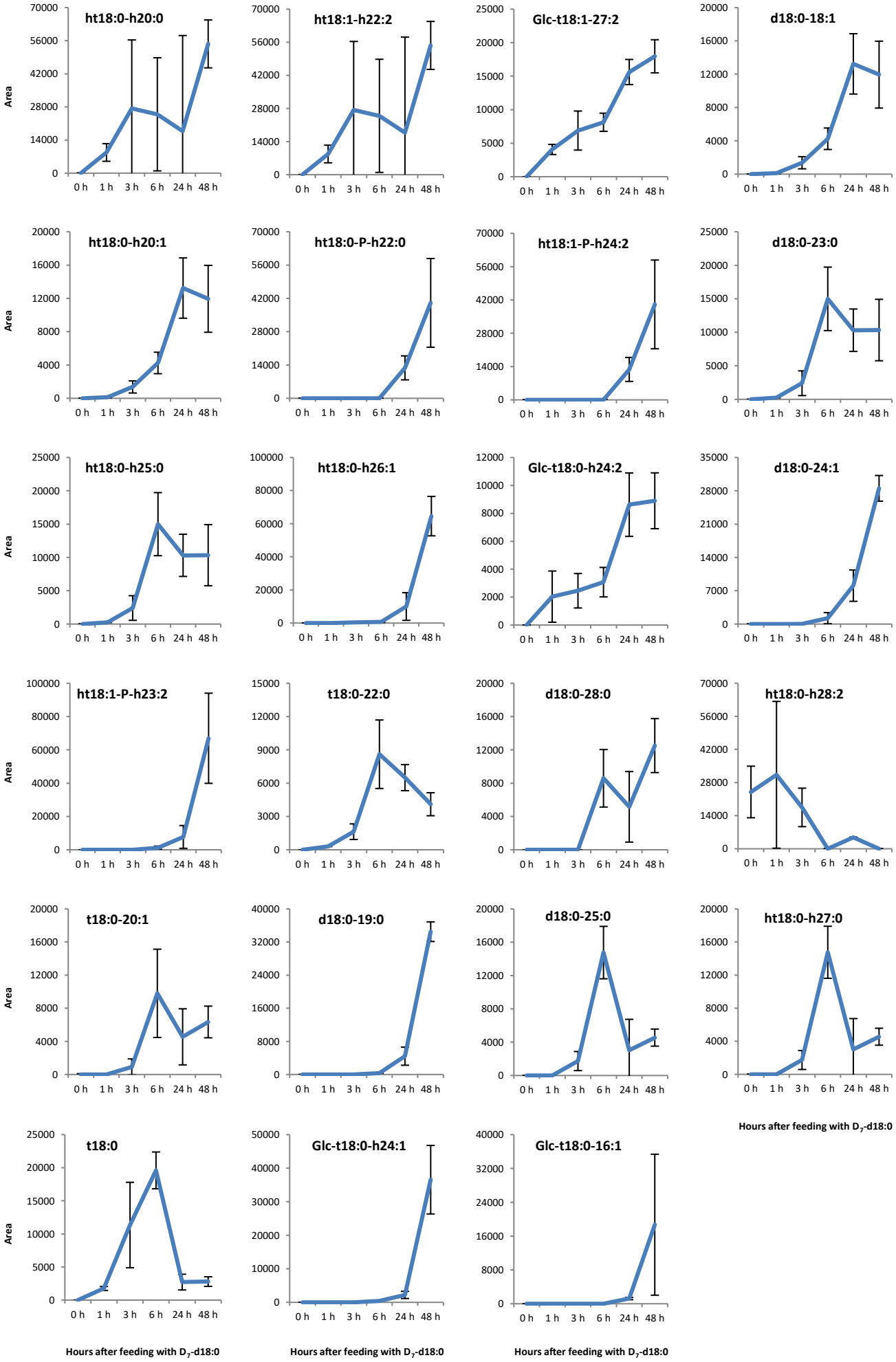
ht18:0-h20:0
ht18:1-h22:2
Glc-t18:1-27:2
d18:0-18:1
ht18:0-h20:1
ht18:0-P-h22:0
ht18:1-P-h24:2
d18:0-23:0
ht18:0-h25:0
ht18:0-h26:1
Glc-t18:0-h24:2
d18:0-24:1
ht18:1-P-h23:2
t18:0-22:0
d18:0-28:0
ht18:0-h28:2
t18:0-20:1
d18:0-19:0
d18:0-25:0
ht18:0-h27:0
t18:0
Glc-t18:0-h24:1
Glc-t18:0-16:1
Area
0 h 1 h 3 h 6 h 24 h 48 h
Hours after feeding with D7-d18:0

Figure 25: Detected labeled ceramides in *A. thaliana* leaves after feeding with D_7-d18:0. Six-week-old leaf discs from *A. thaliana* ecotype Col-0 were incubated in 100 µM D_7-d18:0. Compounds were detected by UPLC-qTOF-MS and assigned to ceramides by matching theoretical molecular weight within a margin of 3 mDa. Average area evolutions of 71 ceramides compounds identified are presented here, ordered from the highest average area at 24 h post-feeding to the lowest average area. Results show means ± SD of six different technical replicates.

3.3.2.3. Ratio of labeled and unlabeled ceramides.

The samples previously analyzed by UPLC-qTOF-MS were next analyzed by targeted analysis by UPLC-ESI-MS/MS in order to quantify ceramides. This quantification allows to determine the incorporation speed and molar ratio of the labeled sphingobase D_7-d18:0 into the leaf discs and how the plant manages to reduce high levels of free sphingobases in the sphingolipid pathway (**Figure 26**). Only an hour was enough time to detect D_7-d18:0 in a large quantity in the leaf discs (**Figure 26**, **A**; 200 nmol / g fresh weight). Increases in the contents of the two close compounds d18:0-P and t18:0 in the sphingolipid's synthesis pathway were observed over time. The compounds d18:0-P and t18:0 were quantified to be 100 times less abundant than d18:0 (up to a maximum of 6 and 5.5 nmol / g fresh weight, respectively).
Labeled ceramides, such as t18:0-16:0, d18:0-16:0 and d18:0-24:0, were detected after 1 h of feeding with D_7-d18:0. More complex ceramides were either not detected or detected at later time points (6 h post-feeding) and in small quantities, such as in the case of t18:1-24:1 (**Figure 26**, **A**). The ratio of sphingolipids and labeled sphingolipids, showed here in percentage, allowed to clearly follow the *de novo* production of ceramides (d18:0-16:0, d18:0-24:0 and d18:0-26:0) in the sphingolipid pathway (**Figure 26**, **B**).

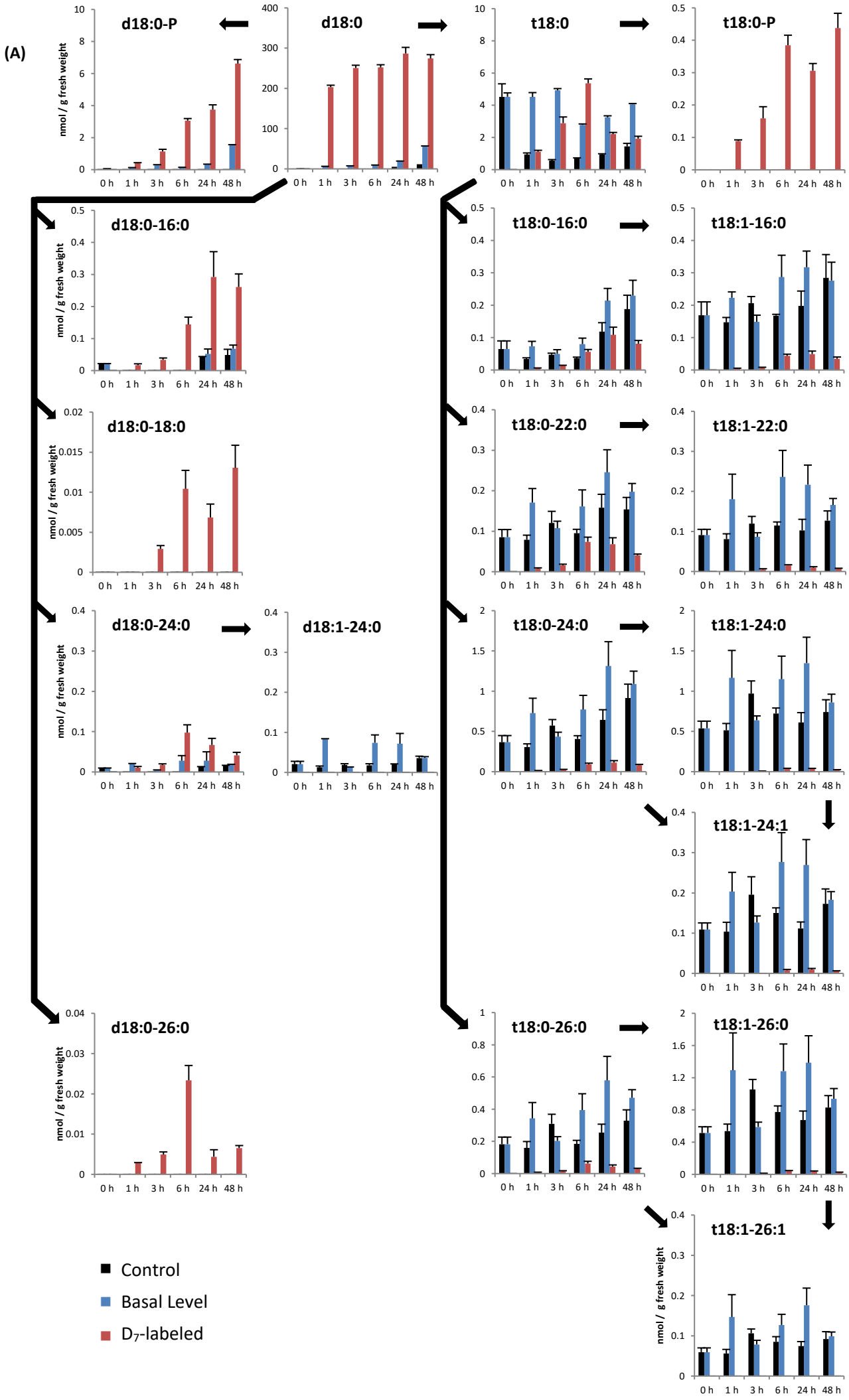
(A)
d18:0-P
d18:0
t18:0
t18:0-P
d18:0-16:0
t18:0-16:0
t18:1-16:0
d18:0-18:0
t18:0-22:0
t18:1-22:0
d18:0-24:0
d18:1-24:0
t18:0-24:0
t18:1-24:0
t18:1-24:1
d18:0-26:0
t18:0-26:0
t18:1-26:0
t18:1-26:1
nmol / g fresh weight
0 h 1 h 3 h 6 h 24 h 48 h
Control
Basal Level
D7-labeled

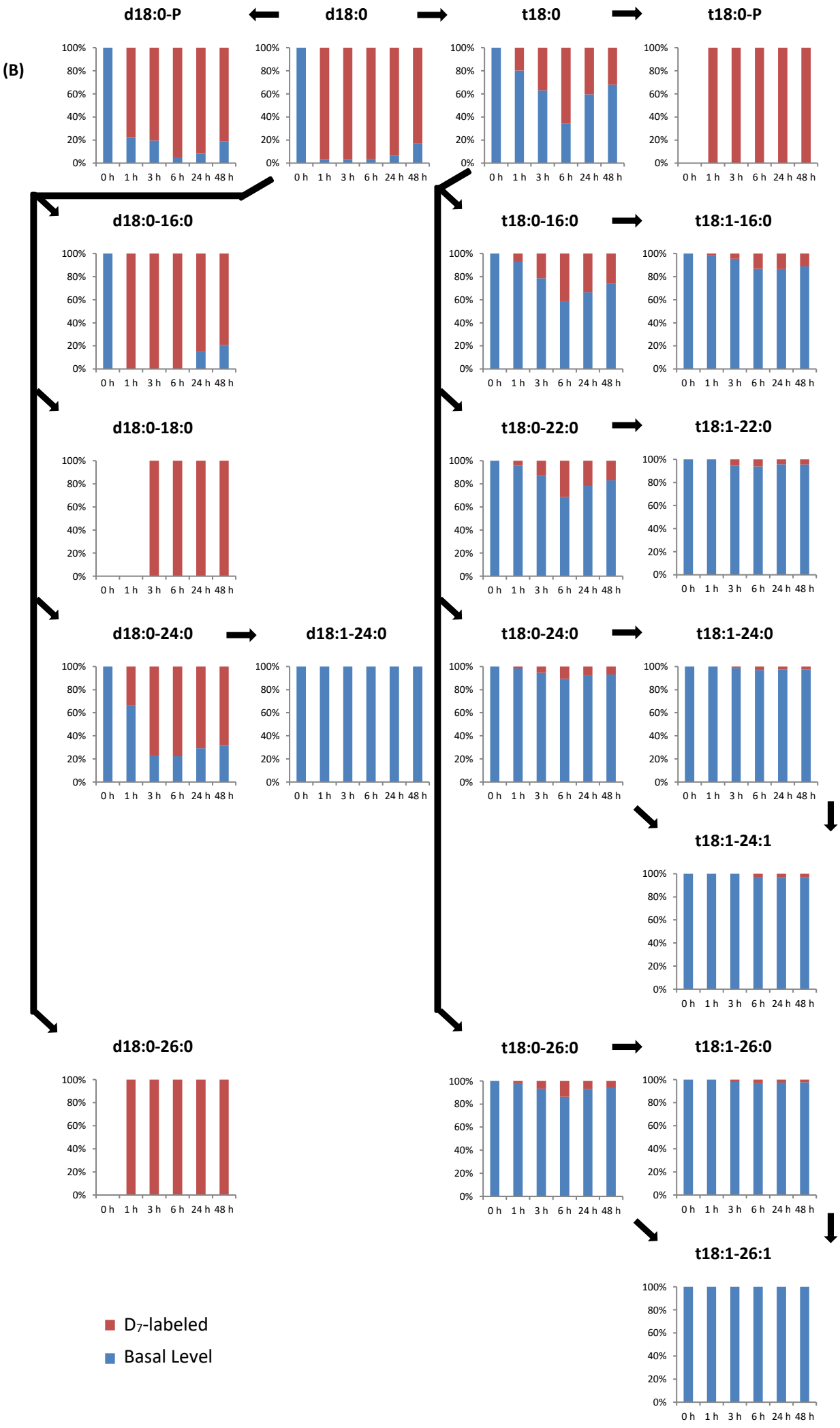
(B)
d18:0-P
d18:0
t18:0
t18:0-P
d18:0-16:0
t18:0-16:0
t18:1-16:0
d18:0-18:0
t18:0-22:0
t18:1-22:0
d18:0-24:0
d18:1-24:0
t18:0-24:0
t18:1-24:0
t18:1-24:1
d18:0-26:0
t18:0-26:0
t18:1-26:0
t18:1-26:1
100%
80%
60%
40%
20%
0%
0 h
1 h
3 h
6 h
24 h
48 h
D7-labeled
Basal Level

Figure 26: Unlabeled and labeled sphingolipids evolution after feeding with D_7-d18:0. Six-week-old leaf discs from *A. thaliana* ecotype Col-0 were incubated in 100 µM D_7-d18:0. Compounds were detected by UPLC-qTOF-MS and UPLC-ESI-MS/MS. Areas were used to determine the quantity of unlabeled and labeled sphingolipids. Changes in the quantity of sphingolipids are shown by absolute quantification (A) as well as by percentage (B) over time. Black arrows indicate the logical synthesis pathway. Results show means ± SD of four different technical replicates.

4. Discussion.

In plant cells, sphingolipids constitute essential components of the plasma membrane, acting not only as structural elements but also as signaling molecules. More importantly, in recent years, sphingolipids have also been described to play an important role in the regulation of PCD during infection by pathogens by acting as secondary messengers. In many cases, the fate of the host plant depends on sphingolipids (Peer *et al*., 2011). Therefore, it is of great importance to understand the defense mechanisms against pathogen infections and the function of sphingolipids. Therefore, one of the aims of this project was to investigate the levels of sphingobases and sphingolipids in several *A. thaliana* mutants of interest in response to infection.

The first step of our approach involved analyzing the sphingolipid levels in thirteen sphingolipid mutant lines of interest as well as the wild-type Col-0 by UPLC-MS/MS with a limit of detection at 0.001 nmol / g fresh weight under our experimental conditions. As mentioned in section 3. 1. 1. Basal levels of sphingolipid contents in sphingolipid metabolism mutant lines, generally, the levels of sphingobases and phosphorylated sphingobases detected in the various plant cell lines tested were different from those reported in the literature (**Figure 4**; Markham and Jaworski, 2007; Shi *et al*., 2007; Dutilleul *et al*., 2012; Nakagawa *et al*., 2012; Magnin-Robert *et al*., 2015). Indeed, under our experimental conditions and in our samples, we detected 0.05 nmol / g fresh weight of d18:0 and 0.6 nmol / g fresh weight of t18:0 and, besides, no phosphorylated sphingobases were detected. In contrast, Markham and Jaworski (2007) reported that *A. thaliana* Col-0 contains 1.25 nmol / g dry weight of d18:0 and 1.5 nmol / g dry weight of t18:0 and, in this case, d18:0-P and t18:0-P were detected although at very low levels (approximately 0.05 nmol / g dry weight). Moreover, the ratio between the levels of sphingobases detected in our samples and those detected in the samples by Markham and Jaworski (2007) are different. Nevertheless, the levels of d18:0 (0.05 nmol / g fresh weight) and t18:0 (0.6 nmol / g fresh weight) detected were comparable to the ones reported in Wu *et al*. (2015). In this thesis and in Markham and Jaworski (2007), the samples of *Arabidopsis* were freeze-dried before extraction of the metabolites, reducing the drying time to preserve perishable materials, such as SPLs. Therefore, the main difference between the experimental conditions used in this thesis and Markham and Jaworski (2007) comes from using fresh weight instead of dry weight for the plant starting material for analysis. Expressing biomass in fresh weight means that the samples have a high-water content. Therefore, more starting biomass material would be required for analysis in comparison to dry weight in order to be able to detect comparable levels of sphingolipid species. This could explain the lower levels of sphingobases detected in this samples in comparison to dry weight samples from the experiments of Markham and Jaworski (2007) as well as the absence of phosphorylated sphingolipids in our samples.

Among the several mutant lines analyzed, five of them were selected due to the different effects that the introduced gene modifications, such as gene overexpression and gene knockdown, would have on the phosphorylation of the sphingobases. The wild-type Col-0 was also employed as a control. The preliminary analysis of the sphingolipid basal levels showed that the two double mutants *sphk1*-OE / *spp1.2* and *dpl1.1* / *spp1.2* showed an excessive accumulation of phosphorylated sphingobases (**Figure 4**, **B** and **D**). Therefore, they represent very interesting candidates to further investigate the importance of accumulating phosphorylated sphingobases during biotic and abiotic stresses. To better understand the combined genetic effects of each mutation in the double mutant lines, the single mutant lines *sphk1*-OE and *dpl1.1* had also been included in the experiments.

The *sphk1*-KD mutant theoretically behaves in the opposite way to sphk1-OE regarding the accumulation of phosphorylated sphingobases. The *sphk1*-OE mutant promotes the phosphorylation

of d18:0 and t18:0 into d18:0-P and t18:0-P, respectively, whereas the *sphk1*-KD mutant tends to repress this step and, as a result, diminish the quantity of phosphorylated sphingobases (Worrall *et al*., 2008). Unfortunately, phosphorylated LCBs were not detected under basal conditions in the mutant lines *sphk1*-OE and *sphk1*-KD and thus this effect could not be confirmed. This aspect was selected to help in the characterization of the two mutant lines *sphk1*-OE / *spp1.2* and *dpl1.1* / *spp1.2*. The three mutant lines *dpl1.1, sphk1*-KD and *sphk1*-OE have been previously described in the literature and thus are useful to compare our results (Tsegaye *et al.*, 2007; Worrall *et al.*, 2008; Magnin-Robert *et al*., 2015; Qin *et al*., 2017; Yanagawa *et al*., 2017; Glenz *et al*., 2019).

4.1. Study of *A. thaliana* sphingolipid metabolism mutant lines after biotic stress.

4.1.1. Study of *A. thaliana* sphingolipid metabolism mutant lines after *P. syringae* infection.

The first step in this thesis was to investigate the role that sphingolipids play in the plant immune response upon infection by *P. syringae* avirulent strain (*Pst AvrRPM1*), which has been shown to trigger PCD (Peer *et al*., 2010). This role was investigated by analyzing several mutant lines that present different levels of specific LCBs and LCB-Ps and examining the different cell death reactions triggered after pathogen recognition. For that, cell death experiments were performed by infiltrating leaf discs with the bacterial pathogen *Pst AvrRPM1* and measuring the electrolyte leakage, which is an indicator of cell death. In fact, plant cells do not form apoptotic bodies, but instead the content of dead cells is directly released into the intercellular fluid, which can be easily measured (Rizhsky *et al*., 2004). This experiment was performed by employing the different *A. thaliana* sphingolipid mutant lines selected previously and the hemibiotrophic pathogen *P. syringae*, in parallel to wild-type plants (Col-0). After leaves were infiltrated with control or infection solution, leaf discs were employed to measure the conductivity over time.

All the mutants showed different trends of cell death in comparison to Col-0, although these differences were not statistically significant, probably because of the variability observed within the samples (**Figure 6**). This variability might be due to differences in the biological material employed, regarding both the plant and the pathogen materials. Moreover, ion leakage measurement might not be the most precise measuring tool to measure small differences between our samples. Indeed, in the literature, a combination of three different methods is suggested for an accurate detection of PCD. The measurement of ion leakage, the measurement of nuclear activity and the detection of DNA fragmentation is the combination of biochemical approaches to measure plant PCD as accurately as possible (Rizhsky *et al*., 2004). On one hand, the sphingolipid mutant line *dpl1.1*, which has a decreased access of phosphorylated sphingobases into the degradation pathway and by consequence accumulates more sphingobases, showed up to 20 % less cell death in comparison to Col-0 after 48 h of infection. Interestingly, these results are in contrast to a published report, in which *A. thaliana dpl1.1* plants exhibited an increased susceptibility to two strains of *P. syringae*, the virulent *Pst* strain DC3000 and the avirulent *Pst* strain *AvrRPM1* (Magnin-Robert *et al*., 2015). The experimental conditions used in both studies were the same, with the exception of plant growth conditions. In Magnin-Robert *et al*. (2015), plants were grown at 12 h light / 12 h dark, 20 °C, 60 % humidity for 35 days whereas, in the experiments in this thesis, plants were grown at 12 h light / 15 h dark, 20 / 22 °C, 70 % humidity for 42 days. Therefore, the age of the plants and the growth

conditions might be affecting the induction of cell death. On the other hand, the two kinase mutants *sphk1*-OE and *sphk1*-KD exhibited opposite results. The presence of phosphorylated sphingobases in *sphk1*-OE mutants after 48 hpi resulted in a stronger reduction of cell death upon *P. syringae* infection, whereas the absence of phosphorylated sphingobases and the accumulation of sphingobases 48 hpi in the *sphk1*-KD mutant led to a slight induction of cell death in response to the pathogen (cell death in Col-0 is used as baseline; **Figure 6**). This suggests that accumulation of sphingobases in plant leaves, without accumulation of phosphorylated sphingobases, is a determinant factor in the susceptibility of the plant to the bacterial strain *P. syringae AvrRPM1*. It might also suggest that accumulation of phosphorylated sphingobases provokes a weaker induction of cell death to *P. syringae*. In fact, the two double mutant lines *sphk1*-OE / *spp1.2* and *dpl1.1* / *spp1.2*, which accumulate phosphorylated sphingobases and have not been previously characterized in the literature, showed a weaker induction of cell death upon *P. syringae AvrRPM1* infection: 17 % and 15 % more resistance, respectively, in comparison to Col-0 (**Figure 6**, **B**).

Following, the sphingolipid profiles of each of these mutant plants were analyzed under basal conditions. The mutant line *dpl1.1* presented similar quantities of d18:0, d18:0-P, and t18:0-P, and ten times more t18:0 compared to the literature (Magnin-Robert *et al*., 2015). In the other mutant lines, *sphk1*-OE, *sphk1*-KD, *sphk1*-OE / *spp1.2*, and *dpl1.1* / *spp1.2*, the quantities of phosphorylated sphingobases detected were in accordance with the results one would expect for these specific genotypes (**Figure 7**).

Then, during *P. syringae* infection, *sphk1*-OE accumulated between six to ten times more phosphorylated sphingobases (t18:0-P and d18:0-P) and the double mutant *sphk1*-OE / *spp1.2* accumulated between two to six times more phosphorylated sphingolipids (d18:0-P and t18:0-P) in comparison to controls. Interestingly, no increases in the contents of d18:0-P and t18:0-P were detected in *sphk1*-OE under basal conditions, indicating that *P. syringae AvrRPM1* infection triggered the accumulation of phosphorylated sphingobases. This observation is further confirmed by the two double mutants, for which higher quantities of LCBs and LCB-Ps were detected after infection. These results would suggest that, as long as there is enough accumulation of phosphorylated sphingobases to balance the presence of sphingobases, cell death can be diminished in comparison to Col-0. The mutant line *sphk1*-KD did not show accumulation of phosphorylated sphingobases during infection and *dpl1.1* / *spp1.2* did not show any significant differences regarding the levels of d18:0-P and t18:0-P in comparison to non-infected plants. In all the plants infected with the pathogen, accumulation of different sphingolipids was observed over time. These results are consistent with the fact that the leaf discs aged and thus the sphingobases are further transformed into more complex ceramides, such as d18:0-16:0 and t18:0-16:0. Plants infected with the pathogens exhibited levels of sphingolipids that reached up to ten times more than in the non-infected controls (**Figure 8**).

The sphingolipids profiles of these mutant plants after infection by *P. syringae* were then analyzed in more detail in these experiments (**Figure 8; Annex 5**). For the mutant line *dpl1.1*, similar results regarding LCBs levels were obtained in comparison to data reported in the literature. Quantities of d18:0 and t18:0 were comparable to those in Magnin-Robert *et al*. (2015) at 48 hpi. However, these increases were transient and significant accumulations were observed in the leaf discs in comparison to the non-infected control at earlier times of the infection. Moreover, no increase in t18:0-P was observed in this experiment after infection with the pathogen, which is in contrast to results published in Magnin-Robert *et al*. (2015), which reported that t18:0-P increased by five times at 48 hpi. Significant accumulations of sphingobases d18:0 and t18:0 in all the mutants tested was observed after infection with *Pst AvrRPM1* in comparison to non-infected plants, according to students *t*-Test with a level smaller than 0.05.

Higher levels of d18:0 and t18:0 are in line with results reported in the literature and, according to Peer *et al*. (2010), could lead to a higher cell death response to *Pst*. The upregulation of t18:0 could be an active process to facilitate PCD and stop the spread of the pathogen. In addition, *sphk1*-OE, *sphk1*-OE / *spp1.2* and *dpl1.1* / *spp1.2*, which were more resistant to the pathogen, accumulated phosphorylated sphingobases d18:0-P and t18:0-P. These results could suggest that, in these lines, the accumulated sphingobases can be rapidly transformed into phosphorylated sphingobases, which can be then degraded, avoiding the toxic effect that they provoke in the plants. The results obtained with *sphk1*-KD mutant line would further support this hypothesis. This mutant did not produce detectable amounts of phosphorylated sphingobases and showed a tendency towards higher susceptibility to *P. syringae*. The mutant *dpl1.1*, slightly more resistant than Col-0 to an avirulent strain *P. syringae*, accumulated some phosphorylated sphingobases although to a very low extent (1.3 nmol / g fresh weight of d18:0-P at 48 hpi and 8.9 nmol / g fresh weight of t18:0-P at 48 hpi).
In conclusion, LCBs d18:0 and t18:0 and the sphingolipids d18:0-16:0 and t18:0-16:0, among all the ones measured, are marker metabolites for the response to the infection by an avirulent strain of *P. syringae* in these mutant lines. It has been shown that the induction of t18:0 was transient in response to the infection by a virulent strain of *P. syringae*, leading to a positive role of t18:0 in the plant response to this pathogen (Peer *et al*., 2010). Based on the data obtained in this work, t18:0 could also play a relevant role in the plant response to the avirulent strain of *P. syringae*.
Future studies could further reveal the sphingolipid profiles under these circumstances by evaluating the effect of different conditions (such as age of plants or infection period), employing inducible mutant lines, performing the treatments on intact plants (instead of only leaves), or using different concentrations of the pathogen. On one hand, harsher conditions than the ones tested in this thesis could reveal more pronounced differences in the sphingolipid profiles that procure the resistance of the plant to the pathogen. On the other hand, the use of inducible lines would allow the manipulation of the enzymatic activity of interest for a short period of time and prevent the plant from adapting to the constitutive overexpression or the knockout of certain enzymes. Altogether, this would provide a more detailed insight into the specific role of the different sphingolipid species as well as the role of their relative contents within the plant in the response of the plant to *P. syringae*.

4.1.2. Study of *A. thaliana* sphingolipid metabolism mutant lines after *V. longisporum* infection.

The *Arabidopsis* sphingolipid metabolism mutant plants were also employed to investigate the role that sphingolipids play in the plant immune response upon infection by the fungi *V. longisporum*. This pathogen was selected for study because it infects Brassicaceae plants and causes severe crop loss in oilseed rape (Iven *et al*., 2012). Moreover, *V. longisporum* displays a different infection mechanism (it infects through the roots) than *P. syringae* (it infects through the leaves), and thus the plant requires different defense mechanisms. Therefore, it is interesting to investigate a potential link between sphingolipid profile and severity of infection. For that, the roots of the different sphingolipid mutant lines were incubated with a solution containing spores of the pathogen. Then, macroscopic infection, quantity of fungal DNA and sphingolipid profiles were investigated in the rosettes of the plants three weeks post-infection. As internal control, the *Arabidopsis* mutant *cyp79 b2/b3*, which has a mutation in the two genes converting the tryptophan into indole-3-acetaldoxime involved in indol glucosinolate biosynthesis, was tested in parallel to the other mutants, since it has been already shown that *cyp79 b2/b3* is highly susceptible to infection by this pathogen (Iven *et al*., 2012).

In all the lines tested, including the wild-type, leaf lesions were detected three weeks post-infection by *V. longisporum.* Moreover, the positive control line *cyp79 b2/b3* showed that the conditions of the experiment also allowed the detection of higher susceptibility (**Figure 10**). Important differences were observed between infected and non-infected plants regarding fresh weight and green rosettes area (**Figure 11**). Infected plants were generally smaller compared to control plants and thus exhibited significant decreases in fresh weight as well as green rosettes area according to students *t*-Test with a level smaller than 0.05. However, no differences were observed among the different infected plant lines, with exception of *sphk1*-OE / *spp1.2*, which was the only mutant line that exhibited signs of lesions although not statistical significance for both tested parameters (green rosette areas and rosette fresh weight) was reached when compared to the non-infected control plants (according to students *t*-Test with a level smaller than 0.05).

Then, the presence of the pathogen was confirmed by quantification of fungal DNA via qPCR three weeks post-infection (**Figure 12**). The susceptible mutant line *cyp79 b2/b3* showed similar results to those already published in Eynck *et al.* (2007), validating our experimental set-up. Regarding the other mutant lines tested, *sphk1*-OE, *sphk1*-KD, *sphk1*-OE / *spp1.2* and *dpl1.1* / *spp1.2* showed significantly higher levels of fungal DNA compared to Col-0. Interestingly, *sphk1*-OE / *spp1.2* presented a higher relative amount of fungal DNA but did not exhibit obvious signs of infection, suggesting that this mutant line is able to resist the pathogen even though it is present. In contrast, the mutant line *dpl1.1*, which showed significant signs of infection, did not present an increase in fungal DNA compared to Col-0. This suggests an increased susceptibility of this mutant line, in which low levels of pathogen cause macroscopical damages.

To gain further understanding of the relationship between the sphingolipids profile and the observed phenotypes after infection with *V. longisporum*, sphingolipids were quantified three weeks after infection (**Figures 10** and **11**). In comparison to Col-0, the susceptible mutant line *cyp79 b2/b3* displayed significantly increased levels of sphingobases d18:0 and t18:0 (0.05 and 2.5 nmol / g of fresh weight, respectively) compared to the levels measured in the wild-type plant (0.03 nmol / g fresh weight of d18:0 and 1.1 nmol /g fresh weight of t18:0). In addition, it did not show accumulation of phosphorylated sphingobases neither variation in the three out of the four most abundant sphingolipids analyzed. Regarding the *dpl1.1*, *sphk1*-KD, *dpl1.1* / *spp1.2* and *cyp79 b2/b3* mutant lines, which all showed macroscopic signs of infection, a significant accumulation of sphingobases was detected. These results are in line with another study that has shown that accumulation of free sphingobases leads the plant to its cellular death (Glenz *et al*., 2019). The two mutant lines *sphk1*-OE / *spp1.2* and *dpl1.1* / *spp1.2* exhibited accumulation of sphingobases (0.15 nmol / g fresh weight of d18:0 and 5 nmol /g fresh weight of t18:0) and phosphorylated sphingobases (3.2 or 3.6 nmol / g fresh weight of d18:0-P and 40 or 17 nmol /g fresh weight of t18:0-P) in comparison to Col-0. However, they both presented different profiles in response to the infection: *dpl1.1* / *spp1.2* presented necrosis while *sphk1*-OE / *spp1.2* did not. The only difference observed between these two lines was regarding the type of sphingolipid accumulated. This would suggest that different sphingolipid profiles could play a role in the resistance or the susceptibility of the plant to the pathogen. The mutant line *sphk1*-OE did not show accumulation of sphingobases, phosphorylated sphingobases or sphingolipids even though presented clear signs of infection. This could suggest that other sphingolipids not measured, such as other ceramides or ceramide-phosphate, might be involved in the response to the process of infection (Siebers *et al*., 2016). However, the possibility that the signs of infection could not be PCD but instead the result of *V. longisporum* infection provoking yellow leaves by damaging or clogging xylem vessels and reducing water supply of some regions of the leaves cannot be excluded. The analysis of sphingolipids was

performed three weeks post-infection when differences in relative leaf area between Col-0 and the mutant of reference, *cyp79 b2/b3*, were noticeable (Iven *et al*., 2012). This selected time point for the measurement of sphingolipids was the endpoint of the infection and not necessarily the most optimal time course of the infection. Indeed, earlier sampling, when the defense of the plant was at stake, could have allowed to observe more clear differences in the sphingolipids content.
In summary, *sphk1*-OE / *spp1.2* and *dpl1.1* / *spp1.2* exhibited strong accumulations of phosphorylated sphingobases with different pathogen phenotypes. The phenotype of the mutant line *sphk1*-OE / *spp1.2* after infection was the same as the control whereas the mutant line *dpl1.1* / *spp1.2* was more sensible to *V. longisporum* (**Figure 11**). The mutant line *sphk1*-OE, which only had elevated LCBs, presented the same phenotype as *dpl1.1* / *spp1.2* after infection. Altogether, it is difficult to draw a firm conclusion regarding which sphingobases or / and sphingolipids play an important role in pathogen resistance. The results suggest that high levels of LCBs might be a consequence rather than a cause of enhanced susceptibility, cell death or disease symptoms.

4.2. Study of the effect of temperature stress on sphingolipid metabolism.

It has been shown that the content of specific lipid species changes during different kinds of abiotic treatments (Dutilleul *et al*., 2012; Mittler *et al*., 2012; Dutilleul *et al*., 2015; Mueller *et al*., 2017). Membranes adapt their lipid composition in response to the environmental changes to maintain optimal properties and increase the chances of survival (Huby *et al*., 2019). In recent years, several studies have reported a role for sphingolipids in response to temperature stress (Dutilleul *et al*., 2012). Therefore, the second part of this thesis is focused on studying the effect that temperature stress, including heat shock, heat acclimation and cold acclimation, has on the sphingolipid metabolism of *Arabidopsis* plants. In particular, the aim was to find out, if within the mutant lines tested, the defects in LCBs and SPLs regulation led to different SPLs level changes upon temperature changes and if they are functionally required for the adaptation to different temperatures. However, it is very complex to draw conclusions between an observed phenotype and the sphingolipids profile measured. In this case, only the most abundant sphingolipids were measured and any changes in their levels that have taken place in response to the temperature stress were detected. Studying other pathways that might be involved could have been another approach to associate sphingolipid profiles to a phenotype.

4.2.1. Temperature acclimation.

The impact of cold and heat acclimation (respectively known as chilling and heat stress in the literature) on the growth and the sphingolipids profile of the seedlings was investigated. The mutants employed were *sphk1*-OE, *sphk1*-KD and *sphk1*-OE / *spp1.2*, which were compared to Col-0. Seedlings were grown for two weeks at 22 °C and then incubated for a few days either at 10 °C to test cold acclimation or 37 °C to test heat acclimation. Control plants were kept at 22 °C. Samples were collected at different time points.

4.2.1.1. Cold acclimation.

Two-week-old wild-type (col-0), *sphk1*-OE, *sphk1*-KD and *sphk1*-OE / *spp1.2* seedlings were grown on MS plates at 22 °C and then transferred to grow at 10 °C for one, three or seven additional days. Regarding the seedling growth, no differences were observed in those seedlings incubated at 10 °C in comparison to the control ones. The germination rate of *sphk1*-KD was very low even in the control seedlings, but this is due to its genotype and not to the treatment. In the sphingolipid profiles of the four different genotypes, an increase in d18:0 and/or t18:0 was observed during incubation at 10 °C (**Figure 19**; **Annex 9**). This observation is in agreement with what was already published in Nagano *et al*. (2014) where the authors show that the total amount of sphingolipids, including GIPCs, increased in wild-type plants after cold treatment and that unsaturated LCBs may be necessary for basic resistance to cold. Phosphorylated sphingobases were significantly increased in Col-0 (d18:0-P and t18:0-P levels at day 1 post-incubation) and *sphk1*-OE / *spp1.2* (t18:0-P at days 3 post-incubation) but not in the other genotypes analyzed according to students *t*-Test with a level smaller than 0.05. Surprisingly, most of the sphingolipid species, even the most abundant sphingolipids measured (such as d18:0-16:0 or t18:0-16:0), remained mainly unchanged after acclimation to 10 °C in comparison to their respective controls grown at 22 °C (**Figure 19**; **Annex 10**).

These results differ from what is published in the literature during cold stress at 4 °C under continuous light, where accumulation of total sphingolipids was observed at low temperature in *Arabidopsis* wild-type plants (Nagano *et al*., 2014). Although the conditions here (10 °C incubation with photoperiod 16 h light/8 h dark) were different to the ones in the study previously mentioned, the results suggest that the specific sphingolipids analyzed here would not play a central role in the process of cold acclimation. The analysis was focused on sphingobases, phosphorylated sphingobases and ceramides, while in Nagano *et al*. (2014), all sphingolipid classes were measured, especially GIPCs and Glc-Cers, which are present at much higher concentrations and are known to be important membrane lipids in eukaryotes (Warnecke and Heinz, 2003; Markham *et al*., 2006; Markham and Jaworski, 2007; Pata *et al*., 2010). Taken together, the absence of variation in ceramide levels would correlate with the fact that they are precursors for the most abundant membrane-localized lipids, Glc-Cers and GIPCs. Indeed, it has been shown that GIPC levels increase in *Arabidopsis* wild-type plants during early stage of cold acclimation, leading to an increase in the total amount of sphingolipids (Nagano *et al*., 2014). This would trigger a decrease in membrane fluidity due to the rigidity of sphingolipids in comparison to glycerolipids (Pata *et al*., 2010). To confirm this hypothesis, a quantification of the enzyme inositol phosphoryl ceramide synthase and glucosylceramide synthase, responsible for the synthesis of more complex ceramides, could be performed. The limiting factor in this pathway would be the quantities of these two enzymes, for which low levels could lead to a saturation of the synthesis capacity.

In conclusion, the sphingolipid levels detected at 10 °C were not too different from the ones detected under control growth conditions. Therefore, this would suggest that the sphingolipid profiles measured here in our *Arabidopsis* lines are not directly linked to cold resistance. In response to different environmental temperatures, changes mostly in the membrane composition are expected to occur in order to maintain the plant healthy. Hence, an analysis of the most abundant membrane lipids, Glc-Cers and GIPCs, would have been more appropriate in this case. As we measured steady-state levels, the possibility that the measured sphingolipids are used up in the pathway as fast as they are synthesized to become more complex sphingolipids cannot be excluded. For instance, the ceramides could be transformed into GIPCs, which were not measured in this experiment. In future studies, by using isotope-labeled LCBs before the treatment (as we perform in the last part of this

thesis), newly synthesized complex sphingolipids could be followed, determining which sphingolipid species are generated within the plant during cold acclimation.

4.2.1.2. Heat acclimation.

Two-week-old wild-type (col-0), *sphk1*-OE, *sphk1*-KD and *sphk1*-OE / *spp1.2* seedlings were grown on MS plates at 22 °C and then transferred to grow at 37 °C for one, three or seven additional days. After heat acclimation at 37°C, the cotyledons of the sphingolipid mutant lines *sphk1*-OE, *sphk1*-KD and *sphk1*-OE / *spp1.2* were much bigger than the respective control cotyledons grown at 22°C. However, this was not the case for Col-0, in which cotyledons remained unchanged after acclimation (**Figure 18**). These results were reproduced in an independent experiment with the same conditions of treatment (2 weeks at 22 °C and then 37 °C for one, three or seven days).
In contrast to low temperature tolerance, the function of sphingolipids in tolerance of high temperature remains poorly characterized (Huby *et al*., 2019). Next, we investigated whether these morphological changes could be related to adjustments in the lipid profiles of these genotypes by analyzing sphingolipids present in all seedlings. Increases in sphingobases, phosphorylated sphingobases and sphingolipids were observed in Col-0 after one day of acclimation at 37 °C. Increases in sphingobases and sphingolipids were also observed in the mutant lines *sphk1*-OE and *sphk1*-KD. Importantly, among all the sphingolipids analyzed, the most noticeable difference between Col-0 and these mutant genotypes is regarding the accumulation of phosphorylated sphingobases. While Col-0 significantly accumulated d18:0-P at day 1 of heat acclimation, the level of phosphorylated sphingobase d18:0-P in the mutant lines *sphk1*-OE and *sphk1*-KD changed only slightly (non-significant difference detected according to students *t*-Test with a level smaller than 0.05). In the case of the double mutant *sphk1*-OE / *spp1.2,* the levels of d18:0-P and t18:0-P were even lower after acclimation (three times lower for d18:0-P and four times lower for t18:0-P at day seven) in comparison to control plants (**Figure 19**; **Annex 9**). This could suggest that these three mutants are able to process phosphorylated sphingobases during heat acclimation as efficiently as during control conditions. However, we could not exclude that the reason for a specific steady-state level of sphingobases could be from the *de novo* production or degradation. Then, it could be speculated that phosphorylated sphingobases are used up further in the sphingolipid pathway in a way that helps these mutants adapting to the harmful effects of warmer temperatures. Phosphorylated sphingobases can also be used to further synthesize other molecules that are not being measured in this experiment, such as phosphorylated ceramides.

4.2.2. Heat shock.

During heat shock response, *Arabidopsis* seedlings, with basal thermotolerance, can survive temperatures as high as 45 °C for a period superior to 2 h (Mueller *et al*., 2017). It has been shown also that, in order to survive variations in temperature, plants modify their metabolism and perform structural remodeling, including lipid contents (Dutilleul *et al*., 2012; Mittler *et al*., 2012; Huang *et al*., 2017). As example, accumulation of triacylglycerols, a type of lipid, has been reported to accumulate and reach maximum levels at temperatures up to 42 °C (Mueller *et al*., 2015). In this thesis, heat shock experiments were performed employing the sphingolipid metabolism mutant lines *dpl1.1*, *sphk1*-OE, *sphk1*-KD, *sphk1*-OE / *spp1.2*, *dpl1.1* / *spp1.2* and *spp1.2* as well as Col-0 to investigate if some sphingolipids species measured were involved in the survival of the plant. Indeed, it is not well understood which SPL species are regulated in response to temperature changes to maintain optimal

properties and increase the chances of survival. The experiment was performed by growing seedlings for two weeks at 22 °C, and then, exposing them to a sudden increase in temperature (45 °C) for a short period of time (90 min). Control plants were kept at 22 °C. Then, the survival (**Figure 18**) and sphingolipid profiles (**Figure 16** and **17**) were evaluated after two weeks of recovery.

The survival rate of Col-0 after heat shock was approximately at 70 %. This result is in agreement with unpublished data obtained previously in our laboratory. Col-0 was defined as reference of well-established test. A significant decrease in survival after heat shock was also observed in all the mutant lines tested, apart from the *sphk1*-KD mutant, which only presented a moderate non-significant decrease in comparison to the non-treated plants according to students *t*-Test with a level smaller than 0.05. The mutant *dpl1.1* was the only line with a higher survival rate than Col-0 after heat shock (78 %) while all the other mutant lines presented survival rates that ranged from 41 % (*dpl1.1* / *spp1.2*) to 69 % (*sphk1*-OE / *spp1.2*).

As sphingolipids are components of the membrane, one can hypothesize that a rearrangement of the sphingolipid profile would occur under a heat stress condition and that certain sphingolipids would protect the plants against such heat shock. To see if any differences could be observed, the level of sphingolipids, sphingobases, phosphorylated sphingobases and main sphingolipids were measured after heat shock (**Figure 16** and **17**). The lines Col-0, *dpl1.1* and *spp1.2* presented no variation on their sphingolipid profiles (except for d18:0-16:0 for *spp1.2*) after treatment, which would explain the similar survival rates observed (59 to 78 %). The mutant line *sphk1*-OE, which presented elevated levels of sphingobases (d18:0 and t18:0), phosphorylated sphingobases (d18:0-P and t18:0-P) and sphingolipids (d18:0-16:0 and t18:0-16:0) after treatment, was more affected by the heat shock and presented an even lower survival rate than Col-0 (58 % of survival rate for *sphk1*-OE and 70 % of survival rate for Col-0). However, the two mutant lines accumulating phosphorylated sphingobases *sphk1*-OE and *spp1.2* presented almost the same survival rate after heat shock (58 % and 59 %, respectively) but did not share either the same sphingobase profiles (d18:0 and t18:0) or the same ceramide profile (t18:0-16:0). This would suggest that other factors, such as more complex sphingolipids, would have a higher impact on the survival of the plant. The survival rate of *sphk1*-KD (64 %), which was the only one not significantly lower after heat shock, showed the same sphingolipids profile than the double mutants tested, *sphk1*-OE / *spp1.2* and *dpl1.1* / *spp1.2*, for which the survival rates observed were 69 % and 41 %, respectively. This last observation would suggest that, at least for these three mutant lines, the sphingolipids measured here do not play an important role in the survival of the plant to heat shock, since there is almost a 30 % difference in survival between them. The results obtained show that increases in sphingolipid levels, including sphingobases and phosphorylated sphingobases, could be the cause of decreased survival, at least regarding the mutant line *sphk1*-OE. Moreover, the mutant lines *sphk1*-KD, *sphk1*-OE / *spp1.2*, *dpl1.1* / *spp1.2* and *spp1.2* have shown diminution in t18:0-24:0 and t18:0-26:0 levels as well as survival after heat shock. These levels were also decreased in Col-0 seedlings after treatment. However, within *dpl1.1*, where the levels of these sphingolipids were not changing after treatment, a better survivability was observed (70 % for Col-0 and 78 % for *dpl1.1*). Together, it can be speculated that diminishment of these sphingolipid species (t18:0-24:0 and t18:0-26:0) could have a negative effect on the survival of these mutants. Nevertheless, in opposition to this hypothesis, the mutant line *sphk1*-OE did not show variation in the levels of VLCFA-sphingolipids but did show a reduced survivability. In these experiments, it would have been interesting to measure the levels of more complex sphingolipids, such as GIPCs or Glc-Cers, in these sphingolipid mutant lines. Even if their production is not supposed to be directly affected by the mutations, a more completed sphingolipid profile could be linked more accurately to a phenotype of survival.

4.3. Study of sphingolipids metabolism pathway.

The LCB moiety is an integral structural part for sphingolipid synthesis, while free LCBs have been shown to act also as signaling molecules, implicated in stomatal closure or pathogen responses, for example (Ng *et al*., 2001; Coursol *et al*., 2005; Worrall *et al*., 2008; Magnin-Robert *et al*., 2015). In the literature, it has also been described that high quantities of LCBs, such as those induced by the toxin Fumonisin B1 from the pathogenic Fusarium clade or by direct application to the plant, lead to cell death (Shi *et al*., 2007; Peer *et al*., 2011; Glenz *et al*., 2019). High levels of LCBs can be processed by the plant via two different ways: downregulation of LCBs via the *de novo* synthesis pathway allowing their incorporation into more complex sphingolipids (Ceramides, Glc-Cers, GIPCs) or degradation via phosphorylation to become LCB-Ps and subsequent degradation by DPL1 into hexadecanal and ethanolamine phosphate (Hannun and Obeid, 2011; Merrill, 2011; González-Solís *et al*., 2020). It has been shown that DPL1 is required for reducing high LCB levels through phosphorylated LCBs after FB1 treatment (Tsegaye *et al*., 2007; Magnin-Robert *et al*., 2015; Glenz *et al*., 2019).

The last part of this thesis focused on investigating the fate of the sphingobase d18:0 in the metabolic pathway after providing a lethal d18:0 quantity to the plant. The purpose of this experiment was to be able to further understand how high levels of LCBs are metabolically processed in the plant. To do so, the changes in sphingolipid levels over time in *A. thaliana* were analyzed by providing a large amount of the sphingobase d18:0, one of the first precursors of the sphingolipid synthesis pathway. The procedure, which required the application of saturating levels of isotope-labeled D_7-d18:0 (also known as feeding), provoked an accumulation of LCBs (200 nmol / g fresh weight 1 h post-feeding) within the plant, which induces cell death (Peer *et al*., 2011). The quantity of labeled LCBs present in the leaf samples corresponded to >97 % of total LCBs and enabled the quantification of LCB products with high and low turnovers.

Determination of the levels of the different labeled sphingolipids located downstream the pathways was carried out by using high-performance liquid chromatography coupled with tandem mass spectrometry using a Quattro Premier Triple Quadrupol instrument (HPLC-MS/MS) or ultra-performance liquid chromatography coupled with a SYNAPT G2 High-Definition Mass Spectrometry™ Quadrupole Time of flight-MS (UPLC-QTOF-MS). The sphingobase d18:0 is the first LCB of the sphingolipid pathway thus it was chosen to be labeled with deuterium (D_7-d18:0) for feeding *A. thaliana* leaf discs. This would help to better understand the incorporation rates of sphingolipids over time since the labeled part of the molecules is conserved during the metabolic process. By performing the feeding with this sphingobase on leaf discs, an unlimited input of this first LCB into the pathway was assured, providing a way of studying the rate of LCB incorporation into different sphingolipid species as well as their turnover. In short, D_7-d18:0 is incorporated and transformed into more complex sphingolipids and the measured quantities reveal the plant's preference and speed of synthesis.

The high incorporation rates of the labeled D_7-d18:0 into d18:0-P and d18:0-16:0 (**Figure 26**), indicated that the labeled LCB is rapidly taken up into the leaf cells and is available for enzymatic processing (0.05 and 0.02 nmol / g fresh weight 1 h post-feeding, respectively). The incorporation rates measured for d18:0-16:0 and t18:0 are in a similar range to those reported in Shi *et al*. 2015. In this study, the authors performed an experiment with ^{15}N-labeled serine in *Arabidopsis* seedlings. In this case, only the single nitrogen atom of the head of the sphingolipids was labeled. The incorporation rate of ^{15}N-labeled serine was different depending on the sphingolipid species. Indeed, its incorporation into simple sphingolipids was between 40 and 65 % and the rate was rather fast. In contrast, the incorporation rate into glucosylceramides was lower in comparison to ceramides and

hydroxyceramides due to the stoichiometry. In this thesis, by using deuterium labeling at the tail of the LCB, the incorporation of the sphingobase into complex sphingolipids can be followed with more accuracy.

Regarding the synthesis of sphingolipids, different "levels of synthesis" can be established, which can help understand the incorporation rate of the newly synthesized sphingolipids (from D_7-d18:0) within the pathways. The first level of synthesis would be comprised of the compounds that use directly D_7-d18:0. For example, as first level of synthesis, D_7-d18:0 can be directly incorporated into sphingolipids such as D_7-d18:0-16:0 by ceramide synthase, hydroxylated into D_7-t18:0 by LCB C4-hydroxylase, or phosphorylated into D_7-d18:0-P by LCB kinase. The second level of synthesis would involve an additional step of enzymatic activity and thus would be comprised of compounds that use those of the first level of synthesis to transform them into other sphingolipids, such as D_7-t18:0-16:0 or D_7-t18:0-P. By using sphingolipid kinase mutant plants in the feeding experiments and then measuring phosphorylated LCB levels, differences in the incorporation rate of D_7-d18:0 and distinctions in the different "levels of synthesis" could be established.

There are two different methods for the analysis of metabolites distributions found in a biological system by mass spectrometry-based metabolomics. Generally, the method of choice method will depend on the biological question asked and on the nature of the compounds to be measured (Kueger *et al*., 2012). The first method, commonly known as targeted metabolomics, measures and profiles known metabolites with known chemical structures (Albinsky *et al*., 2010; Dudley *et al*., 2010). The second method, commonly known as non-targeted analysis, studies compounds beyond the known targets including signals of unknown identity (Hanhineva *et al*., 2008; Tianniam *et al*., 2009).

4.3.1. Investigating sphingolipids incorporation rate by targeted analysis in *Arabidopsis* wild-type plants.

The targeted analysis allows quantification of the metabolites measured by using reference materials, which is considered as the main advantage of this method. However, not all reference materials are available, limiting the number of compounds that can be analyzed. In this thesis, the synthesis of new specific sphingolipid species was analyzed in a targeted experiment by using D_7-d18:0 for feeding.

On one hand, as shown in **Figure 21**, between 200 to 300 nmol per gram of fresh weight, respectively, were detected in the leaf discs from 1 h to 48 h post-feeding with D_7-d18:0. At the same time, the quantity of D_7-d18:0 diminished in the incubating solution over time (66 nmol / g fresh weight at 1 h post-feeding and 4 nmol / g fresh weight at 48 h post-feeding), indicating an uptake of the sphingobase by the leaf discs. Also, a transient increase in D_7-t18:0 was observed, which peaked at 6 h post-feeding with 5.3 nmol / g fresh weight and then returned to 1-2 nmol / g fresh weight at 48 h post-feeding. This suggests that the rate of synthesis of this metabolite and the rate of conversion into more complex sphingolipids during this time period are similar. Other sphingolipids defined in this study as first level of synthesis, such as D_7-d18:0-24:0 and D_7-d18:0-26:0, showed similar patterns to D_7-t18:0. This similarity is defined by a rapid accumulation of the sphingolipids peaking at 3 h or 6 h post-feeding followed by a decrease close to basal levels after 48 h post-feeding. This characteristic transient peak was not observed at 6 h post-feeding for all the measured sphingolipids defined as first level of synthesis. Some others, such as D_7-d18:0-16:0, presented this transient increase at 24 h post-feeding. These transient increases could represent a first accumulation of sphingolipids in the plant until a breaking point is reached, when they are used

up for synthesizing other sphingolipids. They could also be an indication of the time required by the plant for the synthesis and availability of free fatty acids or for the synthesis of enzymes involved in processing these accumulated metabolites into more complex sphingolipids.

On the other hand, for most of the sphingolipids measured in this experiment, a decrease in their quantities was observed at 48 h. This would indicate that, at this time, they are either degraded or processed into other metabolites that are not being measured by the targeted analysis, such as Glc-Cers or GIPCs. To measure those metabolites, reference materials of authentic compounds would be required in order to confirm their existence, avoiding the measurement of artefacts. Unfortunately, such reference materials do not exist. Nevertheless, by considering the results obtained in the untargeted analysis (**Figure 24**), we could speculate that the formation of d18:1-P-26:2 and Glc-d18:0-26:0, which are among the most abundant sphingolipids present after 24 h post-feeding, could originate from one of the first level of sphingolipids synthesized, D_7-d18:0-26:0. This would explain the return to baseline of this sphingolipid.

A constant increase in the phosphorylated sphingobases D_7-d18:0-P and D_7-t18:0-P was observed during the experiment, which could result from the need of the plant to decrease the toxic effect of the accumulation of a large amount of sphingobases. Indeed, as mentioned before, high levels of LCBs can induce cell death and one of the strategies of the plant to downregulate those levels is by phosphorylation of the LCBs and subsequent degradation of LCB-Ps into hexadecanal and ethanolamine phosphate, which is carried out by the enzyme DPL1 (Hannun and Obeid, 2011; Merrill, 2011; Peer *et al*., 2011). Higher steady-state levels of these compounds may indicate a higher activity of LCB kinases. It could be speculated that levels of phosphorylated sphingobases would continue to increase over time until reaching the maximum activity of the enzymes involved in the synthesis and degradation of D_7-d18:0-P and D_7-t18:0-P. If not targeted for degradation, the accumulated phosphorylated sphingobases could also be incorporated into phosphorylated ceramides. However, in this thesis, it was not possible to measure this part of the pathway due to the lack of reference materials of authentic compounds.

Generally, the quantity of sphingolipids that would potentially belong to the second level of synthesis, such as D_7-t18:0-16:0 and D_7-t18:1-16:0, presented a remarkable increase after 6 h post-feeding. These results are consistent with the fact that metabolites from the second level of synthesis would take longer to be produced from the initial LCB, D_7-d18:0, since several enzymatic steps are required. Another limiting factor could be the production of metabolic enzymes, which can be absent or present at low concentrations in the pathway before the feeding. As example, phosphorylated sphingobase levels were not detected under basal conditions in Col-0 (**Figure 4**) but were present in high quantities 48 h post-feeding (**Figure 21**). In the sphingolipid pathway, the reduction of d18:0 levels requires the enzymes SBH1 and SBH2 to create t18:0. All LCBs, phosphorylated and non-phosphorylated, are used for the formation of ceramides by the enzymes LOH1/2/3 and their degradation into hexadecanal and ethanolamine phosphate, after phosphorylation, is conducted by the enzyme DPL1.

A fast accumulation of phosphorylated sphingobases was observed using the targeted analysis. As mentioned, this could represent a strategy of the plant to rapidly degrade the flooded amount of D_7-d18:0. Another strategy in the sphingolipids synthesis pathway to arrive to the degradation path would be the formation of ceramides as fast as possible. Unfortunately, the poor availability of reference compounds in this experiment is a limiting factor to obtain more information about metabolites present in this pathway. One strategy to further investigate this pathway would be to measure the levels of hexadecanal and ethanolamine phosphate, both products of the degradation of phosphorylated sphingobases, generated by DPL1. In future studies, measuring the levels of these

degradation products and/or the activity of the lyase would give an indication of the amount of sphingobases that are being degraded. Unfortunately, in these experiments, sphingolipid levels were measured by evaluating the incorporation of deuterium-labeled LCB moiety, which would be present in hexadecanal but not in ethanolamine phosphates. It could be speculated that higher levels of hexadecanal would be detectable within 1 h to 6 h post-feeding, since it is the timeframe in which increased amounts of phosphorylated sphingobases were observed. Indeed, between 1 h and 6 h post-feeding, the quantities of D_7-d18:0-P and D_7-t18:0-P, produced from the feeding with D_7-d18:0, were at least five times higher and did not show any sign of turnover after 48 h of experiment. For most of the other sphingolipids analyzed, the turnover happened between 6 h and 48 h.
To conclude, sphingolipids defined as first level of synthesis were increasing at earlier time points (3 to 6 h post-feeding) than the ones considered as second level of synthesis (24 h post-feeding). However, an absolute understanding of the sphingolipids pathway by using targeted analysis is almost impossible. The need of reference materials for designing the method and the choice of analytes of interest to be analyzed are the main restrictions of the targeted analysis. In contrast to targeted analysis, high resolution mass spectrometry performed by untargeted analysis allows the detection of many more compounds (markers) over time. Additional experiments or databases using this untargeted analysis would further allow the identification of new metabolites of interest.

4.3.2. Investigating sphingolipids incorporation rate by untargeted analysis in *Arabidopsis* wild-type plants.

An untargeted analysis was employed as a metabolite profiling approach by including a chromatographic separation step upstream of the mass spectrometry measurement. This method is generally employed to analyze a larger set of compounds within a single class of compounds (Last *et al*., 2007; Allwood and Goodacre, 2010). Metabolomic signatures obtained by non-targeted analysis can be analyzed by multivariate statistical methods and provide significantly different metabolic features between the analyzed samples (Bylesjö *et al*., 2007; Sumner *et al*., 2007b). The aim of this analysis was to identify the newly synthesized sphingolipids coming from feeding with D_7-D18:0 to understand the preferences of incorporation of the plant and the speed of synthesis of these sphingolipids. Combining the results gathered using the two methods, targeted and untargeted, it is possible to better understand how the sphingolipid pathways operate under stress conditions. By performing untargeted analysis, 439 markers were detected in leaf discs 48 h post-feeding. Among those markers, 71 sphingolipids could be identified by employing a deuterium-labeled sphingolipids database. This database was created in-house focusing only on sphingolipids and thus other markers among those 439 identified could correspond to other molecules that are not sphingolipids, such as degradation products. For analyzing the results of this experiment, the areas identified for each metabolite were quantified and compared, although these areas are not the perfect reflection of the concentration of the metabolites detected. Indeed, the concentration could not be accurately calculated due to the unavailability of internal standards, the presence of unknown response factors and the different chemical properties of each metabolite. Among all the sphingolipids measured, D_7-d18:0 was present in the highest amount. This is due to the uptake of D_7-d18:0 from the solution by the leaf discs during the experiment, although it could also be due to remaining molecules of D_7-d18:0 that stuck on the outside part of the leaf discs even after washing. Ceramides and hydroxyceramides were among the top ten most abundant sphingolipids detected (e.g. t18:0-24:0, d18:0-24:0 or ht18:0-h18:0), which clearly highlights the importance of the ceramide *de novo* synthesis pathway in the sphingolipid metabolism. Among the most abundant sphingolipids, few

glycosyl-ceramides were also detected, such as Glc-d18:0-20:2 (area: 196036 at 24 h post-feeding), which presented an area that was 10 times smaller than that of the first ceramide detected, t18:0-24:0 (area: 1892921 at 24 h post-feeding). Such a difference in the areas could be due to the fact that the synthesis of this type of sphingolipids involves an enzymatic step, which requires the participation of glycosyl-ceramide synthases, such as GCS2. The action of this enzyme takes place later in the sphingolipid pathway and thus can delay the production of glycosyl-ceramides, which might peak after 48 h post-feeding.

Finally, the most abundant GIPC detected was GIPC-d18:1-20:2, which can be considered to be present in a small amount if compared to the amounts of the top ten most abundant metabolites. It could be speculated that, like for the glycosyl-ceramides, GIPCs synthesis also requires multiple enzymatic steps carried out by several enzymes, such as inositol phosphorylceramide synthase and glucuronosyl transferase, which could delay the synthesis of this type of sphingolipids. For instance, the quantity of GIPC-d18:1-20:2 peaked at 24 h post-feeding. In addition, in comparison to most sphingolipids that are produced in the ER, GIPCs need to be transported into the Golgi apparatus for synthesis, which could also explain why the areas of GIPCs remain lower.

An accumulation of sphingobases during the feeding experiment is highly toxic for the plant (Peer *et al*., 2010) and thus getting these compounds into the degradation pathway would represent a priority for the plant. Considering this, although the incorporation of LCBs into GIPCs would suppose a higher consumption of energy for the plant in comparison to other strategies (e.g. less enzymatic steps required for the production of phosphorylated sphingolipids and their degradation), the production of GIPCs represents a solution to avoid accumulation of LCBs.

In this experiment, the pattern of change of these sphingolipid species over time was also analyzed. In total, three different patterns were observed, including continuous increases, transient increases and continuous decreases in ceramides synthesis. The early continuous increases (1 h post-feeding) correspond to compounds that, using d18:0, require one or two enzymatic steps for the synthesis of ceramides. Also, later continuous increases (6 h post-feeding) were detected, which correspond mainly to compounds that are further downstream the sphingolipid pathway, such as Glc-t18:1-h28:2. The transient increases mostly peaked at 6 h post-feeding before decreasing. This might be due to the time that some particular enzymes need to be produced in higher amounts to be able to process the accumulation of sphingolipids. Only for one compound based on elemental composition calculation within the data, a continuous decrease was observed. The amount of ht18:0-h28:2 was highest at 0-1 h and then drastically decreased. This suggests an immediate and rapid use of this metabolite from the moment of the feeding. In addition, the patterns of the compounds detected by the targeted and the untargeted methods showed similarities (i.e. t18:0 and d18:0-P; **Figure 21** and **25**). It has been shown that flux distributions of LCBs, ceramides and hydroxyceramides composed the highest fraction of total flux. VLCFA-ceramides and hydroxyceramides were defined as important metabolites due to their high flux contribution while the pool sizes of LCBs are rather small in comparison. In contrast, glycosyl-ceramides, had a larger pool size but smaller metabolic fluxes with slow but lasting incorporation rates (Shi *et al*., 2015). Calculated steady-state rates have been recently used for the reconstruction of a metabolic network selecting reactions according to growth measurements and sphingolipid quantifications. Combination of regulatory mechanisms within models of prediction would allow the guidance of experiments and play an important role to engineer crops with higher biotic stress tolerance (Alsiyabi *et al*., 2021).

In conclusion, these data would confirm that sphingolipids that belong to the first and second levels of synthesis are the ones that have incorporated D_7-d18:0 the most. We observed that the capacity of the enzymes involved to process high quantities of LCBs was fast (3 h post-feeding) or near immediate (1 h post-feeding). Some of those enzymatic activities include the hydroxylation of t18:0 from d18:0 (by SBH1/2), the phosphorylation of LCBs by LCB kinases (e.g. LCBK1 or SPHK1) before degradation by DPL1, and the production of ceramides by ceramide synthases (LOH1/2/3). Ceramides with di-hydroxylated LCB, such as d18:0-16:0 and d18:0-24:0, or tri-hydroxylated LCBs, such as t18:0-16:0 and t18:0-24:0, were confirmed to be important in the synthesis pathway by both, targeted and untargeted analysis. Ceramides were further modified by desaturases and hydroxylases and converted into Glc-Cers and GIPCs, which represent pools of highly abundant families of membrane-localized metabolites. Furthermore, the relevance of LCB degradation via phosphorylation and subsequent degradation was highlighted by the presence of high levels and turnover rates of LCB-Ps. A better understanding of the degradation into hexadecanal and ethanolamine phosphate by the enzyme DPL1 and the fine-tuning of the *DPL1* activity could also assist in enhancing the resistance of the plant to high levels of LCBs (such as the increase in LCBs induced by FB_1). In addition, the data obtained during untargeted analysis also illustrates a priority of the plant for ceramides, hydroxyceramides and glycosyl-ceramides pathways in comparison to GIPC pathways. Nevertheless, among these three classes of sphingolipids, no general rule regarding the preference of the plant for sphingolipids synthesis could be drawn concerning the length of the fatty acid or the hydroxylation of the sphingobase. Solving these questions would help define if there is a type of ceramides that are predominantly synthesized in the pathway. A mutant approach could help to decipher which SPLs-modifying enzymes are required for degradation of high LCB levels. As example, a mutant approach using a knockout of *DPL1* had a severe phenotype after FB_1 treatment, making this pathway important. This *dpl1* mutant could also be used in a feeding experiment to try to detect alternative degradation pathways.

Since untargeted analysis allowed the profiling of a large pool of metabolites, it is not to exclude that high level of LCBs might trigger the production of non-sphingolipid candidates. However, their identification is almost impossible with only the knowledge of the elemental composition and the inexistence of reference material, such as the list of marker peaks detected after feeding with D_7-d18:0 presented in **Annex 12**. Complementary experiments measuring additional sphingolipids in positive and negative ESI or increasing the pool of reference materials for the identification of these metabolites would be necessary to be able to determine the preference of LCBs incorporation of the plant in the synthesis pathways.

5. Annexes.

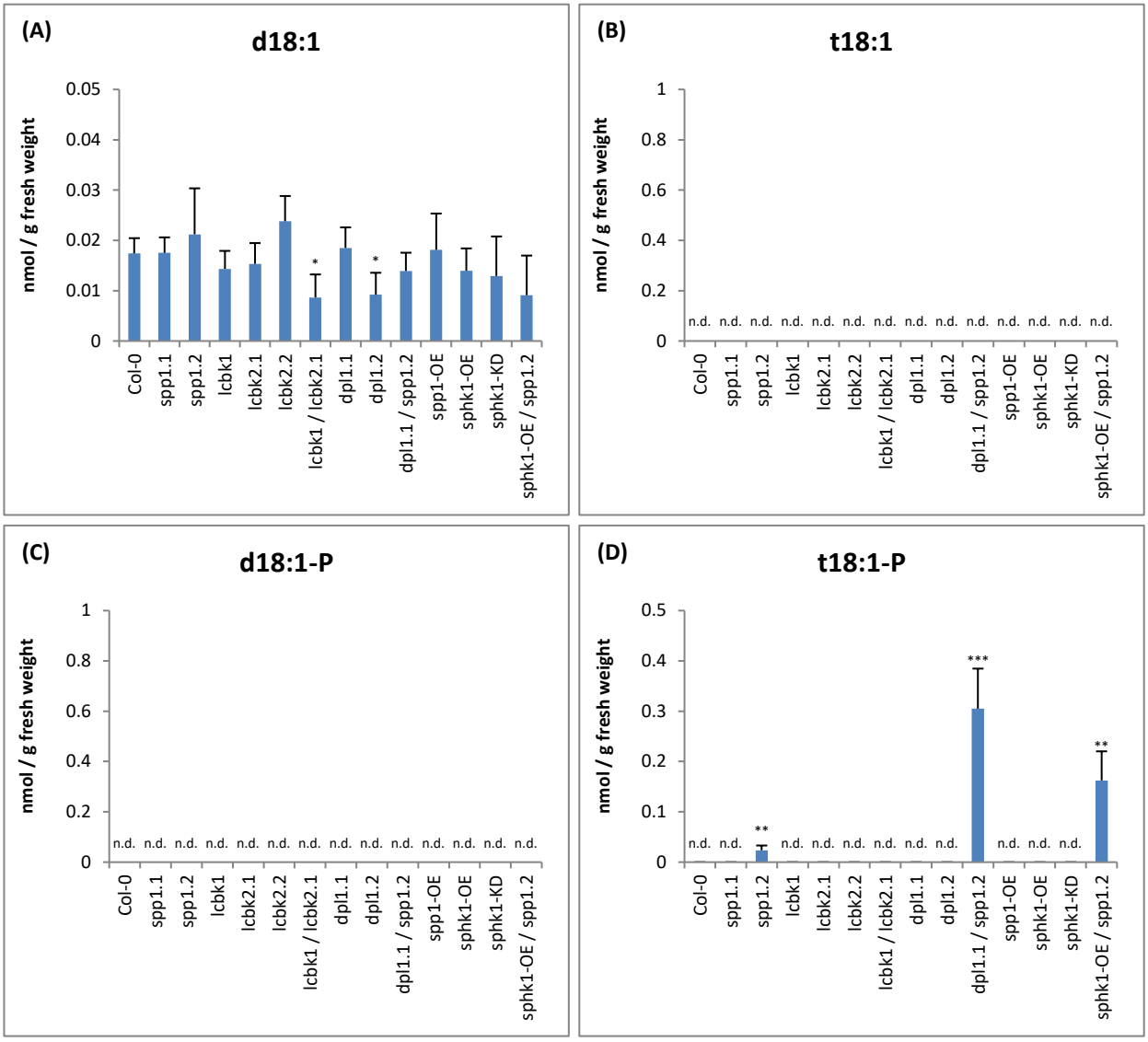

Annex 1: Sphingobase and phosphorylated sphingobase basal levels in *A. thaliana* wild-type ecotype Col-0 and *Arabidopsis* sphingolipid metabolism mutant lines. Sphingobases and phosphorylated sphingobases detected in six-week-old leaves of *A. thaliana* wild-type ecotype (Col-0) and *Arabidopsis* sphingolipid metabolism mutant lines. Levels were calculated by comparison to internal standards using correction factors (Section 2. 2. 4. 2. Targeted analysis) and presented as nano-mole per gram of fresh weight (nmol / g fresh weight). Asterisks indicate significant differences between Col-0 and the corresponding mutant line according to Student's *t*-Test: *, $P < 0.05$; **, $P < 0.01$; and ***, $P < 0.001$ (n.d. stands for non-detected). Results show means ± SD of four different technical replicates. The experiment has been repeated three times with similar results.

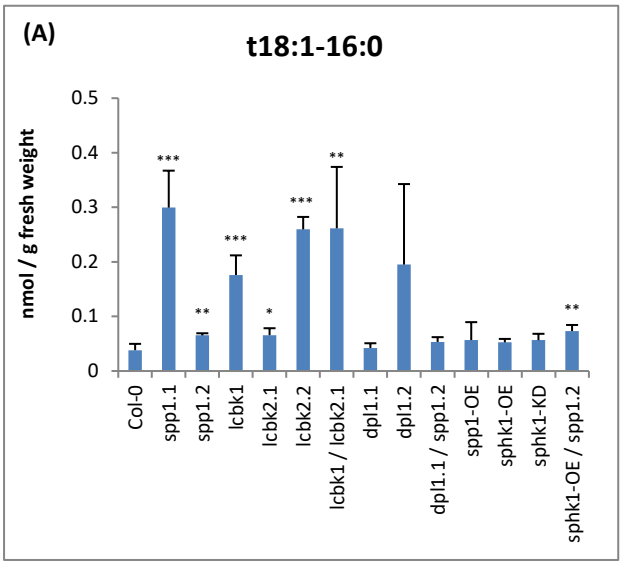
(A)
t18:1-16:0
nmol / g fresh weight
0
0.1
0.2
0.3
0.4
0.5
***
**
***
*
***
**
**
Col-0
spp1.1
spp1.2
lcbk1
lcbk2.1
lcbk2.2
lcbk1 / lcbk2.1
dpl1.1
dpl1.2
dpl1.1 / spp1.2
spp1-OE
sphk1-OE
sphk1-KD
sphk1-OE / spp1.2

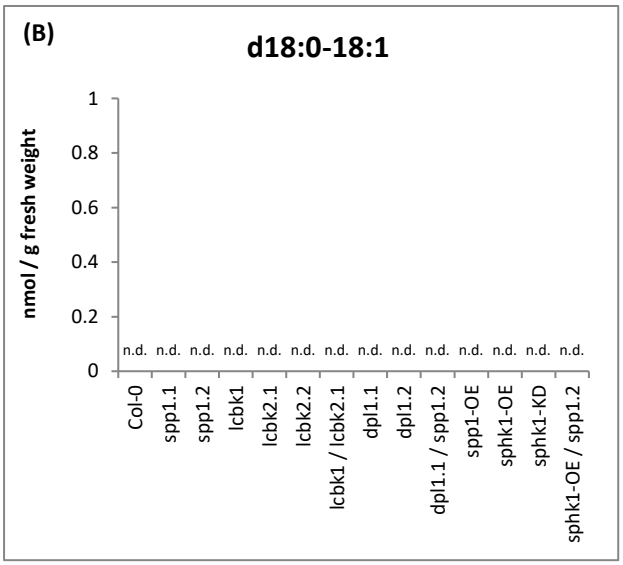
(B)
d18:0-18:1
nmol / g fresh weight
0
0.2
0.4
0.6
0.8
1
n.d.
Col-0
spp1.1
spp1.2
lcbk1
lcbk2.1
lcbk2.2
lcbk1 / lcbk2.1
dpl1.1
dpl1.2
dpl1.1 / spp1.2
spp1-OE
sphk1-OE
sphk1-KD
sphk1-OE / spp1.2

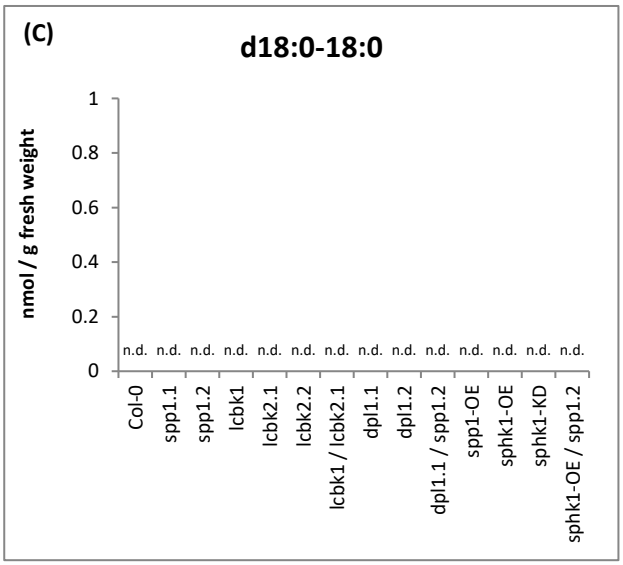
(C)
d18:0-18:0
nmol / g fresh weight
0
0.2
0.4
0.6
0.8
1
n.d.
Col-0
spp1.1
spp1.2
lcbk1
lcbk2.1
lcbk2.2
lcbk1 / lcbk2.1
dpl1.1
dpl1.2
dpl1.1 / spp1.2
spp1-OE
sphk1-OE
sphk1-KD
sphk1-OE / spp1.2

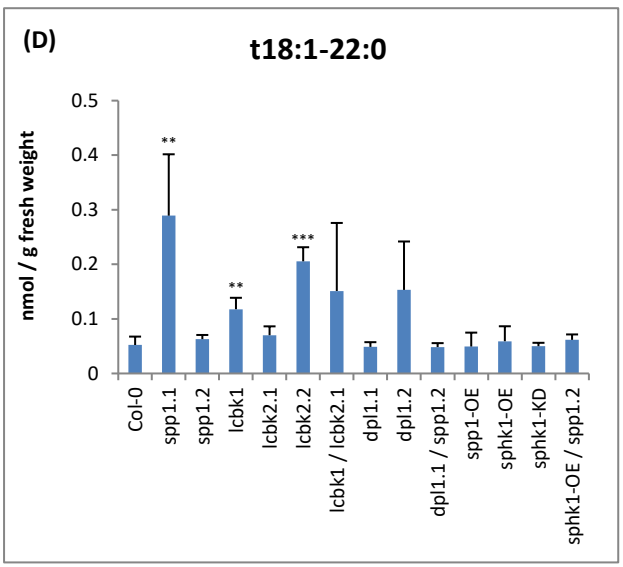
(D)
t18:1-22:0
nmol / g fresh weight
0
0.1
0.2
0.3
0.4
0.5
**
**
***
Col-0
spp1.1
spp1.2
lcbk1
lcbk2.1
lcbk2.2
lcbk1 / lcbk2.1
dpl1.1
dpl1.2
dpl1.1 / spp1.2
spp1-OE
sphk1-OE
sphk1-KD
sphk1-OE / spp1.2

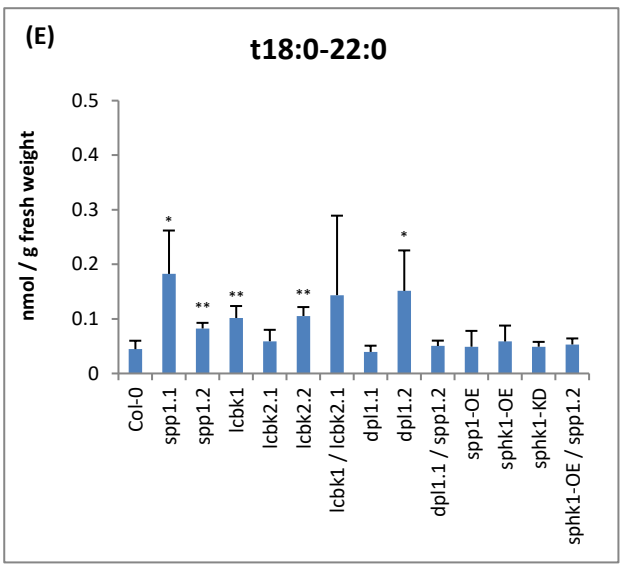
(E)
t18:0-22:0
nmol / g fresh weight
0
0.1
0.2
0.3
0.4
0.5
*
**
**
**
*
Col-0
spp1.1
spp1.2
lcbk1
lcbk2.1
lcbk2.2
lcbk1 / lcbk2.1
dpl1.1
dpl1.2
dpl1.1 / spp1.2
spp1-OE
sphk1-OE
sphk1-KD
sphk1-OE / spp1.2

Annex 2: Long-chain fatty acid ceramide basal levels in *A. thaliana* wild-type ecotype Col-0 and *Arabidopsis* sphingolipid metabolism mutant lines. Long-chain fatty acid ceramides detected in six-week-old leaves of *A. thaliana* wild-type ecotype (Col-0) and *Arabidopsis* sphingolipid metabolism mutant lines. Levels were calculated by comparison to internal standards using correction factors (Section 2. 2. 4. 2. Targeted analysis) and presented as nano-mole per gram of fresh weight (nmol / g fresh weight). Asterisks indicate significant differences between Col-0 and the corresponding mutant line according to Student's *t*-Test: *, P < 0.05; **, P < 0.01; and ***, P < 0.001 (n.d. stands for non-detected). Results show means ± SD of four different technical replicates. The experiment has been repeated three times with similar results.

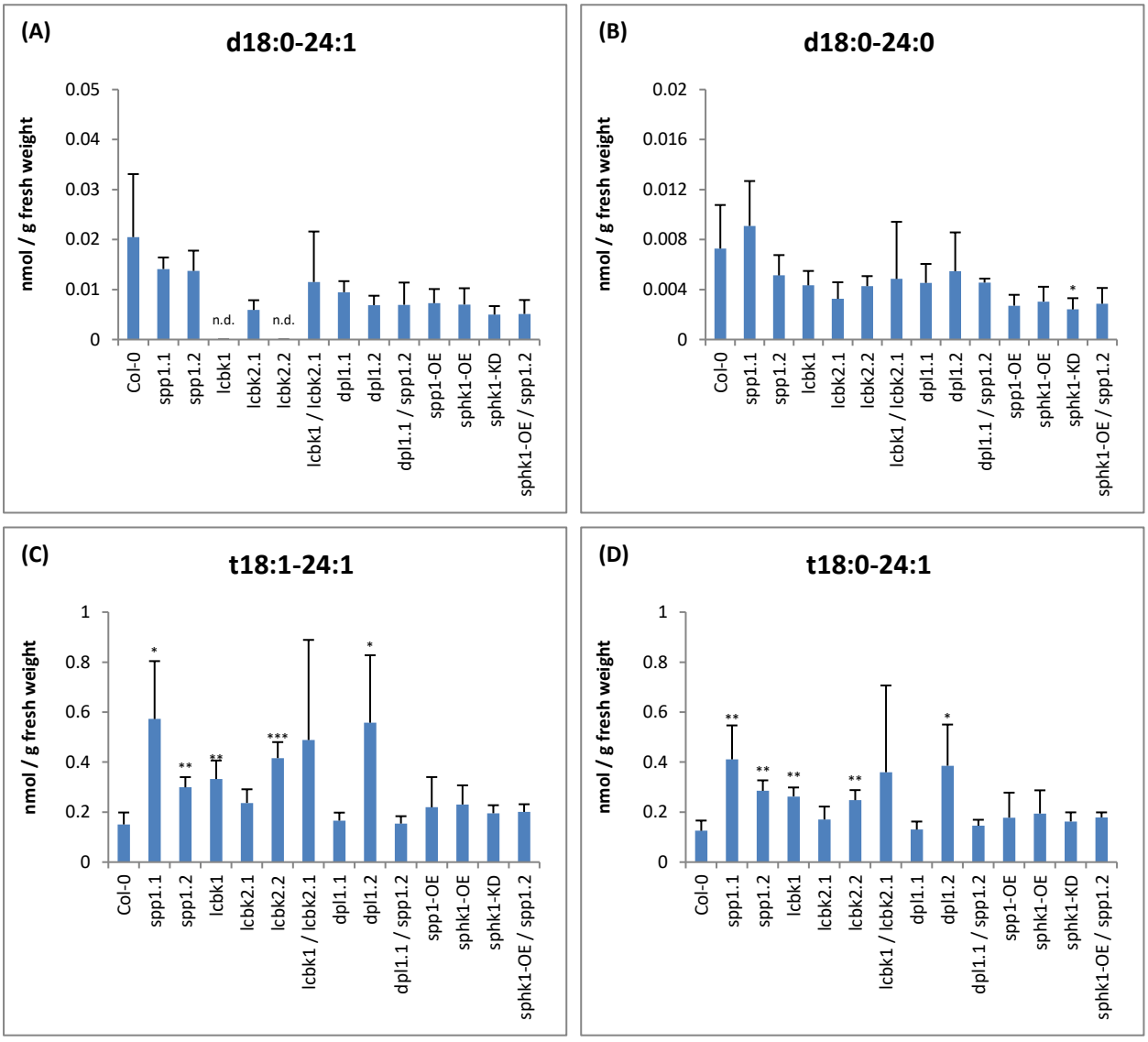

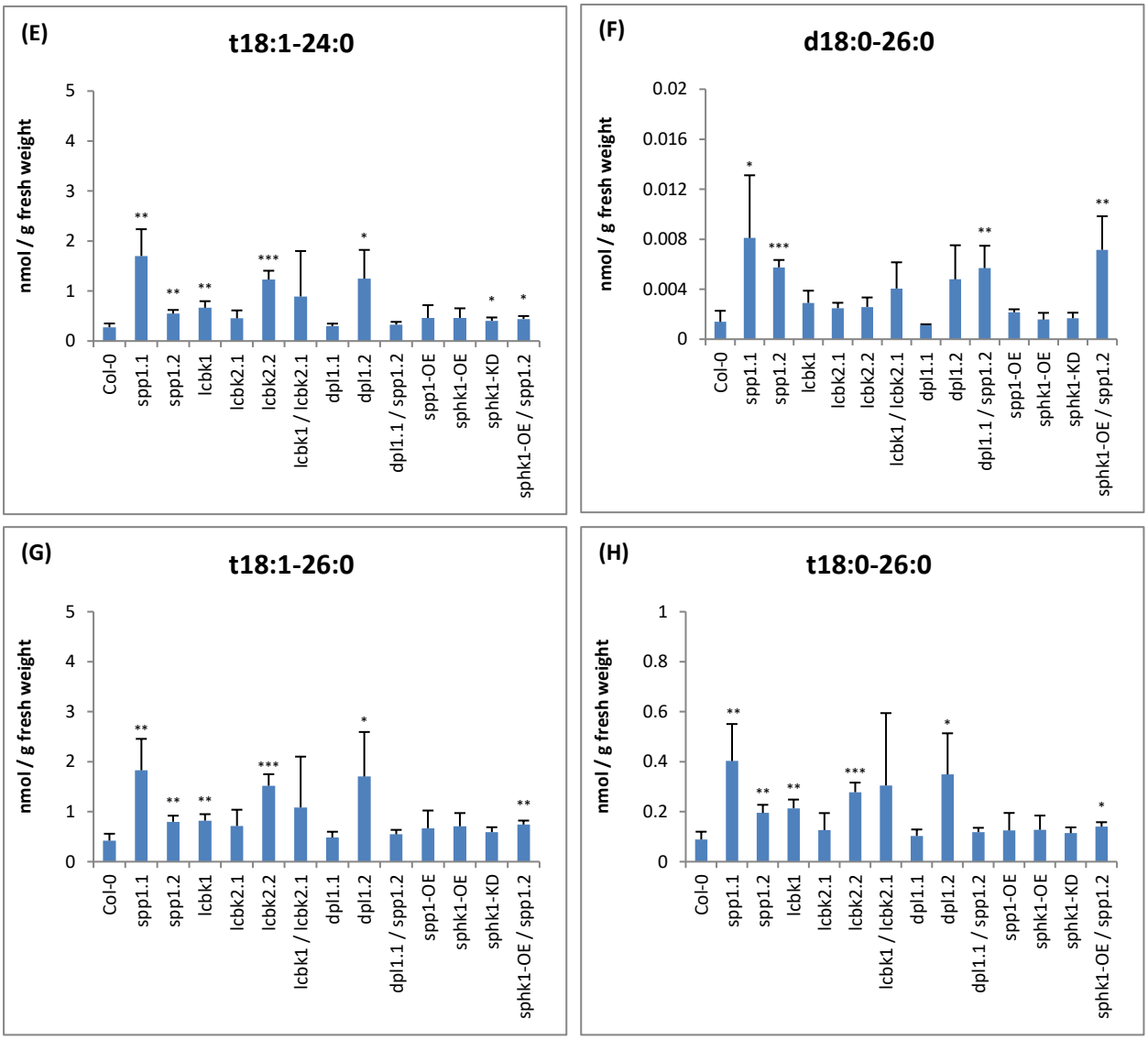

Annex 3: Very-long-chain fatty acid ceramide basal levels in *A. thaliana* wild-type ecotype Col-0 and *Arabidopsis* sphingolipid metabolism mutant lines. Very-long-chain fatty acid ceramides detected in six-week-old leaves of *A. thaliana* wild-type ecotype (Col-0) and *Arabidopsis* sphingolipid metabolism mutant lines. Levels were calculated by comparison to internal standards using correction factors (Section 2. 2. 4. 2. Targeted analysis) and presented as nano-mole per gram of fresh weight (nmol / g fresh weight). Asterisks indicate significant differences between Col-0 and the corresponding mutant line according to Student's *t*-Test: *, $P < 0.05$; **, $P < 0.01$; and ***, $P < 0.001$ (n.d. stands for non-detected). Results show means ± SD of four different technical replicates. The experiment has been repeated three times with similar results.

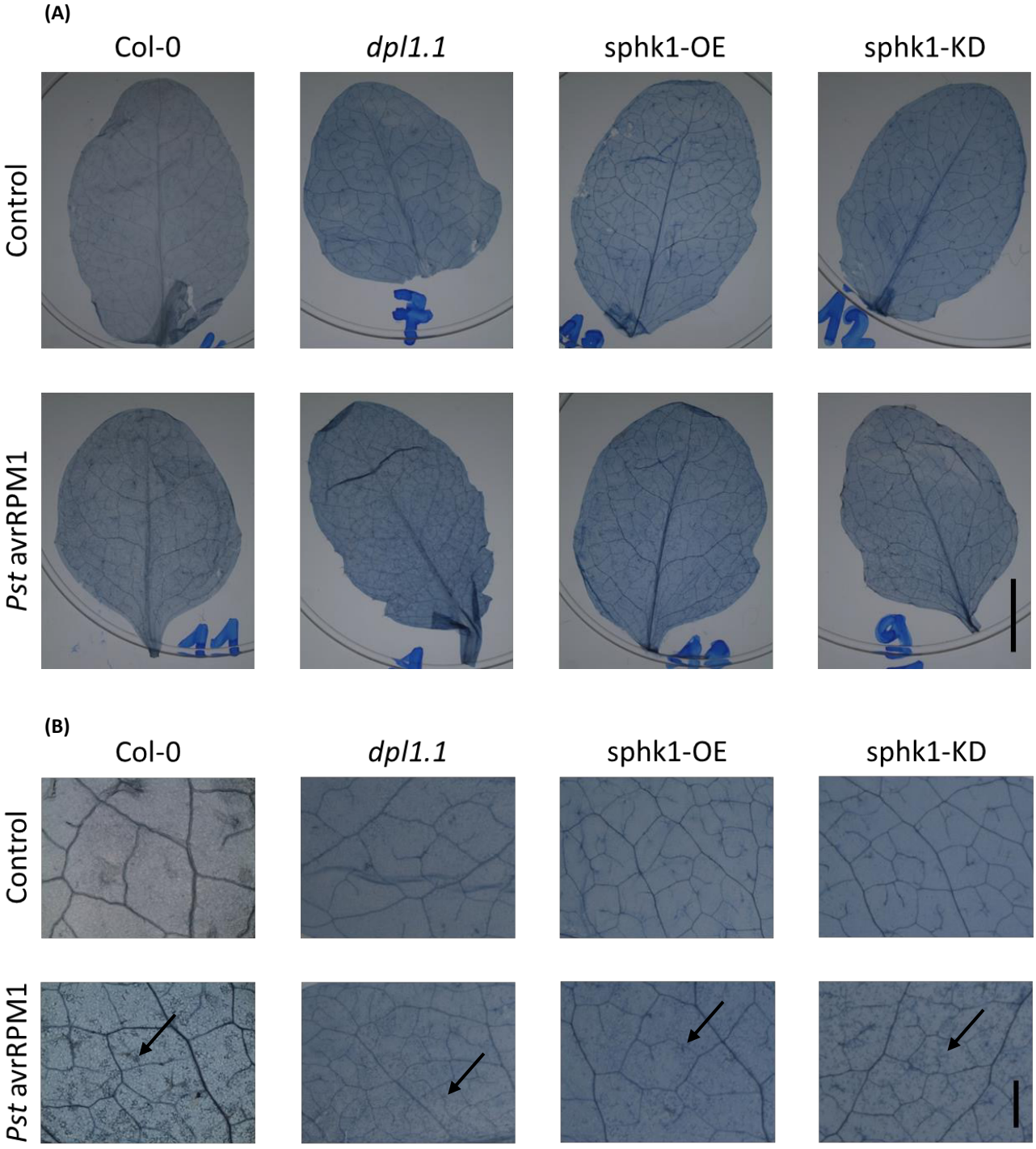

Annex 4: *A. thaliana* cell death induced by *Pst AvrRPM1.* Trypan blue staining was performed to examine cell death induced by *Pst AvrRPM1*. *A. thaliana* leaves were infiltrated with buffer (control) or *Pst AvrRPM1* solution and detached for staining at 24 h after infiltration. Dead cells were stained blue and pointed with a black arrow. Representative images are shown. Scale bars represent 10 mm (A) and 2 mm (B).

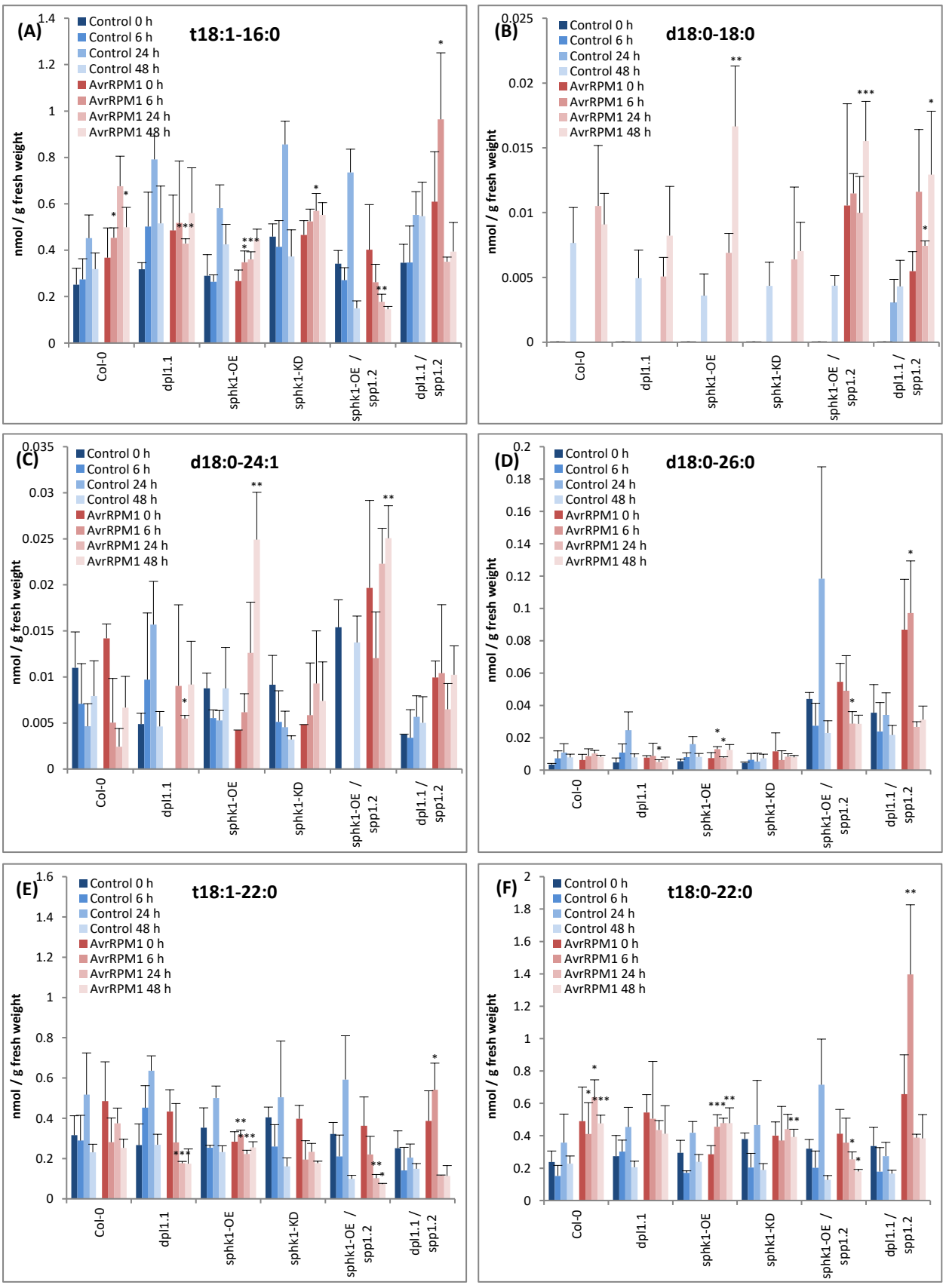
(A)
t18:1-16:0
(B)
d18:0-18:0
(C)
d18:0-24:1
(D)
d18:0-26:0
(E)
t18:1-22:0
(F)
t18:0-22:0
Control 0 h
Control 6 h
Control 24 h
Control 48 h
AvrRPM1 0 h
AvrRPM1 6 h
AvrRPM1 24 h
AvrRPM1 48 h
nmol / g fresh weight
Col-0
dpl1.1
sphk1-OE
sphk1-KD
sphk1-OE / spp1.2
dpl1.1 / spp1.2

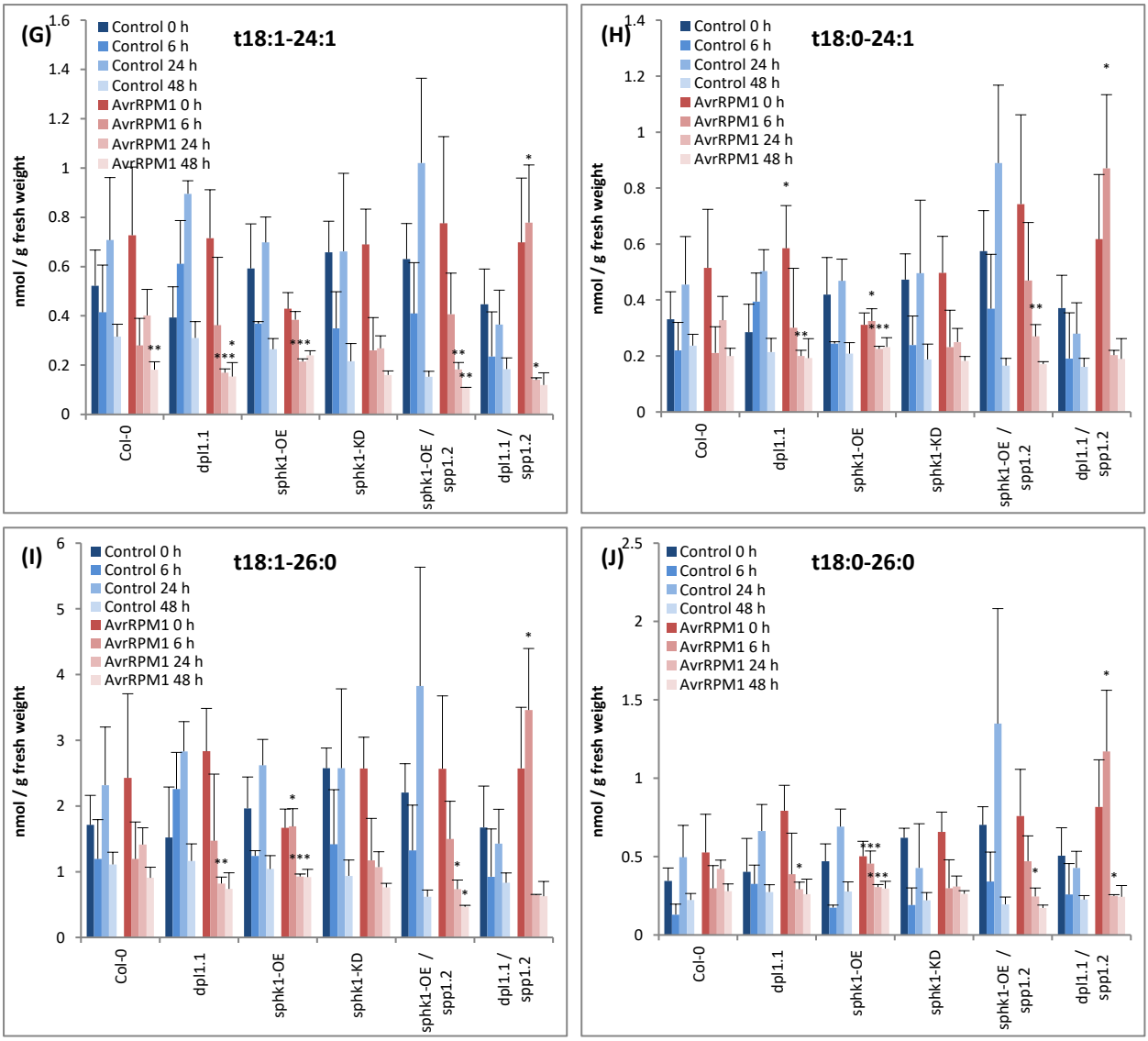

Annex 5: Long-chain fatty acid and very-long-chain fatty acid ceramide accumulations after infection with *Pst* AvrRPM1 in *Arabidopsis* sphingolipid metabolism mutant lines. Leaves of wild-type (Col-0) and sphingolipid metabolism mutant lines were infiltrated with 10 mM $MgCl_2$ as control or *Pst* AvrRPPM1 bacteria solution. Ceramide quantifications were performed over time until 48 hpi. Asterisks indicate significant differences between control pathogen-treated sample and pathogen-treated sample inside the same genotype according to Student's *t*-Test: *, P < 0.05; **, P < 0.01; and ***, P < 0.001. Results show means ± SD of four different technical replicates. The experiment was repeated three times with similar results.

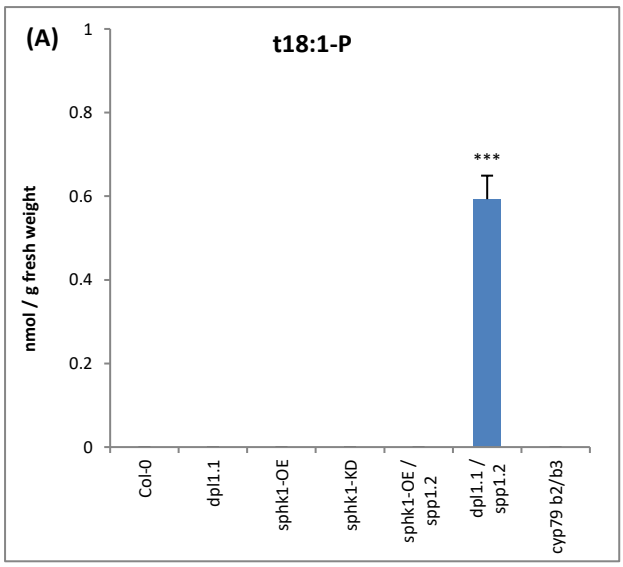
(A)
t18:1-P
nmol / g fresh weight
1
0.8
0.6
0.4
0.2
0
***
Col-0
dpl1.1
sphk1-OE
sphk1-KD
sphk1-OE / spp1.2
dpl1.1 / spp1.2
cyp79 b2/b3

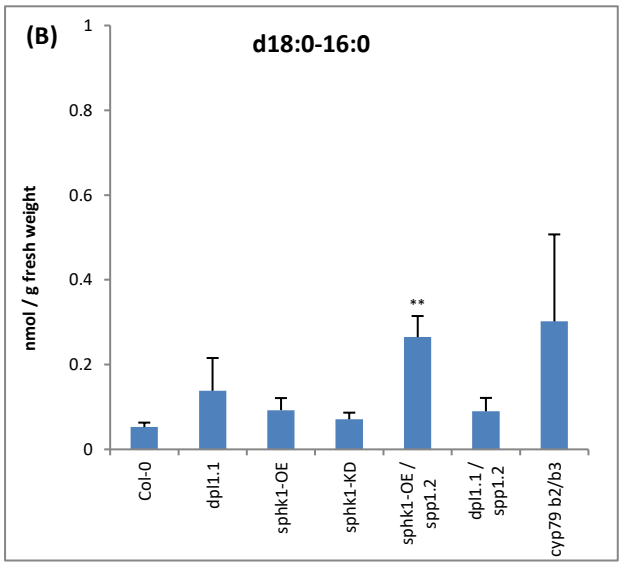
(B)
d18:0-16:0
nmol / g fresh weight
1
0.8
0.6
0.4
0.2
0
**
Col-0
dpl1.1
sphk1-OE
sphk1-KD
sphk1-OE / spp1.2
dpl1.1 / spp1.2
cyp79 b2/b3

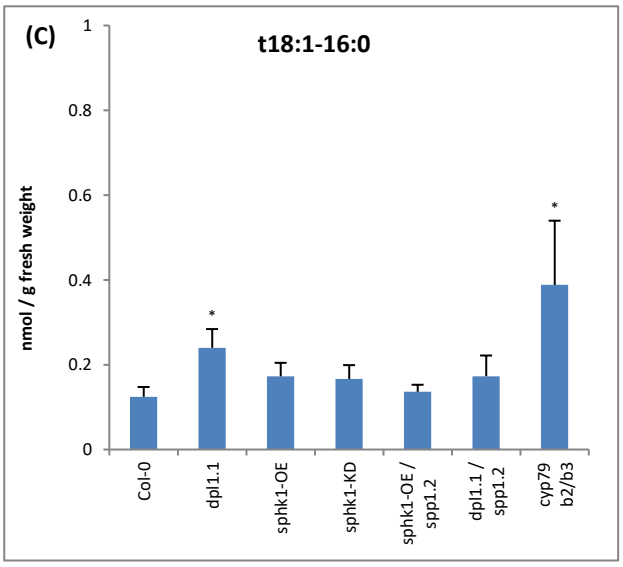
(C)
t18:1-16:0
nmol / g fresh weight
1
0.8
0.6
0.4
0.2
0
*
*
Col-0
dpl1.1
sphk1-OE
sphk1-KD
sphk1-OE / spp1.2
dpl1.1 / spp1.2
cyp79 b2/b3

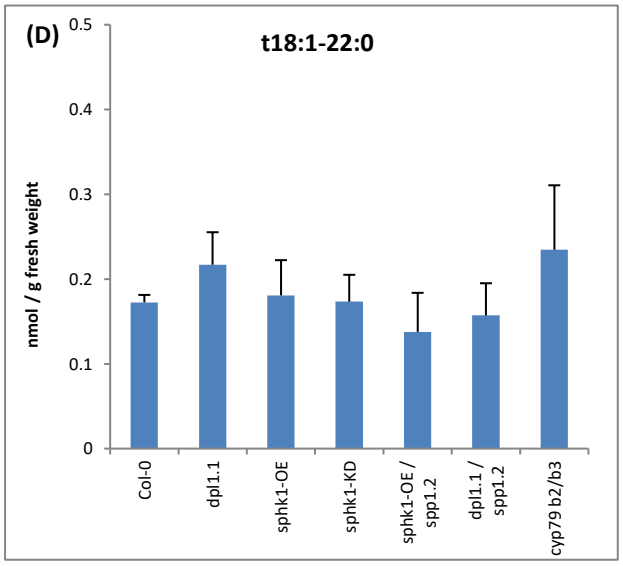
(D)
t18:1-22:0
nmol / g fresh weight
0.5
0.4
0.3
0.2
0.1
0
Col-0
dpl1.1
sphk1-OE
sphk1-KD
sphk1-OE / spp1.2
dpl1.1 / spp1.2
cyp79 b2/b3

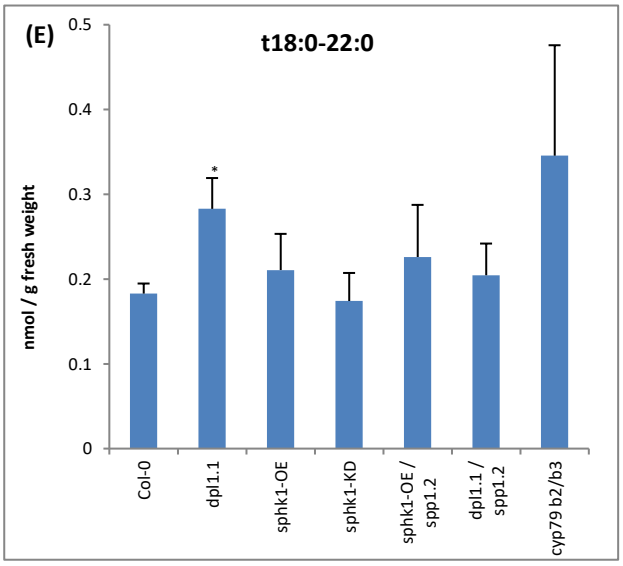
(E)
t18:0-22:0
nmol / g fresh weight
0.5
0.4
0.3
0.2
0.1
0
*
Col-0
dpl1.1
sphk1-OE
sphk1-KD
sphk1-OE / spp1.2
dpl1.1 / spp1.2
cyp79 b2/b3

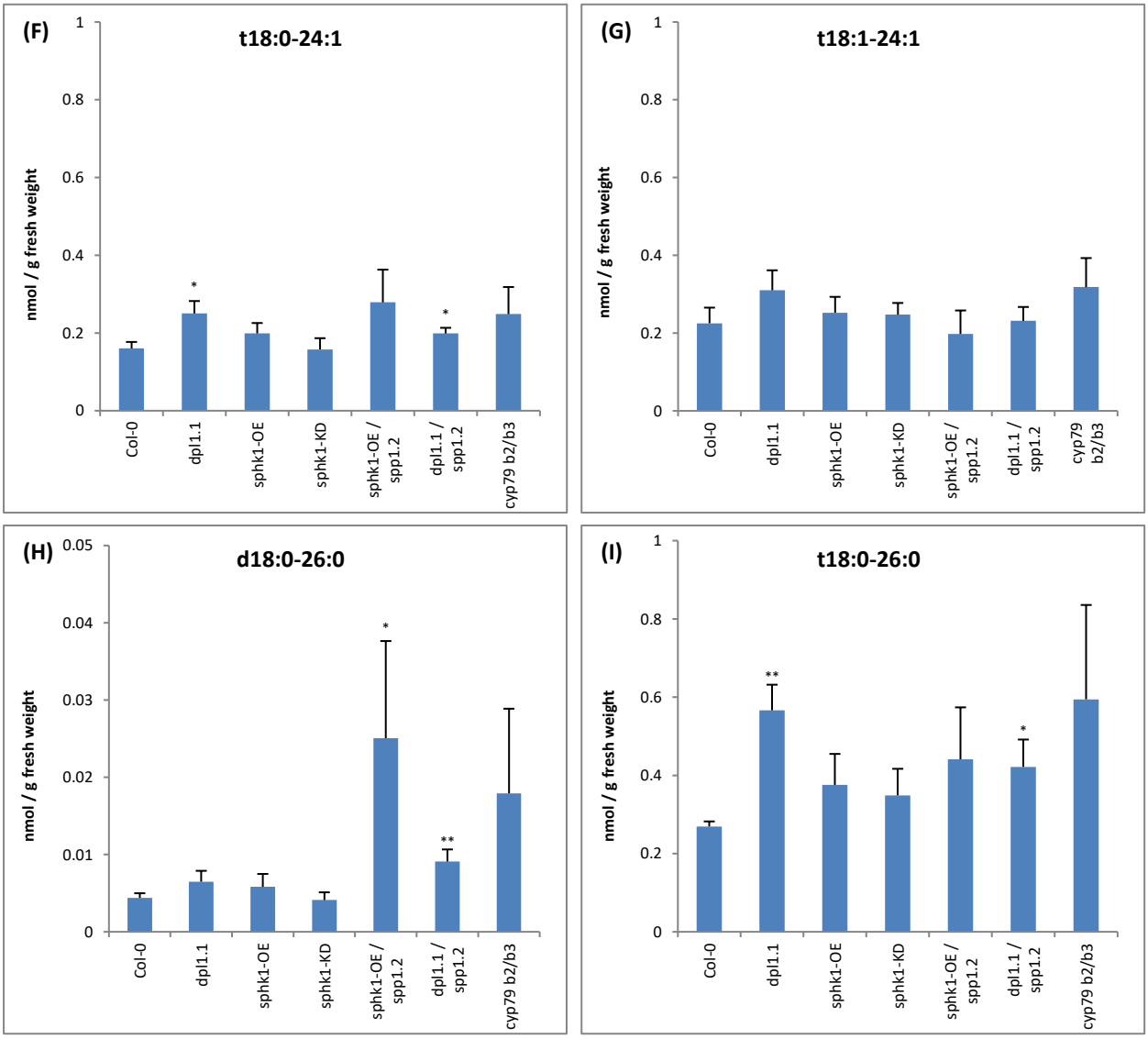

Annex 6: Long-chain fatty acid and very-long-chain fatty acid ceramides accumulation after infection with *V. longisporum* in *Arabidopsis* sphingolipid metabolism mutant lines. Roots of wild-type (Col-0), sphingolipid metabolism mutant lines and the susceptible line *cyp79 b2/b3* were infected with $2*10^6$ spores/mL of fungi solution. Ceramide quantifications were performed three weeks post-infection in rosettes. Asterisks indicate significant differences between Col-0 pathogen-treated sample and the other pathogen-treated plant lines according to Student's *t*-Test: *, P < 0.05; **, P < 0.01; and ***, P < 0.001. Results show means ± SD of three different technical replicates.

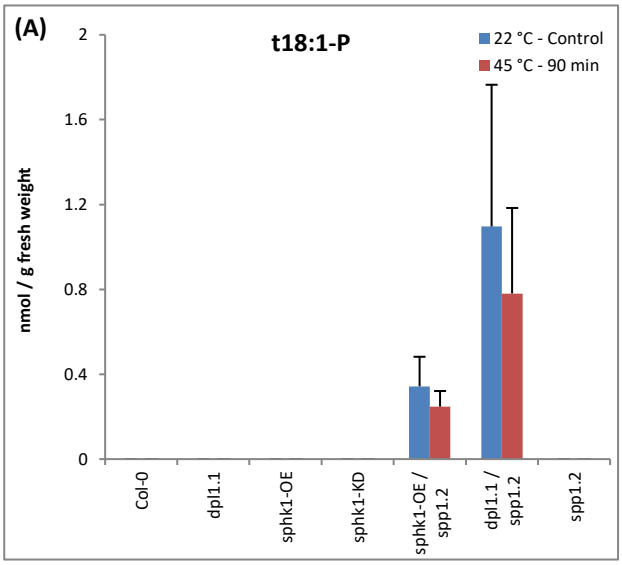
(A)
t18:1-P
22 °C - Control
45 °C - 90 min
nmol / g fresh weight
2
1.6
1.2
0.8
0.4
0
Col-0
dpl1.1
sphk1-OE
sphk1-KD
sphk1-OE / spp1.2
dpl1.1 / spp1.2
spp1.2

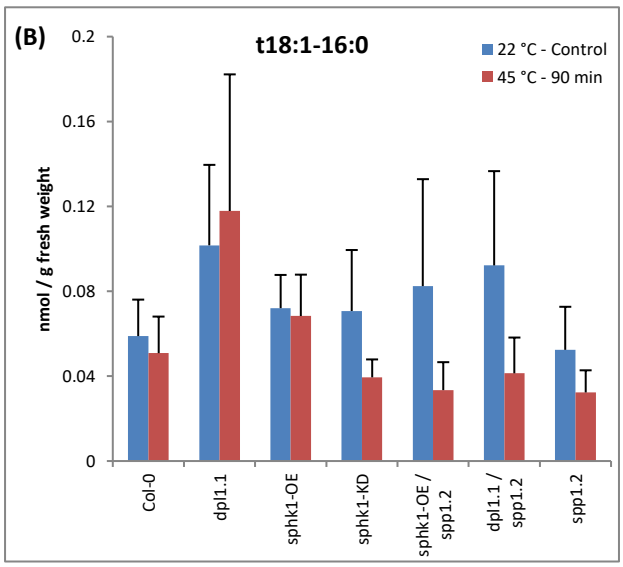
(B)
t18:1-16:0
22 °C - Control
45 °C - 90 min
nmol / g fresh weight
0.2
0.16
0.12
0.08
0.04
0
Col-0
dpl1.1
sphk1-OE
sphk1-KD
sphk1-OE / spp1.2
dpl1.1 / spp1.2
spp1.2

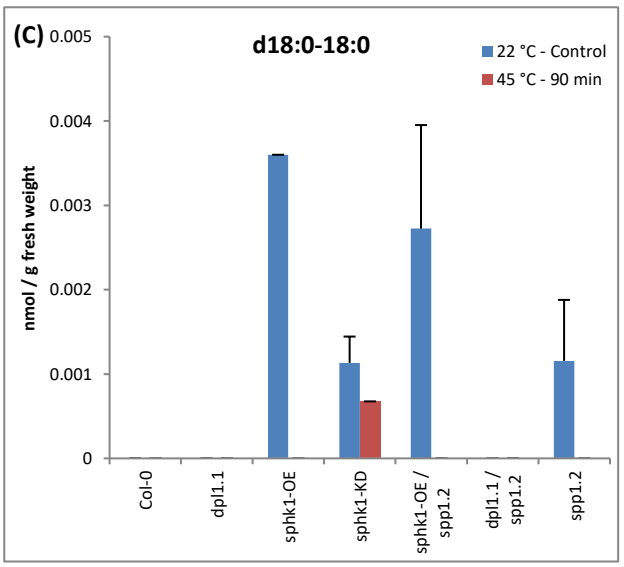
(C)
d18:0-18:0
22 °C - Control
45 °C - 90 min
nmol / g fresh weight
0.005
0.004
0.003
0.002
0.001
0
Col-0
dpl1.1
sphk1-OE
sphk1-KD
sphk1-OE / spp1.2
dpl1.1 / spp1.2
spp1.2

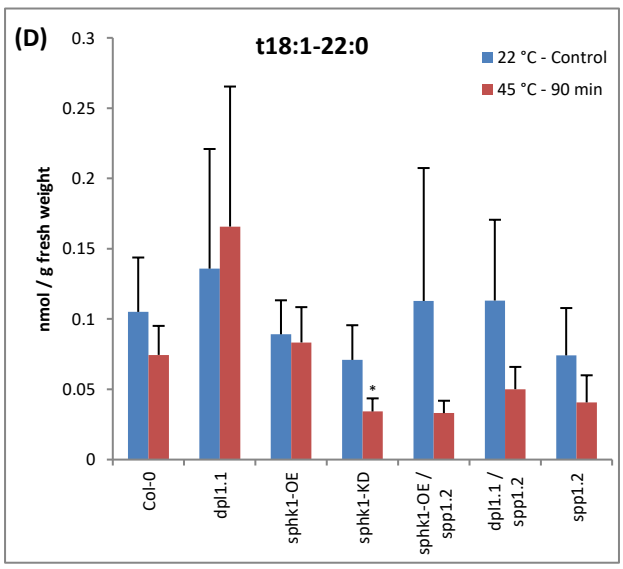
(D)
t18:1-22:0
22 °C - Control
45 °C - 90 min
nmol / g fresh weight
0.3
0.25
0.2
0.15
0.1
0.05
0
*
Col-0
dpl1.1
sphk1-OE
sphk1-KD
sphk1-OE / spp1.2
dpl1.1 / spp1.2
spp1.2

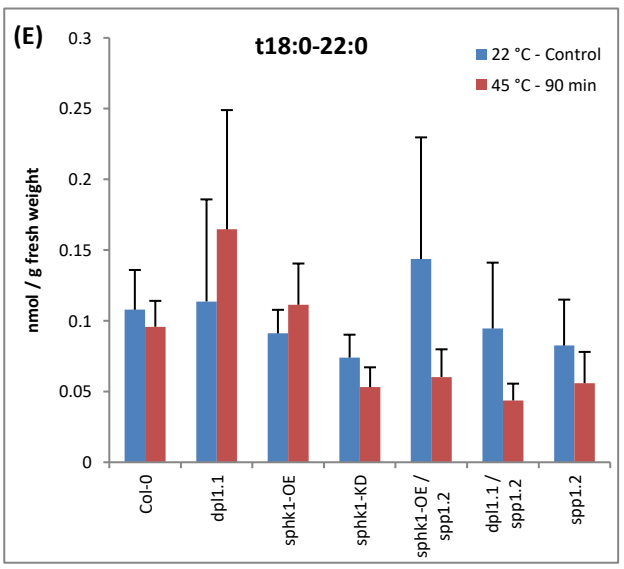
(E)
t18:0-22:0
22 °C - Control
45 °C - 90 min
nmol / g fresh weight
0.3
0.25
0.2
0.15
0.1
0.05
0
Col-0
dpl1.1
sphk1-OE
sphk1-KD
sphk1-OE / spp1.2
dpl1.1 / spp1.2
spp1.2

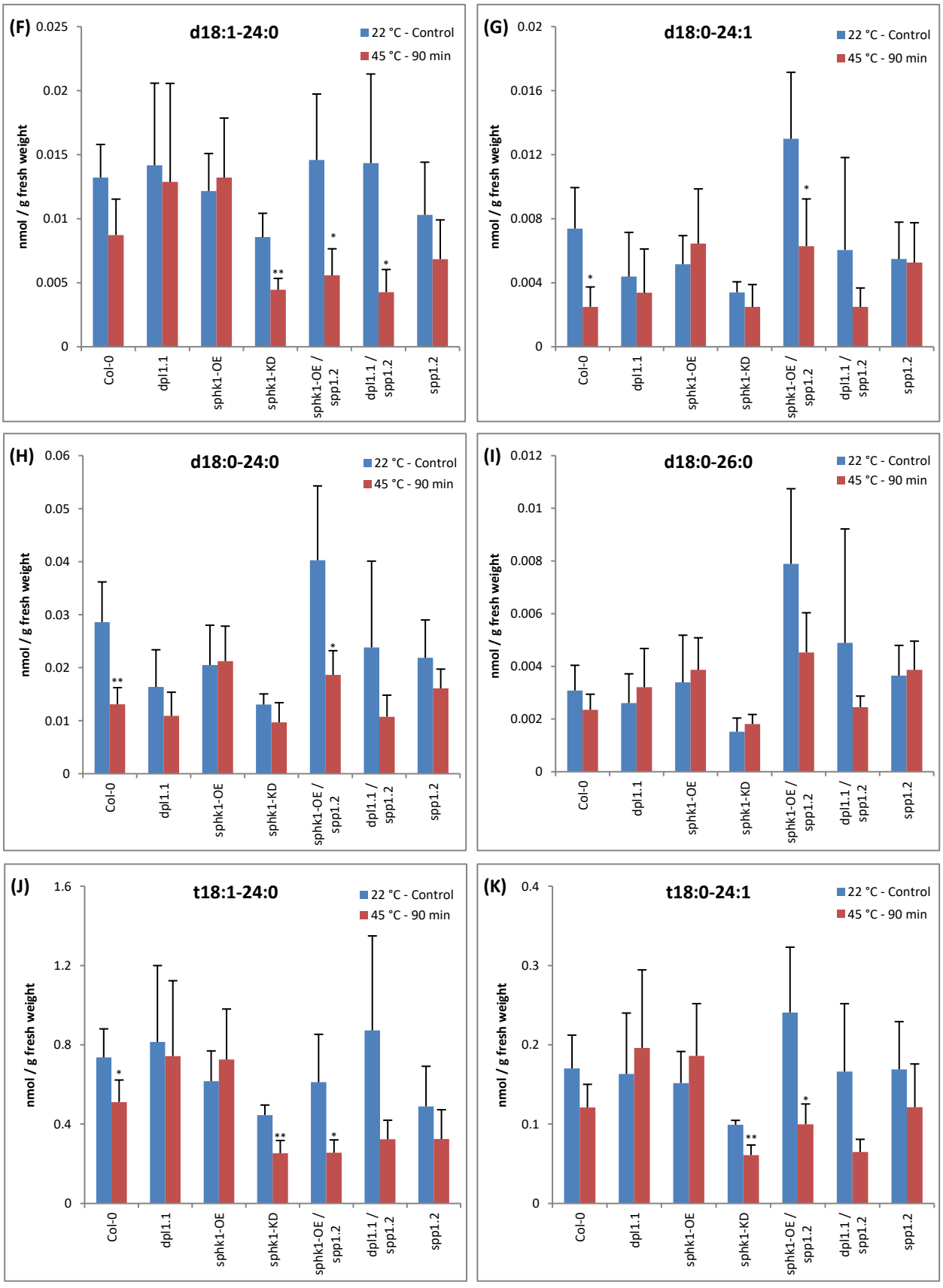
(F)
d18:1-24:0
22 °C - Control
45 °C - 90 min
nmol / g fresh weight
0.025
0.02
0.015
0.01
0.005
0
Col-0
dpl1.1
sphk1-OE
sphk1-KD
sphk1-OE / spp1.2
dpl1.1 / spp1.2
spp1.2
(G)
d18:0-24:1
22 °C - Control
45 °C - 90 min
nmol / g fresh weight
0.02
0.016
0.012
0.008
0.004
0
Col-0
dpl1.1
sphk1-OE
sphk1-KD
sphk1-OE / spp1.2
dpl1.1 / spp1.2
spp1.2
(H)
d18:0-24:0
22 °C - Control
45 °C - 90 min
nmol / g fresh weight
0.06
0.05
0.04
0.03
0.02
0.01
0
Col-0
dpl1.1
sphk1-OE
sphk1-KD
sphk1-OE / spp1.2
dpl1.1 / spp1.2
spp1.2
(I)
d18:0-26:0
22 °C - Control
45 °C - 90 min
nmol / g fresh weight
0.012
0.01
0.008
0.006
0.004
0.002
0
Col-0
dpl1.1
sphk1-OE
sphk1-KD
sphk1-OE / spp1.2
dpl1.1 / spp1.2
spp1.2
(J)
t18:1-24:0
22 °C - Control
45 °C - 90 min
nmol / g fresh weight
1.6
1.2
0.8
0.4
0
Col-0
dpl1.1
sphk1-OE
sphk1-KD
sphk1-OE / spp1.2
dpl1.1 / spp1.2
spp1.2
(K)
t18:0-24:1
22 °C - Control
45 °C - 90 min
nmol / g fresh weight
0.4
0.3
0.2
0.1
0
Col-0
dpl1.1
sphk1-OE
sphk1-KD
sphk1-OE / spp1.2
dpl1.1 / spp1.2
spp1.2

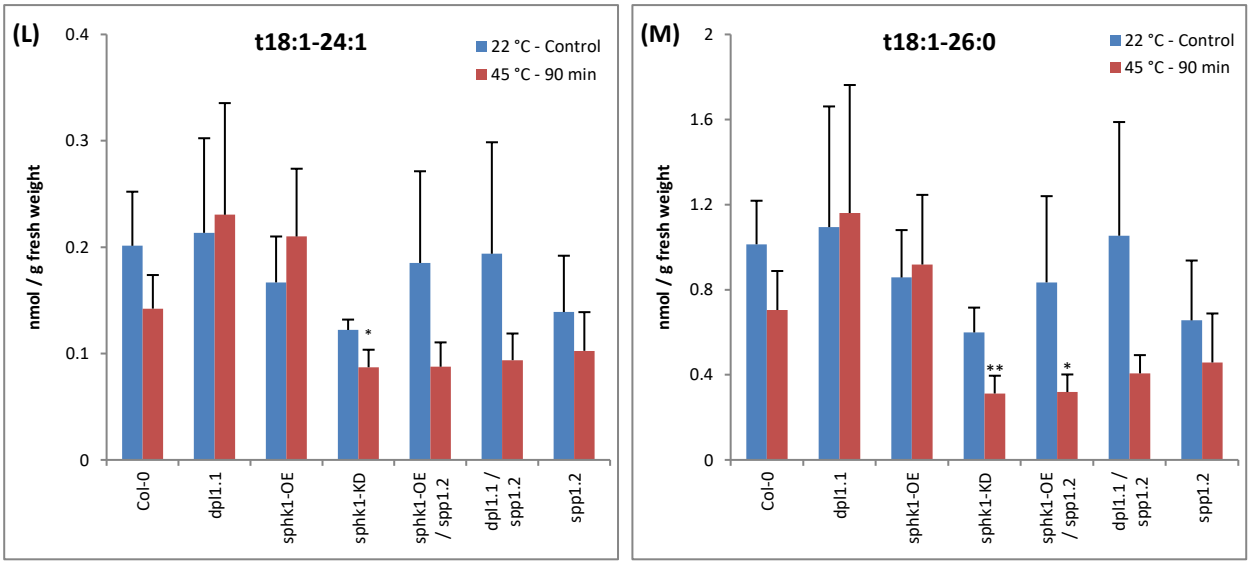

Annex 7: Long-chain and very-long-chain fatty acid ceramides accumulation after heat shock at 45 °C of *A. thaliana* wild-type ecotype Col-0 and *Arabidopsis* sphingolipid metabolism mutant lines. Two-week-old seedlings of wild-type (Col-0) and sphingolipid metabolism mutant lines were incubated either at 22 °C for control or at 45 °C for heat shock. Long-chain and very-long-chain fatty acid ceramides quantifications were measured after 90 min. Asterisks indicate significant differences between control-incubated samples and heat shock-incubated samples according to Student's *t*-Test: *, $P < 0.05$; **, $P < 0.01$; and ***, $P < 0.001$. Results show means ± SD of four different technical replicates. The experiment was repeated two times with similar results.

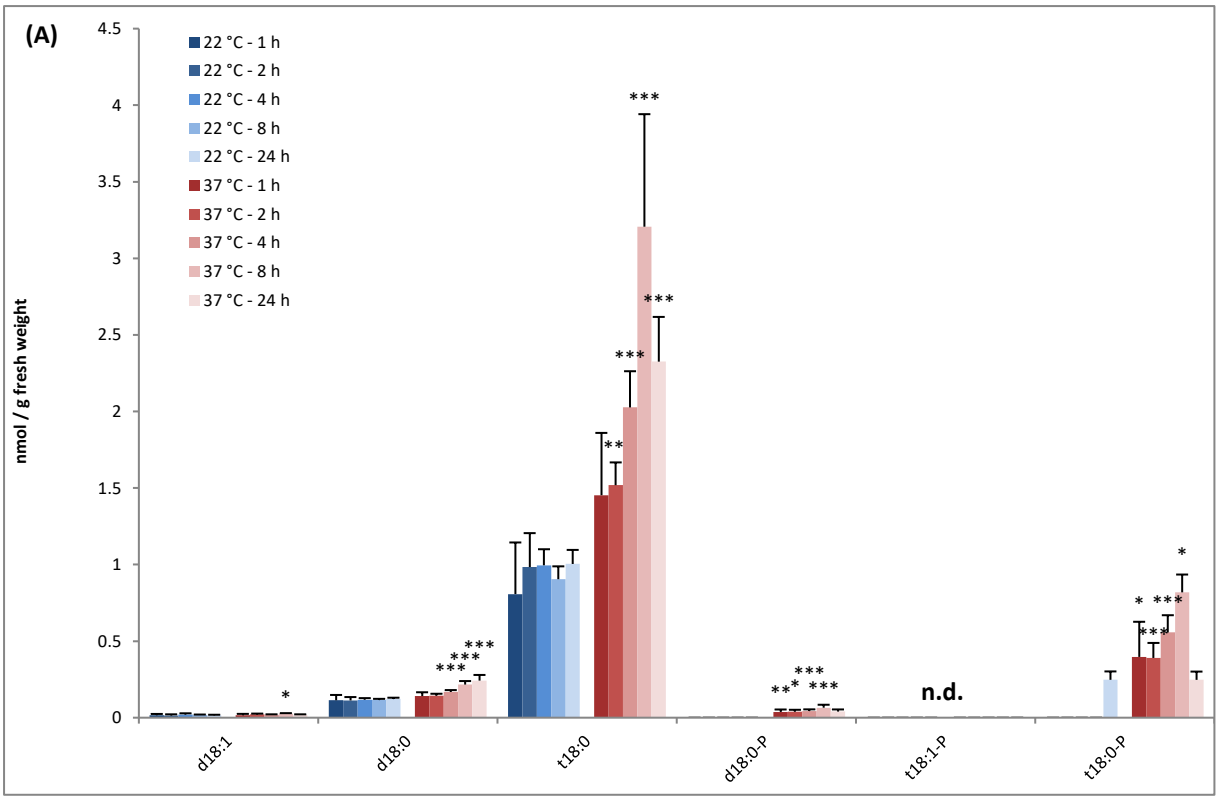
(A)
nmol / g fresh weight
22 °C - 1 h
22 °C - 2 h
22 °C - 4 h
22 °C - 8 h
22 °C - 24 h
37 °C - 1 h
37 °C - 2 h
37 °C - 4 h
37 °C - 8 h
37 °C - 24 h
n.d.
d18:1
d18:0
t18:0
d18:0-P
t18:1-P
t18:0-P

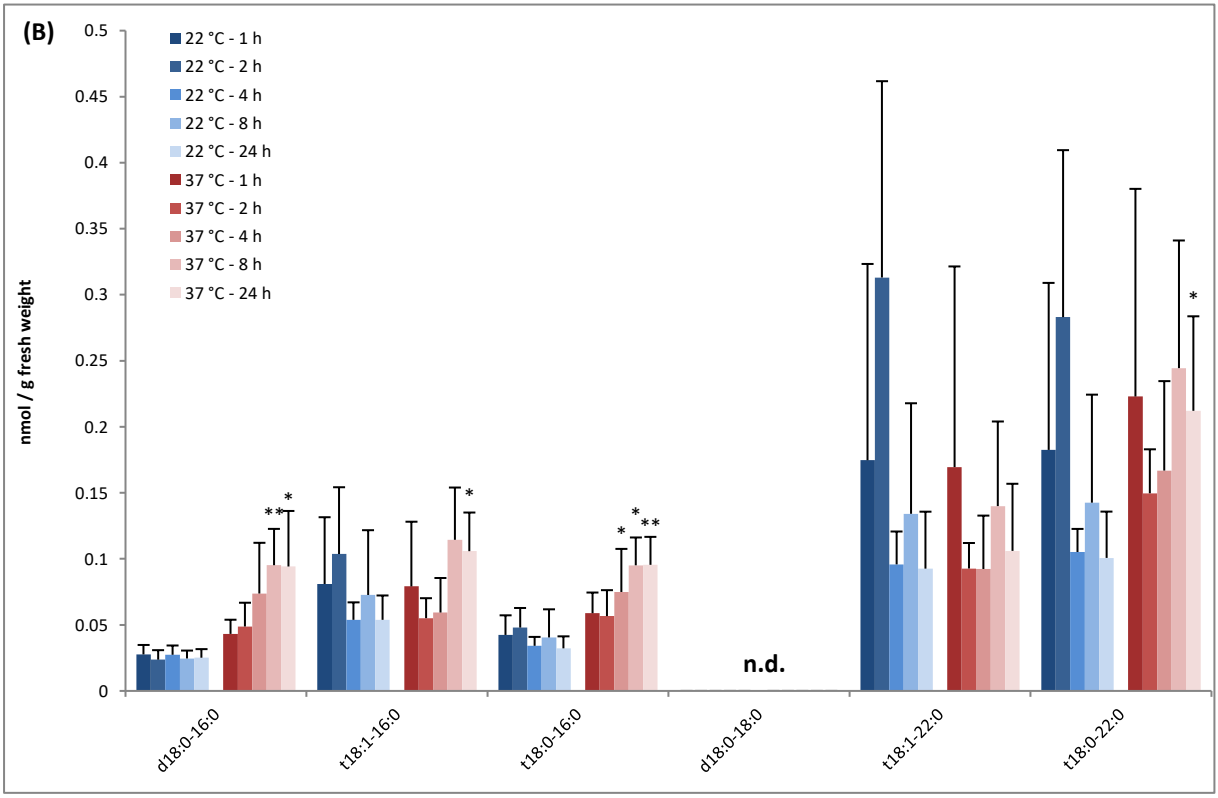
(B)
nmol / g fresh weight
22 °C - 1 h
22 °C - 2 h
22 °C - 4 h
22 °C - 8 h
22 °C - 24 h
37 °C - 1 h
37 °C - 2 h
37 °C - 4 h
37 °C - 8 h
37 °C - 24 h
n.d.
d18:0-16:0
t18:1-16:0
t18:0-16:0
d18:0-18:0
t18:1-22:0
t18:0-22:0

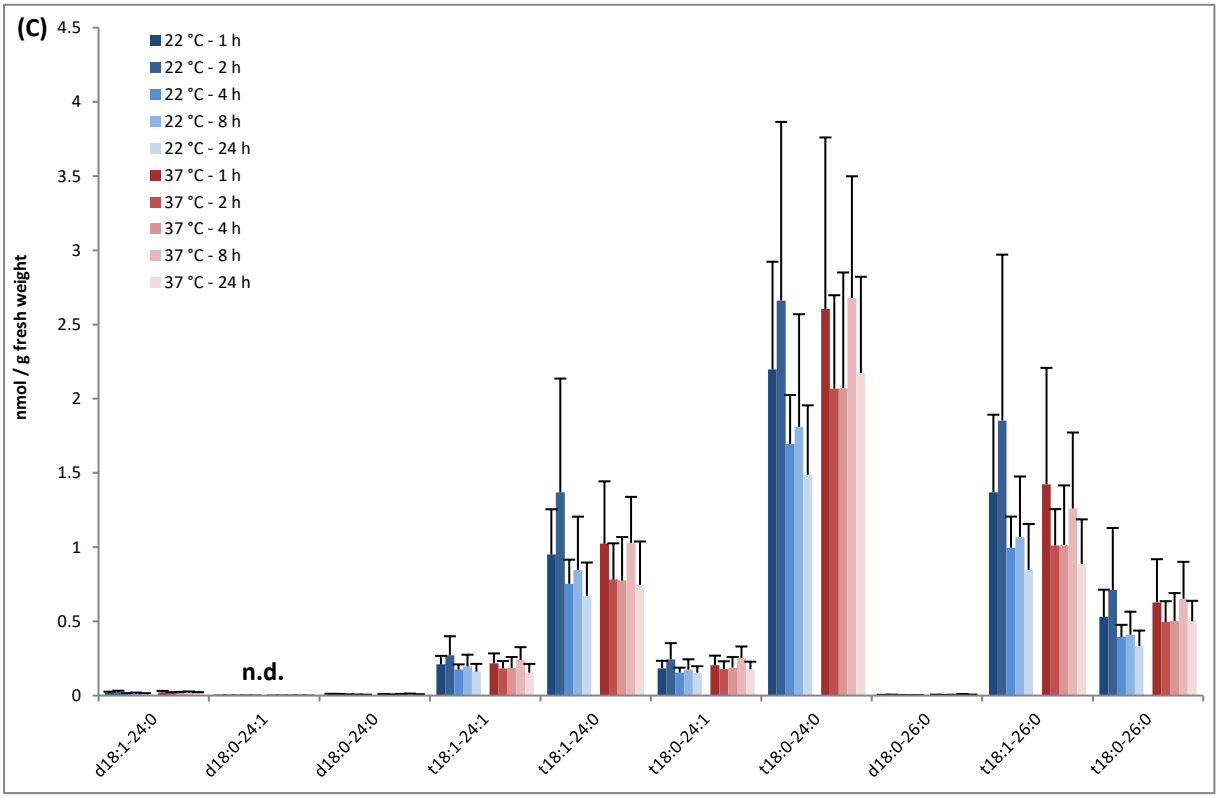

Annex 8: Free LCB, LCB-P, long-chain fatty acid and very-long-chain fatty acid ceramides accumulation during heat adaptation at 37 °C of *A. thaliana* wild-type ecotype Col-0. Two-week-old seedlings of wild-type (Col-0) were incubated either at 22 °C for control or at 37 °C for heat adaptation. LCB and LCB-P (A), long-chain fatty acid ceramides (B), and very-long-chain fatty acid ceramides (C) were measured during 24 h. Asterisks indicate significant differences between control-incubated samples and heat adaptation-incubated samples according to Student's *t*-Test: *, $P < 0.05$; **, $P < 0.01$; and ***, $P < 0.001$. n.d. stands for not detected. Results show means ± SD of four different technical replicates.

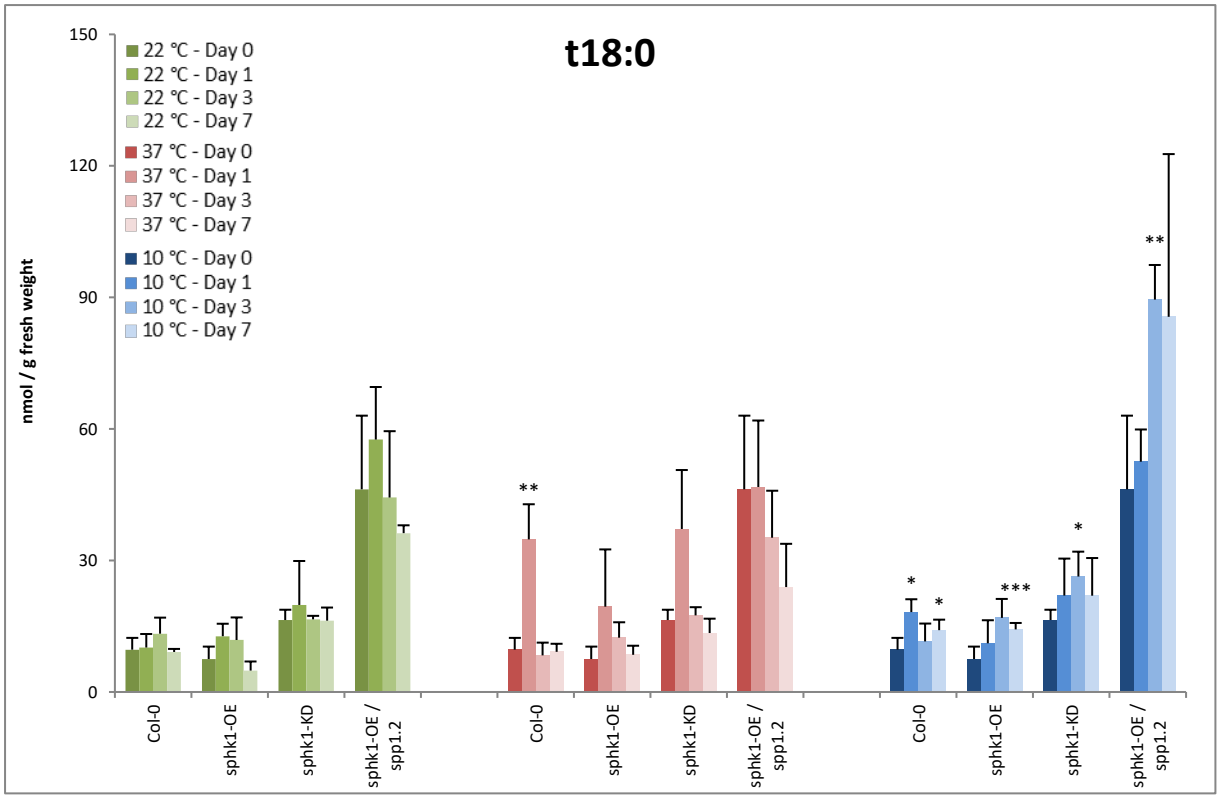
t18:0
nmol / g fresh weight
150
120
90
60
30
0
22 °C - Day 0
22 °C - Day 1
22 °C - Day 3
22 °C - Day 7
37 °C - Day 0
37 °C - Day 1
37 °C - Day 3
37 °C - Day 7
10 °C - Day 0
10 °C - Day 1
10 °C - Day 3
10 °C - Day 7
Col-0
sphk1-OE
sphk1-KD
sphk1-OE / spp1.2
Col-0
sphk1-OE
sphk1-KD
sphk1-OE / spp1.2
Col-0
sphk1-OE
sphk1-KD
sphk1-OE / spp1.2

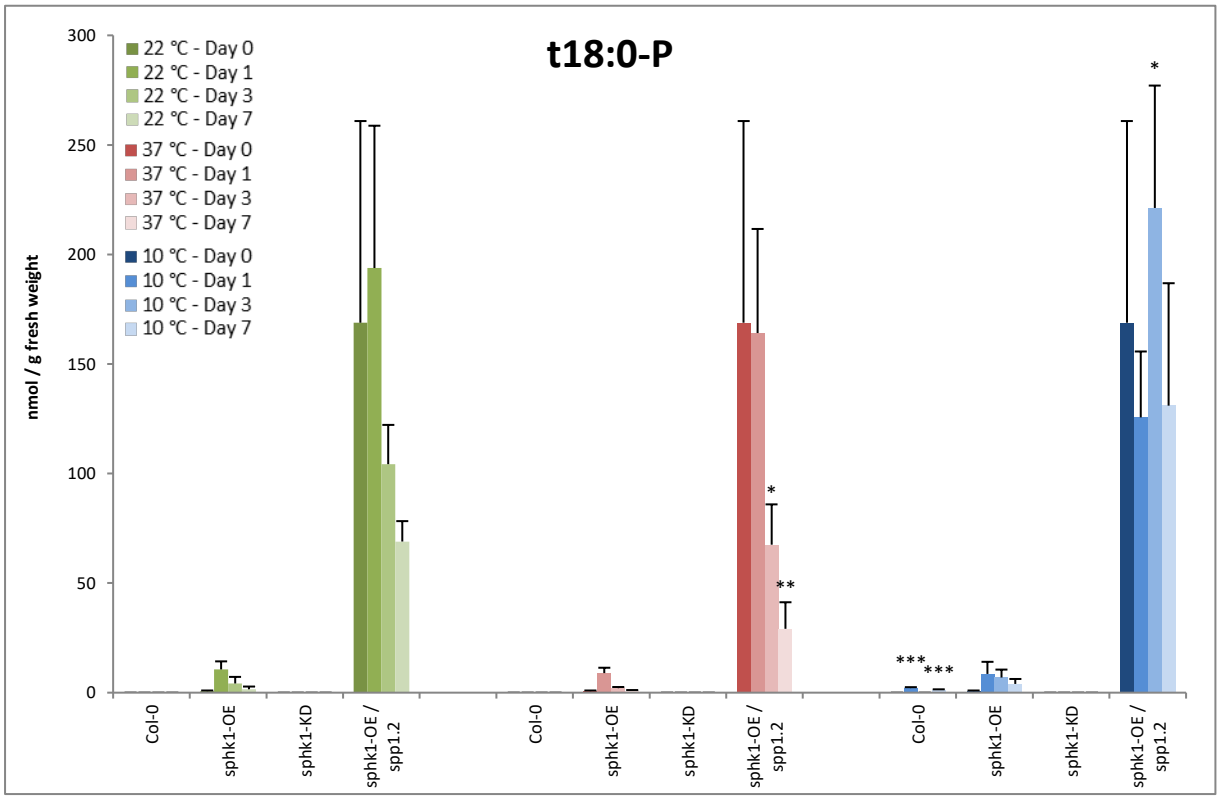
t18:0-P
nmol / g fresh weight
300
250
200
150
100
50
0
22 °C - Day 0
22 °C - Day 1
22 °C - Day 3
22 °C - Day 7
37 °C - Day 0
37 °C - Day 1
37 °C - Day 3
37 °C - Day 7
10 °C - Day 0
10 °C - Day 1
10 °C - Day 3
10 °C - Day 7
Col-0
sphk1-OE
sphk1-KD
sphk1-OE / spp1.2
Col-0
sphk1-OE
sphk1-KD
sphk1-OE / spp1.2
Col-0
sphk1-OE
sphk1-KD
sphk1-OE / spp1.2

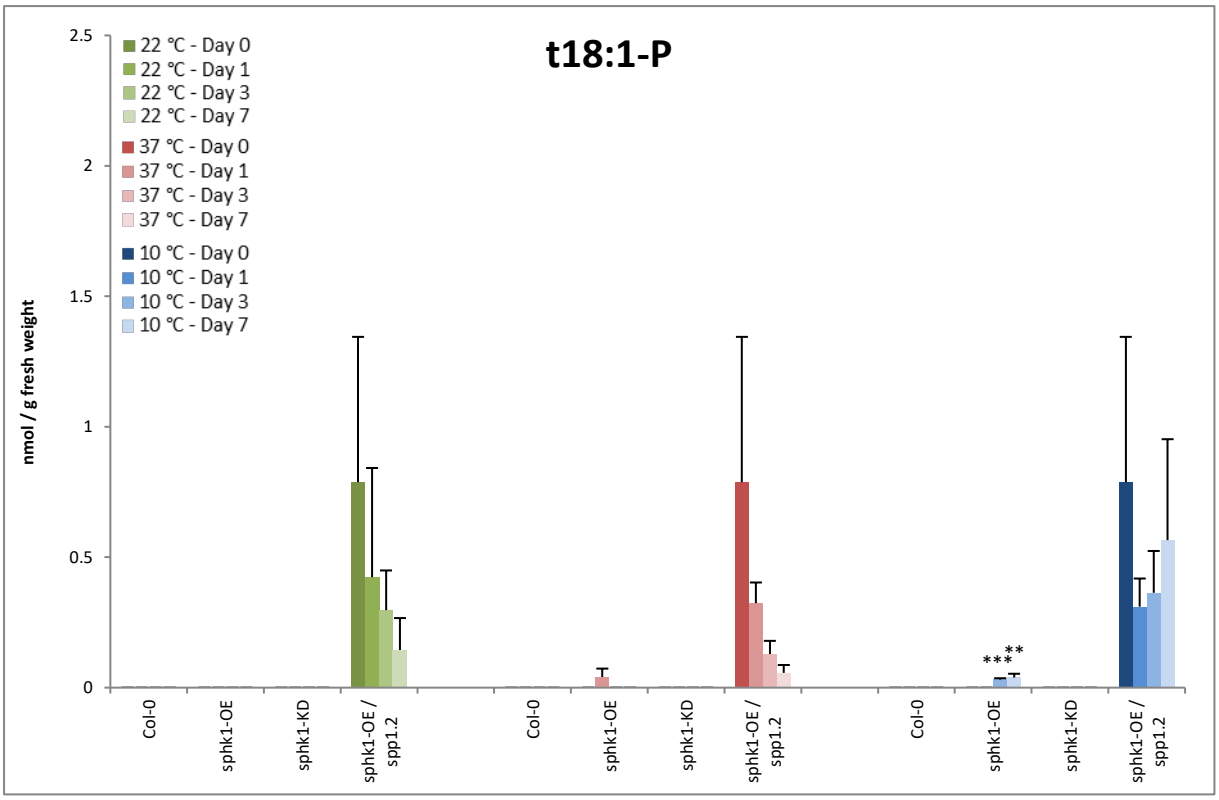

Annex 9: LCBs accumulation during temperature adaptation of *A. thaliana* wild-type ecotype Col-0 and *Arabidopsis* sphingolipid metabolism mutant lines. Two-week-old seedlings of wild-type (Col-0) and *Arabidopsis* sphingolipid metabolism mutant lines were incubated either at 22 °C for control, at 37 °C for heat adaptation or at 10 °C for cold adaptation. Long-chain fatty acid ceramides were measured at day 0, 1, 3 and 7. Asterisks indicate significant differences between control-incubated samples and heat adaptation-incubated samples or between control-incubated samples and cold adaptation-incubated samples according to Student's *t*-Test: *, $P < 0.05$; **, $P < 0.01$; and ***, $P < 0.001$. Results show means ± SD of four different technical replicates.

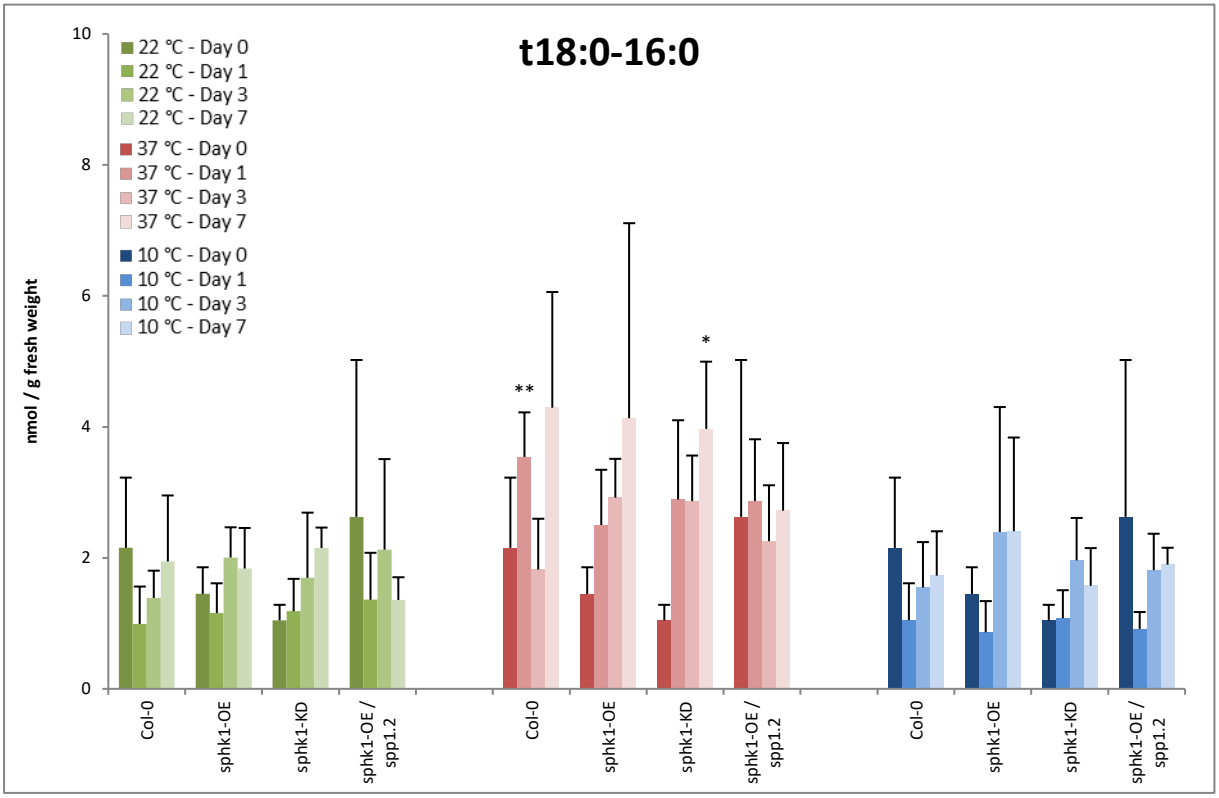
t18:0-16:0
nmol / g fresh weight
22 °C - Day 0
22 °C - Day 1
22 °C - Day 3
22 °C - Day 7
37 °C - Day 0
37 °C - Day 1
37 °C - Day 3
37 °C - Day 7
10 °C - Day 0
10 °C - Day 1
10 °C - Day 3
10 °C - Day 7
Col-0
sphk1-OE
sphk1-KD
sphk1-OE / spp1.2

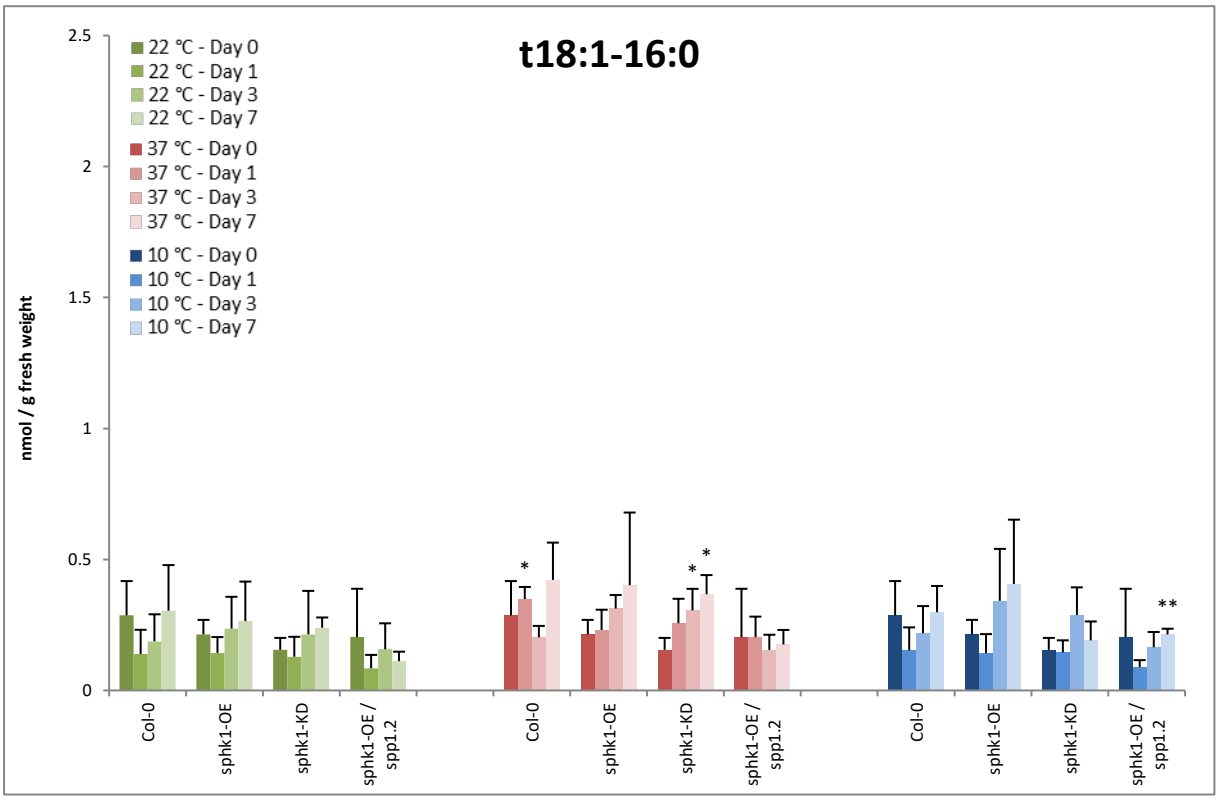
t18:1-16:0
nmol / g fresh weight
22 °C - Day 0
22 °C - Day 1
22 °C - Day 3
22 °C - Day 7
37 °C - Day 0
37 °C - Day 1
37 °C - Day 3
37 °C - Day 7
10 °C - Day 0
10 °C - Day 1
10 °C - Day 3
10 °C - Day 7
Col-0
sphk1-OE
sphk1-KD
sphk1-OE / spp1.2

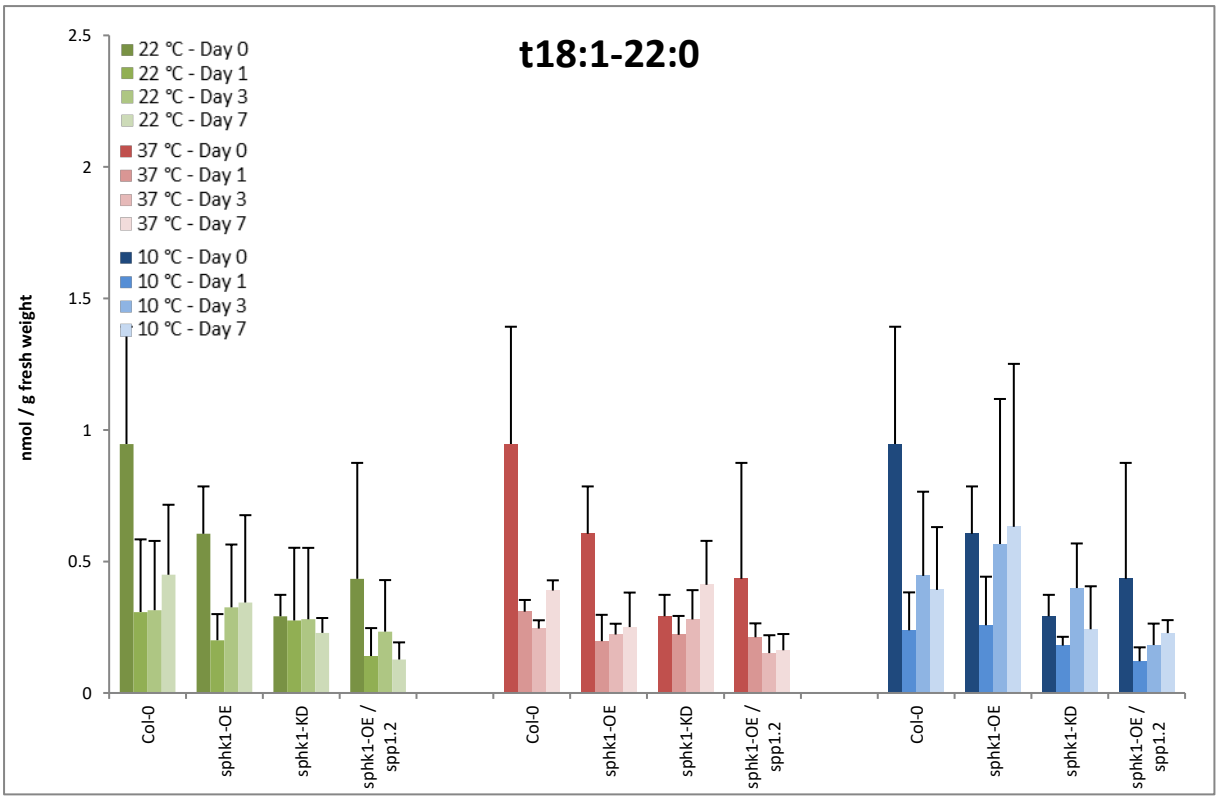
t18:1-22:0
nmol / g fresh weight
22 °C - Day 0
22 °C - Day 1
22 °C - Day 3
22 °C - Day 7
37 °C - Day 0
37 °C - Day 1
37 °C - Day 3
37 °C - Day 7
10 °C - Day 0
10 °C - Day 1
10 °C - Day 3
10 °C - Day 7
Col-0
sphk1-OE
sphk1-KD
sphk1-OE / spp1.2

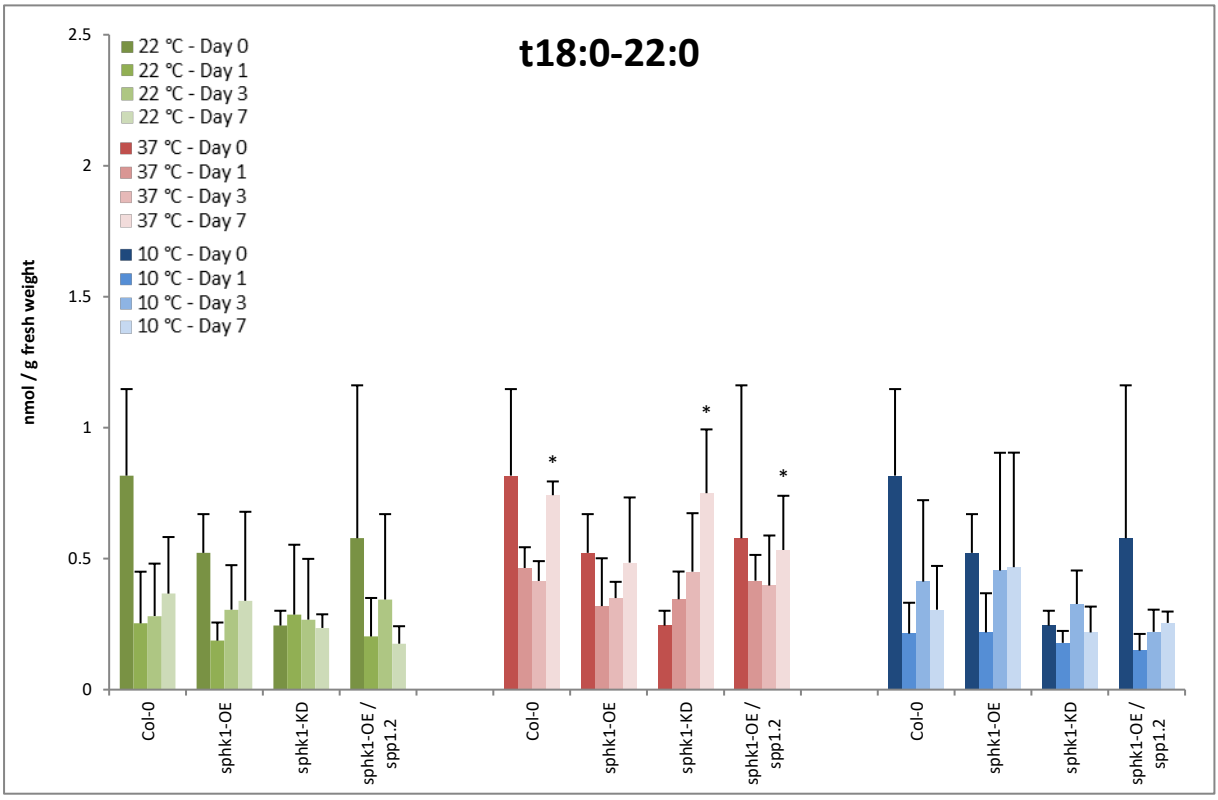
t18:0-22:0
nmol / g fresh weight
22 °C - Day 0
22 °C - Day 1
22 °C - Day 3
22 °C - Day 7
37 °C - Day 0
37 °C - Day 1
37 °C - Day 3
37 °C - Day 7
10 °C - Day 0
10 °C - Day 1
10 °C - Day 3
10 °C - Day 7
Col-0
sphk1-OE
sphk1-KD
sphk1-OE / spp1.2

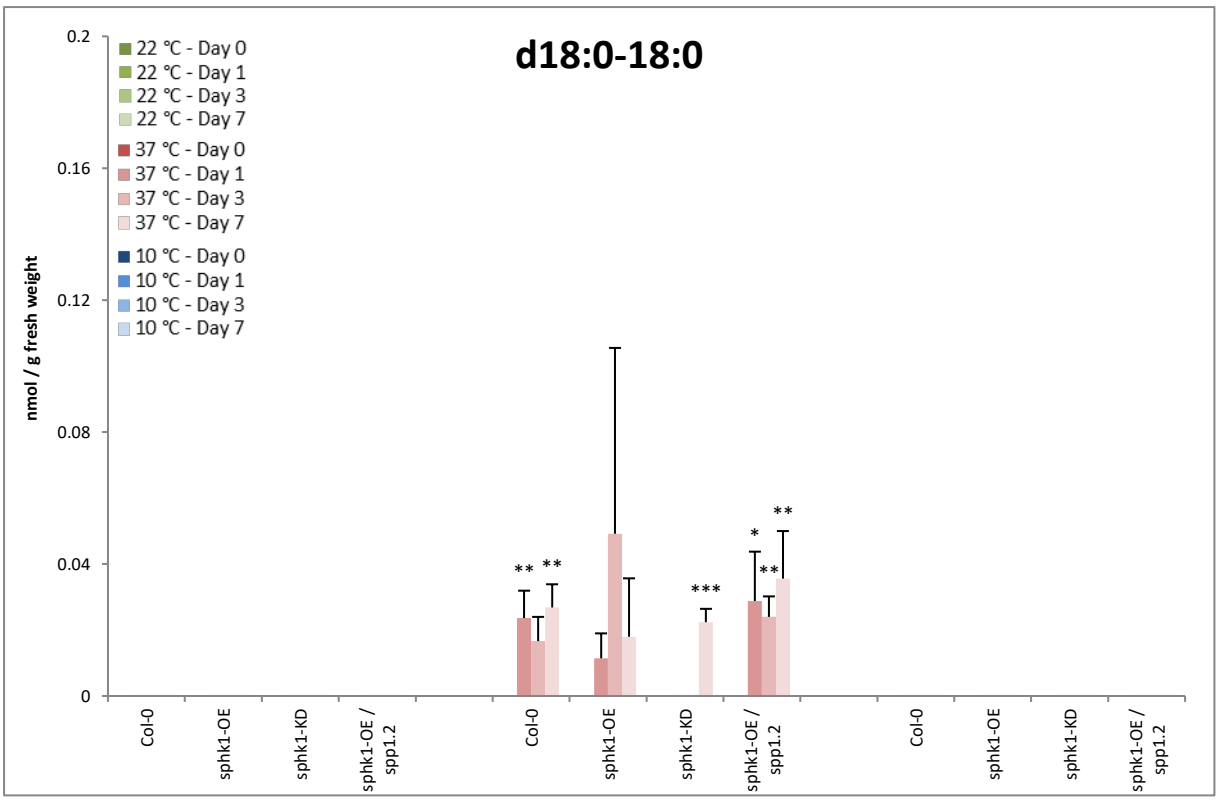
d18:0-18:0
nmol / g fresh weight
0.2
0.16
0.12
0.08
0.04
0
22 °C - Day 0
22 °C - Day 1
22 °C - Day 3
22 °C - Day 7
37 °C - Day 0
37 °C - Day 1
37 °C - Day 3
37 °C - Day 7
10 °C - Day 0
10 °C - Day 1
10 °C - Day 3
10 °C - Day 7
Col-0
sphk1-OE
sphk1-KD
sphk1-OE / spp1.2

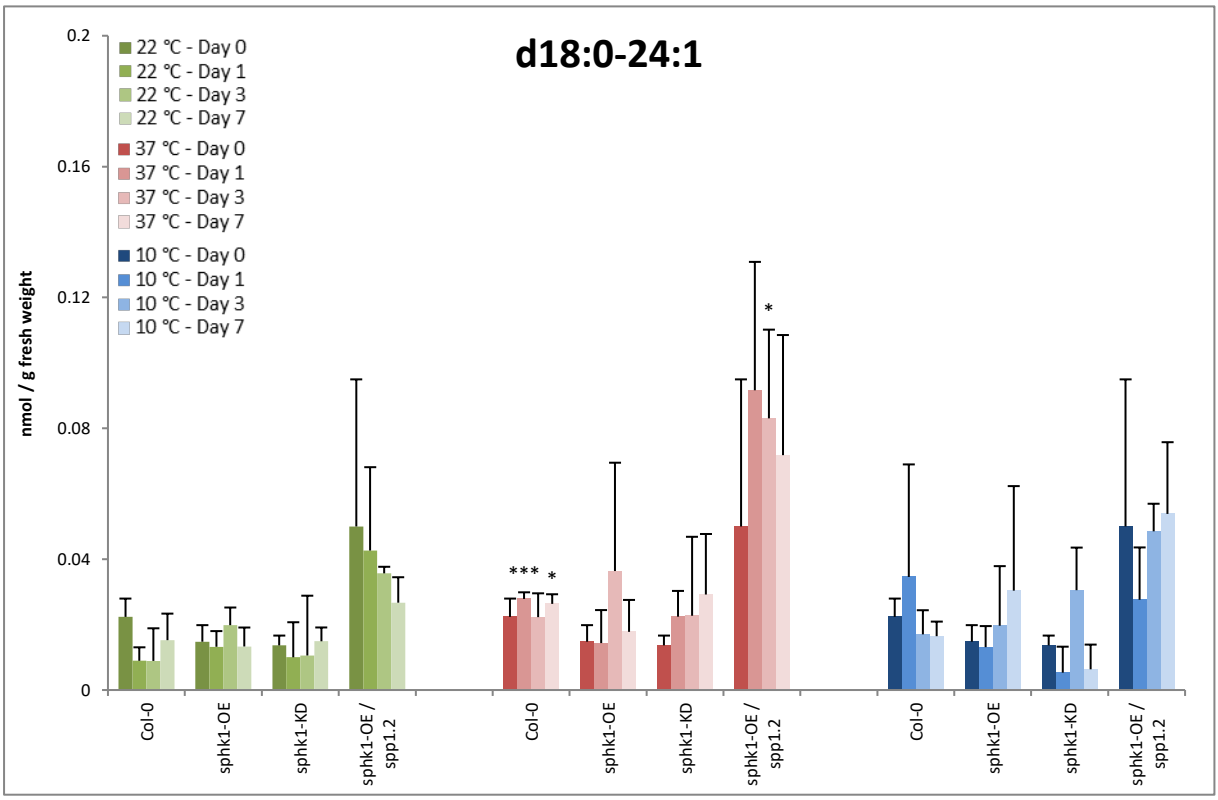
d18:0-24:1
nmol / g fresh weight
0.2
0.16
0.12
0.08
0.04
0
22 °C - Day 0
22 °C - Day 1
22 °C - Day 3
22 °C - Day 7
37 °C - Day 0
37 °C - Day 1
37 °C - Day 3
37 °C - Day 7
10 °C - Day 0
10 °C - Day 1
10 °C - Day 3
10 °C - Day 7
Col-0
sphk1-OE
sphk1-KD
sphk1-OE / spp1.2

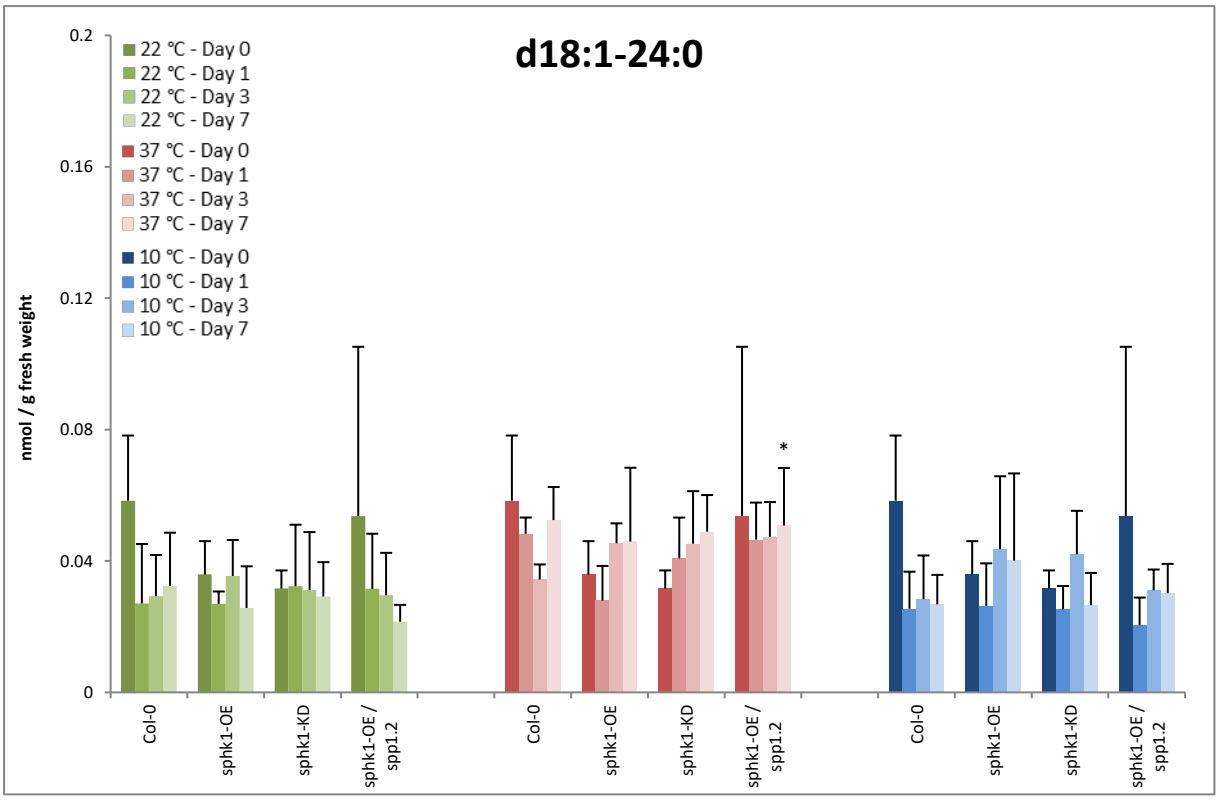
d18:1-24:0
nmol / g fresh weight
0.2
0.16
0.12
0.08
0.04
0
22 °C - Day 0
22 °C - Day 1
22 °C - Day 3
22 °C - Day 7
37 °C - Day 0
37 °C - Day 1
37 °C - Day 3
37 °C - Day 7
10 °C - Day 0
10 °C - Day 1
10 °C - Day 3
10 °C - Day 7
*
Col-0
sphk1-OE
sphk1-KD
sphk1-OE / spp1.2
Col-0
sphk1-OE
sphk1-KD
sphk1-OE / spp1.2
Col-0
sphk1-OE
sphk1-KD
sphk1-OE / spp1.2

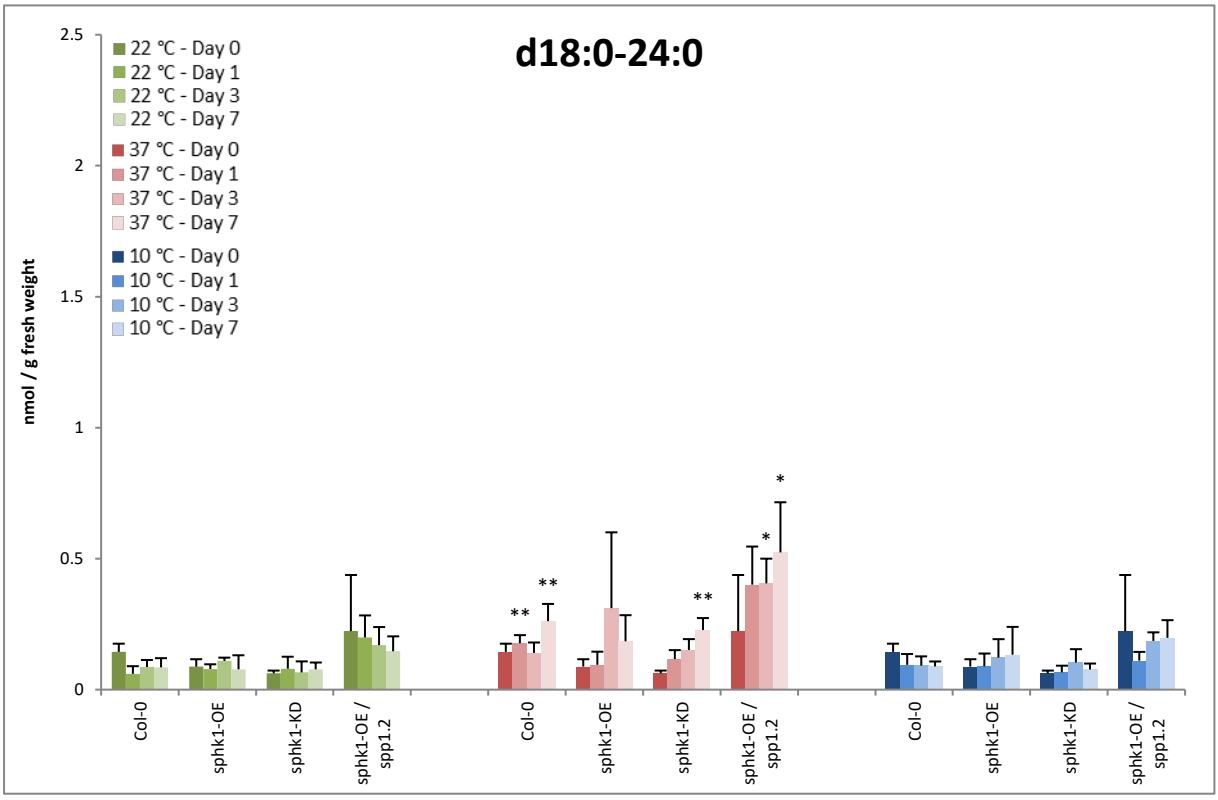
d18:0-24:0
nmol / g fresh weight
2.5
2
1.5
1
0.5
0
22 °C - Day 0
22 °C - Day 1
22 °C - Day 3
22 °C - Day 7
37 °C - Day 0
37 °C - Day 1
37 °C - Day 3
37 °C - Day 7
10 °C - Day 0
10 °C - Day 1
10 °C - Day 3
10 °C - Day 7
**
**
**
*
*
Col-0
sphk1-OE
sphk1-KD
sphk1-OE / spp1.2
Col-0
sphk1-OE
sphk1-KD
sphk1-OE / spp1.2
Col-0
sphk1-OE
sphk1-KD
sphk1-OE / spp1.2

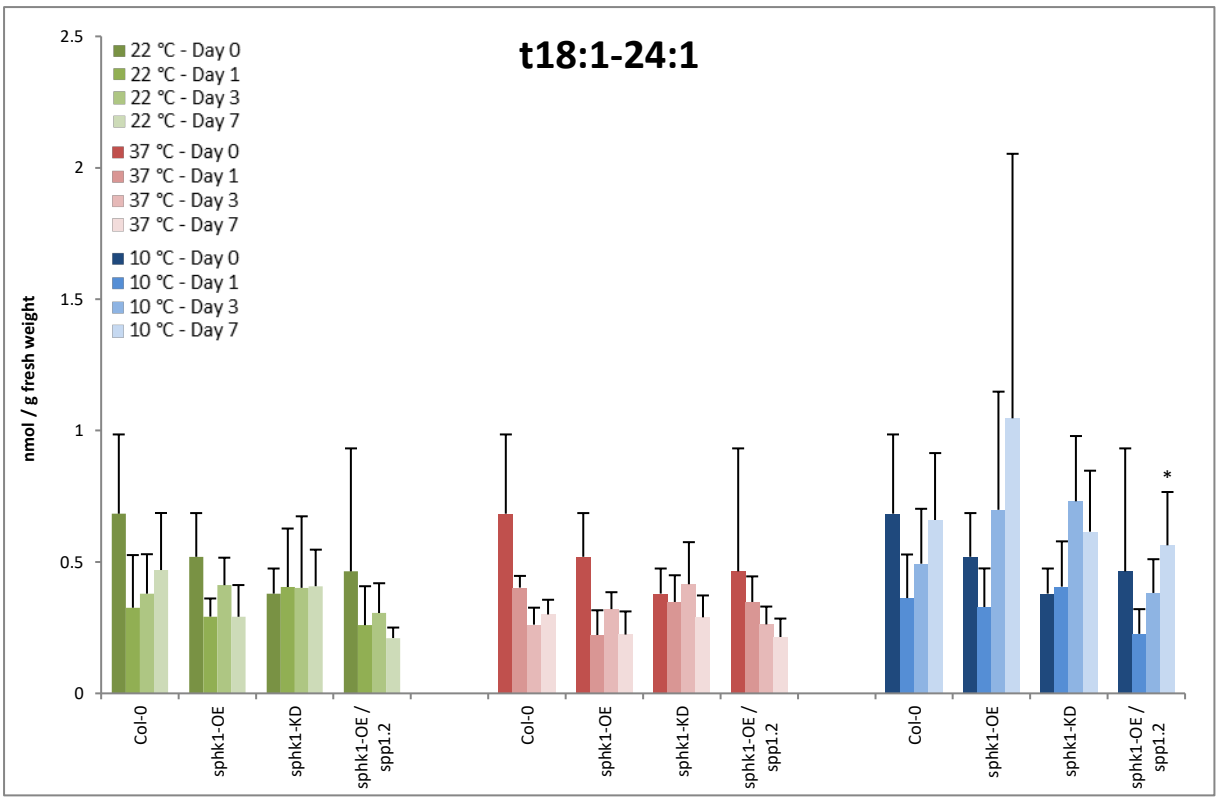
t18:1-24:1
nmol / g fresh weight
2.5
2
1.5
1
0.5
0
22 °C - Day 0
22 °C - Day 1
22 °C - Day 3
22 °C - Day 7
37 °C - Day 0
37 °C - Day 1
37 °C - Day 3
37 °C - Day 7
10 °C - Day 0
10 °C - Day 1
10 °C - Day 3
10 °C - Day 7
*
Col-0
sphk1-OE
sphk1-KD
sphk1-OE / spp1.2
Col-0
sphk1-OE
sphk1-KD
sphk1-OE / spp1.2
Col-0
sphk1-OE
sphk1-KD
sphk1-OE / spp1.2

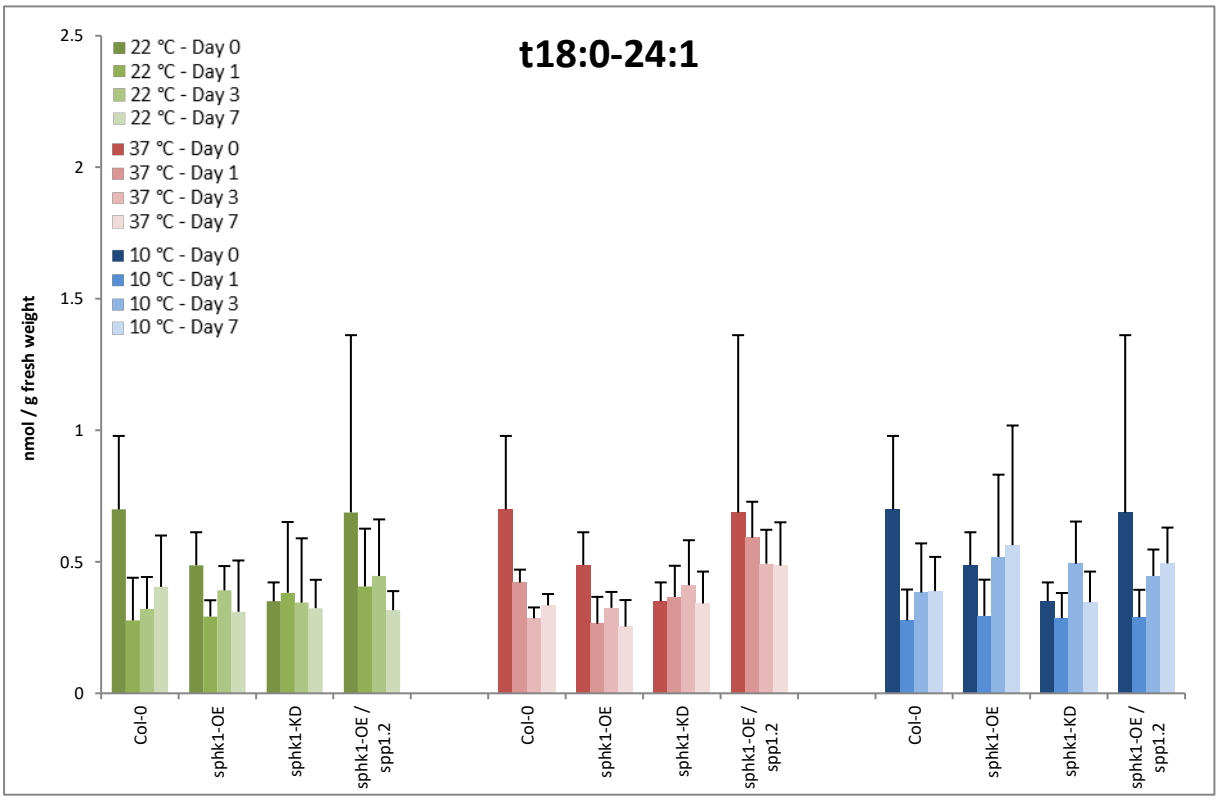
t18:0-24:1
nmol / g fresh weight
2.5
2
1.5
1
0.5
0
22 °C - Day 0
22 °C - Day 1
22 °C - Day 3
22 °C - Day 7
37 °C - Day 0
37 °C - Day 1
37 °C - Day 3
37 °C - Day 7
10 °C - Day 0
10 °C - Day 1
10 °C - Day 3
10 °C - Day 7
Col-0
sphk1-OE
sphk1-KD
sphk1-OE / spp1.2
Col-0
sphk1-OE
sphk1-KD
sphk1-OE / spp1.2
Col-0
sphk1-OE
sphk1-KD
sphk1-OE / spp1.2

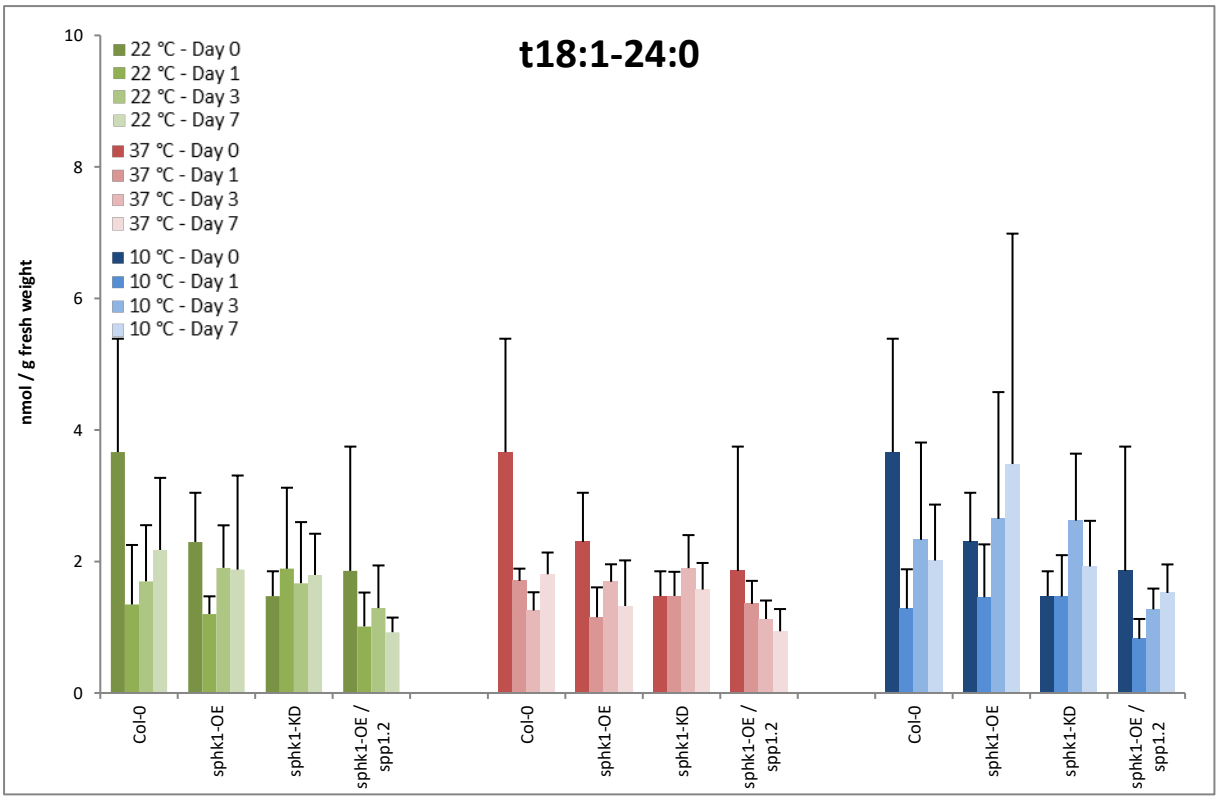
t18:1-24:0
nmol / g fresh weight
22 °C - Day 0
22 °C - Day 1
22 °C - Day 3
22 °C - Day 7
37 °C - Day 0
37 °C - Day 1
37 °C - Day 3
37 °C - Day 7
10 °C - Day 0
10 °C - Day 1
10 °C - Day 3
10 °C - Day 7
Col-0
sphk1-OE
sphk1-KD
sphk1-OE / spp1.2

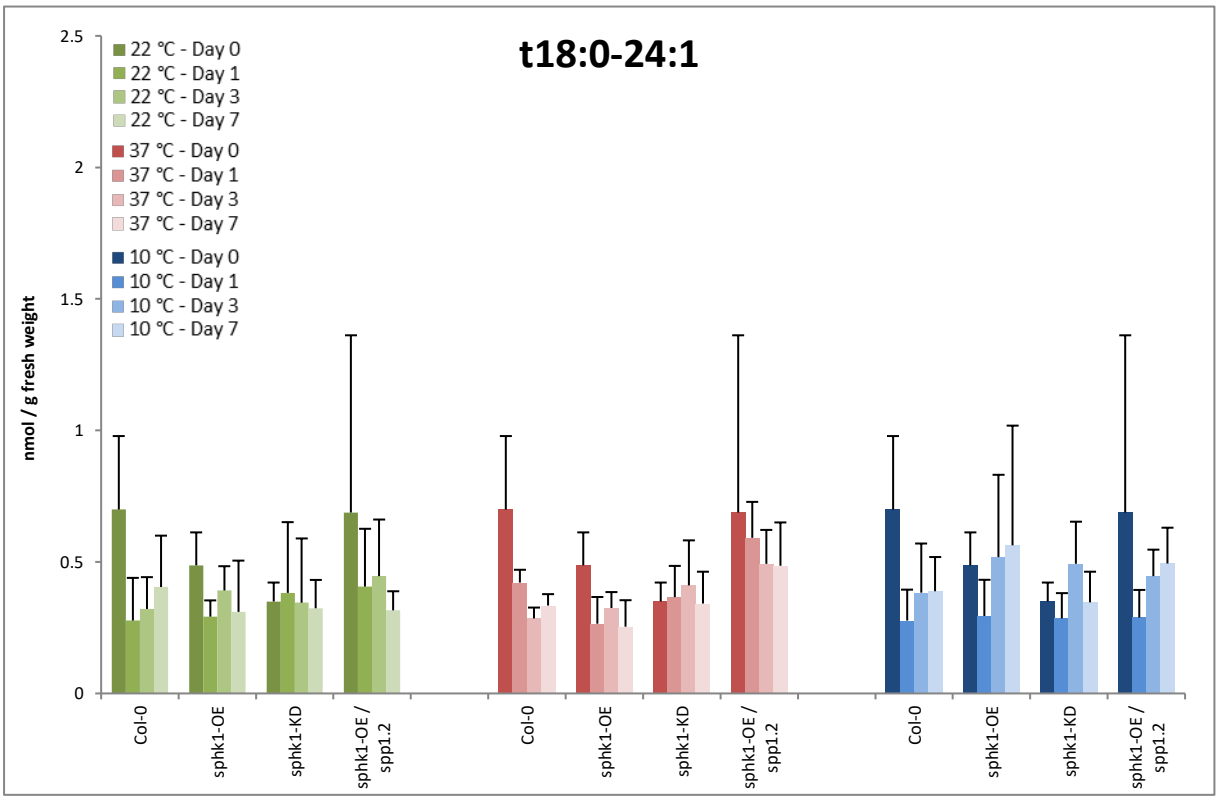
t18:0-24:1
nmol / g fresh weight
22 °C - Day 0
22 °C - Day 1
22 °C - Day 3
22 °C - Day 7
37 °C - Day 0
37 °C - Day 1
37 °C - Day 3
37 °C - Day 7
10 °C - Day 0
10 °C - Day 1
10 °C - Day 3
10 °C - Day 7
Col-0
sphk1-OE
sphk1-KD
sphk1-OE / spp1.2

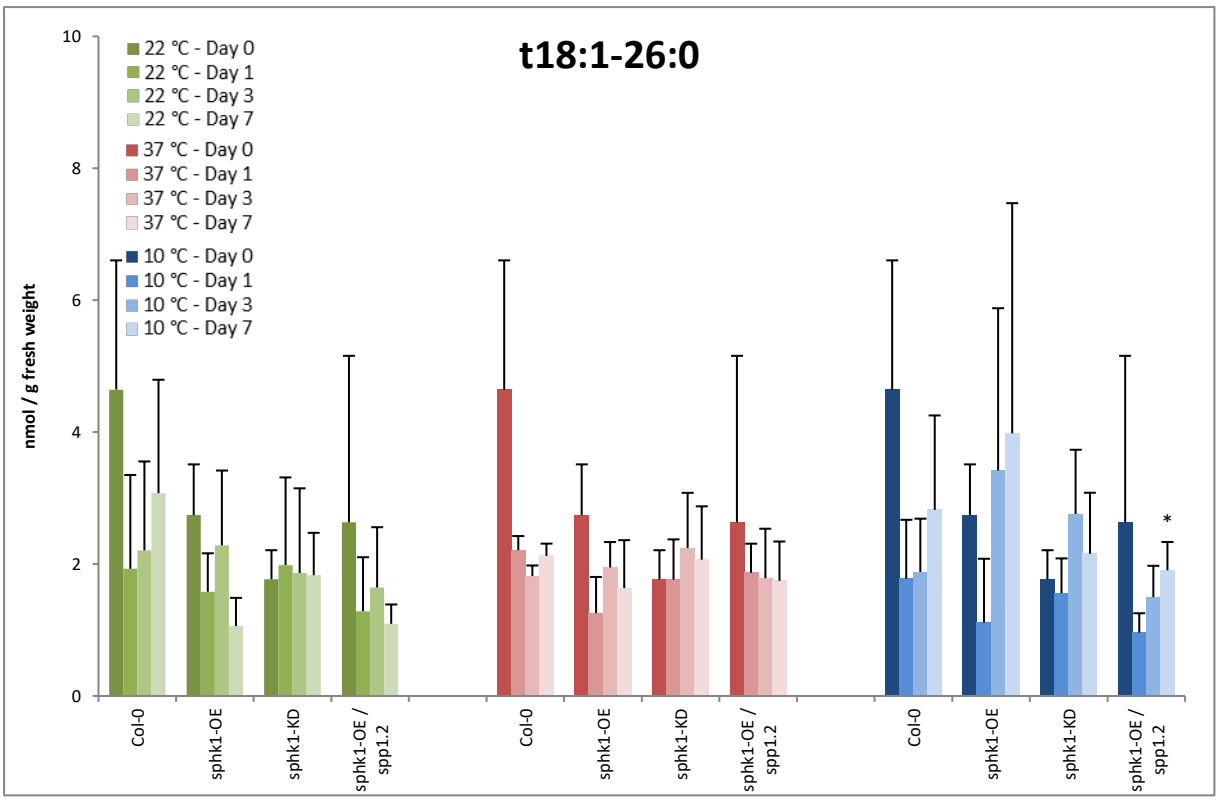
t18:1-26:0
nmol / g fresh weight
22 °C - Day 0
22 °C - Day 1
22 °C - Day 3
22 °C - Day 7
37 °C - Day 0
37 °C - Day 1
37 °C - Day 3
37 °C - Day 7
10 °C - Day 0
10 °C - Day 1
10 °C - Day 3
10 °C - Day 7
Col-0
sphk1-OE
sphk1-KD
sphk1-OE / spp1.2

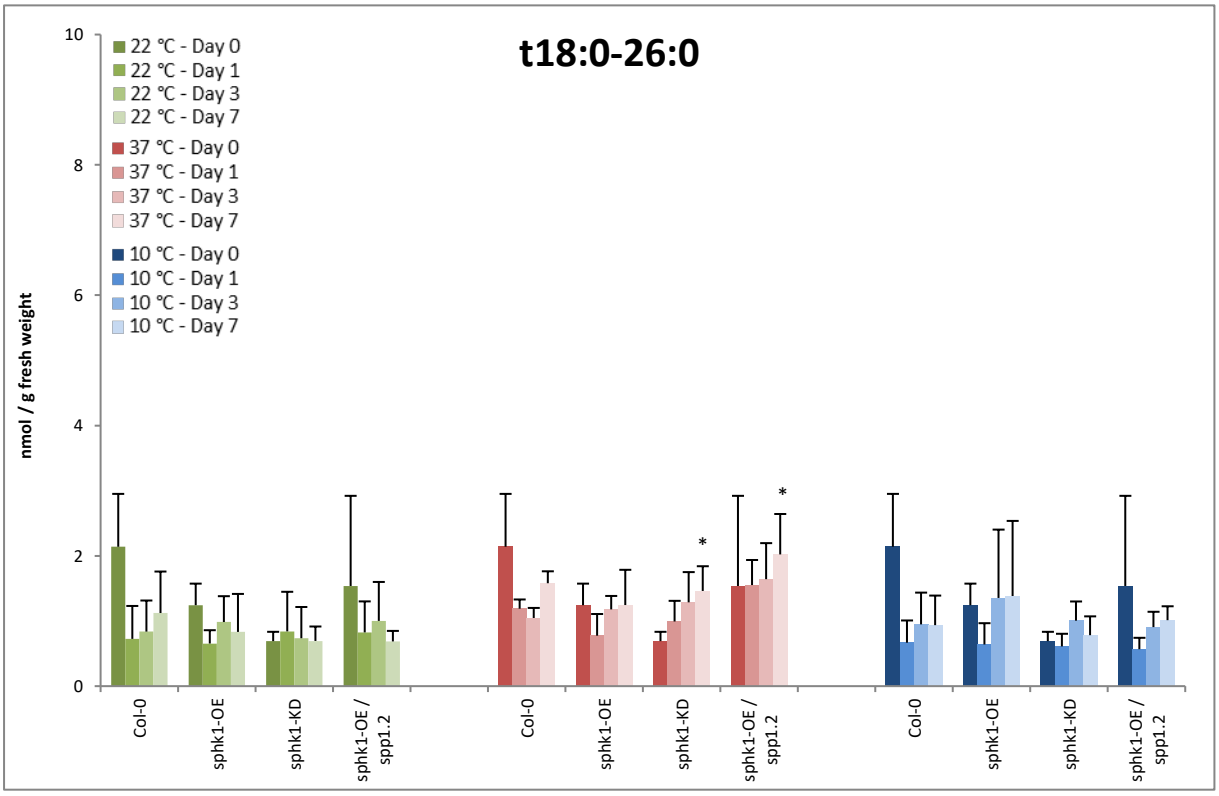
t18:0-26:0
nmol / g fresh weight
22 °C - Day 0
22 °C - Day 1
22 °C - Day 3
22 °C - Day 7
37 °C - Day 0
37 °C - Day 1
37 °C - Day 3
37 °C - Day 7
10 °C - Day 0
10 °C - Day 1
10 °C - Day 3
10 °C - Day 7
Col-0
sphk1-OE
sphk1-KD
sphk1-OE / spp1.2

Annex 10: Ceramides accumulation during temperature adaptation of *A. thaliana* wild-type ecotype Col-0 and *Arabidopsis* sphingolipid metabolism mutant lines. Two-week-old seedlings of wild-type (Col-0) and *Arabidopsis* sphingolipid metabolism mutant lines were incubated either at 22 °C for control, at 37 °C for heat adaptation or at 10 °C for cold adaptation. Very-long-chain fatty acid ceramides were measured at day 0, 1, 3 and 7. Asterisks indicate significant differences between control-incubated samples and heat adaptation-incubated samples or between control-incubated samples and cold adaptation-incubated samples according to Student's *t*-Test: *, P < 0.05; **, P < 0.01; and ***, P < 0.001. Results show means ± SD of four different technical replicates.

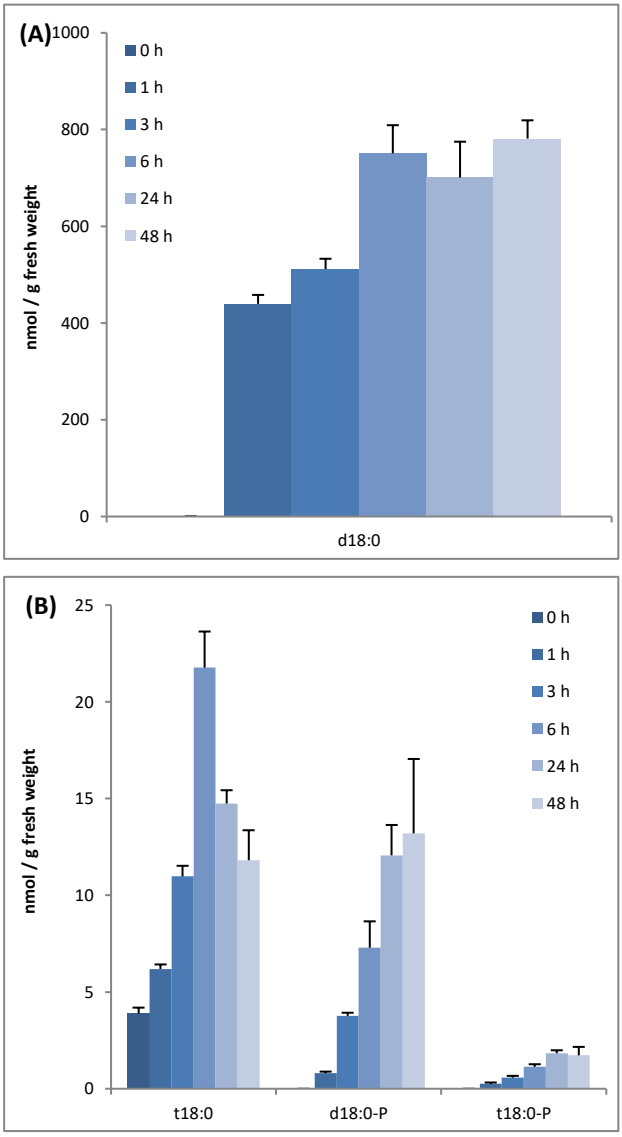

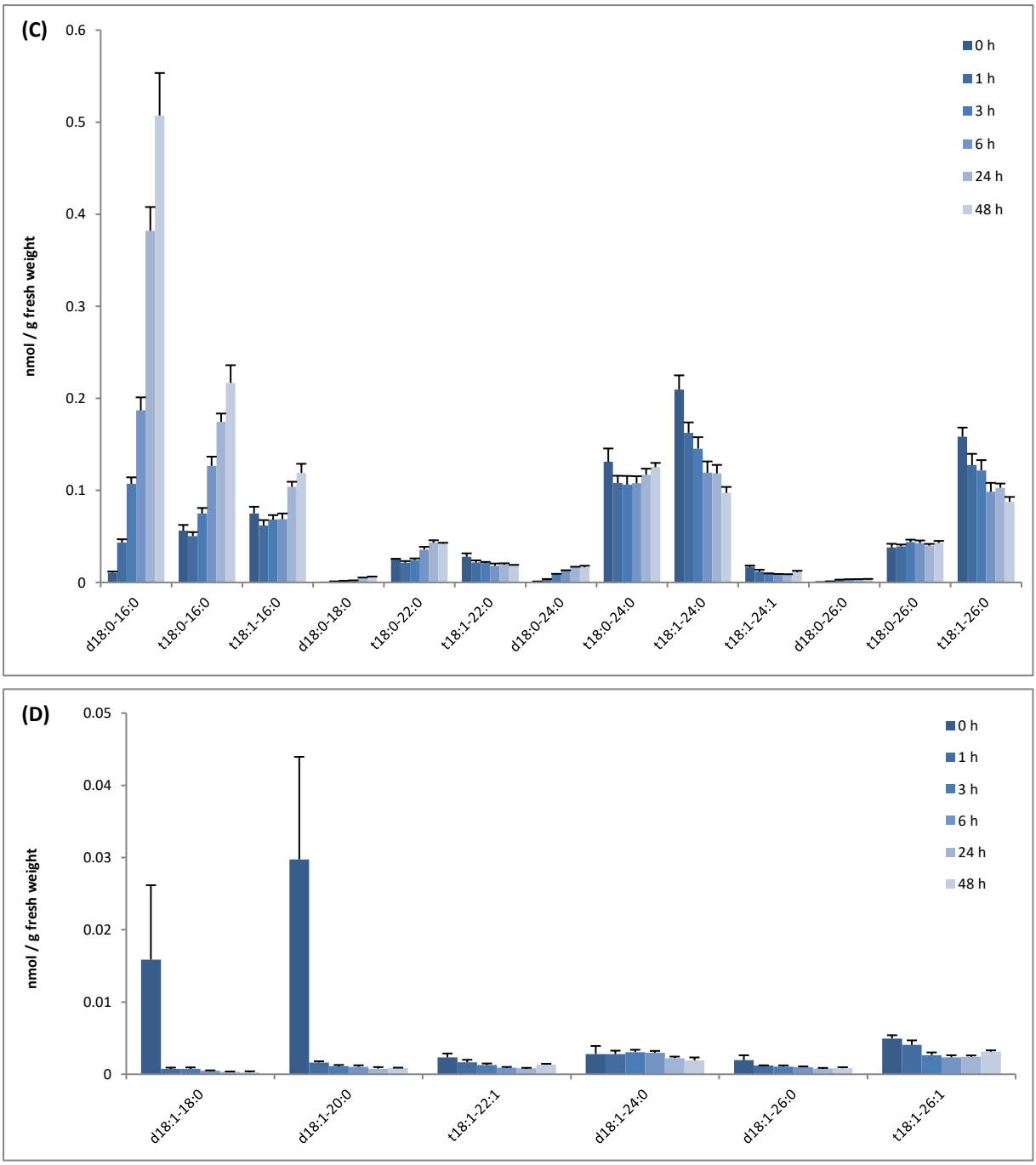

Annex 11: Sphingolipids detected during leaf discs feeding in *A. thaliana* wild-type Col-0. Six-week-old leaf discs from *A. thaliana* ecotype Col-0 were incubated in 100 µM d18:0 solutions. Leaf discs were collected over time and Sphingolipids were quantified. LCBs are presented on figures on (A) and (B) and ceramides are presented on figure (C) and (D). Results show means ± SD of four different technical replicates. Similar results were obtained in three different biological replicates.

Compound	ESI Mode	RT	D_7-m/z	m/z	Found in Experiment
No match	Negative	1.47	351.3238	344,2797	
No match	Negative	2.17	419.3131	412,269	
No match	Negative	2.22	278.2711	271,227	B/F/H/I/J/K/L/P/R
No match	Negative	2.27	519.3301	512,286	
No match	Negative	2.41	493.3505	486,3064	
No match	Negative	2.46	497.3452	490,3011	
t18:2, d18:1-P-26:2, Glc-d18:0-20:2	Negative	2.48	379.3186	372,2745	
No match	Negative	2.51	621.3612	614,3171	
No match	Negative	2.53	521.3412	514,2971	
No match	Negative	2.54	468.3124	461,2683	D
d18:0-P	Negative	2.55	387.3029	380,2588	K/L
Glc-t18:0-h24:2	Negative	2.55	423.345	416,3009	
No match	Negative	2.59	400.3058	393,2617	
No match	Negative	2.62	292.2868	285,2427	F/G/H/I/J/K/L
No match	Negative	2.71	354.2272	347,1831	
No match	Negative	2.76	630.3614	623,3173	
No match	Negative	2.84	320.2816	313,2375	
No match	Negative	2.93	568.3837	561,3396	
No match	Negative	3.16	568.3827	561,3386	B/V/W
t18:0	Negative	3.17	323,3285	316,2844	
No match	Negative	3.19	477.4281	470,384	
No match	Negative	3.21	470.3854	463,3413	
No match	Negative	3.23	379.3532	372,3091	
Glc-d18:0-17:2	Negative	3.26	358.2961	351,252	
No match	Negative	3.27	550.3665	543,3224	
Glc-d18:0-19:2	Negative	3.27	372.3118	365,2677	
No match	Negative	3.32	248.2607	241,2166	B/C/F/G/H/I/J/K/L/V/W
t18:1, t18:0-22:1	Negative	3.35	321.3133	314,2692	
No match	Negative	3.39	497.3458	490,3017	
No match	Negative	3.4	544.346	537,3019	
Glc-t18:1-27:2	Negative	3.42	435.3665	428,3224	
No match	Negative	3.42	516.3357	509,2916	
Glc-t18:0-h24:0	Negative	3.43	425.3606	418,3165	
No match	Negative	3.45	846.3035	839,2594	
No match	Negative	3.45	414.285	407,2409	
No match	Negative	3.5	379.355	372,3109	
t18:0-26:1	Negative	3.5	349.3442	342,3001	
Glc-d18:0-19:2	Negative	3.52	372.3114	365,2673	
No match	Negative	3.59	389.3038	382,2597	
d18:0-P-28:1, Glc-d18:0-22:0	Negative	3.6	395.3503	388,3062	U
No match	Negative	3.61	439.4053	432,3612	
No match	Negative	3.62	273.2926	266,2485	
d18:0	Negative	3.63	307,3337	300,2896	J/V/W
No match	Negative	3.63	615.6759	608,6318	
No match	Negative	3.64	343.3084	336,2643	
No match	Negative	3.64	563.5738	556,5297	

Compound	ESI Mode	RT	D7-m/z	m/z	Found in Experiment
No match	Negative	3.64	411.3134	404,2693	
No match	Negative	3.64	547.3612	540,3171	
No match	Negative	3.66	350.3404	343,2963	
No match	Negative	3.66	480.4331	473,389	
No match	Negative	3.69	389.3384	382,2943	
No match	Negative	3.72	419.3487	412,3046	
No match	Negative	3.72	423.3503	416,3062	
No match	Negative	3.74	557.3265	550,2824	
No match	Negative	3.74	411.3767	404,3326	
No match	Negative	3.74	500.3557	493,3116	
d18:1	Negative	3.75	365.3395	358,2954	
d18:2	Negative	3.77	363.3247	356,2806	
No match	Negative	3.78	389.3634	382,3193	
No match	Negative	3.8	444.3777	437,3336	
No match	Negative	3.8	521.3463	514,3022	
No match	Negative	3.81	598.6134	591,5693	
No match	Negative	3.82	927.9044	920,8603	
ht18:0-h17:1	Negative	3.83	590.5632	583,5191	
No match	Negative	3.83	261.2701	254,226	
No match	Negative	3.84	563.5742	556,5301	
No match	Negative	3.84	366.2587	359,2146	
No match	Negative	3.84	70.029	62,9849	
No match	Negative	3.86	664.6189	657,5748	
No match	Negative	3.87	408.3337	401,2896	
d18:0-16:0, ht18:0-h18:0	Negative	3.88	605.5852	598,5411	
t18:0-18:2	Negative	3.88	645.5797	638,5356	
ht18:0-h18:1	Negative	3.88	663.5916	656,5475	
ht18:0-h18:1	Negative	3.89	604.5788	597,5347	
t18:0-26:0	Negative	3.9	349,3443	342,3002	J/K/L/U
No match	Negative	3.92	342.3007	335,2566	G/H/I
No match	Negative	3.92	140.0347	132,9906	
No match	Negative	3.94	361.3085	354,2644	
No match	Negative	3.94	623.3223	616,2782	
No match	Negative	3.95	456.3033	449,2592	
d18:2	Negative	3.97	303.303	296,2589	
No match	Negative	3.99	458.3972	451,3531	
No match	Negative	4.01	548.3562	541,3121	
No match	Negative	4.02	509.3452	502,3011	
No match	Negative	4.03	526.3357	519,2916	
No match	Negative	4.03	498.3099	491,2658	
No match	Negative	4.03	623.3226	616,2785	
No match	Negative	4.04	927.6893	920,6452	
No match	Negative	4.06	920.6447	913,6006	
No match	Negative	4.08	466.3942	459,3501	
No match	Negative	4.09	430.4022	423,3581	
No match	Negative	4.09	519.2918	512,2477	

Compound	ESI Mode	RT	D_7-m/z	m/z	Found in Experiment
No match	Negative	4.13	1133.6418	1126,5977	
No match	Negative	4.13	930.7048	923,6607	
No match	Negative	4.13	797.6584	790,6143	
No match	Negative	4.14	1190.6093	1183,5652	
No match	Negative	4.14	545.3381	538,294	
No match	Negative	4.16	303.2995	296,2554	
No match	Negative	4.16	827.7075	820,6634	
No match	Negative	4.17	456.2956	449,2515	
t18:0-28:1	Negative	4.17	363.36	356,3159	
No match	Negative	4.17	492.2725	485,2284	
Glc-d18:0-26:0	Negative	4.19	423.381	416,3369	
No match	Negative	4.19	356.3157	349,2716	
No match	Negative	4.23	417.3683	410,3242	
No match	Negative	4.26	431.3123	424,2682	
No match	Negative	4.28	494.3615	487,3174	
No match	Negative	4.28	276.2917	269,2476	B/F/H/I/J/K/L/O/Q/V/W
Glc-t18:1-h28:2	Negative	4.3	450.3711	443,327	
No match	Negative	4.32	487.3172	480,2731	
Glc-d18:0-28:1	Negative	4.36	436.3914	429,3473	
No match	Negative	4.41	622.3716	615,3275	
No match	Negative	4.41	459,322	452,2779	
No match	Negative	4.47	450.3711	443,327	
No match	Negative	4.47	606.3769	599,3328	
No match	Negative	4.5	478.3645	471,3204	
No match	Negative	4.5	347.3657	340,3216	
No match	Negative	4.53	540.3889	533,3448	
No match	Negative	4.57	304,287	297,2429	
No match	Negative	4.6	496.3623	489,3182	
No match	Negative	4.64	493.4227	486,3786	
No match	Negative	4.67	646.3925	639,3484	
ht18:0-h22:1	Negative	4.8	719,652	712,6079	
No match	Negative	4.8	361.3074	354,2633	
No match	Negative	4.83	428.3837	421,3396	
No match	Negative	4.98	345.2426	338,1985	
No match	Negative	4.99	426.3708	419,3267	
No match	Negative	5.02	428.3862	421,3421	
No match	Negative	5.05	405,4064	398,3623	
No match	Negative	5.1	836.5437	829,4996	
No match	Negative	5.26	432.3603	425,3162	
No match	Negative	5.4	644.5246	637,4805	
No match	Negative	5.62	524.3927	517,3486	
No match	Negative	5.82	401.3417	394,2976	
No match	Negative	5.85	719.4651	712,421	
No match	Negative	6.12	838.548	831,5039	
No match	Negative	6.4	676.4935	669,4494	K/R
No match	Negative	6.47	840.5659	833,5218	

Compound	ESI Mode	RT	D_7-m/z	m/z	Found in Experiment
No match	Negative	6.53	718.5411	711,497	J/K/O
No match	Negative	6.71	678.5097	671,4656	D/J/K
No match	Negative	6.82	573,45	566,4059	
No match	Negative	6.85	651.5191	644,475	
No match	Negative	6.88	1006.5341	999,49	
No match	Negative	6.9	512.4677	505,4236	
d18:0-14:1, ht18:0-h16:1	Negative	6.97	575.5374	568,4933	H/I/J/K/L
No match	Negative	7.05	734.5737	727,5296	
No match	Negative	7.1	761.6879	754,6438	
No match	Negative	7.11	556.4939	549,4498	
No match	Negative	7.13	626.6093	619,5652	
No match	Negative	7.14	622.5383	615,4942	H/I/J/K/L
No match	Negative	7.14	719.5222	712,4781	
No match	Negative	7.16	400.3342	393,2901	
Glc-d18:0-16:1, Glc-t18:0-h18:1	Negative	7.17	765.6226	758,5785	B/J/L/O
No match	Negative	7.2	640.5469	633,5028	B/J
No match	Negative	7.22	736.6071	729,563	
ht18:0-h17:1	Negative	7.29	589.5571	582,513	L/M/N/O
No match	Negative	7.3	584,598	577,5539	
No match	Negative	7.35	624.5545	617,5104	B/D/G/H/I/J
d18:0-18:1, ht18:0-h20:1	Negative	7.35	631.5982	624,5541	
No match	Negative	7.35	607.5684	600,5243	
No match	Negative	7.35	653.6106	646,5665	
t18:0-16:0	Negative	7.36	561,5584	554,5143	B/D/F/G/H/I/J/K/L/U/V/W/X
No match	Negative	7.42	710.628	703,5839	
No match	Negative	7.46	691.6438	684,5997	
d18:0-18:2, ht18:0-h20:2	Negative	7.5	629.5874	622,5433	J
No match	Negative	7.52	579.5244	572,4803	J/M/N/O/P
d18:0-16:1	Negative	7.53	543,5479	536,5038	B/C/H/I/J/K/L/M/N/O/P/V/W
No match	Negative	7.53	602.5648	595,5207	
No match	Negative	7.54	669.6709	662,6268	
No match	Negative	7.55	594.5424	587,4983	
d18:0-14:0, ht18:0-h16:0	Negative	7.55	577.5559	570,5118	J/K/L
No match	Negative	7.58	631.5961	624,552	
No match	Negative	7.6	964.9999	957,9558	
No match	Negative	7.6	1092.6733	1085,6292	
No match	Negative	7.61	957.9563	950,9122	A/B/H/I/J/K/L/M/N/O/P/W
No match	Negative	7.61	402.4331	395,389	D/E
No match	Negative	7.62	939.9433	932,8992	
t18:0-20:1	Negative	7.73	615.6046	608,5605	
No match	Negative	7.74	551,6017	544,5576	
No match	Negative	7.74	1017.9575	1010,9134	H/I/J/K/L/V/W
d18:0-15:0, ht18:0-h17:0	Negative	7.75	591.5703	584,5262	J/K/L/M/N/O/P/V/W
No match	Negative	7.75	1159.2012	1152,1571	
No match	Negative	7.75	630.5806	623,5365	
No match	Negative	7.75	941.9606	934,9165	

Compound	ESI Mode	RT	D_7-m/z	m/z	Found in Experiment
No match	Negative	7.77	1152.1577	1145,1136	
d18:0-16:0	Negative	7.77	544,5573	537,5132	
No match	Negative	7.78	1145.1142	1138,0701	J/K/L
No match	Negative	7.83	631.5944	624,5503	
No match	Negative	7.83	1098.5199	1091,4758	
No match	Negative	7.86	640.6249	633,5808	
No match	Negative	7.9	603.5928	596,5487	
t18:0-20:1	Negative	8.01	675.628	668,5839	D/E/H/I/J/K/P/X
No match	Negative	8.03	658.5641	651,52	X
No match	Negative	8.04	580.6026	573,5585	
No match	Negative	8.06	566.6229	559,5788	
No match	Negative	8.08	606.5863	599,5422	
No match	Negative	8.1	752.6906	745,6465	
No match	Negative	8.11	640.6242	633,5801	
d18:0-18:0	Negative	8.16	573,5951	566,551	
ht18:0-h24:2	Negative	8.18	685,6476	678,6035	H/I
ht18:0-h22:1	Negative	8.2	659,6308	652,5867	
No match	Negative	8.2	719.4442	712,4001	
No match	Negative	8.22	656.6531	649,609	
No match	Negative	8.3	909.7424	902,6983	
d18:0-22:1, ht18:0-h24:1	Negative	8.38	687.6646	680,6205	H/I
No match	Negative	8.4	622.6113	615,5672	
No match	Negative	8.48	671.6731	664,629	B/J/K/L/V/W
No match	Negative	8.49	691.6602	684,6161	
No match	Negative	8.51	704.6714	697,6273	
No match	Negative	8.52	624.6274	617,5833	
t18:0-24:1	Negative	8.65	671,6693	664,6252	
No match	Negative	8.65	734.6707	727,6266	
t18:0-22:0	Negative	8.69	645,652	638,6079	B/J/K/L/P
No match	Negative	8.72	930.4717	923,4276	
t18:0-26:1	Negative	8.76	759.7216	752,6775	D/E/H/I/W/X
No match	Negative	8.77	719.6949	712,6508	
d18:0-22:0	Negative	8.78	629,659	622,6149	
No match	Negative	8.78	833.6674	826,6233	
No match	Negative	8.78	895.6658	888,6217	
t18:0-24:0	Negative	8.8	673,686	666,6419	B/D
ht18:0-h26:1	Negative	8.82	775.7177	768,6736	H/I
d18:0-23:0, ht18:0-h25:0	Negative	8.92	703.6956	696,6515	B/H/I/O
No match	Negative	8.93	747.7266	740,6825	
No match	Negative	8.93	762.6995	755,6554	
No match	Negative	8.96	733.7123	726,6682	
d18:0-24:0	Negative	9.05	657,6885	650,6444	
t18:0-26:0,	Negative	9.05	701,7172	694,6731	W
No match	Negative	9.05	764.7158	757,6717	
t18:0-28:1	Negative	9.17	787.7532	780,7091	C/D/E/G/H/I/O/W
d18:0-25:0, ht18:0-h27:0	Negative	9.17	731.7269	724,6828	

Compound	ESI Mode	RT	D_7-m/z	m/z	Found in Experiment
No match	Negative	9.21	932.9706	925,9265	
d18:0-26:0, ht18:0-h28:0	Negative	9.28	745.7417	738,6976	M/N/O/P
No match	Negative	9.43	960.9633	953,9192	
d18:0-28:0	Negative	9.49	773.7739	766,7298	U
No match	Negative	9.88	829.7082	822,6641	
No match	Negative	9.99	930.8473	923,8032	
t18:1	Positive	1.69	323.3287	316,2846	
No match	Positive	10.22	808.791	801,7469	
No match	Positive	10.28	1016.9183	1009,8742	
No match	Positive	10.31	938.8696	931,8255	
No match	Positive	10.46	876.8539	869,8098	
t18:1	Positive	2.07	323.3281	316,284	
No match	Positive	2.23	589.2452	582,2011	
No match	Positive	2.27	1034.7172	1027,6731	
No match	Positive	2.43	530.2331	523,189	
t18:0	Positive	2.51	325.3445	318,3004	
d18:0-P	Positive	2.54	389.3164	382,2723	
No match	Positive	2.58	409.3641	402,32	
No match	Positive	2.62	772.4815	765,4374	
No match	Positive	2.7	263.3078	256,2637	
d18:1	Positive	2.77	307.3341	300,29	
No match	Positive	3.01	1148.7844	1141,7403	
No match	Positive	3.03	538.4274	531,3833	
No match	Positive	3.18	339.3601	332,316	V/W
No match	Positive	3.27	552.3845	545,3404	
No match	Positive	3.29	667.3129	660,2688	
No match	Positive	3.32	321.3497	314,3056	
No match	Positive	3.33	506.4371	499,393	
d18:1	Positive	3.42	307.3344	300,2903	V/W
No match	Positive	3.48	385.3808	378,3367	
No match	Positive	3.49	470.3973	463,3532	
No match	Positive	3.51	693.4206	686,3765	
No match	Positive	3.53	464.3579	457,3138	
No match	Positive	3.55	935.5879	928,5438	
GIPC-d18:1-20:2	Positive	3.55	1176.6938	1169,6497	
ht18:0-h20:0, ht18:1-h22:2	Positive	3.56	657.6162	650,5721	
No match	Positive	3.57	910.7724	903,7283	
No match	Positive	3.57	1083.81	1076,7659	
No match	Positive	3.58	1175.8931	1168,849	
No match	Positive	3.6	1101.8202	1094,7761	
d18:0	Positive	3.62	309,3512	302,3071	J/U
No match	Positive	3.62	617,6928	610,6487	
No match	Positive	3.62	625.678	618,6339	
No match	Positive	3.62	261.3284	254,2843	
No match	Positive	3.63	292.4414	285,3973	
No match	Positive	3.66	1119.8665	1112,8224	

Compound	ESI Mode	RT	D_7-m/z	m/z	Found in Experiment
No match	Positive	3.68	1157.8831	1150,839	
No match	Positive	3.69	909.7696	902,7255	
No match	Positive	3.7	411.3827	404,3386	
No match	Positive	3.72	445.3458	438,3017	
No match	Positive	3.73	1013.7849	1006,7408	
No match	Positive	3.74	353.3758	346,3317	
No match	Positive	3.75	717.6182	710,5741	
No match	Positive	3.81	909.7694	902,7253	
d18:0-23:0	Positive	3.83	645.6868	638,6427	
No match	Positive	3.86	955.8106	948,7665	
d18:0-24:0	Positive	3.88	659.7014	652,6573	
No match	Positive	3.88	490.3372	483,2931	
No match	Positive	3.89	332.3363	325,2922	
No match	Positive	3.93	464.3493	457,3052	
No match	Positive	3.93	447.3939	440,3498	
ht18:0-h25:1	Positive	3.94	703.6926	696,6485	
No match	Positive	3.99	484.8325	477,7884	
No match	Positive	3.99	1160.9006	1153,8565	
d18:1	Positive	4.02	307.3346	300,2905	
No match	Positive	4.02	487.3374	480,2933	
No match	Positive	4.03	538.4288	531,3847	
No match	Positive	4.04	464.3491	457,305	
No match	Positive	4.06	468.4158	461,3717	
No match	Positive	4.1	351.3954	344,3513	
No match	Positive	4.14	929.7055	922,6614	
No match	Positive	4.19	351.3651	344,321	
No match	Positive	4.2	346.3587	339,3146	
No match	Positive	4.21	965.7957	958,7516	
No match	Positive	4.22	1069.8292	1062,7851	
No match	Positive	4.22	364.3699	357,3258	
No match	Positive	4.24	277.324	270,2799	
No match	Positive	4.25	556.4275	549,3834	
No match	Positive	4.3	421.4015	414,3574	
No match	Positive	4.3	319.334	312,2899	
No match	Positive	4.38	464.3896	457,3455	
No match	Positive	4.44	696.5271	689,483	
No match	Positive	4.45	387.4439	380,3998	
No match	Positive	4.48	625.4703	618,4262	
No match	Positive	4.51	379,3921	372,348	
No match	Positive	4.52	482.3998	475,3557	
No match	Positive	4.53	360.3749	353,3308	
No match	Positive	4.54	365.3761	358,332	
No match	Positive	4.55	608.4767	601,4326	
No match	Positive	4.61	395.3863	388,3422	
No match	Positive	4.63	417.4088	410,3647	
No match	Positive	4.68	319.334	312,2899	

Compound	ESI Mode	RT	D_7-m/z	m/z	Found in Experiment
No match	Positive	4.7	365.3759	358,3318	
No match	Positive	4.78	453.4259	446,3818	
No match	Positive	4.78	402.4071	395,363	
No match	Positive	4.79	471.3816	464,3375	
No match	Positive	4.81	591.4248	584,3807	
No match	Positive	4.92	435.4174	428,3733	
No match	Positive	4.92	347.3651	340,321	
No match	Positive	4.93	409.4016	402,3575	
No match	Positive	4.97	389.3754	382,3313	
No match	Positive	5.02	430.4019	423,3578	
No match	Positive	5.16	389.3765	382,3324	
No match	Positive	5.21	1002.6067	995,5626	
No match	Positive	5.27	418.415	411,3709	
No match	Positive	5.3	506.4357	499,3916	
No match	Positive	5.37	513.4647	506,4206	
No match	Positive	5.37	530.2356	523,1915	
No match	Positive	5.46	992.7425	985,6984	
No match	Positive	5.56	389.3756	382,3315	
No match	Positive	5.57	437.4335	430,3894	
No match	Positive	5.61	359.3655	352,3214	
No match	Positive	5.64	598.4771	591,433	
No match	Positive	5.65	437.4334	430,3893	
No match	Positive	5.71	710.2544	703,2103	
t18:0-24:2	Positive	5.75	693.6516	686,6075	
No match	Positive	5.84	403.3912	396,3471	
No match	Positive	5.89	373.3809	366,3368	
No match	Positive	5.93	523.4344	516,3903	
No match	Positive	5.93	419.561	412,5169	
No match	Positive	5.99	451.4489	444,4048	
No match	Positive	6.01	785.543	778,4989	
No match	Positive	6.01	275.265	268,2209	
No match	Positive	6.06	415.358	408,3139	
No match	Positive	6.31	726.5002	719,4561	
No match	Positive	6.43	417.4068	410,3627	
No match	Positive	6.48	978.7628	971,7187	
No match	Positive	6.6	274.3107	267,2666	
ht18:1-P-h23:2	Positive	6.76	751.6005	744,5564	U
No match	Positive	6.82	263.1653	256,1212	
No match	Positive	6.85	610.5415	603,4974	
No match	Positive	6.89	619.5419	612,4978	
ht18:0-P-h22:0, ht18:1-P-h24:2	Positive	6.91	765.6129	758,5688	
No match	Positive	6.92	763.6004	756,5563	A/B/U
No match	Positive	7.03	721.552	714,5079	A
Glc-t18:0-16:1	Positive	7.07	723.6136	716,5695	
No match	Positive	7.09	527.4822	520,4381	
No match	Positive	7.11	498.4879	491,4438	

Compound	ESI Mode	RT	D_7-m/z	m/z	Found in Experiment
No match	Positive	7.13	649.5517	642,5076	
t18:0-16:1	Positive	7.14	561.558	554,5139	B/J/W
No match	Positive	7.23	653.6912	646,6471	
No match	Positive	7.35	723.5685	716,5244	B
t18:0-16:0	Positive	7.36	563.5738	556,5297	B/J/V/W
No match	Positive	7.4	937.7539	930,7098	
d18:0-24:1	Positive	7.46	657.6864	650,6423	
No match	Positive	7.49	560.5042	553,4601	
No match	Positive	7.49	650.5729	643,5288	
d18:0-18:2	Positive	7.5	571.5793	564,5352	
No match	Positive	7.51	295,1915	288,1474	
No match	Positive	7.52	552.6076	545,5635	
d18:0-16:1	Positive	7.53	545,5636	538,5195	J/W
No match	Positive	7.54	263.1647	256,1206	
d18:0-15:0	Positive	7.55	533.5633	526,5192	
No match	Positive	7.55	247.1703	240,1262	
t18:0-16:0	Positive	7.61	563.5736	556,5295	J/W/X
ht18:0-h28:2	Positive	7.61	760.7505	753,7064	
No match	Positive	7.62	562.5225	555,4784	
No match	Positive	7.66	277.1807	270,1366	
No match	Positive	7.71	625.6602	618,6161	
No match	Positive	7.73	612.6758	605,6317	
No match	Positive	7.74	554.623	547,5789	
No match	Positive	7.74	605.6323	598,5882	J/W
No match	Positive	7.77	1094.1558	1087,1117	
No match	Positive	7.78	770.5701	763,526	
No match	Positive	7.82	683.6844	676,6403	
d18:0-19:0	Positive	7.89	589.6247	582,5806	
No match	Positive	7.91	555.5137	548,4696	
No match	Positive	7.92	631.5769	624,5328	
No match	Positive	7.98	851.7265	844,6824	
No match	Positive	8.01	741.6978	734,6537	
No match	Positive	8.03	730.6481	723,604	
No match	Positive	8.03	584.6329	577,5888	
No match	Positive	8.04	705.6136	698,5695	
No match	Positive	8.06	1161.1497	1154,1056	
No match	Positive	8.06	567.6323	560,5882	
No match	Positive	8.1	754.7024	747,6583	
No match	Positive	8.11	950.8035	943,7594	
No match	Positive	8.12	554.6228	547,5787	
No match	Positive	8.15	631.5777	624,5336	
d18:0-18:0	Positive	8.16	575.61	568,5659	
No match	Positive	8.22	598.6487	591,6046	
No match	Positive	8.24	554.6228	547,5787	
Glc-t18:0-h24:1	Positive	8.31	851.7339	844,6898	
No match	Positive	8.33	598.6489	591,6048	

Compound	ESI Mode	RT	D_7-m/z	m/z	Found in Experiment
t18:0-22:1	Positive	8.36	645.6524	638,6083	
No match	Positive	8.37	698.2553	691,2112	
No match	Positive	8.38	612.6648	605,6207	
ht18:0-h24:1	Positive	8.54	689.6791	682,635	
No match	Positive	8.58	768.6657	761,6216	
No match	Positive	8.63	772.2744	765,2303	
t18:0-24:1	Positive	8.67	673.6839	666,6398	X/W
ht18:0-h24:0	Positive	8.69	691.6958	684,6517	B
t18:0-24:0	Positive	8.8	675.6994	668,6553	B
No match	Positive	8.81	949.8201	942,776	
t18:0-26:1	Positive	8.93	701.7149	694,6708	
No match	Positive	9.03	977.8505	970,8064	
No match	Positive	9.07	574.5565	567,5124	
No match	Positive	9.08	908.7943	901,7502	
No match	Positive	9.17	846.9699	839,9258	
No match	Positive	9.21	874.9648	867,9207	
No match	Positive	9.27	616.5667	609,5226	
No match	Positive	9.35	824.9293	817,8852	
No match	Positive	9.42	866.7855	859,7414	
No match	Positive	9.46	656.5994	649,5553	
No match	Positive	9.5	644.5980	637,5539	
No match	Positive	9.72	672.6293	665,5852	
No match	Positive	9.79	935.8481	928,804	
No match	Positive	9.87	872.8664	865,8223	
No match	Positive	9.87	967.8438	960,7997	

Annex 12: List of marker peaks detected after feeding with D_7-d18:0. The final list of 203 marker peaks detected in positive ESI and 236 marker peaks detected in negative ESI. Each marker peak is characterized by a sphingolipid compound name if possible, the ESI mode, the retention time (RT), the labeled mass to charge ratio (D_7-m/z), the mass to charge ratio (m/z) and the experiment letter label where it has been measured.

Experiments	Genotypes	Treatment's methods	Treatment's specifics	Treatment time points	Plant tissues	Plant material age
A	Col-0	Dexamethasone spray solution	100 nM	1, 4, 7, 25 and 49 h	Leaves	Six-week-old
B	Col-0	Dexamethasone spray solution	200 nM	1, 4, 7, 25 and 49 h	Leaves	Six-week-old
C	Col-0	Hydrogen peroxide spray solution	10 mM	1 and 7 days	Leaves	Six-week-old
D	Col-0	Deoxynivalenol spray solution	150 µM	1 and 7 days	Leaves	Six-week-old
E	Col-0	Salicylic acid spray solution	150 µM	1 and 7 days	Leaves	Six-week-old
F	Col-0	Hydroponic stock solution	Stock 1	48 h	Roots	Eight-week-old
G	Col-0	Hydroponic stock solution	Stock 2	48 h	Roots	Eight-week-old
H	Col-0	Hydroponic stock solution	Stock 3	48 h	Roots	Eight-week-old
I	Col-0	Hydroponic stock solution	Stock 4	48 h	Roots	Eight-week-old
J	Col-0	*P. syringae* infiltration	10^7 cfu/mL	48 h	Leaf discs	Six-week-old
K	*sphk1*-OE	*P. syringae* infiltration	10^7 cfu/mL	48 h	Leaf discs	Six-week-old
L	*sphk1*-OE /spp1.2	*P. syringae* infiltration	10^7 cfu/mL	48 h	Leaf discs	Six-week-old
M	Col-0	Heat adaptation incubation	37 °C	0, 1, 3 and 7 days	Seedlings	Two-week-old
N	*sphk1*-OE	Heat adaptation incubation	37 °C	0, 1, 3 and 7 days	Seedlings	Two-week-old
O	*sphk1*-OE /spp1.2	Heat adaptation incubation	37 °C	0, 1, 3 and 7 days	Seedlings	Two-week-old
P	*sphk1*-KD	Heat adaptation incubation	37 °C	0, 1, 3 and 7 days	Seedlings	Two-week-old
Q	Col-0	Cold adaptation incubation	10 °C	0, 1, 3 and 7 days	Seedlings	Two-week-old
R	*sphk1*-OE	Cold adaptation incubation	10 °C	0, 1, 3 and 7 days	Seedlings	Two-week-old
S	*sphk1*-OE /spp1.2	Cold adaptation incubation	10 °C	0, 1, 3 and 7 days	Seedlings	Two-week-old
T	*sphk1*-KD	Cold adaptation incubation	10 °C	0, 1, 3 and 7 days	Seedlings	Two-week-old
U	Col-0	FB1 spray solution	30 µM	1 and 6 days	Leaves	Six-week-old
V	Col-0	FB1 hydroponic solution	250 nM	3 days	Roots	Eight-week-old
W	Col-0	Hydrogen peroxide hydroponic solution	3 mM	3 days	Roots	Eight-week-old
X	DEX:AVR	Dexamethasone hydroponic solution	1 µM	24 h	Leaves	Eight-week-old

Annex 13: Sphingolipid measurement experiments summary. Experiment details where sphingolipids measurements were performed and used as database to determine where the newly sphingolipids after feeding with D_7-d18:0 were also found.

LCBs	FA	Hydroxy FA	Head group	Adducts
d18:0	10:0	h10:0	Glucosylceramide (Glc-ceramide)	Monoisotopic
d18:1	12:0	h12:0	(Glycosyl)Inositol-phosphate ceramide (GIPC)	$[M-H^+]^-$
d18:2	14:0	h14:0		$[M-2H^+]^-$
t18:0	15:0	h15:0		$[M+Acetate^-]^-$
t18:1	16:0	h16:0		$[M+H]^+$
t18:2	17:0	h17:0		$[M+NH_4^+]^+$
d18:0-P	18:0	h18:0		$[M+Na^+]^+$
d18:1-P	19:0	h19:0		
d18:2-P	20:0	h20:0		
t18:0-P	22:0	h22:0		
t18:1-P	23:0	h23:0		
t18:2-P	24:0	h24:0		
	25:0	h25:0		
	26:0	h26:0		
	27:0	h27:0		
	28:0	h28:0		
	10:1	h10:1		
	12:1	h12:1		
	14:1	h14:1		
	15:1	h15:1		
	16:1	h16:1		
	17:1	h17:1		
	18:1	h18:1		
	19:1	h19:1		
	20:1	h20:1		
	22:1	h22:1		
	23:1	h23:1		
	24:1	h24:1		
	25:1	h25:1		
	26:1	h26:1		
	27:1	h27:1		
	28:1	h28:1		
	10:2	h10:2		
	12:2	h12:2		
	14:2	h14:2		
	15:2	h15:2		
	16:2	h16:2		
	17:2	h17:2		
	18:2	h18:2		
	19:2	h19:2		
	20:2	h20:2		
	22:2	h22:2		
	23:2	h23:2		
	24:2	h24:2		
	25:2	h25:2		
	26:2	h26:2		
	27:2	h27:2		
	28:2	h28:2		

Annex 14: Ceramide database creation. Six-week-old leaf discs from *A. thaliana* ecotype Col-0 were incubated in 100 µM D_7-d18:0. Compounds were detected by UPLC-qTOF-MS and compared to molecular weight D_7-ceramides databases combining all possibilities between LBCs, FA, Hydroxy FA, Head groups and Adducts.

6. References.

Abbas, H. K., Tanaka, T., Duke, S. O., Porter, J. K., Wray, E. M., Hodges, L., Sessions, A. E., Wang, E., Merrill, A. H., Jr, and Riley, R. T. (1994). Fumonisin- and AAL-Toxin-Induced Disruption of Sphingolipid Metabolism with Accumulation of Free Sphingoid Bases. *Plant physiology*, 106(3):1085-1093.

Albinsky, D., Sawada, Y., Kuwahara, A., Nagano, M., Hirai, A., Saito, K., and Hirai, M. Y. (2010). Widely targeted metabolomics and coexpression analysis as tools to identify genes involved in the side-chain elongation steps of aliphatic glucosinolate biosynthesis. *Amino acids*, 39(4):1067-1075.

Alden, K. P., Dhondt-Cordelier, S., McDonald, K. L., Reape, T. J., Ng, C. K. Y., McCabe, P. F., and Leaver, C. J. (2011). Sphingolipid long-chain base phosphates can regulate apoptotic-like programmed cell death in plants. *Biochem. Biophys. Res. Commun*., 410(3):574-580.

Allocati, N., Masulli, M., Di Ilio, C., and De Laurenzi, V. (2015). Die for the community: an overview of programmed cell death in bacteria. *Cell Death Dis*., 6(1):e1609.

Allwood, J. W., and Goodacre, R. (2010). An introduction to liquid chromatography-mass spectrometry instrumentation applied in plant metabolomic analyses. *Phytochemical analysis : PCA*, 21(1):33-47.

Alonso, J. M., Stepanova, A. N., Leisse, T. J., Kim, C. J., Chen, H., Shinn, P., Stevenson, D. K., Zimmerman, J., Barajas, P., Cheuk, R., Gadrinab, C., Heller, C., Jeske, A., Koesema, E., Meyers, C. C., Parker, H., Prednis, L., Ansari, Y., Choy, N., … and Ecker, J. R. (2003). Genome-Wide Insertional Mutagenesis of *Arabidopsis thaliana*. *Science*, 301(5633):653-657.

Alsiyabi, A., Solis, A. G., Cahoon, E. B., and Saha, R. (2021). Dissecting the regulatory roles of ORM proteins in the sphingolipid pathway of plants. *PLoS computational biology*, 17(1):e1008284.

Asai, T., Stone, J. M., Heard, J. E., Kovtun, Y., Yorgey, P., Sheen, J., and Ausubel, F. M. (2000). Fumonisin B1-Induced cell death in *Arabidopsis* protoplasts requires jasmonate-, ethylene-, and salicylate-dependent signaling pathways. *Plant Cell*, 12(10):1823-1835.

Ausubel, F. M. (2005). Are innate immune signaling pathways in plants and animals conserved?. *Nat. Immunol*., 6(10):973-979.

Baxter, A., Mittler, R., and Suzuki, N. (2014). ROS as key players in plant stress signalling. *J. Exp. Bot*., 65(5):1229-1240.

Bayer, E. M., Mongrand, S., and Tilsner, J. (2014). Specialized membrane domains of plasmodesmata, plant intercellular nanopores. *Front. Plant Sci*, 5:507.

Benton, H. P., Want, E. J., and Ebbels, T. M. (2010). Correction of mass calibration gaps in liquid chromatography-mass spectrometry metabolomics data. *Bioinformatics (Oxford, England)*, 26(19):2488-2489.

Berkey, R., Bendigeri, D., and Xiao, S. (2012). Sphingolipids and plant defense/disease: the “death” connection and beyond. *Front. Plant Sci*., 3:68.

Beynon, R. J., and Pratt, J. M. (2005). Metabolic labeling of proteins for proteomics. *Molecular and cellular proteomics : MCP*, 4(7):857-872.

Bi, F. C., Liu, Z., Wu, J. X., Liang, H., Xi, X. L., Fang, C., Sun, T. J., Yin, J., Dai, G. Y., Rong, C., Greenberg, J. T., Su, W. W., and Yao, N. (2014). Loss of ceramide kinase in *Arabidopsis* impairs defenses and promotes ceramide accumulation and mitochondrial H_2O_2 bursts. *Plant Cell*, 26(8):3449-3467.

Bigeard, J., Colcombet, J., and Hirt, H. (2015). Signaling mechanisms in pattern-triggered immunity (PTI). *Mol. Plant*, 8(4):521-539.

Bohn, M., Heinz, E., and Lüthje, S. (2001). Lipid composition and fluidity of plasma membranes isolated from corn (Zea mays L.) roots. *Archives Biochem. Biophys.*, 387(1):35-40.

Boller, T., and Felix, G. (2009). A Renaissance of Elicitors: Perception of Microbe-Associated Molecular Patterns and Danger Signals by Pattern-Recognition Receptors. *Annu. Rev. Plant Biol*., 60:379-406.

Borner, G. H., Sherrier, D. J., Weimar, T., Michaelson, L. V., Hawkins, N. D., Macaskill, A., Napier, J. A., Beale, M. H., Lilley, K. S., and Dupree, P. (2005). Analysis of detergent-resistant membranes in *Arabidopsis*. Evidence for plasma membrane lipid rafts. *Plant Physiol.*, 137(1):104-116.

Brinkmann, V., Billich, A., Baumruker, T., Heining, P., Schmouder, R., Francis, G., Aradhye, S., and Burtin, P. (2010). Fingolimod (FTY720): discovery and development of an oral drug to treat multiple sclerosis. *Nature Rev. Drug Discovery*, 9(11):883-897.

Brodersen, P., Petersen, M., Pike, H. M., Olszak, B., Skov, S., Odum, N., Jørgensen, L. B., Brown, R. E., and Mundy, J. (2002). Knockout of *Arabidopsis* accelerated-cell-death11 encoding a sphingosine transfer protein causes activation of programmed cell death and defense. *Genes & Dev.*, 16(4):490-502.

Buré, C., Cacas, J. L., Wang, F., Gaudin, K., Domergue, F., Mongrand, S., and Schmitter, J. M. (2011). Fast screening of highly glycosylated plant sphingolipids by tandem mass spectrometry. *Rapid Commun. Mass Spectrom*., 25(20):3131-3145.

Büttner, D. (2016). Behind the lines-actions of bacterial type III effector proteins in plant cells. *FEMS Microbiol. Rev*., 40(6):894-937.

Bylesjö, M., Eriksson, D., Kusano, M., Moritz, T., and Trygg, J. (2007). Data integration in plant biology: the O2PLS method for combined modeling of transcript and metabolite data. *The Plant journal : for cell and molecular biology*, 52(6):1181-1191.

Cacas, J. L., Buré, C., Furt, F., Maalouf, J. P., Badoc, A., Cluzet, S., Schmitter, J. M., Antajan, E., and Mongrand, S. (2013). Biochemical survey of the polar head of plant glycosylinositolphosphoceramides unravels broad diversity. *Phytochem.*, 96:191-200.

Cacas, J. L., Buré, C., Grosjean, K., Gerbeau-Pissot, P., Lherminier, J., Rombouts, Y., Maes, E., Bossard, C., Gronnier, J., Furt, F., Fouillen, L., Germain, V., Bayer, E., Cluzet, S., Robert, F., Schmitter, J. M., Deleu, M., Lins, L., Simon-Plas, F., and Mongrand, S. (2016). Revisiting Plant Plasma Membrane Lipids in Tobacco: A Focus on Sphingolipids. *Plant Physiol*., 170(1):367-384.

Cahoon, E. B., and Lynch, D. V. (1991). Analysis of Glucocerebrosides of Rye (Secale cereale L. cv Puma) Leaf and Plasma Membrane. *Plant Phys.*, 95(1):58-68.

Chalfant, C. E., Szulc, Z., Roddy, P., Bielawska, A., and Hannun, Y. A. (2004). The structural requirements for ceramide activation of serine-threonine protein phosphatases. *J. Lipid Res.*, 45(3):496-506.

Chen, M., Han, G., Dietrich, C. R., Dunn, T. M., and Cahoon, E. B. (2006). The essential nature of sphingolipids in plants as revealed by the functional identification and characterization of the *Arabidopsis* LCB1 subunit of serine palmitoyltransferase. *Plant Cell*, 18(12):3576-3593.

Chen, M., Markham, J. E., Dietrich, C. R., Jaworski, J. G., and Cahoon, E. B. (2008). Sphingolipid long-chain base hydroxylation is important for growth and regulation of sphingolipid content and composition in *Arabidopsis*. *Plant Cell*, 20(7):1862-1878.

Chen, Y., Liu, Y., Sullards, M. C., and Merrill, A. H. Jr. (2010). An introduction to sphingolipid metabolism and analysis by new technologies. *Neuromol. Med*., 12:306-319.

Chen, M., Markham, J. E., and Cahoon, E. B. (2012). Sphingolipid Δ8 unsaturation is important for glucosylceramide biosynthesis and low-temperature performance in *Arabidopsis*. *Plant J. : for cell and mol. Biol.*, 69(5):769-781.

Chen, L. Y., Shi, D. Q., Zhang, W. J., Tang, Z. S., Liu, J., and Yang, W. C. (2015). The *Arabidopsis* alkaline ceramidase TOD1 is a key turgor pressure regulator in plant cells. *Nature Com*., 6:6030.

Chisholm, S. T., Coaker, G., Day, B., and Staskawicz, B. J. (2006). Host-microbe interactions: shaping the evolution of the plant immune response. *Cell*, 124(4):803-814.

Coll, N. S., Epple, P., and Dangl, J. L. (2011). Programmed cell death in the plant immune system. *Cell Death Differ*., 18:1247-1256.

Coursol, S., Fan, L. M., Le Stunff, H., Spiegel, S., Gilroy, S., and Assmann, S. M. (2003). Sphingolipid signalling in *Arabidopsis* guard cells involves heterotrimeric G proteins. *Nature*, 423:651-654.

Coursol, S., Le Stunff, H., Lynch, D. V., Gilroy, S., Assmann, S. M., and Spiegel, S. (2005). *Arabidopsis* sphingosine kinase and the effects of phytosphingosine-1-phosphate on stomatal aperture. *Plant Physiol*., 137(2):724-737.

Coursol, S., Fromentin, J., Noirot, E., Brière, C., Robert, F., Morel, J., Liang, Y. K., Lherminier, J., and Simon-Plas, F. (2015). Long-chain bases and their phosphorylated derivatives differentially regulate cryptogein-induced production of reactive oxygen species in tobacco (Nicotiana tabacum) BY-2 cells. *New Phytologist*, 205(3):1239-1249.

Da Silva, D., Lachaud, C., Cotelle, V., Brière, C., Grat, S., Mazars, C., and Thuleau, P. (2011). Nitric oxide production is not required for dihydrosphingosine-induced cell death in tobacco BY-2 cells. *Plant Signal* Behav., 6(5):736-739.

De Gara, L., de Pinto, M. C., and Tommasi, F. (2003). The antioxidant systems vis-à-vis reactive oxygen species during plant-pathogen interaction. *Plant Physio. and Biochem*., 41(10):863-870.

Dickson, R. C. (1998). Sphingolipid functions in Saccharomyces cerevisiae: comparison to mammals. *Annu. Rev. Biochem*., 67:27-48.

Dietrich, C. R., Han, G., Chen, M., Berg, R. H., Dunn, T. M., and Cahoon, E. B. (2008). Loss-of-function mutations and inducible RNAi suppression of *Arabidopsis LCB2* genes reveal the critical role of sphingolipids in gametophytic and sporophytic cell viability. *Plant J*., 54(2):284-298.

Dudley, E., Yousef, M., Wang, Y., and Griffiths, W. J. (2010). Targeted metabolomics and mass spectrometry. *Advances in protein chemistry and structural biology*, 80:45-83.

Dunn, T. M., Lynch, D. V., Michaelson, L. V., and Napier, J. A. (2004). A post-genomic approach to understanding sphingolipid metabolism in *Arabidopsis thaliana*. *Ann. Bot*., 93(5):483-497.

Dutilleul, C., Benhassaine-Kesri, G., Demandre, C., Rézé, N., Launay, A., Pelletier, S., Renou, J. P., Zachowski, A., Baudouin, E., and Guillas, I. (2012). Phytosphingosine phosphate is a signal for AtMPK6 activation and *Arabidopsis* response to chilling. *New Phytol*., 194:181-191.

Dutilleul, C., Chavarria, H., Rézé, N., Sotta, B., Baudouin, E., and Guillas, I. (2015). Evidence for ACD5 ceramide kinase activity involvement in *Arabidopsis* response to cold stress. *Plant, cell & environment*, *38*(12):2688-2697.

Engelsberger, W. R., Erban, A., Kopka, J., and Schulze, W. X. (2006). Metabolic labeling of plant cell cultures with K(15)NO3 as a tool for quantitative analysis of proteins and metabolites. *Plant methods*, 2:14.

Eynck, C., Koopmann, B., Grunewaldt-Stoecker, G., Karlowsky, P. and Von Tiedemann, A. (2007). Differential interactions of *Verticilium longisporum* and *V. dahlia* with *Brassica napus* with molecular and histological techniques. *Eur. J. Plant Pathol*., 118:259-274.

Fukuda, H. (1996). Xylogenesis: initiation, progression, and cell death. *Annu. Rev. Plant Physiol*. *Plant Mol. Biol*., 47:299-325.

Futerman, A. H., and Hannun, Y. A. (2004). The complex life of simple sphingolipids. *EMBO Rep*., 5(8):777-782.

Fröschel, C., Iven, T., Walper, E., Bachmann, V., Weiste, C., and Dröge-Laser, W. (2019). A Gain-of-Function Screen Reveals Redundant ERF Transcription Factors Providing Opportunities for Resistance Breeding Toward the Vascular Fungal Pathogen *Verticillium longisporum*. *Mol. Plant-Microbe Interact.*, *32*(9):1095-1109.

Galluzzi, L., Vitale, I., Aaronson, S. A., Abrams, J. M., Adam, D., Agostinis, P., Alnemri, E. S., Altucci, L., Amelio, I., Andrews, D. W., Annicchiarico-Petruzzelli, M., Antonov, A. V., Arama, E., Baehrecke, E. H., Barlev, N. A., Bazan, N. G., Bernassola, F., Bertrand, M., Bianchi, K., Blagosklonny, M. V., … Kroemer, G. (2018). Molecular mechanisms of cell death: recommendations of the Nomenclature Committee on Cell Death 2018. *Cell death and differentiation*, 25(3):486-541.

Gault, C. R., Obeid, L. M., and Hannun, Y. (2010). An overview of sphingolipid metabolism: from synthesis to breakdown. *Adv. Epx. Med. Biol*., 688:1-23.

Giavalisco, P., Köhl, K., Hummel, J., Seiwert, B., and Willmitzer, L. (2009). 13C isotope-labeled metabolomes allowing for improved compound annotation and relative quantification in liquid chromatography-mass spectrometry-based metabolomic research. *Analytical chemistry*, 81(15): 6546-6551.

Giavalisco, P., Li, Y., Matthes, A., Eckhardt, A., Hubberten, H. M., Hesse, H., Segu, S., Hummel, J., Köhl, K., and Willmitzer, L. (2011). Elemental formula annotation of polar and lipophilic metabolites using (13) C, (15) N and (34) S isotope labelling, in combination with high-resolution mass spectrometry. *The Plant journal : for cell and molecular biology*, 68(2):364-376.

Glazebrook, J. (2005). Contrasting mechanisms of defense against biotrophic and necrotrophic pathogens. *Annu. Rev. Phytol*., 43:205-227.

Glenz, R. (2019). *Die Rolle von Sphingobasen in der pflanzlichen Zelltodreaktion* [Doctoral thesis, Pharmacology Institute at Julius-Maximilians University of Wuerzburg]. https://opus.bibliothek.uni-wuerzburg.de/opus4-wuerzburg/frontdoor/deliver/index/docId/18790/file/Glenz_Rene_Dissertation.pdf

Glenz, R., Schmalhaus, D., Krischke, M., Mueller, M. J., and Waller, F. (2019). Elevated Levels of Phosphorylated Sphingobases Do Not Antagonize Sphingobase- or Fumonisin B1-Induced Plant Cell Death. *Plant Cell Physiol.*, 60(5):1109-1119.

Gonzalez-Solis, A., Han, G., Gan, L., Li, Y., Markham, J. E., Cahoon, R. E., Dunn, T. M., and Cahoon, E. B. (2020). Unregulated Sphingolipid Biosynthesis in Gene-Edited *Arabidopsis ORM* Mutants Results in Nonviable Seeds with Strongly Reduced Oil Content. *The Plant cell*, 32(8):2474-2490.

Greenberg, J. T., Silverman, F. P., and Liang, H. (2000). Uncoupling salicylic acid-dependent cell death and defense-related responses from disease resistance in the *Arabidopsis* mutant acd5. *Genetics*, 156(1):341-350.

Gunawardena, A. H. L. A. N. (2008). Programmed cell death and tissue remodelling in plants. *J. Exp. Bot*., 59(3):445-451.

Guo, L., Mishra, G., Taylor, K., and Wang, X. (2011). Phosphatidic acid binds and stimulates *Arabidopsis* sphingosine kinases. *J. Biol. Chem*., 286(15):13336-13345.

Hamann, T. (2012). Plant cell wall integrity maintenance as an essential component of biotic stress response mechanisms. *Front. Plant Sci*., 3:77.

Hanada, K. (2003). Serine palmitoyltransferase, a key enzyme of sphingolipid metabolism. *Biochim. Biophys. Acta.* 1632(1-3):16-30.

Hanhineva, K., Rogachev, I., Kokko, H., Mintz-Oron, S., Venger, I., Kärenlampi, S., and Aharoni, A. (2008). Non-targeted analysis of spatial metabolite composition in strawberry (Fragariaxananassa) flowers. *Phytochemistry*, 69(13):2463-2481.

Hannun, Y. A., and Obeid, L. M. (2011). Many ceramides. *The Journal of biological chemistry*, 286(32):27855-27862.

Hannun, Y. A., and Obeid, L. M. (2018). Sphingolipids and their metabolism in physiology and disease. *Nat. Rev. Mol. Cell Biol*., 19:175-191.

Harada, K., Fukusaki, E., Bamba, T., Sato, F., and Kobayashi, A. (2006). In vivo 15N-enrichment of metabolites in suspension cultured cells and its application to metabolomics. *Biotechnology progress*, 22(4):1003-1011.

Hara-Nishimura, I., and Hatsugai, N. (2011). The role of vacuole in plant cell death. *Cell Death Differ*., 18(8):1298-1304.

Hatsugai, N., Yamada, K., Goto-Yamada, S., and Hara-Nishimura, I. (2015). Vacuolar processing enzyme in plant programmed cell death. *Front. Plant Sci*., 6:234.

Haynes, C. A., Allegood, J. C., Park, H., and Sullards, M. C. (2009). Sphingolipidomics: Methods for the comprehensive analysis of sphingolipids. *J. Chromatogr. B. Analyt. Technol. Biomed. Life Sci*., 877:2696-2708.

Heaver, S. L., Johnson, E. L., and Ley, R. E. (2018). Sphingolipids in host-microbial interactions. *Curr. Opin. Microbiol*., 43:92-99.

Hegeman, A. D., Schulte, C. F., Cui, Q., Lewis, I. A., Huttlin, E. L., Eghbalnia, H., Harms, A. C., Ulrich, E. L., Markley, J. L., and Sussman, M. R. (2007). Stable isotope assisted assignment of elemental compositions for metabolomics. *Analytical chemistry*, 79(18):6912-6921.

Hegeman A. D. (2010). Plant metabolomics--meeting the analytical challenges of comprehensive metabolite analysis. *Briefings in functional genomics*, 9(2):139-148.

Huang, X., Zhang, Y., Zhang, X., and Shi, Y. (2017). Long-chain base kinase1 affects freezing tolerance in *Arabidopsis thaliana*. *Plant Sci.,* 259:94-103.

Huby, E., Napier, J. A., Baillieul, F., Michaelson, L. V., and Dhondt-Cordelier, S. (2020). Sphingolipids: towards an integrated view of metabolism during the plant stress response. *The New phytologist*, 225(2):659-670.

Hückelhoven, R., and Kogel, K.-H. (1998). Tissue-specific superoxide generation at interaction sites in resistant and susceptible near-isogenic barley lines attacked by the powdery mildew fungus (*Erysiphe graminis f.sp. hord*ei). *Mol. Plant-Microbe*. Interact., 11:292-300.

Igarashi, D., Bethke, G., Xu, Y., Tsuda, K., Glazebrook, J., and Katagiri, F. (2013). Pattern-triggered immunity suppresses programmed cell death triggered by fumonisin b1. *PloS one*, 8(4):e60769.

Imai, H., Ohnishi, M., Kinoshita, M., Kojima, M., and Ito, S. (1995). Structure and Distribution of Cerebroside Unsaturated Hydroxy Fatty Acids in Plant Leaves. *Biosci. Biotech. Biochem*., 59(7):1309-1313.

Imai, H., and Nishiura, H. (2005). Phosphorylation of sphingoid long-chain bases in *Arabidopsis*: functional characterization and expression of the first sphingoid long-chain base Kinase gene in plants. *Plant Cell Physiol*., 46(2):375-380.

Islam, M. N., Jacquemot, M. P., Coursol, S., and Ng, C. K. Y. (2012). Sphingosine in plants -- more riddles from the Sphinx? *New Phytol*., 193(1):51-57.

Iven, T., König, S., Singh, S., Braus-Stromeyer, S. A., Bischoff, M., Tietze, L. F., Braus, G. H., Lipka, V., Feussner, I., and Dröge-Laser, W. (2012). Transcriptional activation and production of tryptophan-derived secondary metabolites in *Arabidopsis* roots contributes to the defense against the fungal vascular pathogen *Verticillium longisporum*. *Mol. Plant*, 5(6):1389-1402.

Jones, J. D. G., and Dangl, J. L. (2006). The plant immune system. *Nature*, 444(7117):323-329.

Kikuchi, J., and Hirayama, T. (2007). Practical aspects of uniform stable isotope labeling of higher plants for heteronuclear NMR-based metabolomics. *Methods in molecular biology (Clifton, N.J.)*, 358:273-286.

Kim, H. K., Choi, Y. H., and Verpoorte, R. (2011). NMR-based plant metabolomics: where do we stand, where do we go?. *Trends in biotechnology*, 29(6):267-275.

Kimberlin, A. N., Majumder, S., Han, G., Chen, M., Cahoon, R. E., Stone, J. M., Dunn, T. M., and Cahoon, E. B. (2013). *Arabidopsis* 56-amino acid serine palmitoyltransferase-interacting proteins stimulate sphingolipid synthesis, are essential, and affect mycotoxin sensitivity. *Plant Cell*, 25(11):4627-4639.

Kimberlin, A. N., Han, G., Luttgeharm, K. D., Chen, M., Cahoon, R. E., Stone, J. M., Markham, J. E., Dunn, T. M., and Cahoon, E. B. (2016). *ORM* Expression Alters Sphingolipid Homeostasis and Differentially Affects Ceramide Synthase Activity. *Plant Physiol*., 172(2):889-900.

Kitatani, K., Idkowiak-Baldys, J., and Hannun, Y. A. (2008). The sphingolipid salvage pathway in ceramide metabolism and signaling. *Cell Signal*., 20(6):1010-1018.

Kleinboelting, N., Huep, G., Kloetgen, A., Viehoever, P., and Weisshaar, B. (2012). GABI-Kat SimpleSearch: new features of the *Arabidopsis thaliana* T-DNA mutant database. *Nucleic Acids Res*., 40:D1211-D1215.

Kueger, S., Steinhauser, D., Willmitzer, L., and Giavalisco, P. (2012). High-resolution plant metabolomics: from mass spectral features to metabolites and from whole-cell analysis to subcellular metabolite distributions. *The Plant journal : for cell and molecular biology*, 70(1):39-50.

Lachaud, C., Da Silva, D., Cotelle, V., Thuleau, P., Xiong, T. C., Jauneau, A., Brière, C., Graziana, A., Bellec, Y., Faure, J. D., Ranjeva, R., and Mazars, C. (2010). Nuclear calcium controls the apoptotic-like cell death induced by D-erythro-sphinganine in tobacco cells. *Cell Calcium*, 47(1):92-100.

Last, R. L., Jones, A. D., and Shachar-Hill, Y. (2007). Towards the plant metabolome and beyond. *Nature reviews. Molecular cell biology*, 8(2):167-174.

Li, J., Bi, F. C., Yin, J., Wu, J. X., Rong, C., Wu, J. L., and Yao, N. (2015). An *Arabidopsis* neutral ceramidase mutant ncer1 accumulates hydroxyceramides and is sensitive to oxidative stress. *Front. Plant Sci*., 6:460.

Liang, H., Yao, N., Song, J. T., Luo, S., Lu, H. and Greenberg, J. T. (2003). Ceramides modulate programmed cell death in plants. *Genes Dev*., 17:2636-2641.

Lisec, J., Schauer, N., Kopka, J., Willmitzer, L., and Fernie, A. R. (2006). Gas chromatography mass spectrometry-based metabolite profiling in plants. *Nature protocols*, 1(1):387-396.

Lockshin, A., and Zakeri, Z. (2004). Apoptosis, autophagy, and more. *Int. J. Biochem. Cell Biol*., 36(12):2405-2419.

Lukasik, E. and Takken, F. L. W. (2009). STANDing strong, resistance proteins instigators of plant defence. *Curr. Opi. in Plant Biol*., 12(4):427-436.

Luttgeharm, K. D., Chen, M., Mehra, A., Cahoon, R. E., Markham, J. E., and Cahoon, E. B. (2015). Overexpression of *Arabidopsis* Ceramide Synthases Differentially Affects Growth, Sphingolipid Metabolism, Programmed Cell Death, and Mycotoxin Resistance. *Plant Physiol*., 169(2):1108-1117.

Lynch, D. V., Caffrey, M., Hogan, J. L., and Steponkus, P. L. (1992). Calorimetric and x-ray diffraction studies of rye glucocerebroside mesomorphism. *Biophys. J.*, 61(5):1289-1300.

Lynch, D. V., and Dunn, T. M. (2004). An introduction to plant sphingolipids and a review of recent advances in understanding their metabolism and function. *New Phytol*., 161(3):677-702.

Magnin-Robert, M., Le Bourse, D., Markham, J., Dorey, S., Clément, C., Baillieul, F., and Dhondt-Cordelier, S. (2015). Modifications of Sphingolipid Content Affect Tolerance to Hemibiotrophic and Necrotrophic Pathogens by Modulating Plant Defense Responses in *Arabidopsis*. *Plant Physiol*., 169(3):2255-2274.

Mao, C., and Obeid, L. M. (2008). Ceramidases: regulators of cellular responses mediated by ceramide, sphingosine, and sphingosine-1-phosphate. *Biochim. Biophys. Acta*, 1781(9):424-434.

Markham, J. E., Li, J., Cahoon, E. B., and Jaworski, J. G. (2006). Separation and identification of major plant sphingolipid classes from leaves. *J. Biol. Chem*., 281(32):22684-22694.

Markham, J. E., and Jaworski, J. G. (2007). Rapid measurement of sphingolipids from *Arabidopsis thaliana* by reversed-phase high-performance liquid chromatography coupled to electrospray ionization tandem mass spectrometry. *Rapid Commun Mass Spectrom*., 21(7):1304-1314.

Markham, J. E., Molino, D., Gissot, L., Bellec, Y., Hématy, K., Marion, J., Belcram, K., Palauqui, J. C., Satiat-JeuneMaître, B., and Faure, J. D. (2011). Sphingolipids containing very-long-chain fatty acids define a secretory pathway for specific polar plasma membrane protein targeting in *Arabidopsis*. *Plant Cell*, 23(6):2362-2378.

McElver, J., Tzafrir, I., Aux, G., Rogers, R., Ashby, C., Smith, K., Thomas, C., Schetter, A., Zhou, Q., Cushman, M. A., Tossberg, J., Nickle, T., Levin, J. Z., Law, M., Meinke, D., and Patton, D. (2001). Insertional Mutagenesis of Genes Required for Seed Development in *Arabidopsis thaliana*. *Genetics*, 159(4):1751-1763.

Melser, S., Batailler, B., Peypelut, M., Poujol, C., Bellec, Y., Wattelet-Boyer, V., Maneta-Peyret, L., Faure, J. D., and Moreau, P. (2010). Glucosylceramide biosynthesis is involved in Golgi morphology and protein secretion in plant cells. *Traffic*, 11(4):479-490.

Merrill, A. H. Jr., Sullards, M. C., Wang, E., Voss, K. A., and Riley, R. T. (2001). Sphingolipid Metabolism: Roles in Signal Transduction and Disruption by Fumonisins. *Environ. Health Perspect*., 109(2):283-289.

Merrill, A. H. Jr., Stokes, T. H., Momin, A., Park, H., Portz, B. J., Kelly, S., Wang, E., Sullards, M. C., and Wang, M. D. (2009). Sphingolipidomics: a valuable tool for understanding the roles of sphingolipids in biology and disease. *J. Lipid Res*., 50(Suppl):S97-S102.

Merrill, A. H. Jr. (2011). Sphingolipid and Glycosphingolipid Metabolic Pathways in the Era of Sphingolipidomics. *Chem Rev*., 111(10):6387-6422.

Michaelson, L. V., Zäuner, S., Markham, J. E., Haslam, R. P., Desikan, R., Mugford, S., Albrecht, S., Warnecke, D., Sperling, P., Heinz, E., and Napier, J. A. (2009). Functional Characterization of a Higher Plant Sphingolipid Δ4-Desaturase: Defining the Role of Sphingosine and Sphingosine-1-Phosphate in *Arabidopsis*. *Plant Physiol*., 149(1):487-498.

Michaelson, L. V., Napier, J. A., Molino, D., and Faure, J. D. (2016). Plant sphingolipids: Their importance in cellular organization and adaption. *Biochim. Biophys. Acta*, 1861(9):1329-1335.

Mina, J. G., Okada, Y., Wansadhipathi-Kannangara, N. K., Pratt, S., Shams-Eldin, H., Schwarz, R. T., Steel, P. G., Fawcett, T., and Denny, P. W. (2010). Functional analyses of differentially expressed isoforms of the *Arabidopsis* inositol phosphorylceramide synthase. *Plant Mol. Biol*., 73(4-5):399-407.

Mirocha, C. J., Gilchrist, D. G., Shier, W. T., Abbas, H. K., Wen, Y., and Vesonder, R. F. (1992). AAL toxins, fumonisins (biology and chemistry) and host-specificity concepts. *Mycopathologia*, 117(1-2):47-56.

Mishina, T. E., and Zeier, J. (2007). Pathogen-associated molecular pattern recognition rather than development of tissue necrosis contributes to bacterial induction of systemic acquired resistance in *Arabidopsis*. *Plant J*., 50(3):500-513.

Mittler, R. (2002). Oxidative stress, antioxidants and stress tolerance. *Trends Plant Sci*., 7(9):405-410.

Mittler, R., Finka, A., and Goloubinoff, P. (2012). How do plants feel the heat?. *Trends Biochem. Sci.*, 37(3):118-125.

Mongrand, S., Morel, J., Laroche, J., Claverol, S., Carde, J. P., Hartmann, M. A., Bonneu, M., Simon-Plas, F., Lessire, R., and Bessoule, J. J. (2004). Lipid rafts in higher plant cells: purification and characterization of Triton X-100-insoluble microdomains from tobacco plasma membrane. *J. Biol. Chem.*, 279(35):36277-36286.

Mortimer, J. C., Yu, X., Albrecht, S., Sicilia, F., Huichalaf, M., Ampuero, D., Michaelson, L. V., Murphy, A. M., Matsunaga, T., Kurz, S., Stephens, E., Baldwin, T. C., Ishii, T., Napier, J. A., Weber, A. P. M., Handford, M. G., and Dupree, P. (2013). Abnormal glycosphingolipid mannosylation triggers salicylic acid-mediated responses in *Arabidopsis*. *Plant Cell*, 25(5):1881-1894.

Msanne, J., Chen, M., Luttgeharm, K. D., Bradley, A. M., Mays, E. S., Paper, J. M., Boyle, D. L., Cahoon, R. E., Schrick, K., and Cahoon, E. B. (2015). Glucosylceramides are critical for cell-type differentiation and organogenesis, but not for cell viability in *Arabidopsis*. *Plant J*., 84(1):188-201.

Mueller, S. P., Krause, D. M., Mueller, M. J., and Fekete, A. (2015). Accumulation of extra-chloroplastic triacylglycerols in *Arabidopsis* seedlings during heat acclimation. *Journal of experimental botany*, 66(15):4517-4526.

Mueller, S. P., Unger, M., Guender, L., Fekete, A., and Mueller, M. J. (2017). Phospholipid:Diacylglycerol Acyltransferase-Mediated Triacylglyerol Synthesis Augments Basal Thermotolerance. *Plant Physiol.*, 175(1):486-497.

Mur, L. A. J., Kenton, P., Lloyd, A. J., Ougham, H., and Prats, E. (2008). The hypersensitive response; the centenary is upon us but how much do we know? *J. Exp. Bot*., 59(3):501-520.

Nagano, M., Ishikawa, T., Ogawa, Y., Iwabuchi, M., Nakasone, A., Shimamoto, K., Uchimiya, H., and Kawai-Yamada, M. (2014). *Arabidopsis* Bax inhibitor-1 promotes sphingolipid synthesis during cold stress by interacting with ceramide-modifying enzymes. *Planta*, 240(1):77-89.

Nagata, S. (2018). Apoptosis and Clearance of Apoptotic Cells. *Annu. Rev. Immunol*., 36:489-517.

Nakabayashi, R., Kusano, M., Kobayashi, M., Tohge, T., Yonekura-Sakakibara, K., Kogure, N., Yamazaki, M., Kitajima, M., Saito, K., and Takayama, H. (2009). Metabolomics-oriented isolation and structure elucidation of 37 compounds including two anthocyanins from *Arabidopsis thaliana*. *Phytochemistry*, 70(8):1017-1029.

Nakagawa, N., Kato, M., Takahashi, Y., Shimazaki, K., Tamura, K., Tokuji, Y., Kihara, A., and Imai, H. (2012). Degradation of long-chain base 1-phosphate (LCBP) in *Arabidopsis*: functional characterization of LCBP phosphatase involved in the dehydration stress response. *J. Plant Res*., 125(3):439-449.

Ng, C. K. Y., Carr, K., McAinsh, M. R., Powell, B., and Hetherington, A. M. (2001). Drought-induced guard cell signal transduction involves sphingosine-1-phosphate. *Nature*, 410:596-599.

Nishikawa, M., Hosokawa, K., Ishiguro, M., Minamioka, H., Tamura, K., Hara-Nishimura, I., Takahashi, Y., Shimazaki, K., and Imai, H. (2008). Degradation of sphingoid long-chain base 1-phosphates (LCB-1Ps): functional characterization and expression of AtDPL1 encoding LCB-1P lyase Involved in the dehydration stress response in *Arabidopsis*. *Plant Cell Physiol*., 49(11):1758-1763.

Norberg, P., Nilsson, R., Nyiredy, S., and Liljenberg, C. (1996). Glucosylceramides of oat root plasma membranes--physicochemical behaviour in natural and in model systems. *Biochim. Biophys. Acta*, 1299(1):80-86.

Ogasawara, Y., Kaya, H., Hiraoka, G., Yumoto, F., Kimura, S., Kadota, Y., Hishinuma, H., Senzaki, E., Yamagoe, S., Nagata, K., Nara, M., Suzuki, K., Tanokura, M., and Kuchitsu, K. (2008). Synergistic activation of the *Arabidopsis* NADPH oxidase AtrbohD by Ca^{2+} and phosphorylation. *J. Biol. Chem*., 283(14):8885-8892.

Oliver, S. G., Winson, M. K., Kell, D. B., and Baganz, F. (1998). Systematic functional analysis of the yeast genome. *Trends in biotechnology*, 16(9):373-378.

Oliver, R. P., and Ipcho, S. V. S. (2004). *Arabidopsis* pathology breathes new life into the necrotrophs-vs.-biotrophs classification of fungal pathogens. *Mol. Plant Pathol*., 5(4):347-352.

Pata, M. O., Hannun, Y. A., and Ng, C. K. Y. (2010). Plant sphingolipids: decoding the enigma of the Sphinx. *New Phytol*., 185(3):611-630.

Peer, M., Stegmann, M., Mueller, M. J., and Waller, F. (2010). Pseudomonas syringae infection triggers de novo synthesis of phytosphingosine from sphinganine in *Arabidopsis thaliana*. *FEBS Lett*., 584(18):4053-4056.

Peer, M., Bach, M., Mueller, M. J., and Waller, F. (2011). Free sphingobases induce RBOHD-dependent reactive oxygen species production in *Arabidopsis* leaves. *FEBS Lett*., 585(19):3006-3010.

Pluskal, T., Castillo, S., Villar-Briones, A., and Oresic, M. (2010). MZmine 2: modular framework for processing, visualizing, and analyzing mass spectrometry-based molecular profile data. *BMC bioinformatics*, 11:395.

Pruett, S. T., Bushnev, A., Hagedorn, K., Adiga, M., Haynes, C. A., Sullards, M. C., Liotta, D. C. and Merrill, A. H. Jr. (2008). Biodiversity of sphingoid bases ("sphingosines") and related amino alcohols. *J. Lipid Res*., 49(8):1621-1639.

Qin, X., Zhang, R. X., Ge, S., Zhou, T., and Liang, Y. K. (2017). Sphingosine kinase AtSPHK1 functions in fumonisin B1-triggered cell death in *Arabidopsis*. *Plant Physiol. Biochem*., 119:70-80.

Quartacci, M. F., Cosi, E., and Navari-Izzo, F. (2001). Lipids and NADPH-dependent superoxide production in plasma membrane vesicles from roots of wheat grown under copper deficiency or excess. *J. Exp. Botany*, 52(354):77-84.

Rennie, E. A., Ebert, B., Miles, G. P., Cahoon, R. E., Christiansen, K. M., Stonebloom, S., Khatab, H., Twell, D., Petzold, C. J., Adams, P. D., Dupree, P., Heazlewood, J. L., Cahoon, E. B., and Scheller, H. V. (2014). Identification of a sphingolipid α-glucuronosyltransferase that is essential for pollen function in *Arabidopsis*. *Plant Cell*, 26(8):3314-3325.

Rizhsky, L., Shulaev, V., and Mittler, R. (2004). Measuring programmed cell death in plants. *Methods in Mol. Biol. (Clifton, N.J.)*, 282:179-189.

Saiki, R. K., Gelfand, D. H., Stoffel, S., Scharf, S. J., Higuchi, R., Horn, G. T., Mullis, K. B., and Erlich, H. A. (1988). Primer-directed enzymatic amplification of DNA with a thermostable DNA polymerase. *Science*, 239(4839):487-491.

Saito, K., and Matsuda, F. (2010). Metabolomics for functional genomics, systems biology, and biotechnology. *Annual rev. of Plant Biol.*, 61:463-489.

Saucedo-García, M., González-Solís, A., Rodríguez-Mejía, P., Olivera-Flores, T. de J., Vázquez-Santana, S., Cahoon, E. B., and Gavilanes-Ruiz, M. (2011). Reactive oxygen species as transducers of sphinganine-mediated cell death pathway. *Plant Signal Behav*., 6(10):1616-1619.

Scherer, M., Leuthäuser-Jaschinski, K., Ecker, J., Schmitz, G., and Liebisch, G. (2010). A rapid and quantitative LC-MS/MS method to profile sphingolipids. *J. Lipid Res*., 51:2001-2011.

Scholl, R. L., May, S. T., and Ware, D. H. (2000). Seed and molecular resources for *Arabidopsis*. *Plant Physiol.*, 124(4):1477-1480.

Shaner, R. L., Allegood, J. C., Park, H., Wang, E., Kelly, S., Haynes, C. A., Sullards, M. C., and Merrill, A. H., Jr (2009). Quantitative analysis of sphingolipids for lipidomics using triple quadrupole and quadrupole linear ion trap mass spectrometers. *J. Lipid Res.*, 50(8):1692-1707.

Shi, L., Bielawski, J., Mu, J., Dong, H., Teng, C., Zhang, J., Yang, X., Tomishige, N., Hanada, K., Hannun, Y. A., and Zuo, J. (2007). Involvement of sphingoid bases in mediating reactive oxygen intermediate production and programmed cell death in *Arabidopsis*. *Cell Res*., 17(12):1030-1040.

Shi, C., Yin, J., Liu, Z., Wu, J. X., Zhao, Q., Ren, J., and Yao, N. (2015). A systematic simulation of the effect of salicylic acid on sphingolipid metabolism. *Frontiers in plant science*, 6:186.

Siebers, M., Brands, M., Wewer, V., Duan, Y., Hölzl, G., and Dörmann, P. (2016). Lipids in plant-microbe interactions. *Biochim. Biophys. Acta*, 1861(9 Pt B):1379-1395.

Siehler, S., and Manning, D. R. (2002). Pathways of transduction engaged by sphingosine 1-phosphate through G protein-coupled receptors. *Biochim. Biophys. Acta*, 1582(1-3):94-99.

Simanshu, D. K., Zhai, X., Munch, D., Hofius, D., Markham, J. E., Bielawski, J., Bielawska, A., Malinina, L., Molotkovsky, J. G., Mundy, J. W., Patel, D. J., and Brown, R. E. (2014). *Arabidopsis* accelerated cell death 11, ACD11, is a ceramide-1-phosphate transfer protein and intermediary regulator of phytoceramide levels. *Cell Rep*., 6(2):388-399.

Spassieva, S., and Hille, J. (2003). Plant sphingolipids today - Are they still enigmatic?. *Plant Biol*., 5(2):123-136.

Sperling, P., Zähringer, U., and Heinz, E. (1998). A sphingolipid desaturase from higher plants. Identification of a new cytochrome b5 fusion protein. *J. biol. Chem.*, 273(44):28590-28596.

Sperling, P., Ternes, P., Moll, H., Franke, S., Zähringer, U., and Heinz, E. (2001). Functional characterization of sphingolipid C4-hydroxylase genes from *Arabidopsis thaliana*. *FEBS Lett*., 494(1-2):90-94.

Sperling, P., and Heinz, E. (2003). Plant sphingolipids: structural diversity, biosynthesis, first genes and functions. *Biochim. Biophys. Acta*, 1632(1-3):1-15.

Sperling, P., Franke, S., Lüthje, S., and Heinz, E. (2005). Are glucocerebrosides the predominant sphingolipids in plant plasma membranes?. *Plant Physiol. Biochem.*, 43(12):1031-1038.

Spiegel, S., and Milstien, S. (2003). Sphingosine-1-phosphate: an enigmatic signalling lipid. *Nat. Rev. Mol. Cell Biol*., 4:397-407.

Stockmann-Juvala, H., Alenius, H., and Savolainen, K. (2008). Effects of fumonisin B(1) on the expression of cytokines and chemokines in human dendritic cells. *Food Chem. Toxicol.*, 46(5):1444-1451.

Sullards, M. C. (2000). Analysis of sphingomyelin, glucosylceramide, ceramide, sphingosine, and sphingosine 1-phosphate by tandem mass spectrometry. *Methods Enzymol*., 312:32-45.

Sullards, M. C., and Merrill, A. H., Jr (2001). Analysis of sphingosine 1-phosphate, ceramides, and other bioactive sphingolipids by high-performance liquid chromatography-tandem mass spectrometry. *Sci. STKE.,* 2001(67):pl1.

Sumner, L. W., Amberg, A., Barrett, D., Beale, M. H., Beger, R., Daykin, C. A., Fan, T. W., Fiehn, O., Goodacre, R., Griffin, J. L., Hankemeier, T., Hardy, N., Harnly, J., Higashi, R., Kopka, J., Lane, A. N., Lindon, J. C., Marriott, P., Nicholls, A. W., Reily, … Viant, M. R. (2007a). Proposed minimum reporting standards for chemical analysis Chemical Analysis Working Group (CAWG) Metabolomics Standards Initiative (MSI). *Metabolomics*, 3(3):211-221.

Sumner, L. W., Urbanczyk-Wochniak, E., and Broeckling, C. D. (2007b). Metabolomics data analysis, visualization, and integration. *Methods in molecular biology (Clifton, N.J.)*, 406:409-436.

Tafesse, F. G., and Holthuis, J. C. M. (2010). Cell biology: a brake on lipid synthesis. *Nature*, 463(7284):1028-1029.

Teng, C., Dong, H., Shi, L., Deng, Y., Mu, J., Zhang, J., Yang, X., and Zuo, J. (2008). Serine palmitoyltransferase, a key enzyme for de novo synthesis of sphingolipids, is essential for male gametophyte development in *Arabidopsis*. *Plant Physiol*., 146(3):1322-1332.

Ternes, P., Feussner, K., Werner, S., Lerche, J., Iven, T., Heilmann, I., Riezman, H., and Feussner, I. (2011). Disruption of the ceramide synthase LOH1 causes spontaneous cell death in *Arabidopsis thaliana*. *New Phytol*., 192(4):841-854.

Thuleau, P., Aldon, D., Cotelle, V., Brière, C., Ranty, B., Galaud, J. P., and Mazars, C. (2013). Relationships between calcium and sphingolipid-dependent signalling pathways during the early steps of plant-pathogen interactions. *Biochim. Biophys. Acta*, *1833*(7):1590-1594.

Tianniam, S., Bamba, T., and Fukusaki, E. (2009). Non-targeted metabolite fingerprinting of oriental folk medicine Angelica acutiloba roots by ultra performance liquid chromatography time-of-flight mass spectrometry. *Journal of separation science*, 32(13):2233-2244.

Tohge, T., and Fernie, A. R. (2009). Web-based resources for mass-spectrometry-based metabolomics: a user's guide. *Phytochemistry*, 70(4), 450-456.

Townley, H. E., McDonald, K., Jenkins, G. I., Knight, M. R., and Leaver, C. J. (2005). Ceramides induce programmed cell death in *Arabidopsis* cells in a calcium-dependent-manner. *Biol. Chem*., 386(2):161-166.

Trinel, P. A., Maes, E., Zanetta, J. P., Delplace, F., Coddeville, B., Jouault, T., Strecker, G., and Poulain, D. (2002). Candida albicans phospholipomannan, a new member of the fungal mannose inositol phosphoceramide family. *J. Biol. Chem.*, 277(40):37260-37271.

Tsegaye, Y., Richardson, C. G., Bravo, J. E., Mulcahy, B. J., Lynch, D. V., Markham, J. E., Jaworski, J. G., Chen, M., Cahoon, E. B., and Dunn, T. M. (2007). *Arabidopsis* mutants lacking long-chain base phosphate lyase are fumonisin-sensitive and accumulate trihydroxy-18:1 long-chain base phosphate. *J. Biol. Chem*., 282:28195-28206.

Tukey, J. W. (1949). Comparing individual means in the analysis of variance. *Biometrics*, 5(2):99-114.

Van der Hoorn, R. A. L., and Kamoun, S. (2008). From guard to decoy: A new model for perception of plant pathogen effectors. *The plant Cell*, 20:2009-2017.

Van Doorn, W. G. (2011). Classes of programmed cell death in plants, compared to those animals. *J. Exp. Bot*., 62(14):4749-4761.

Vleeshouwers, V. G. A. A., and Oliver, R. P. (2014). Effectors as tools in disease resistance breeding against biotrophic, hemibiotrophic, and necrotrophic plant pathogens. *Mol. Plant Microbe Interact*., 27(3):196-206.

Wadsworth, J. M., Clarke, D. J., McMahon, S. A., Lowther, J. P., Beattie, A. E., Langridge-Smith, P. R., Broughton, H. B., Dunn, T. M., Naismith, J. H., and Campopiano, D. J. (2013). The chemical basis of serine palmitoyltransferase inhibition by myriocin. *J. American Chem. Soci.*, 135(38):14276-14285.

Wang, W., Yang, X., Tangchaiburana, S., Ndeh, R., Markham, J. E., Tsegaye, Y., Dunn, T. M., Wang, G. L., Bellizzi, M., Parsons, J. F., Morrissey, D., Bravo, J. E., Lynch, D. V., and Xiao, S. (2008). An inositolphosphorylceramide synthase is involved in regulation of plant programmed cell death associated with defense in *Arabidopsis*. *Plant Cell*, 20(11):3163-3179.

Wang, Y., Xiao, J., Suzek, T. O., Zhang, J., Wang, J., and Bryant, S. H. (2009). PubChem: a public information system for analyzing bioactivities of small molecules. *Nucleic acids research*, 37(Web Server issue):W623-W633.

Warnecke, D., and Heinz, E. (2003). Recently discovered functions of glucosylceramides in plants and fungi. *Cell. Mol. Life Sci.*, 60(5):919-941.

Winter, E., and Ponting, C. P. (2002). TRAM, LAG1 and CLN8: members of a novel family of lipid-sensing domains?. *Trends Biochem. Sci.*, 27(8):381-383.

Worrall, D., Liang, Y. K., Alvarez, S., Holroyd, G. H., Spiegel, S., Panagopulos, M., Gray, J. E., and Hetherington, A. M. (2008). Involvement of sphingosine kinase in plant cell signalling. *Plant J*., 56(1):64-72.

Wu, J. X., Li, J., Liu, Z., Yin, J., Chang, Z. Y., Rong, C., Wu, J. L., Bi, F. C., and Yao, N. (2015). The *Arabidopsis* ceramidase AtACER functions in disease resistance and salt tolerance. *Plant J*., 81(5):767-780.

Xie, L. J., Chen, Q. F., Chen, M. X., Yu, L. J., Huang, L., Chen, L., Wang, F. Z., Xia, F. N., Zhu, T. R., Wu, J. X., Yin, J., Liao, B., Shi, J., Zhang, J. H., Aharoni, A., Yao, N., Shu, W., and Xiao, S. (2015). Unsaturation of very-long-chain ceramides protects plant from hypoxia-induced damages by modulating ethylene signaling in *Arabidopsis*. *PLoS Genet*., 11(3):e1005143.

Yanagawa, D., Ishikawa, T., and Imai, H. (2017). Synthesis and degradation of long-chain base phosphates affect fumonisin B_1-induced cell death in *Arabidopsis thaliana*. *Journal of plant research*, 130(3):571-585.

Zeise, K., and Von Tiedemann, A. (2002). Host specialization among vegetative compatibility groups of *Verticillium dahlia* in relation to *Verticillium longisporum*. *J. Phytopathol.*, 150(3):112-119.

Zhang, G., Slaski, J., Archambault, D., and Taylor, G. (2006). Alteration of plasma membrane lipids in aluminum-resistant and aluminum-sensitive wheat genotypes in response to aluminum stress. *Phys. Plantarum*, 99:302-308.

Zhao, Y., Hull, A. K., Gupta, N. R., Goss, K. A., Alonso, J., Ecker, J. R., Normanly, J., Chory, J., and Celenza, J. L. (2002). Trp-dependent auxin biosynthesis in *Arabidopsis*: involvement of cytochrome P450s CYP79B2 and CYP79B3. *Genes & Dev.*, 16(23):3100-3112.

Zheng, P., Wu, J. X., Sahu, S. K., Zeng, H. Y., Huang, L. Q., Liu, Z., Xiao, S., and Yao, N. (2018). Loss of alkaline ceramidase inhibits autophagy in *Arabidopsis* and plays an important role during environmental stress response. *Plant Cell Environ.*, 41(4):837-849.

7. Acknowledgments.

This journey would not have been possible without the support of my supervisors, colleagues, family, and friends. I would like to express my gratitude to my supervisor Prof. Dr. Frank Waller for giving me the opportunity to perform the PhD thesis in his group. For his friendly supervision, patience and advice while guiding me through this experience. Your suggestions gave me motivation and were an essential contribution to my dissertation. I would like to thank Prof. Dr. Martin J. Müller for recruiting me, for his feedback during each of our meetings, and for the valuable discussions about this project. Also, I would like to thank Prof. Dr. Dirk Becker for providing an expert opinion on my thesis.

I would like to particularly thank Agnes Fekete and Markus Krischke for introducing me to the analysis of metabolites through HPLC-MS/MS, for answering my many questions on sphingolipids analysis and for measuring my large number of samples even during the weekend. I am very grateful to Prof. Dr. Wolfgang Dröge-Laser and his group for being so kind with me while working in their laboratory. Special thanks to Christoph Weiste for always transmitting happiness and for helping me with technical questions. I am very greatful to Christian Fröschel for his help with the pathogen infection studies during my thesis, for his patience and for sharing with me his knowledge on the subject.

I would also like to thank all former and present members of the department of pharmaceutical biology for their help in the laboratory and the delightful, shared moments during lunch time. The day-to-day interactions were amusing and lovely and I always felt welcome. Special thanks to my colleagues Elena Ferber, Pamela Korte, Stephanie Müller, Manuel Lange, Beeke Tappe, Pyroozeh Peirovnaziri, Stefan Schäbler, Mohamed Osman, Niklas Reichelt, Theresa Damm, Kelechi Amatobi, and René Glenz, with whom I shared those 3 years and a half, for their friendly support and for the pleasant and relaxed atmosphere in the office. I particularly thank Pamela Korte for her help with the German translation in this thesis. My gratitude also goes to the interns and students Agnes Kaiping, Vanessa Bachmann, Quynh Nhu Truong, and Steven Steinwand who helped me daily and actively supported me with this project with practical work in the laboratory, contributing to the success of this thesis.

I wish to thank my family for their unconditional support and encouragement throughout this journey, for their advice and for believing in me. *Je vous remercie de ne pas avoir perdu espoir, d'avoir cru en moi, de m'avoir conseillé et encouragé durant ces années loin de vous. Je finis finalement l'écriture de ma thèse, mais bon, j'étais large. Doucement mais sûrement, comme on dit. Merci beaucoup, je vous aime.* Last, but not least, thank you Cristina for helping me, motivating me, and pushing me through this adventure when I needed it. This would not have been possible without you being by my side.